BNL-102434-2013

Seismic Soil-Structure Interaction Analyses of a Deeply Embedded Model Reactor – SASSI Analyses

J. Nie, J. Braverman, M. Costantino

October 2013

Nuclear Science & Technology Department

Brookhaven National Laboratory

U.S. Department of Energy
Office of Nuclear Energy

Notice: This manuscript has been authored by employees of Brookhaven Science Associates, LLC under Contract No. DE-AC02-98CH10886 with the U.S. Department of Energy. The publisher by accepting the manuscript for publication acknowledges that the United States Government retains a non-exclusive, paid-up, irrevocable, world-wide license to publish or reproduce the published form of this manuscript, or allow others to do so, for United States Government purposes.

DISCLAIMER

This report was prepared as an account of work sponsored by an agency of the United States Government. Neither the United States Government nor any agency thereof, nor any of their employees, nor any of their contractors, subcontractors, or their employees, makes any warranty, express or implied, or assumes any legal liability or responsibility for the accuracy, completeness, or any third party's use or the results of such use of any information, apparatus, product, or process disclosed, or represents that its use would not infringe privately owned rights. Reference herein to any specific commercial product, process, or service by trade name, trademark, manufacturer, or otherwise, does not necessarily constitute or imply its endorsement, recommendation, or favoring by the United States Government or any agency thereof or its contractors or subcontractors. The views and opinions of authors expressed herein do not necessarily state or reflect those of the United States Government or any agency thereof..

BNL-102434-2013

Seismic Soil-Structure Interaction Analyses of a Deeply Embedded Model Reactor – SASSI Analyses

October 31, 2013

Jinsuo R. Nie[1], Joseph I. Braverman[1], and Michael Costantino[2]

[1] Brookhaven National Laboratory
[2] CJC & Associates

ABSTRACT

This report summarizes the SASSI analyses of a deeply embedded reactor model performed by BNL and CJC & Associates, as part of the seismic soil-structure interaction (SSI) simulation capability project for the NEAMS (Nuclear Energy Advanced Modeling and Simulation) Program of the Department of Energy. The SASSI analyses included three cases: 0.2 g, 0.5 g, and 0.9g, all of which refer to nominal peak accelerations at the top of the bedrock. The analyses utilized the modified subtraction method (MSM) for performing the seismic SSI evaluations. Each case consisted of two analyses: input motion in one horizontal direction (X) and input motion in the vertical direction (Z), both of which utilized the same in-column input motion.

Besides providing SASSI results for use in comparison with the time domain SSI results obtained using the DIABLO computer code, this study also leads to the recognition that the frequency-domain method should be modernized so that it can better serve its mission-critical role for analysis and design of nuclear power plants.

TABLE OF CONTENTS

ABSTRACT iii

LIST OF TABLES vii

LIST OF FIGURES ix

ACRONYMS xix

1 INTRODUCTION 1

2 DEVELOPMENT OF SASSI HOUSE MODELS 3

2.1 General Procedure 3
2.2 Pictures of the SASSI Models 7

3 THE CASE OF 0.2 g 15

3.1 Summary of SASSI Results 15
3.2 Acceleration Time Histories and ISRS for the X Directional Input Motion 24
3.3 Acceleration Time Histories and ISRS for the Z Directional Input Motion 55

4 THE CASE OF 0.5 g 87

4.1 Summary of SASSI Results 87
4.2 Acceleration Time Histories and ISRS for the X Directional Input Motion 96
4.3 Acceleration Time Histories and ISRS for the Z Directional Input Motion 128

5 The Case of 0.9 g 161

5.1 Summary of SASSI Results 161
5.2 Acceleration Time Histories and ISRS for the X Directional Input Motion 171
5.3 Acceleration Time Histories and ISRS for the Z Directional Input Motion 203

6 SUMMARY AND RECOMMENDATIONS 237

LIST OF TABLES

Table 3-1 SASSI Results for the Case of 0.2 g 16
Table 4-1 SASSI Results for the Case of 0.5 g 88
Table 5-1 SASSI Results for the Case of 0.9 g 162

LIST OF FIGURES

Figure 2-1 ATF Comparison at the Center of the Basemat of the Quarter Model for Horizontal Input Motion at Basemat Level 4
Figure 2-2 ATF Comparison at a Corner of the Basemat of the Quarter Model for Horizontal Input Motion at Basemat Level 4
Figure 2-3 ATF Comparison at a Corner of the Structure of the Quarter Model for Horizontal Input Motion at Basemat Level 5
Figure 2-4 ATF Comparison at the Center of the Basemat of the Quarter Model for Vertical Input Motion at Basemat Level 5
Figure 2-5 ATF Comparison at a Corner of the Basemat of the Quarter Model for Vertical Input Motion at Basemat Level 6
Figure 2-6 ATF Comparison at a Corner of the Structure of the Quarter Model for Vertical Input Motion at Basemat Level 6
Figure 2-7 Effectiveness of GLP Points 7
Figure 2-8 Structural Model 8
Figure 2-9 Comparison of Original and New Basemat Models 9
Figure 2-10 Structural Soil Model 10
Figure 2-11 Bottom and Top Views of the Structural Soil below Basemat 10
Figure 2-12 Excavated Soil Model 11
Figure 2-13 Interaction Nodes for DM (All Nodes of Excavated Soil) 11
Figure 2-14 Interaction Nodes for SM (Only Boundary Nodes on the Sides and Bottom) 12
Figure 2-15 Interaction Nodes for MSM (Boundary Nodes plus Nodes on Ground Surface) 12
Figure 2-16 Interaction Nodes for MSM2 (MSM + Alternating Internal Nodes) 13
Figure 2-17 One Example of the Interaction Nodes for ESM (Boundary Nodes + GLP Internal Nodes) 13
Figure 3-1 Response Acceleration Time Histories and ISRS at Node 1021 for X Input Motion (0.2 g) 24
Figure 3-2 Response Acceleration Time Histories and ISRS at Node 1182 for X Input Motion (0.2 g) 25
Figure 3-3 Response Acceleration Time Histories and ISRS at Node 1887 for X Input Motion (0.2 g) 26
Figure 3-4 Response Acceleration Time Histories and ISRS at Node 1942 for X Input Motion (0.2 g) 27
Figure 3-5 Response Acceleration Time Histories and ISRS at Node 2949 for X Input Motion (0.2 g) 28
Figure 3-6 Response Acceleration Time Histories and ISRS at Node 4905 for X Input Motion (0.2 g) 29
Figure 3-7 Response Acceleration Time Histories and ISRS at Node 13774 for X Input Motion (0.2 g) 30
Figure 3-8 Response Acceleration Time Histories and ISRS at Node 13886 for X Input Motion (0.2 g) 31
Figure 3-9 Response Acceleration Time Histories and ISRS at Node 14364 for X Input Motion (0.2 g) 32
Figure 3-10 Response Acceleration Time Histories and ISRS at Node 14522 for X Input Motion (0.2 g) 33
Figure 3-11 Response Acceleration Time Histories and ISRS at Node 15095 for X Input Motion (0.2 g) 34
Figure 3-12 Response Acceleration Time Histories and ISRS at Node 18132 for X Input Motion (0.2 g) 35
Figure 3-13 Response Acceleration Time Histories and ISRS at Node 22080 for X Input Motion (0.2 g) 36

Figure 3-14 Response Acceleration Time Histories and ISRS at Node 27184 for X Input Motion (0.2 g) 37
Figure 3-15 Response Acceleration Time Histories and ISRS at Node 27296 for X Input Motion (0.2 g) 38
Figure 3-16 Response Acceleration Time Histories and ISRS at Node 27782 for X Input Motion (0.2 g) 39
Figure 3-17 Response Acceleration Time Histories and ISRS at Node 27948 for X Input Motion (0.2 g) 40
Figure 3-18 Response Acceleration Time Histories and ISRS at Node 28514 for X Input Motion (0.2 g) 41
Figure 3-19 Response Acceleration Time Histories and ISRS at Node 31566 for X Input Motion (0.2 g) 42
Figure 3-20 Response Acceleration Time Histories and ISRS at Node 32546 for X Input Motion (0.2 g) 43
Figure 3-21 Response Acceleration Time Histories and ISRS at Node 35500 for X Input Motion (0.2 g) 44
Figure 3-22 Response Acceleration Time Histories and ISRS at Node 38274 for X Input Motion (0.2 g) 45
Figure 3-23 Response Acceleration Time Histories and ISRS at Node 38328 for X Input Motion (0.2 g) 46
Figure 3-24 Response Acceleration Time Histories and ISRS at Node 38557 for X Input Motion (0.2 g) 47
Figure 3-25 Response Acceleration Time Histories and ISRS at Node 38569 for X Input Motion (0.2 g) 48
Figure 3-26 Response Acceleration Time Histories and ISRS at Node 38876 for X Input Motion (0.2 g) 49
Figure 3-27 Response Acceleration Time Histories and ISRS at Node 39041 for X Input Motion (0.2 g) 50
Figure 3-28 Response Acceleration Time Histories and ISRS at Node 39274 for X Input Motion (0.2 g) 51
Figure 3-29 Response Acceleration Time Histories and ISRS at Node 39962 for X Input Motion (0.2 g) 52
Figure 3-30 Response Acceleration Time Histories and ISRS at Node 39976 for X Input Motion (0.2 g) 53
Figure 3-31 Response Acceleration Time Histories and ISRS at Node 40333 for X Input Motion (0.2 g) 54
Figure 3-32 Response Acceleration Time Histories and ISRS at Node 1021 for Z Input Motion (0.2 g) 55
Figure 3-33 Response Acceleration Time Histories and ISRS at Node 1182 for Z Input Motion (0.2 g) 56
Figure 3-34 Response Acceleration Time Histories and ISRS at Node 1887 for Z Input Motion (0.2 g) 57
Figure 3-35 Response Acceleration Time Histories and ISRS at Node 1942 for Z Input Motion (0.2 g) 58
Figure 3-36 Response Acceleration Time Histories and ISRS at Node 2949 for Z Input Motion (0.2 g) 59
Figure 3-37 Response Acceleration Time Histories and ISRS at Node 4905 for Z Input Motion (0.2 g) 60

Figure 3-38 Response Acceleration Time Histories and ISRS at Node 13774 for Z Input Motion (0.2 g) 61
Figure 3-39 Response Acceleration Time Histories and ISRS at Node 13886 for Z Input Motion (0.2 g) 62
Figure 3-40 Response Acceleration Time Histories and ISRS at Node 14364 for Z Input Motion (0.2 g) 63
Figure 3-41 Response Acceleration Time Histories and ISRS at Node 14522 for Z Input Motion (0.2 g) 64
Figure 3-42 Response Acceleration Time Histories and ISRS at Node 15095 for Z Input Motion (0.2 g) 65
Figure 3-43 Response Acceleration Time Histories and ISRS at Node 18132 for Z Input Motion (0.2 g) 66
Figure 3-44 Response Acceleration Time Histories and ISRS at Node 22080 for Z Input Motion (0.2 g) 67
Figure 3-45 Response Acceleration Time Histories and ISRS at Node 27184 for Z Input Motion (0.2 g) 68
Figure 3-46 Response Acceleration Time Histories and ISRS at Node 27296 for Z Input Motion (0.2 g) 69
Figure 3-47 Response Acceleration Time Histories and ISRS at Node 27782 for Z Input Motion (0.2 g) 70
Figure 3-48 Response Acceleration Time Histories and ISRS at Node 27948 for Z Input Motion (0.2 g) 71
Figure 3-49 Response Acceleration Time Histories and ISRS at Node 28514 for Z Input Motion (0.2 g) 72
Figure 3-50 Response Acceleration Time Histories and ISRS at Node 31566 for Z Input Motion (0.2 g) 73
Figure 3-51 Response Acceleration Time Histories and ISRS at Node 32546 for Z Input Motion (0.2 g) 74
Figure 3-52 Response Acceleration Time Histories and ISRS at Node 35500 for Z Input Motion (0.2 g) 75
Figure 3-53 Response Acceleration Time Histories and ISRS at Node 38274 for Z Input Motion (0.2 g) 76
Figure 3-54 Response Acceleration Time Histories and ISRS at Node 38328 for Z Input Motion (0.2 g) 77
Figure 3-55 Response Acceleration Time Histories and ISRS at Node 38557 for Z Input Motion (0.2 g) 78
Figure 3-56 Response Acceleration Time Histories and ISRS at Node 38569 for Z Input Motion (0.2 g) 79
Figure 3-57 Response Acceleration Time Histories and ISRS at Node 38876 for Z Input Motion (0.2 g) 80
Figure 3-58 Response Acceleration Time Histories and ISRS at Node 39041 for Z Input Motion (0.2 g) 81

Figure 3-59 Response Acceleration Time Histories and ISRS at Node 39274 for Z Input Motion (0.2 g) 82
Figure 3-60 Response Acceleration Time Histories and ISRS at Node 39962 for Z Input Motion (0.2 g) 83
Figure 3-61 Response Acceleration Time Histories and ISRS at Node 39976 for Z Input Motion (0.2 g) 84
Figure 3-62 Response Acceleration Time Histories and ISRS at Node 40333 for Z Input Motion (0.2 g) 85
Figure 4-1 Response Acceleration Time Histories and ISRS at Node 1021 for X Input Motion (0.5 g) 96
Figure 4-2 Response Acceleration Time Histories and ISRS at Node 1182 for X Input Motion (0.5 g) 97
Figure 4-3 Response Acceleration Time Histories and ISRS at Node 1887 for X Input Motion (0.5 g) 98
Figure 4-4 Response Acceleration Time Histories and ISRS at Node 1942 for X Input Motion (0.5 g) 99
Figure 4-5 Response Acceleration Time Histories and ISRS at Node 2949 for X Input Motion (0.5 g) 100
Figure 4-6 Response Acceleration Time Histories and ISRS at Node 4904 for X Input Motion (0.5 g) 101
Figure 4-7 Response Acceleration Time Histories and ISRS at Node 4905 for X Input Motion (0.5 g) 102
Figure 4-8 Response Acceleration Time Histories and ISRS at Node 13774 for X Input Motion (0.5 g) .. 103
Figure 4-9 Response Acceleration Time Histories and ISRS at Node 13886 for X Input Motion (0.5 g) .. 104
Figure 4-10 Response Acceleration Time Histories and ISRS at Node 14364 for X Input Motion (0.5 g) 105
Figure 4-11 Response Acceleration Time Histories and ISRS at Node 14522 for X Input Motion (0.5 g) 106
Figure 4-12 Response Acceleration Time Histories and ISRS at Node 15095 for X Input Motion (0.5 g) 107
Figure 4-13 Response Acceleration Time Histories and ISRS at Node 18132 for X Input Motion (0.5 g) 108
Figure 4-14 Response Acceleration Time Histories and ISRS at Node 22080 for X Input Motion (0.5 g) 109
Figure 4-15 Response Acceleration Time Histories and ISRS at Node 27184 for X Input Motion (0.5 g) 110
Figure 4-16 Response Acceleration Time Histories and ISRS at Node 27296 for X Input Motion (0.5 g) 111
Figure 4-17 Response Acceleration Time Histories and ISRS at Node 27782 for X Input Motion (0.5 g) 112
Figure 4-18 Response Acceleration Time Histories and ISRS at Node 27948 for X Input Motion (0.5 g) 113
Figure 4-19 Response Acceleration Time Histories and ISRS at Node 28514 for X Input Motion (0.5 g) 114
Figure 4-20 Response Acceleration Time Histories and ISRS at Node 31566 for X Input Motion (0.5 g) 115
Figure 4-21 Response Acceleration Time Histories and ISRS at Node 32546 for X Input Motion (0.5 g) 116

Figure 4-22 Response Acceleration Time Histories and ISRS at Node 35500 for X Input Motion (0.5 g) 117
Figure 4-23 Response Acceleration Time Histories and ISRS at Node 38274 for X Input Motion (0.5 g) 118
Figure 4-24 Response Acceleration Time Histories and ISRS at Node 38328 for X Input Motion (0.5 g) 119
Figure 4-25 Response Acceleration Time Histories and ISRS at Node 38557 for X Input Motion (0.5 g) 120
Figure 4-26 Response Acceleration Time Histories and ISRS at Node 38569 for X Input Motion (0.5 g) 121
Figure 4-27 Response Acceleration Time Histories and ISRS at Node 38876 for X Input Motion (0.5 g) 122
Figure 4-28 Response Acceleration Time Histories and ISRS at Node 39041 for X Input Motion (0.5 g) 123
Figure 4-29 Response Acceleration Time Histories and ISRS at Node 39274 for X Input Motion (0.5 g) 124
Figure 4-30 Response Acceleration Time Histories and ISRS at Node 39962 for X Input Motion (0.5 g) 125
Figure 4-31 Response Acceleration Time Histories and ISRS at Node 39976 for X Input Motion (0.5 g) 126
Figure 4-32 Response Acceleration Time Histories and ISRS at Node 40333 for X Input Motion (0.5 g) 127
Figure 4-33 Response Acceleration Time Histories and ISRS at Node 1021 for Z Input Motion (0.5 g) .. 128
Figure 4-34 Response Acceleration Time Histories and ISRS at Node 1182 for Z Input Motion (0.5 g) .. 129
Figure 4-35 Response Acceleration Time Histories and ISRS at Node 1887 for Z Input Motion (0.5 g) .. 130
Figure 4-36 Response Acceleration Time Histories and ISRS at Node 1942 for Z Input Motion (0.5 g) .. 131
Figure 4-37 Response Acceleration Time Histories and ISRS at Node 2949 for Z Input Motion (0.5 g) .. 132
Figure 4-38 Response Acceleration Time Histories and ISRS at Node 4904 for Z Input Motion (0.5 g) .. 133
Figure 4-39 Response Acceleration Time Histories and ISRS at Node 4905 for Z Input Motion (0.5 g) .. 134
Figure 4-40 Response Acceleration Time Histories and ISRS at Node 13774 for Z Input Motion (0.5 g) 135
Figure 4-41 Response Acceleration Time Histories and ISRS at Node 13886 for Z Input Motion (0.5 g) 136
Figure 4-42 Response Acceleration Time Histories and ISRS at Node 14364 for Z Input Motion (0.5 g) 137
Figure 4-43 Response Acceleration Time Histories and ISRS at Node 14522 for Z Input Motion (0.5 g) 138
Figure 4-44 Response Acceleration Time Histories and ISRS at Node 15095 for Z Input Motion (0.5 g) 139
Figure 4-45 Response Acceleration Time Histories and ISRS at Node 18132 for Z Input Motion (0.5 g) 140

Figure 4-46 Response Acceleration Time Histories and ISRS at Node 22080 for Z Input Motion (0.5 g) 141
Figure 4-47 Response Acceleration Time Histories and ISRS at Node 27184 for Z Input Motion (0.5 g) 142
Figure 4-48 Response Acceleration Time Histories and ISRS at Node 27296 for Z Input Motion (0.5 g) 143
Figure 4-49 Response Acceleration Time Histories and ISRS at Node 27782 for Z Input Motion (0.5 g) 144
Figure 4-50 Response Acceleration Time Histories and ISRS at Node 27948 for Z Input Motion (0.5 g) 145
Figure 4-51 Response Acceleration Time Histories and ISRS at Node 28514 for Z Input Motion (0.5 g) 146
Figure 4-52 Response Acceleration Time Histories and ISRS at Node 31566 for Z Input Motion (0.5 g) 147
Figure 4-53 Response Acceleration Time Histories and ISRS at Node 32546 for Z Input Motion (0.5 g) 148
Figure 4-54 Response Acceleration Time Histories and ISRS at Node 35500 for Z Input Motion (0.5 g) 149
Figure 4-55 Response Acceleration Time Histories and ISRS at Node 38274 for Z Input Motion (0.5 g) 150
Figure 4-56 Response Acceleration Time Histories and ISRS at Node 38328 for Z Input Motion (0.5 g) 151
Figure 4-57 Response Acceleration Time Histories and ISRS at Node 38557 for Z Input Motion (0.5 g) 152
Figure 4-58 Response Acceleration Time Histories and ISRS at Node 38569 for Z Input Motion (0.5 g) 153
Figure 4-59 Response Acceleration Time Histories and ISRS at Node 38876 for Z Input Motion (0.5 g) 154
Figure 4-60 Response Acceleration Time Histories and ISRS at Node 39041 for Z Input Motion (0.5 g) 155
Figure 4-61 Response Acceleration Time Histories and ISRS at Node 39274 for Z Input Motion (0.5 g) 156
Figure 4-62 Response Acceleration Time Histories and ISRS at Node 39962 for Z Input Motion (0.5 g) 157
Figure 4-63 Response Acceleration Time Histories and ISRS at Node 39976 for Z Input Motion (0.5 g) 158
Figure 4-64 Response Acceleration Time Histories and ISRS at Node 40333 for Z Input Motion (0.5 g) 159
Figure 5-1 Response Acceleration Time Histories and ISRS at Node 1021 for X Input Motion (0.9 g) 171
Figure 5-2 Response Acceleration Time Histories and ISRS at Node 1182 for X Input Motion (0.9 g) 172
Figure 5-3 Response Acceleration Time Histories and ISRS at Node 1887 for X Input Motion (0.9 g) 173
Figure 5-4 Response Acceleration Time Histories and ISRS at Node 1942 for X Input Motion (0.9 g) 174
Figure 5-5 Response Acceleration Time Histories and ISRS at Node 2949 for X Input Motion (0.9 g) 175

Figure 5-6 Response Acceleration Time Histories and ISRS at Node 4904 for X Input Motion (0.9 g) 176
Figure 5-7 Response Acceleration Time Histories and ISRS at Node 4905 for X Input Motion (0.9 g) 177
Figure 5-8 Response Acceleration Time Histories and ISRS at Node 13774 for X Input Motion (0.9 g) .. 178
Figure 5-9 Response Acceleration Time Histories and ISRS at Node 13886 for X Input Motion (0.9 g) .. 179
Figure 5-10 Response Acceleration Time Histories and ISRS at Node 14364 for X Input Motion (0.9 g) 180
Figure 5-11 Response Acceleration Time Histories and ISRS at Node 14522 for X Input Motion (0.9 g) 181
Figure 5-12 Response Acceleration Time Histories and ISRS at Node 15095 for X Input Motion (0.9 g) 182
Figure 5-13 Response Acceleration Time Histories and ISRS at Node 18132 for X Input Motion (0.9 g) 183
Figure 5-14 Response Acceleration Time Histories and ISRS at Node 22080 for X Input Motion (0.9 g) 184
Figure 5-15 Response Acceleration Time Histories and ISRS at Node 27184 for X Input Motion (0.9 g) 185
Figure 5-16 Response Acceleration Time Histories and ISRS at Node 27296 for X Input Motion (0.9 g) 186
Figure 5-17 Response Acceleration Time Histories and ISRS at Node 27782 for X Input Motion (0.9 g) 187
Figure 5-18 Response Acceleration Time Histories and ISRS at Node 27948 for X Input Motion (0.9 g) 188
Figure 5-19 Response Acceleration Time Histories and ISRS at Node 28514 for X Input Motion (0.9 g) 189
Figure 5-20 Response Acceleration Time Histories and ISRS at Node 31566 for X Input Motion (0.9 g) 190
Figure 5-21 Response Acceleration Time Histories and ISRS at Node 32546 for X Input Motion (0.9 g) 191
Figure 5-22 Response Acceleration Time Histories and ISRS at Node 35500 for X Input Motion (0.9 g) 192
Figure 5-23 Response Acceleration Time Histories and ISRS at Node 38274 for X Input Motion (0.9 g) 193
Figure 5-24 Response Acceleration Time Histories and ISRS at Node 38328 for X Input Motion (0.9 g) 194
Figure 5-25 Response Acceleration Time Histories and ISRS at Node 38557 for X Input Motion (0.9 g) 195
Figure 5-26 Response Acceleration Time Histories and ISRS at Node 38569 for X Input Motion (0.9 g) 196
Figure 5-27 Response Acceleration Time Histories and ISRS at Node 38876 for X Input Motion (0.9 g) 197
Figure 5-28 Response Acceleration Time Histories and ISRS at Node 39041 for X Input Motion (0.9 g) 198

Figure 5-29 Response Acceleration Time Histories and ISRS at Node 39274 for X Input Motion (0.9 g) 199
Figure 5-30 Response Acceleration Time Histories and ISRS at Node 39962 for X Input Motion (0.9 g) 200
Figure 5-31 Response Acceleration Time Histories and ISRS at Node 39976 for X Input Motion (0.9 g) 201
Figure 5-32 Response Acceleration Time Histories and ISRS at Node 40333 for X Input Motion (0.9 g) 202
Figure 5-33 Response Acceleration Time Histories and ISRS at Node 1021 for Z Input Motion (0.9 g) .. 203
Figure 5-34 Response Acceleration Time Histories and ISRS at Node 1182 for Z Input Motion (0.9 g) .. 204
Figure 5-35 Response Acceleration Time Histories and ISRS at Node 1887 for Z Input Motion (0.9 g) .. 205
Figure 5-36 Response Acceleration Time Histories and ISRS at Node 1942 for Z Input Motion (0.9 g) .. 206
Figure 5-37 Response Acceleration Time Histories and ISRS at Node 2949 for Z Input Motion (0.9 g) .. 207
Figure 5-38 Response Acceleration Time Histories and ISRS at Node 4904 for Z Input Motion (0.9 g) .. 208
Figure 5-39 Response Acceleration Time Histories and ISRS at Node 4905 for Z Input Motion (0.9 g) .. 209
Figure 5-40 Response Acceleration Time Histories and ISRS at Node 13774 for Z Input Motion (0.9 g) 210
Figure 5-41 Response Acceleration Time Histories and ISRS at Node 13886 for Z Input Motion (0.9 g) 211
Figure 5-42 Response Acceleration Time Histories and ISRS at Node 14364 for Z Input Motion (0.9 g) 212
Figure 5-43 Response Acceleration Time Histories and ISRS at Node 14522 for Z Input Motion (0.9 g) 213
Figure 5-44 Response Acceleration Time Histories and ISRS at Node 15095 for Z Input Motion (0.9 g) 214
Figure 5-45 Response Acceleration Time Histories and ISRS at Node 18132 for Z Input Motion (0.9 g) 215
Figure 5-46 Response Acceleration Time Histories and ISRS at Node 22080 for Z Input Motion (0.9 g) 216
Figure 5-47 Response Acceleration Time Histories and ISRS at Node 27184 for Z Input Motion (0.9 g) 217
Figure 5-48 Response Acceleration Time Histories and ISRS at Node 27296 for Z Input Motion (0.9 g) 218
Figure 5-49 Response Acceleration Time Histories and ISRS at Node 27782 for Z Input Motion (0.9 g) 219
Figure 5-50 Response Acceleration Time Histories and ISRS at Node 27948 for Z Input Motion (0.9 g) 220
Figure 5-51 Response Acceleration Time Histories and ISRS at Node 28514 for Z Input Motion (0.9 g) 221
Figure 5-52 Response Acceleration Time Histories and ISRS at Node 31566 for Z Input Motion (0.9 g) 222

Figure 5-53 Response Acceleration Time Histories and ISRS at Node 32546 for Z Input Motion (0.9 g) 223
Figure 5-54 Response Acceleration Time Histories and ISRS at Node 35500 for Z Input Motion (0.9 g) 224
Figure 5-55 Response Acceleration Time Histories and ISRS at Node 38274 for Z Input Motion (0.9 g) 225
Figure 5-56 Response Acceleration Time Histories and ISRS at Node 38328 for Z Input Motion (0.9 g) 226
Figure 5-57 Response Acceleration Time Histories and ISRS at Node 38557 for Z Input Motion (0.9 g) 227
Figure 5-58 Response Acceleration Time Histories and ISRS at Node 38569 for Z Input Motion (0.9 g) 228
Figure 5-59 Response Acceleration Time Histories and ISRS at Node 38876 for Z Input Motion (0.9 g) 229
Figure 5-60 Response Acceleration Time Histories and ISRS at Node 39041 for Z Input Motion (0.9 g) 230
Figure 5-61 Response Acceleration Time Histories and ISRS at Node 39274 for Z Input Motion (0.9 g) 231
Figure 5-62 Response Acceleration Time Histories and ISRS at Node 39962 for Z Input Motion (0.9 g) 232
Figure 5-63 Response Acceleration Time Histories and ISRS at Node 39976 for Z Input Motion (0.9 g) 233
Figure 5-64 Response Acceleration Time Histories and ISRS at Node 40333 for Z Input Motion (0.9 g) 234

ACRONYMS

ATF	Acceleration Transfer Function
BNL	Brookhaven National Laboratory
CJCA	CJC and Associates
DM	Direct Method
DOE	Department of Energy
ESM	Enhanced Subtraction Method
ESSI	Nonlinear Earthquake Soil/Rock Structure Interaction
GLP	Good-Lattice Points
ISRS	In-Structure Response Spectra
LBNL	Lawrence Berkeley National Laboratory
LLNL	Lawrence Livermore National Laboratory
MSM	Modified Subtraction Method
NEAMS	Nuclear Energy Advanced Modeling and Simulation Program
ORNL	Oak Ridge National Laboratory
SASSI	A System for Analysis of Soil-Structure Interaction
SM	Subtraction Method

1 INTRODUCTION

This report summarizes the SASSI analyses performed by Brookhaven National Laboratory (BNL) and CJC & Associates, for the DOE NEAMS - Seismic Soil Structure Interaction Simulation Capability project. The prototype of the reactor model was developed based on inputs from LLNL, BNL, and other national laboratories, and is described separately in a report prepared by LLNL.

The SASSI analyses included all three cases: 0.2 g, 0.5 g, and 0.9 g corresponding to three levels of earthquakes. The modified subtraction method (MSM) was determined to be the most appropriate method in SASSI for this task based on a comparison study using a quarter model of the reactor model. Due to the large size of the model, CJC & Associates' SDE-SASSI v2.0 was used to perform the calculation. This version of SASSI has the capability to solve large scale SSI problems.

The structural model for the containment and reactor vessel was developed in Cubit by LLNL. The basemat in the Cubit model was replaced with a regular mesh that has an element aspect ratio near unity. This allows for a consistent interaction node spacing as well as a uniform excavated soil model which is consistent with guidance defined for SASSI implementations.

The analyses included a case with an input motion in one horizontal direction (X) and a case with the same input motion in the vertical direction (Z). For the purpose of comparison of the SASSI (frequency domain solution) results with those calculated with LLNL's nonlinear time-domain structural mechanics code DIABLO, it was agreed that it would be sufficient to consider input in these two directions. The input motions were specified as the in-column ground motions at a depth of 112.776 m (370 ft). The same input acceleration time histories were assumed for both the X direction and the Z direction.

This report discusses the maximum acceleration and in-structure response spectra (ISRS) for all the nodes that were selected for comparison with DIABLO. The soil pressure and other member forces/moments are not readily available; however, this data could be calculated in a future expansion of this project.

The SASSI computer code provides the results for acceleration time histories. Integration of the acceleration time histories should not be used to obtain velocity or displacement time histories.

Section 2 of this report describes the development of the SASSI models based on the structural model provided by LLNL; Sections 3 through 5 present the results for the case of 0.2 g, 0.5 g, and 0.9 g, respectively. Section 6 provides a summary of the SASSI analyses and recommendations for future work to modernize the frequency domain soil-structure interaction (SSI) method.

This report was prepared in order to provide the results of the BNL SASSI analysis of the reactor model to be used by the DOE NEAMS team for comparison with the DIABLO results. A separate report will be written by the DOE NEAMS team in more detail to summarize the overall study.

2 DEVELOPMENT OF SASSI HOUSE MODELS

2.1 General Procedure

The reactor model developed by LLNL, BNL, and other national laboratories for the NEAMS seismic simulation project, consisted of a box-type containment structure, a cylindrical reactor pressure vessel, stick models of various frequencies to represent major equipment, a large water tank, and other auxiliary structural elements. LLNL developed a finite element model for the reactor model for time-domain analysis. Based on the structural part of the finite element model provided by LLNL (the soil model was not provided because it was developed for the time-domain solution and a different model must be developed for the SASSI analysis), BNL developed the SASSI models for its frequency-domain soil-structure interaction analysis. As for damping, 4% was used for the steel components and the lumped-mass "stick" elements, and 7% for the concrete elements. The same damping ratios were used in the DIABLO analysis. However, it should be noted that SASSI assumes hysteresis damping, as compared to the viscous damping used in the DIABLO analysis.

The development of the SASSI models involved the following steps:

1. Convert the LLNL structural model in Cubit format to an LS-DYNA model;
2. Perform modal analyses of the LS-DYNA structural model to check model consistency with the DIABLO structural model;
3. Replace the original basemat model with a more uniform basemat model in order to develop a regular mesh for the excavated soil model for SASSI analysis;
4. Develop the SASSI models including structural soil model and excavated soil model in LS-PrePost;
5. Generate interaction nodes for the subtraction method (SM), modified subtraction method (MSM), direct method (DM), and enhanced subtraction method (ESM, more interaction nodes were added to SM using good-lattice points (GLP));
6. Translate the SASSI models in LS-DYNA format to SASSI house models, including structure, structural soil, and excavated soil;
7. Perform SASSI analyses of a quarter model using DM, SM, MSM, and ESM for benchmark purpose.

The modal analysis of the fixed base structure identified that fundamental frequencies were about 4.6 Hz in the horizontal directions and 12.5 Hz in the vertical direction. The lowest natural frequency for the stick models was confirmed to be 1 Hz.

GLP are low discrepancy points used in multidimensional quadrature, simulation, and experimental design. It has been previously used to estimate structural system reliability. A feature of GLP is that for a given number of points in a set, they are more uniformly distributed than randomly selected points such as those used in Monte Carlo simulation.

By comparing acceleration transfer functions (ATFs) of a quarter model (see Figure 2-1 through Figure 2-6 for examples), MSM was determined to be the most appropriate method for this model. Therefore, the MSM was utilized in the SASSI analyses for the 0.2 g, 0.5 g, and 0.9 g cases. However, it should be noted that the modal analyses showed that ESM had a large advantage in increasing the fundamental frequency of the excavated soil model (see Figure 2-7), which has been identified as an indicator that the SM or MSM may start to produce spurious results for some problems.

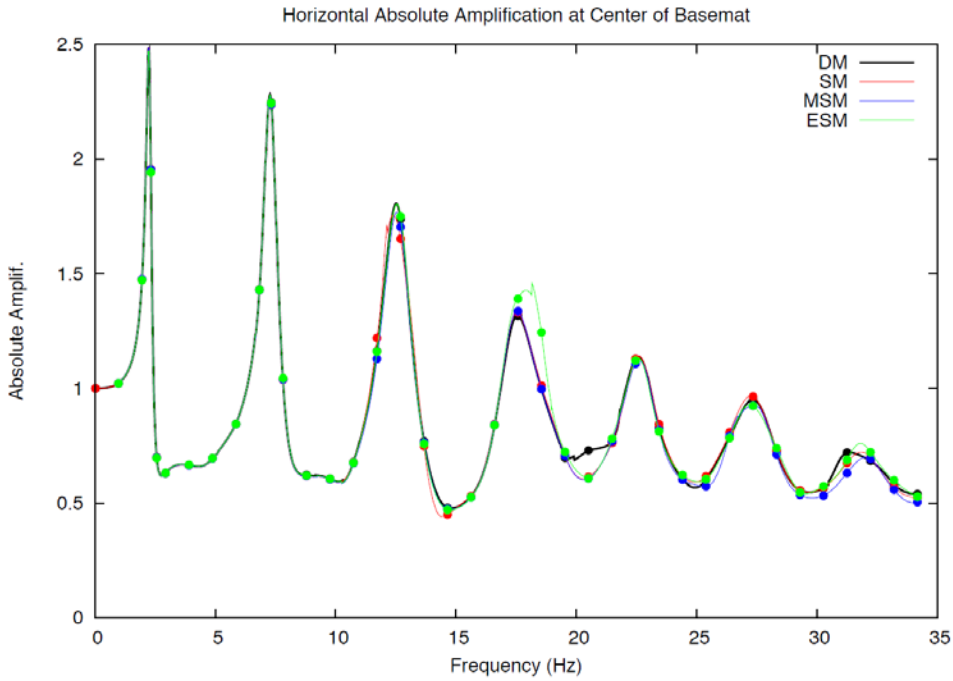

Figure 2-1 ATF Comparison at the Center of the Basemat of the Quarter Model for Horizontal Input Motion at Basemat Level

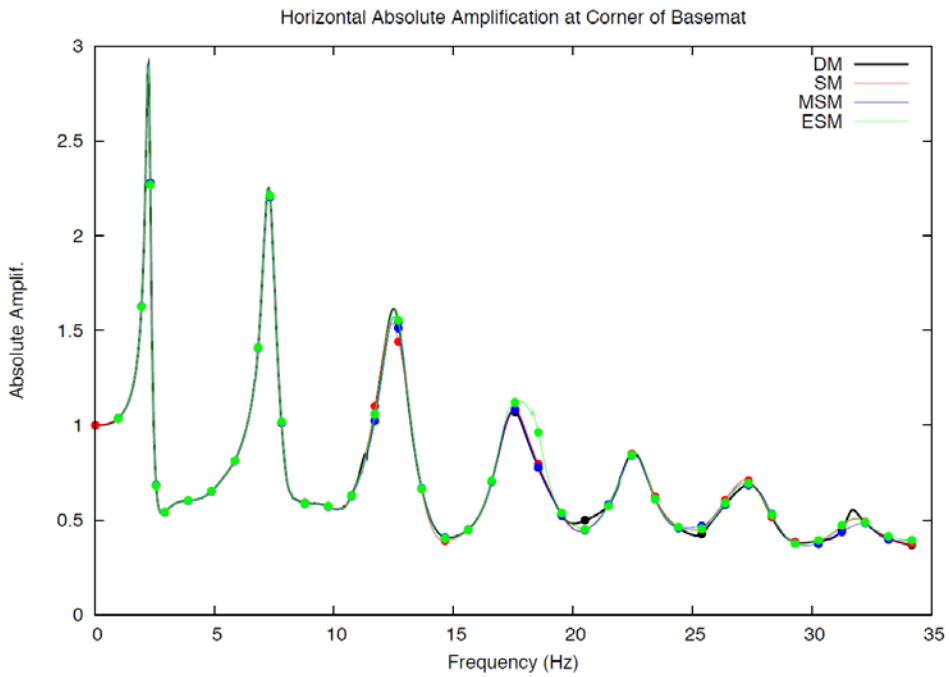

Figure 2-2 ATF Comparison at a Corner of the Basemat of the Quarter Model for Horizontal Input Motion at Basemat Level

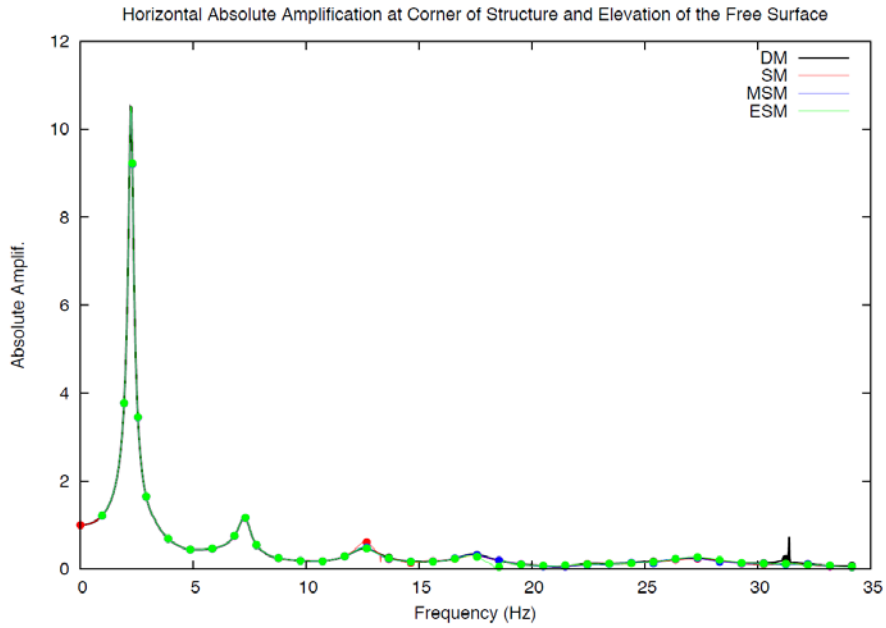

Figure 2-3 ATF Comparison at a Corner of the Structure of the Quarter Model for Horizontal Input Motion at Basemat Level

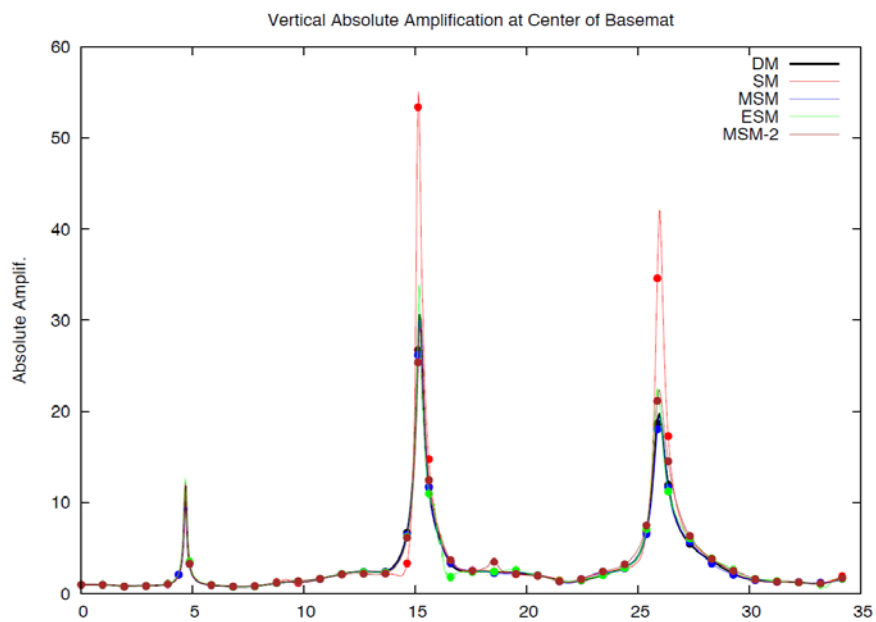

Figure 2-4 ATF Comparison at the Center of the Basemat of the Quarter Model for Vertical Input Motion at Basemat Level

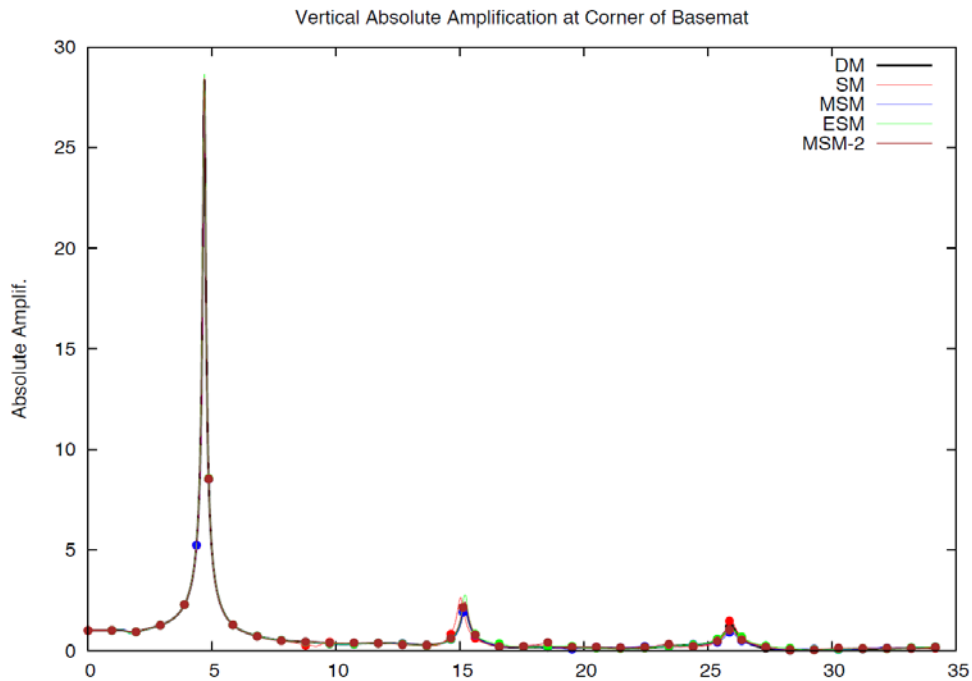

Figure 2-5 ATF Comparison at a Corner of the Basemat of the Quarter Model for Vertical Input Motion at Basemat Level

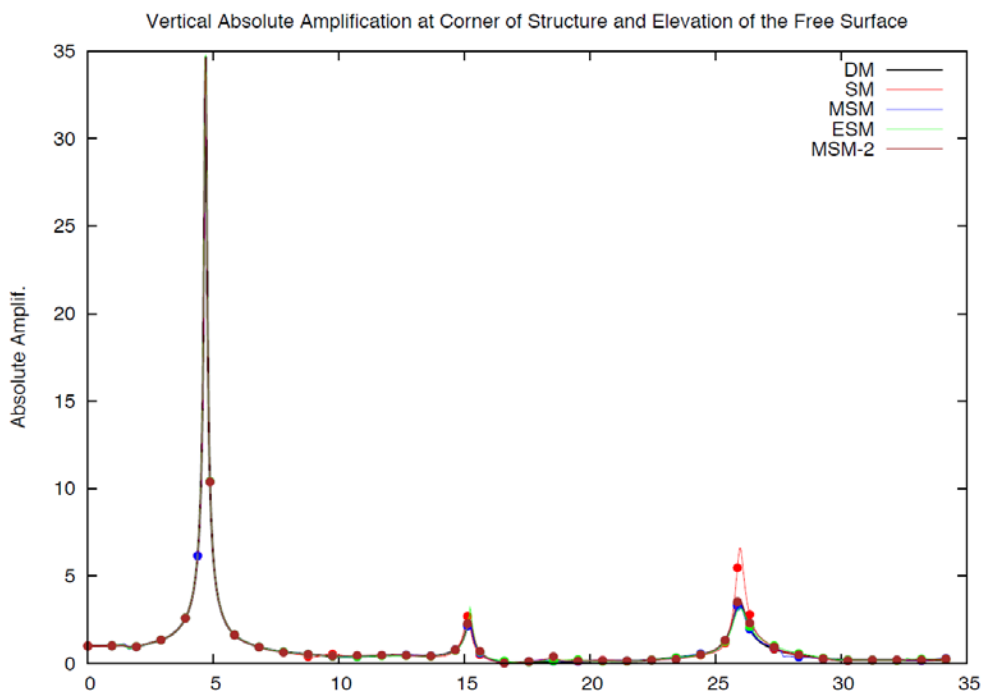

Figure 2-6 ATF Comparison at a Corner of the Structure of the Quarter Model for Vertical Input Motion at Basemat Level

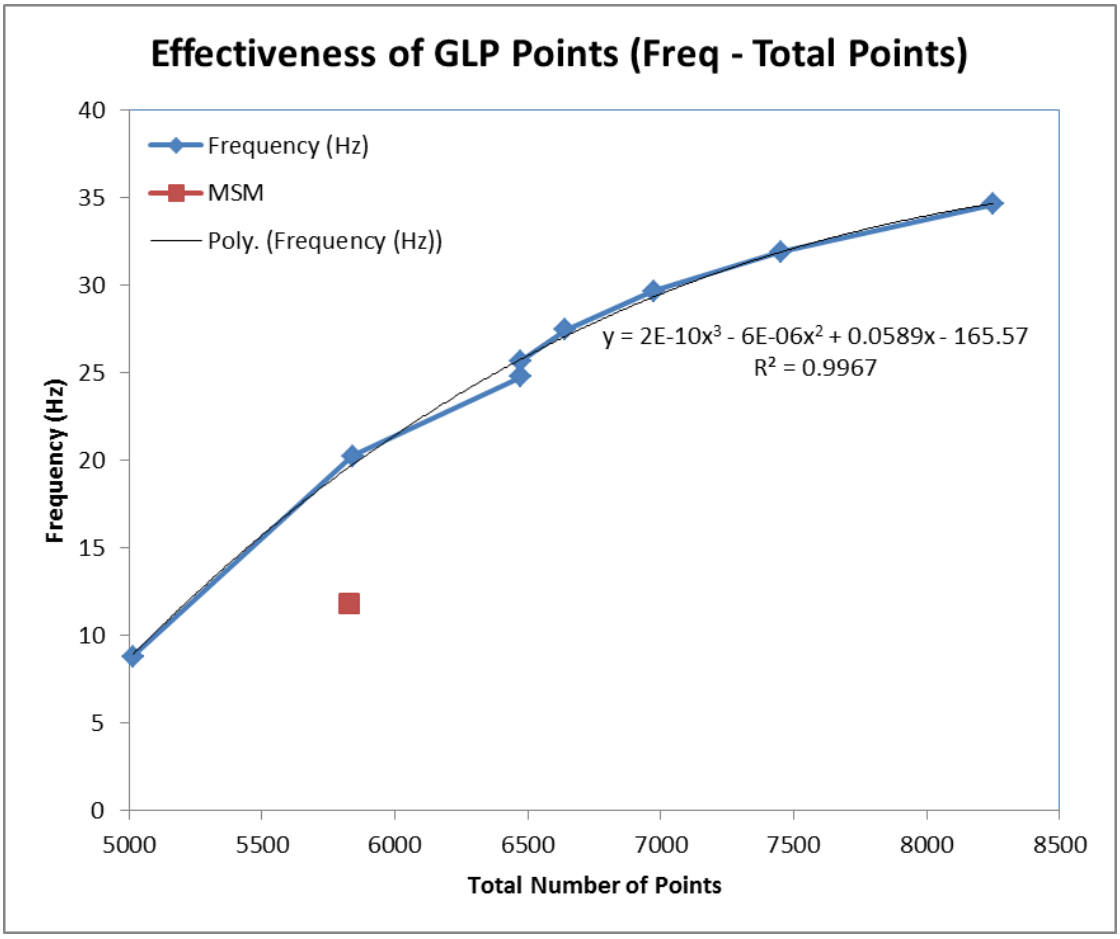

Figure 2-7 Effectiveness of GLP Points

2.2 Pictures of the SASSI Models

An external view of the finite element model for the containment and reactor vessel is shown in Figure 2-8 and a comparison of the original basemat model and the new basemat model is shown in Figure 2-9. Figure 2-10 shows the structural soil model, which consists of a single layer of solid elements of soil properties surrounding the structure. The structural soil model was included to obtain soil pressure if needed and to achieve the transition of the irregular structural mesh to the regular excavated soil mesh, as shown in Figure 2-11.

The excavated soil model and the interaction nodes are critical in a successful SASSI analysis. Figure 2-12 shows the excavated soil model and Figure 2-13 through Figure 2-17 show the interaction nodes for various analysis methods in SASSI.

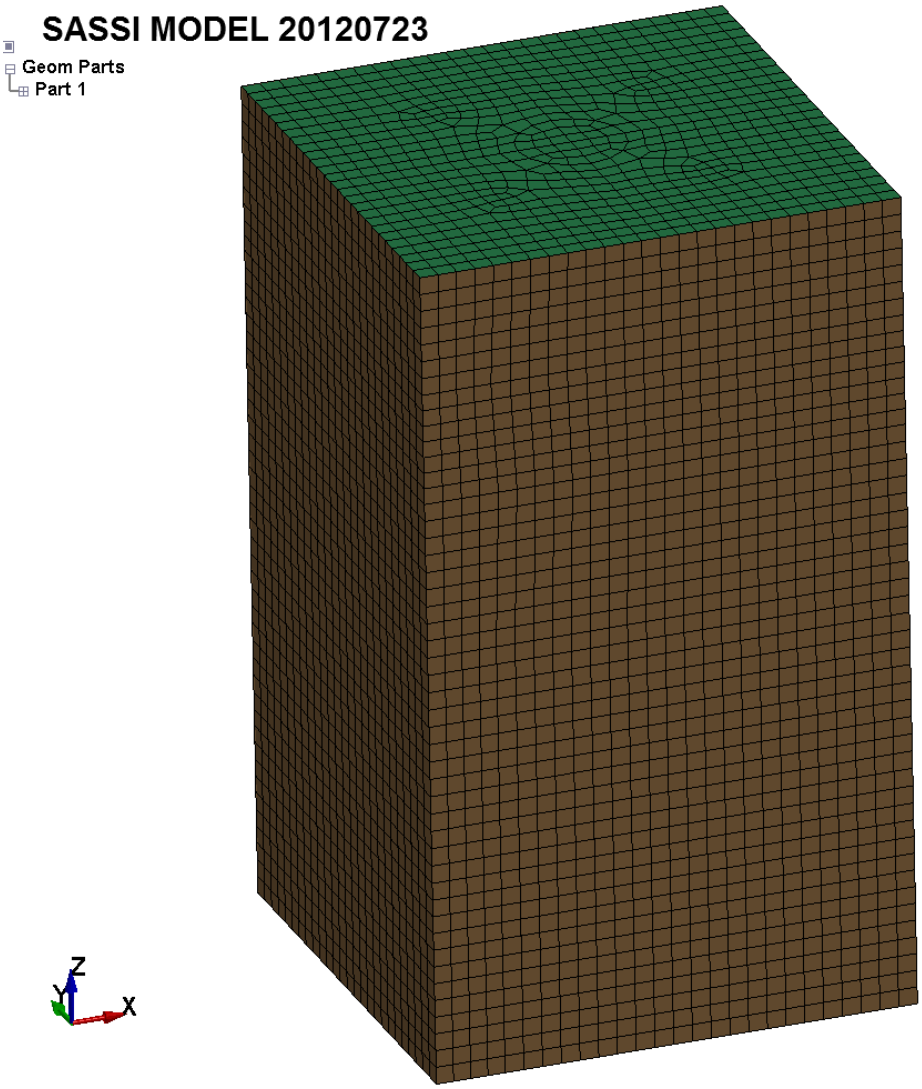

Figure 2-8 The Structural Model

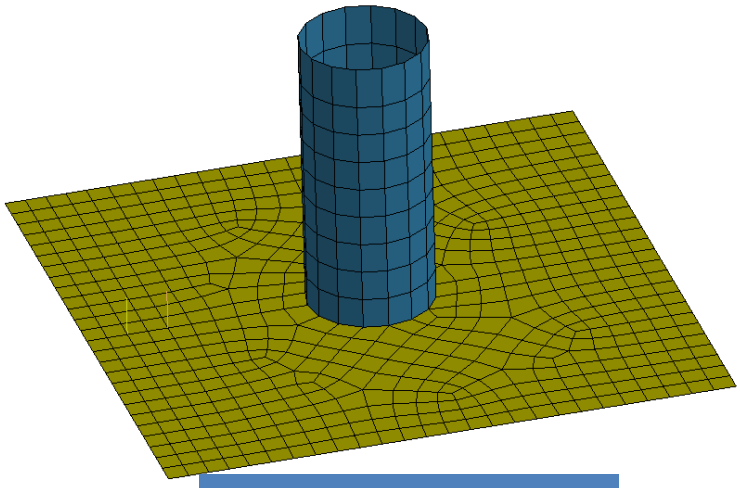

Original Basemat Model

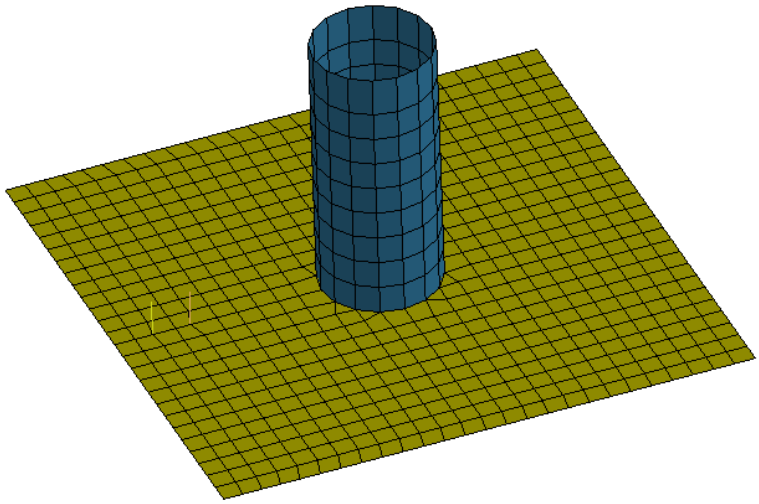

New Basemat Model for Resolving Potential Effects of Irregular Excavated Soil Model (minor adjustment to match the cylinder and the beams)

Figure 2-9 Comparison of Original and New Basemat Models

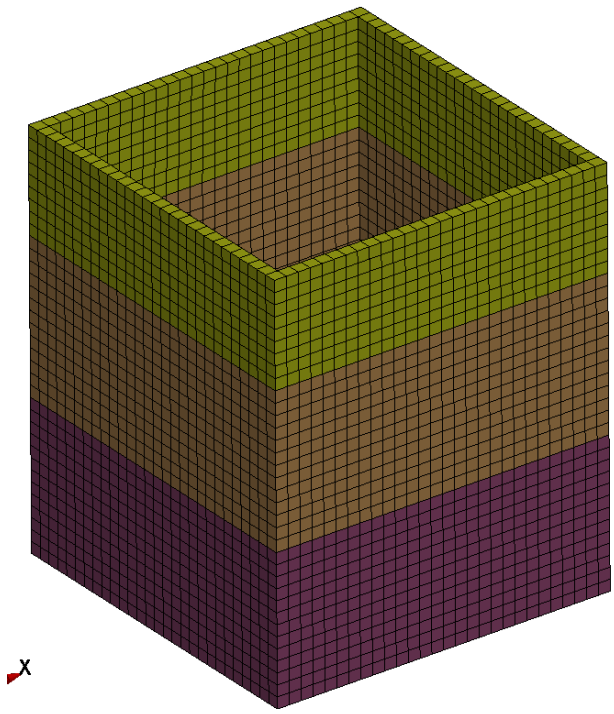

Figure 2-10 Structural Soil Model

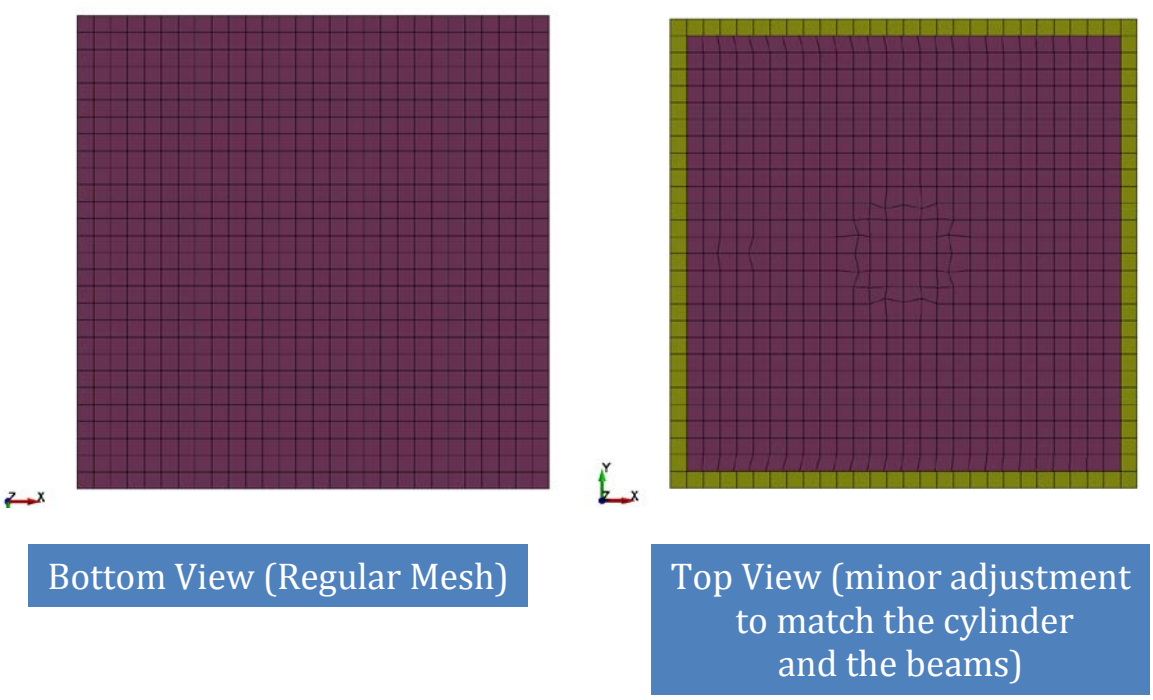

Figure 2-11 Bottom and Top Views of the Structural Soil below Basemat

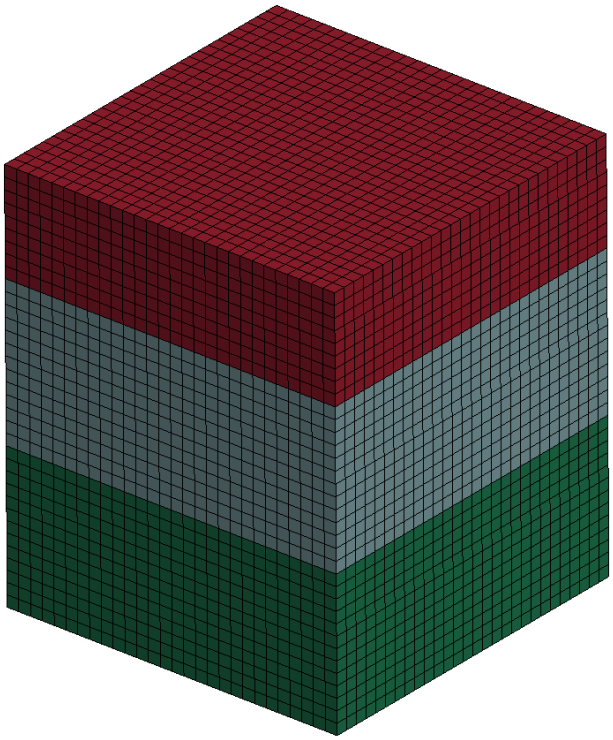

Figure 2-12 Excavated Soil Model

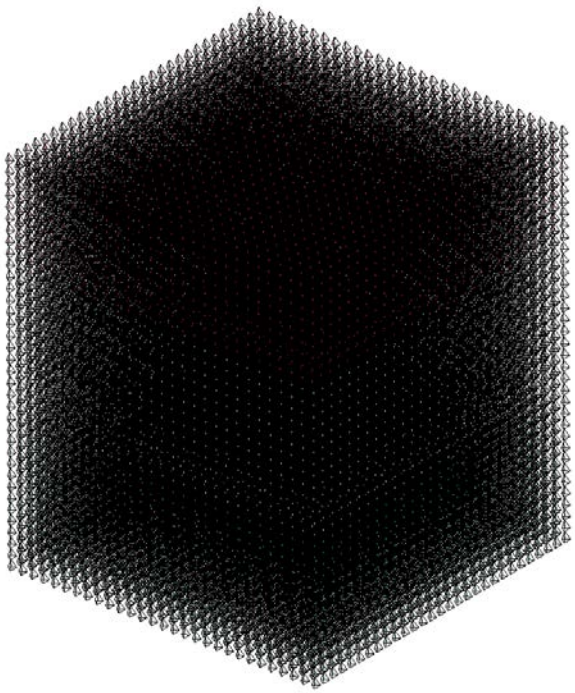

Figure 2-13 Interaction Nodes for DM (All Nodes of Excavated Soil)

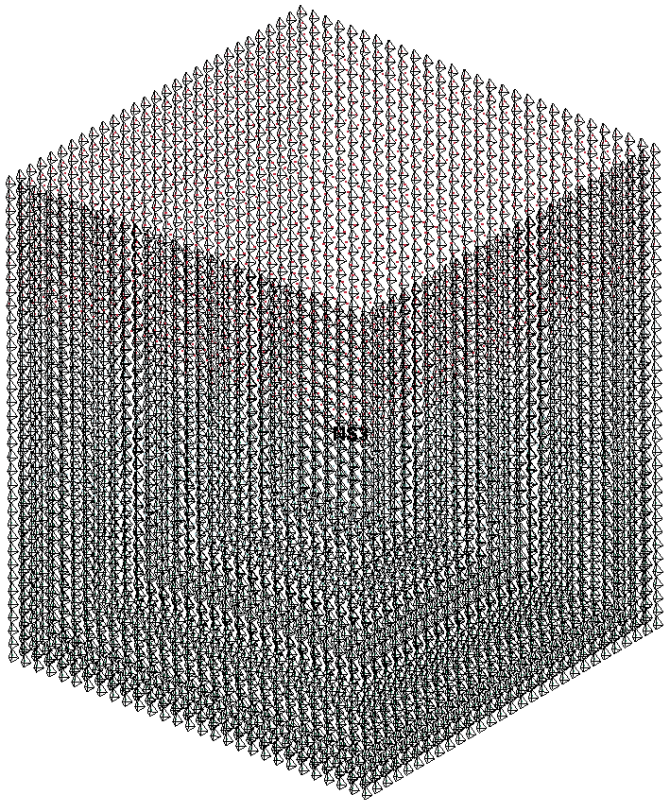

Figure 2-14 Interaction Nodes for SM (Only Boundary Nodes on the Sides and Bottom)

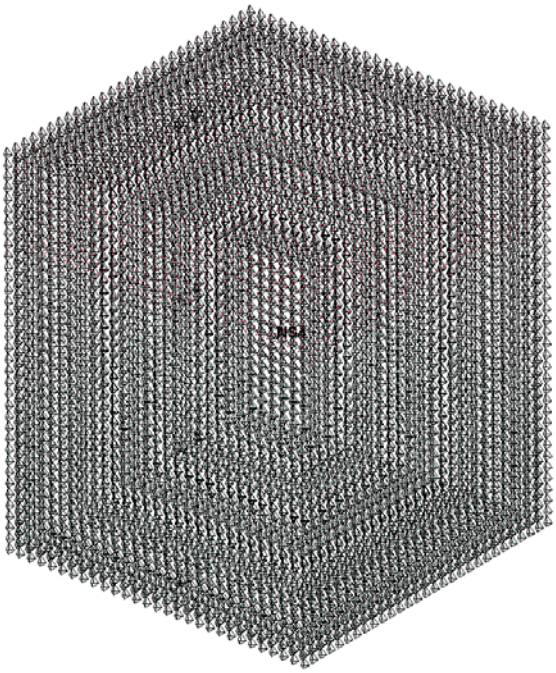

Figure 2-15 Interaction Nodes for MSM (Boundary Nodes plus Nodes on Ground Surface)

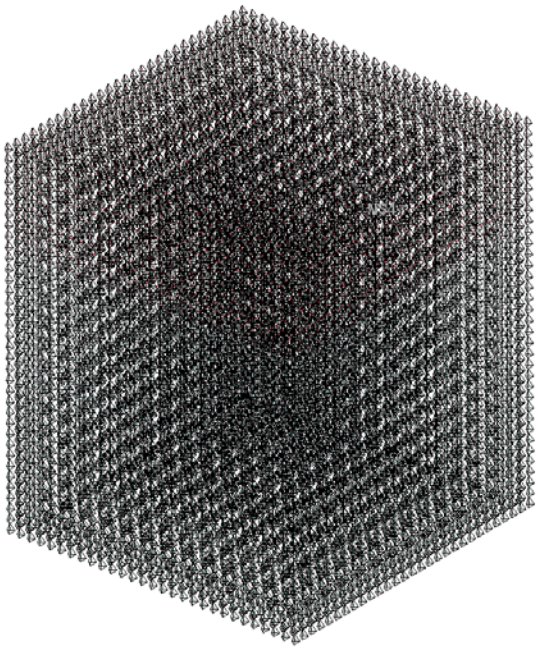

Figure 2-16 Interaction Nodes for MSM2 (MSM + Alternating Internal Nodes)

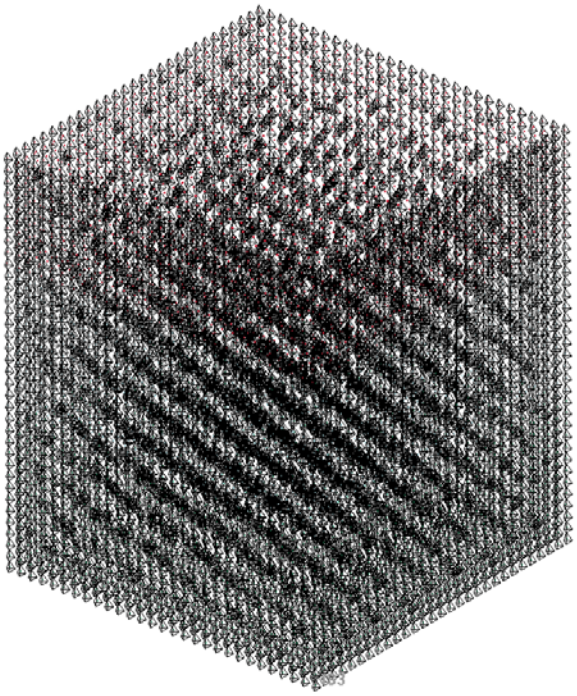

Figure 2-17 One Example of the Interaction Nodes for ESM (Boundary Nodes + GLP Internal Nodes)

3 THE CASE OF 0.2 g

3.1 Summary of SASSI Results

This section describes the SASSI results for the case of a nominal bedrock peak acceleration of 0.2 g.

Section 3.2 includes acceleration time history and response spectral figures for the X directional input, while Section 3.3 includes figures for the Z directional input.

The acceleration time histories are output directly from the SASSI computer code. The ISRS were calculated outside of SASSI for each of these acceleration time histories, separately for the two input motions in the X and Z directions. All maximum acceleration values are rounded to the second decimal place. It should be noted that the input motion, used in both DIABLO and SASSI analyses, was not baseline-corrected, and neither were the response accelerations shown in this document. In addition, the acceleration time histories should not be integrated to obtain velocity or displacement time histories.

In summary, results are presented as follows:

Accelerations – Maximum values and time history plots
ISRS – Acceleration response spectra

The table and the footnotes were provided to BNL by LLNL in order for BNL to enter the SASSI results. All items in red denote SASSI node/element information. Where an "x" is presented in the table, the data is not available.

Table 3-1 SASSI Results for the Case of 0.2 g

Roof Slab			
Response Parameter (unit) & Location	**Response Parameter Value for**		**Remarks**
	X-Dir Input Motion	**Vertical (Z) Input Motion**	
Maximum[(1)] X, Y, Z-Directional Accelerations m/s^2) at Node xx near the center of Roof Slab	2.85 0.00 0.04	0.10 0.00 6.20	Node (EXODUS:4140, CUBIT:8789, SASSI-39962): Located (0.0,0.0,13.5)m
Maximum[(1)] X, Y, Z-Directional Displacements (m) at Node xx near the center of Roof Slab	x	x	Node (EXODUS:4140, CUBIT:8789, SASSI-39962): Located (0.0,0.0,13.5)m
Maximum[(1)] out-of-plane Bending Moment about X and Y axes (N-m/m) at Node xx near the center of the Roof Slab	x	x	Element (EXODUS:4452, CUBIT:9444, SASSI- (710, 8, 3)): Located (0.0,0.0,13.5)m
X, Y, Z-Directional Acceleration ISRSs (in 'g'unit) at Node xx near the center of Roof Slab	See figure for 39962	See figure for 39962	Node (EXODUS:4140, CUBIT:8789, SASSI-39962): Located (0.0,0.0,13.5)m
X, Y, Z-Directional Acceleration ISRSs (in 'g'unit) at Node xx and Node YY near the edges of Roof Slab	See figures for 40333 and 39976	See figures for 40333 and 39976	Node (EXODUS:3962, CUBIT:4922, SASSI-40333): Located (14.0,0.0,13.5)m Node (EXODUS:4145, CUBIT:1142, SASSI-39976): Located (0.0,14.0,13.5)m
Third Floor Slab			
Maximum[(1)] X, Y, Z-Directional Accelerations (m/s^2) at Node xx near the center of Slab	2.36 0.00 0.04	0.08 0.00 5.94	Node (EXODUS:3436, CUBIT:8193, SASSI-38557): Located (0.0, 0.0, 6.5) m
Maximum[(1)] X, Y, Z-Directional Displacements m) at Node xx near the center of Slab	x	x	Node (EXODUS:3436, CUBIT:8193, SASSI-38557): Located (0.0, 0.0, 6.5) m
Maximum[(1)] out-of-plane Bending Moment about X and Y axes N-m/m) at Node xx near the center of the Slab	x	x	Element (EXODUS:3258, CUBIT:8250, SASSI- (146, 7, 3)): Located (0.0, 0.0, 6.5) m
X, Y, Z-Directional Acceleration ISRSs (in 'g'unit) at Node xx near the center of Slab	See figure for 38557	See figure for 38557	Node (EXODUS:3436, CUBIT:8193, SASSI-38557): Located (0.0, 0.0, 6.5) m

X, Y, Z-Directional Acceleration ISRSs (in 'g'unit) at Node xx and Node YY near the edges of Slab	See figures for 38876 and 38569	See figures for 38876 and 38569	Node (EXODUS:3321, CUBIT:4747, SASSI-38876): Located (14.0,0.0,6.5)m Node (EXODU:3493, CUBIT:39, SASSI-38569): Located (0.0,14.0,6.5)m
Second Floor Slab			
Maximum[1] X, Y, Z-Directional Accelerations m/s^2) at Node xx near the center of Slab	1.70 0.00 0.29	0.13 0.00 5.12	Node (EXODUS:675, CUBIT:5718, SASSI-27948): Located (3.125, 0.0, -9.144)m
Maximum[1] X, Y, Z-Directional Displacements (m) at Node xx near the center of Slab	x	x	Node (EXODUS:675, CUBIT:5718, SASSI-27948): Located (3.125, 0.0, -9.144)m
Maximum[1] out-of-plane Bending Moment about X and Y axes (N-m/m) at Node xx near the center of the Slab	x	x	Element (EXODUS:2627, CUBIT:7619, SASSI- (65, 6, 3)): Located (3.125, 0.0, -9.144)m
X, Y, Z-Directional Acceleration ISRSs (in 'g'unit) at Node xx near the center of Slab	See figure for 27948	See figure for 27948	Node (EXODUS:675, CUBIT:5718, SASSI-27948): Located (3.125, 0.0, -9.144)m
X, Y, Z-Directional Acceleration ISRSs (in 'g'unit) at Node xx and Node YY near the edges of Slab	See figures for 28514 and 27782	See figures for 28514 and 27782	Node (EXODUS:2676, CUBIT:3872, SASSI-28514): Located (14.0,0.0,-9.144)m Node (EXODUS:2993, CUBIT:231, SASSI- 27782) Located (-0.1818,14.0,-9.144)m
First Floor Slab			
Maximum[1] X, Y, Z-Directional Accelerations m/s^2) at Node xx near the center of Slab	1.79 0.00 0.30	0.16 0.00 4.52	Node (EXODUS:435, CUBIT:5532, SASSI-14522): Located(3.125,0.0,-22.5552)m
Maximum[1] X, Y, Z-Directional Displacements (m) at Node xx near the center of Slab	x	x	Node (EXODUS:435, CUBIT:5532, SASSI-14522): Located(3.125,0.0,-22.5552)m
Maximum[1] out-of-plane Bending Moment about X and Y axes (N-m/m) at Node xx near the center of the Slab	x	x	Element (EXODUS:2224, CUBIT:7216, SASSI- (279, 5, 3)): Located(3.125,0.0,-22.5552)m

X, Y, Z-Directional Acceleration ISRSs (in 'g'unit) at Node xx near the center of Slab	See figure for 14522	See figure for 14522	Node (EXODUS:435, CUBIT:5532, SASSI-14522): Located(3.125,0.0,-22.5552)m
X, Y, Z-Directional Acceleration ISRSs (in 'g'unit) at Node xx and Node YY near the edges of Slab	See figures for 15095 and 14364	See figures for 15095 and 14364	Node (EXODUS:2055, CUBIT:4122, SASSI-15095): Located (14.00,0.0,-22.5552) Node (EXODUS:2363, CUBIT:486, SASSI- 14364): Located(-0.1818,14.0,-22.5552)
Base Mat			
Maximum[(1)] X, Y, Z-Directional Accelerations (m/s^2) at Node xx near the center of Slab	1.85 0.00 0.02	0.03 0.00 4.36	Node (EXODUS:1319, CUBIT:6413, New basemat 9828, SASSI- 1942): Located (0.0,0.0,-34.5)
Maximum[(1)] X, Y, Z-Directional Displacements (m) at Node xx near the center of Slab	x	x	Node (EXODUS:1319, CUBIT:6413, New basemat 9828, SASSI- 1942): Located (0.0,0.0,-34.5)
Maximum[(1)] out-of-plane Bending Moment about X and Y axes (N-m/m) at Node xx near the center of the Slab	x	x	Element (EXODUS:1299, CUBIT:6413, New basemat 19363 (+X+Y to node 9828), SASSI- (351, 4, 3)): Located (0.0,0.0,-34.5)
X, Y, Z-Directional Acceleration ISRSs (in 'g'unit) at Node xx near the center of Slab	See figure for 1942	See figure for 1942	Node (EXODUS:1319, CUBIT:6413, New basemat 9828, SASSI- 1942): Located (0.0,0.0,-34.5)
X, Y, Z-Directional Acceleration ISRSs (in 'g'unit) at Node xx and Node YY near the edges of Slab	See figures for 2949 And 1887	See figures for 2949 And 1887	Node (EXODUS:1384, CUBIT:4447, SASSI- 2949): Located (14,0.0,-34.5)m Node (EXODUS:1700, CUBIT:835, SASSI- 1887): Located (0.909,14.0,-34.5)m
Reactor Vessel and Supports			
Maximum[(1)] X, Y, Z-Directional Displacements (m) at Node xx near the top Cover Plate of the Reactor Vessel	x	x	Node (EXODUS:27, CUBIT:5122, SASSI-32546): Located (0.0,0.0,-4.5)m

Maximum[1] out-of-plane Bending Moments about X and Y axes (N-m/m) at Node xx near the top Cover Plate of the Reactor Vessel	x	x	Element (EXODUS:14, CUBIT:5006, SASSI- (14, 1, 3)): Located (0.0,0.0,-4.5)m
Maximum[1] out-of-plane Bending Moments about X and Y axes (N-m/m) at Node xx of the Reactor Support Ring Plate		x	Element (EXODUS:4460, CUBIT:9452, SASSI- (2, 9, 3)): Located (2.0,0.0,-20.5)m Element (EXODUS:4486. CUBIT:9478, SASSI- (28, 9, 3)): Located (0.0,2.0,-20.5)m
Reactor Building Walls			
Maximum out-of-plane bending moments about X and Y axes (N-m/m) at Elev XX (4 Nodes, one in each wall near the center)	x	x	Elevation 1 Element (EXODUS:4503, CUBIT:13), SASSI- (13, 10, 3) located: (0.0,14.0,0.0)m Element(EXODUS: 8351, CUBIT:3861), SASSI- (3861, 10, 3) Located: (14.0,0.0,0.0) Element (EXODUS:5751, CUBIT:1261) , SASSI- (1261, 10, 3) Located: (0.0, -14.0,0.0)m Element(EXODUS: 6999, CUBIT:2509) SASSI- (2509, 10, 3) Located: (-14.0, 0.0, 0.0)m Elevation 2 Element (EXODUS:7571, CUBIT:3081), SASSI- (3081, 10, 3) Located: (-14.0,0.0, -16.36541)m Element (EXODUS:6323, CUBIT:1833) SASSI- (1833, 10, 3) Located: (-0.1818, -14.00, -16.36541)m Element (EXODUS:8637, CUBIT:4147), SASSI- (4147, 10, 3)Located: (14.00, 0.0, -16.36541)m Element (EXODUS:5075, CUBIT:585) SASSI- (585, 10, 3): Located: (-0.1818, 14.00, -16.36541)m

Maximum soil pressure in X and Y direction (in psi Pa) at 4 Nodes, one in each outer wall near the center	x	x	Elevation 1 Element(EXODUS: 8351, CUBIT:3861) StructSoil: 24702, SASSI-(900, 101, 1) Located: (14.0,0.0,0.0) Element Element(EXODUS: 6999, CUBIT:2509) Located: (-14.0, 0.0, 0.0)m Elevation 2 Element (EXODUS:7571, CUBIT:3081) StructSoil: 22828, SASSI-(1060, 102, 1) Located: (-14.0,0.0, -16.36541)m Element (EXODUS:6323, CUBIT:1833) StructSoil: 22282, SASSI-(514, 102, 1) Located: (-0.1818, -14.00, -16.36541)m Element (EXODUS:8637, CUBIT:4147) StructSoil: 22321, SASSI-(553, 102, 1) Located: (14.00, 0.0, -16.36541)m Element (EXODUS:5075, CUBIT:585): StructSoil: 22516, SASSI-(748, 102, 1) Located: (-0.1818, 14.00, -16.36541)m

Maximum in-plane shear stress(Pa) in the reactor building X and Y-Dir outer walls at 8 Nodes, two in each outer wall (one near the center, one near the edge)			Set 1 Element (EXODUS:5544, CUBIT:1054) SASSI- (1054, 10, 3) Located: (-0.1818,14.00,-34.5) Element (EXODUS:5554, CUBIT:1064) SASSI- (1064, 10, 3) Located: (10.7272,14.00,-34.5) Set 2 Element (EXODUS:9106, CUBIT:4616) SASSI- (4616, 10, 3) Located: (14.00, 0.0, -34.5) Element (EXODUS:9116, CUBIT:4626) SASSI- (4626, 10, 3) Located: (14.00,-10.7692,-34.5) Set 3 Element (EXODUS:6791, CUBIT:2301) SASSI- (2301, 10, 3) Located: (-0.1818,-14.00,-34.5) Element (EXODUS:6781, CUNIT:2291) SASSI- (2291, 10, 3) Located: (-11.00, -14.00,-34.5) Set 4 Element (EXODUS:8039, CUBIT:3549) SASSI- (3549, 10, 3) Located: (-14.00, 0.0, -34.5)
Lumped-Mass Stick Models			

X, Y, Z-Directional Acceleration ISRSs (in 'g'unit) at the top and the bottom node of each stick	See figures for the ISRSs for these nodes. Note that for node 9396 (SASSI 4904), the results cannot be provided for the SASSI 0.2 g case.	See figures for the ISRSs for these nodes. Note that for node 9396 (SASSI 4904), the results cannot be provided for the SASSI 0.2 g case.	Node EXODUS 1893, Cubit 9396 Node EXODUS 1330, Cubit 9400 Node EXODUS 2554, Cubit 9404 Node EXODUS 2001, Cubit 9420 Node EXODUS 3163, Cubit 9428 Node EXODUS 2674, Cubit 9436 Node EXODUS 3830, Cubit 9452 Node EXODUS 3619, Cubit 9456 See the following for beam bottom and top Node CUBIT 6918, Cubit 9396 SASSI-1021, ~~4904~~ Node CUBIT 6426, 9400 SASSI- 1182, 4905 Node CUBIT 7475, 9404 SASSI-13774, 22080 Node CUBIT 6993, 9420 SASSI-13886, 18132 Node CUBIT 7980, 9428 SASSI-27184, 31566 Node CUBIT 7550, 9436 SASSI-27296, 35500 Node CUBIT 8543, 9452 SASSI-38274, 39041 Node CUBIT 8338, 9456 SASSI-38328, 39274
Maximum Accelerations (m/s^2) at the top and bottom nodes of each "stick.	1.85	3.93	CUBIT 6918, 9396 SASSI-1021, ~~4904~~
	1.85 4.09	3.92 3.89	CUBIT 6426, 9400 SASSI- 1182, 4905
	1.87 4.83	4.34 4.35	CUBIT 7475, 9404 SASSI-13774, 22080

	1.85 1.83	4.82 4.83	CUBIT 6993, 9420 SASSI-13886, 18132
	1.70 2.56	4.61 4.61	CUBIT 7980, 9428 SASSI-27184, 31566
	1.70 5.51	4.57 4.57	CUBIT 7550, 9436 SASSI-27296, 35500
	2.35 7.67	4.82 4.82	CUBIT 8543, 9452 SASSI-38274, 39041
	2.35 3.01	4.96 4.96	CUBIT 8338, 9456 SASSI-38328, 39274

Notes:

(1) The term "Maximum" is used to mean the maximum considering the entire time period for which the time-history analysis was performed.

3.2 Acceleration Time Histories and ISRS for the X Directional Input Motion

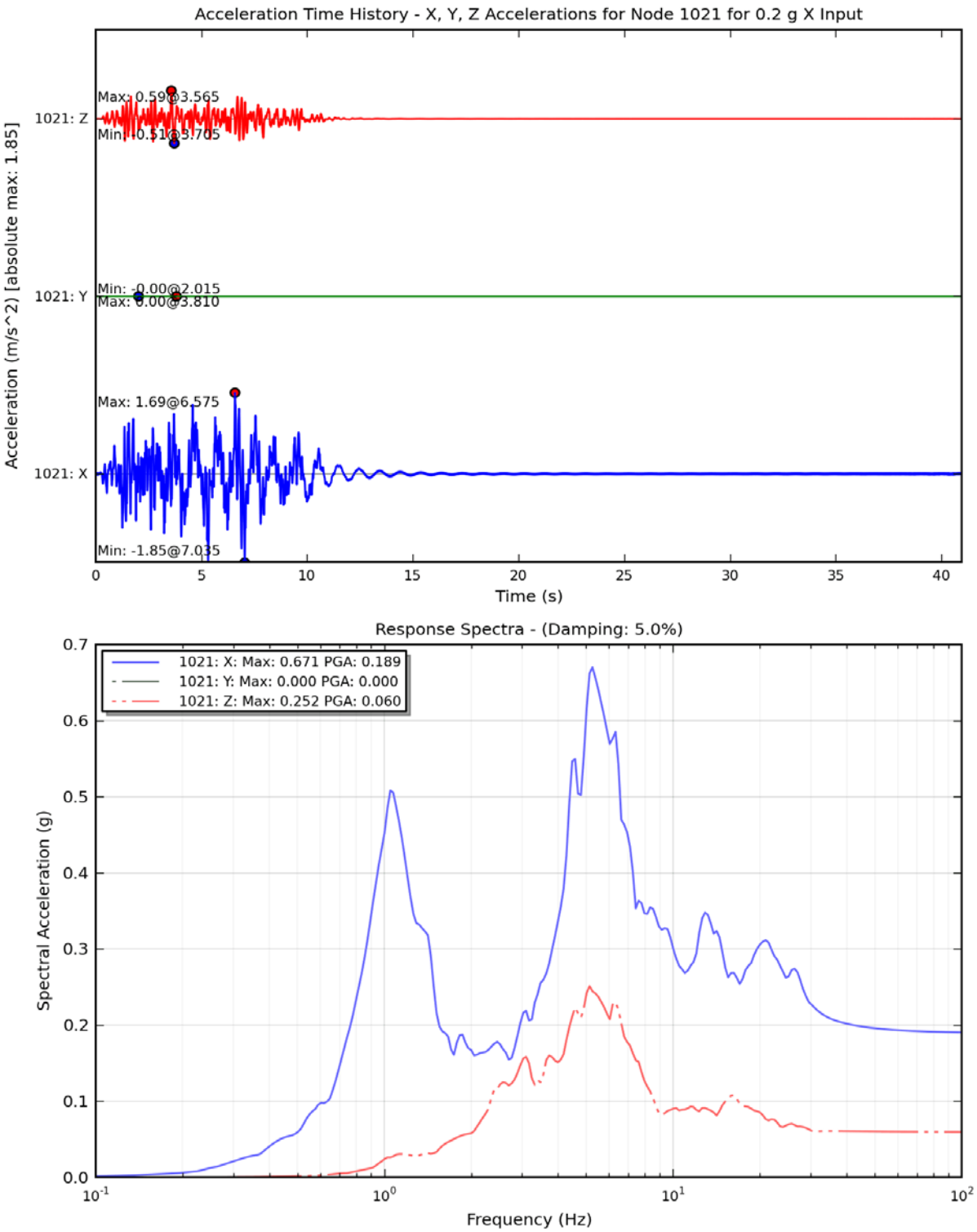

Figure 3-1 Response Acceleration Time Histories and ISRS at Node 1021 for X Input Motion (0.2 g)

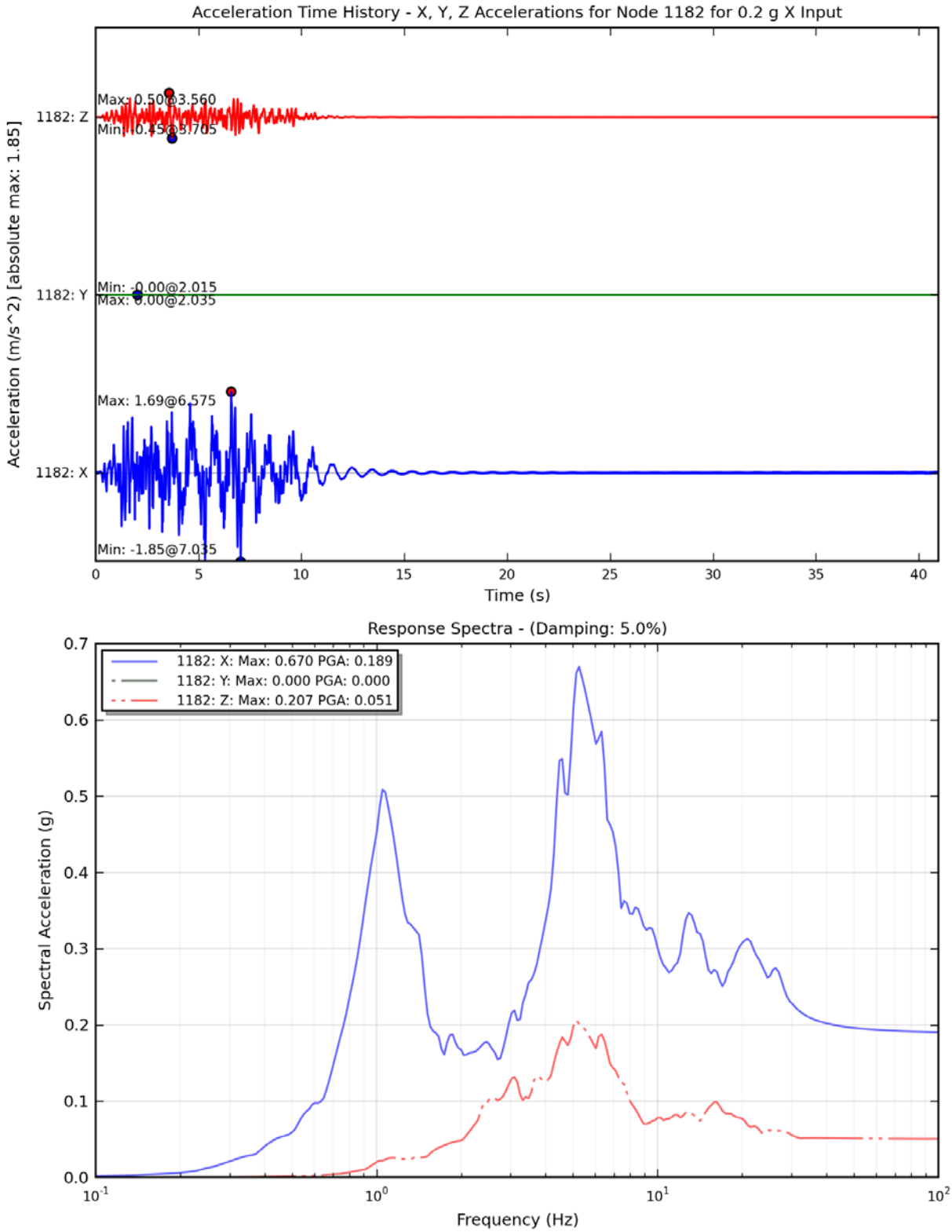

Figure 3-2 Response Acceleration Time Histories and ISRS at Node 1182 for X Input Motion (0.2 g)

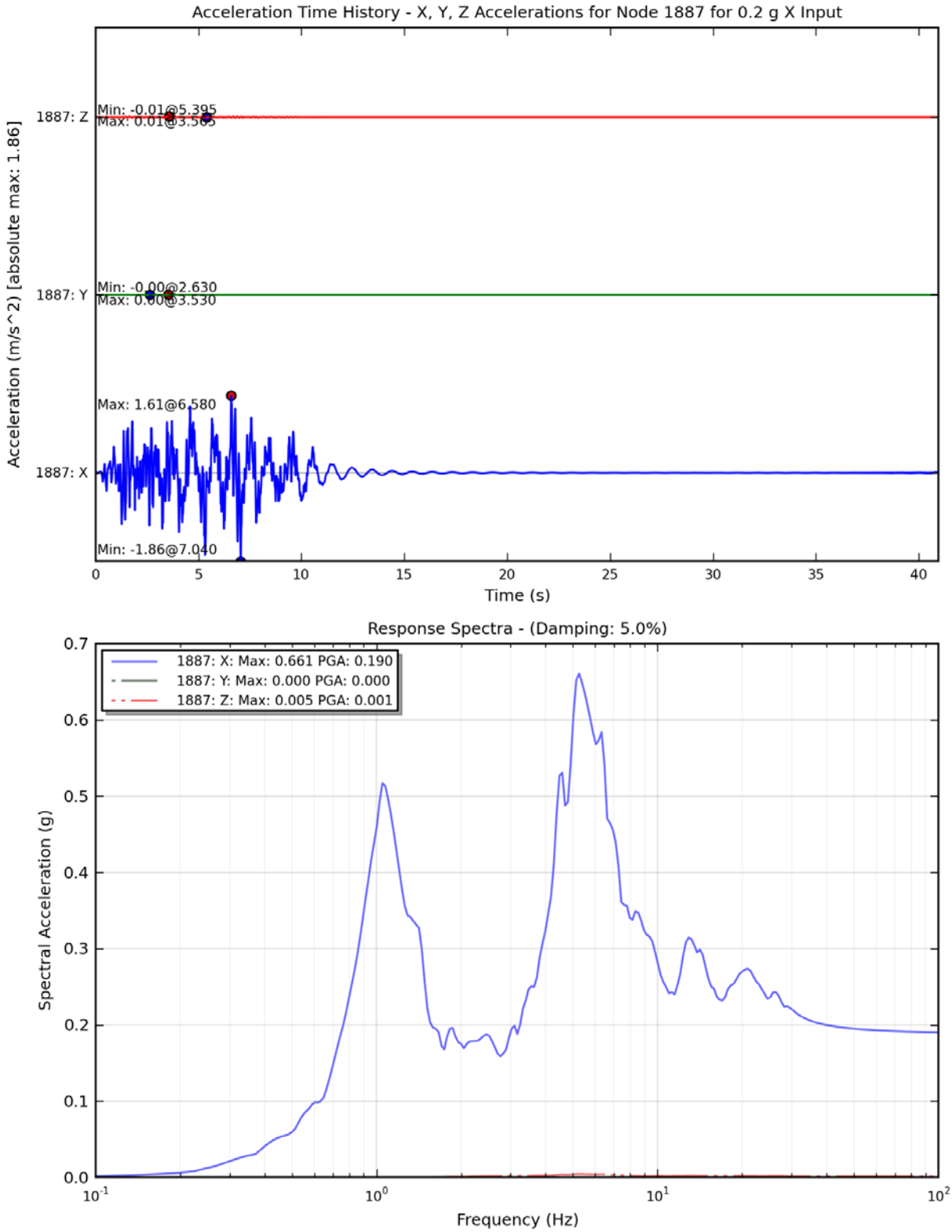

Figure 3-3 Response Acceleration Time Histories and ISRS at Node 1887 for X Input Motion (0.2 g)

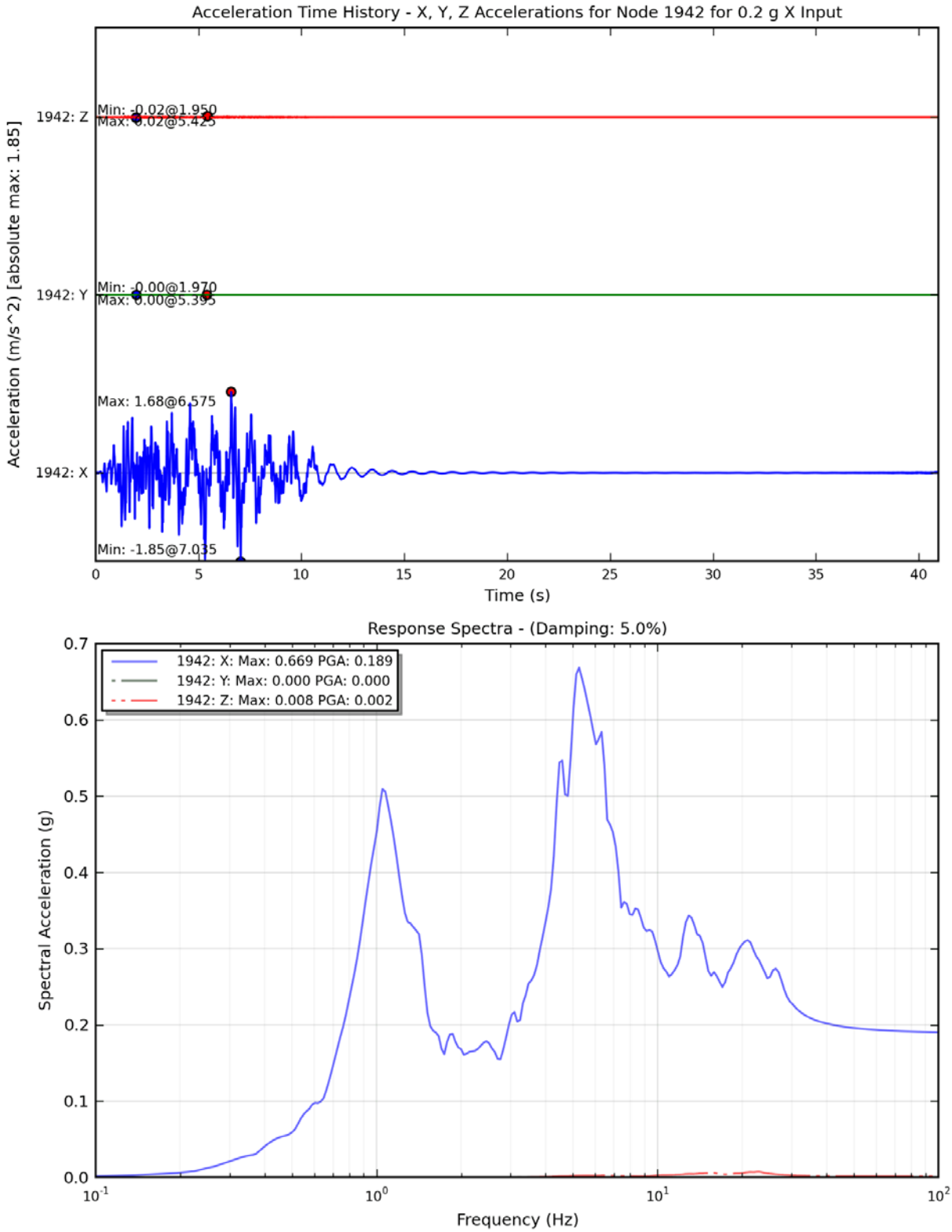

Figure 3-4 Response Acceleration Time Histories and ISRS at Node 1942 for X Input Motion (0.2 g)

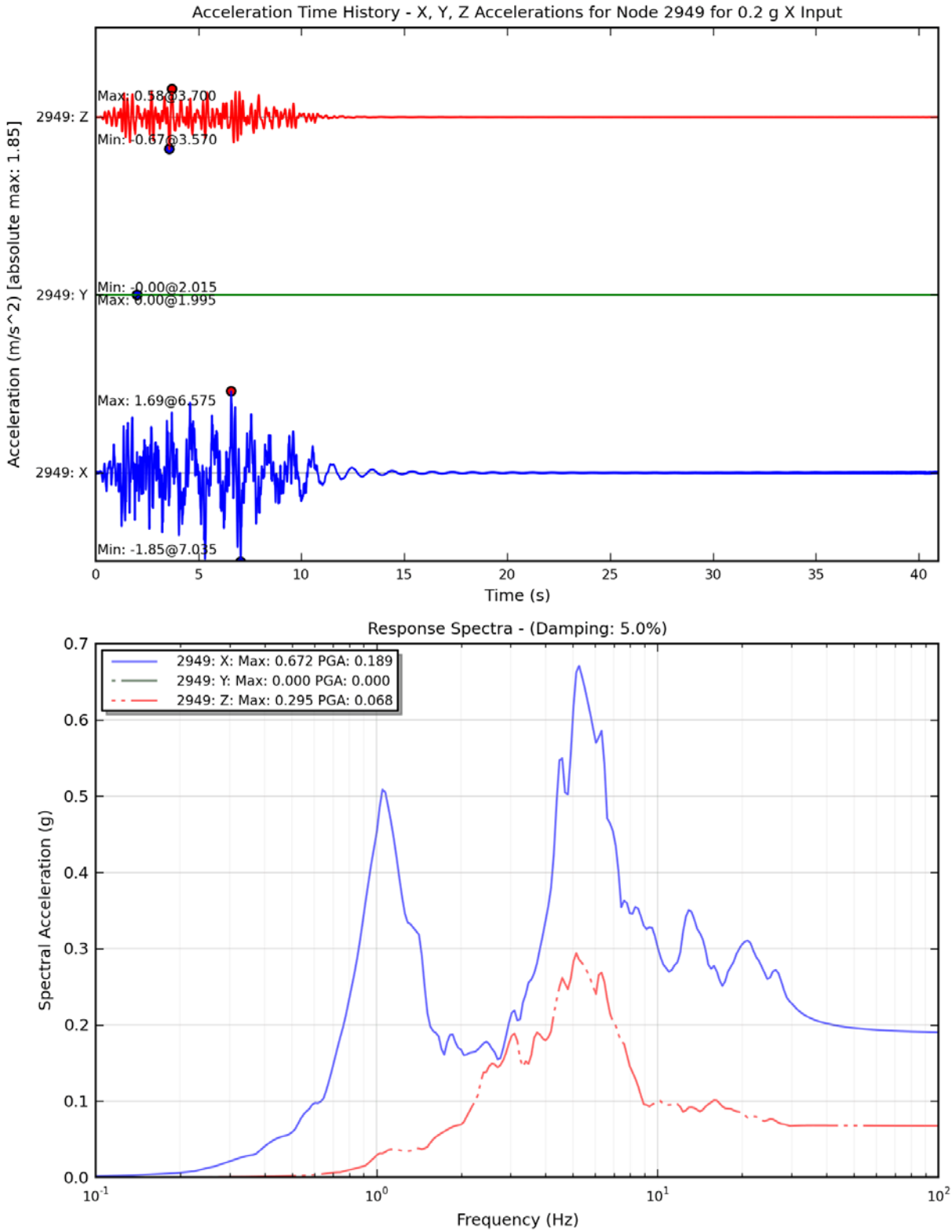

Figure 3-5 Response Acceleration Time Histories and ISRS at Node 2949 for X Input Motion (0.2 g)

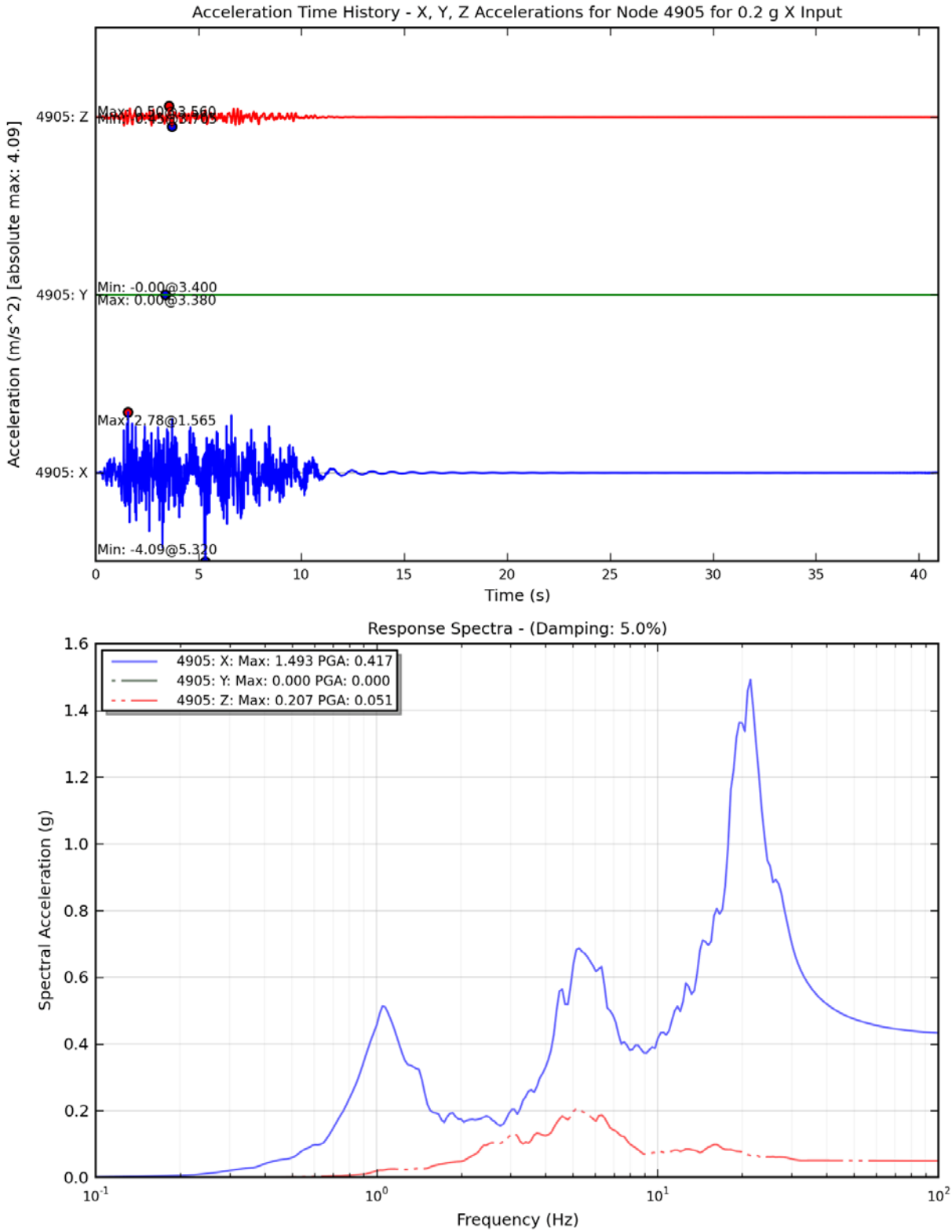

Figure 3-6 Response Acceleration Time Histories and ISRS at Node 4905 for X Input Motion (0.2 g)

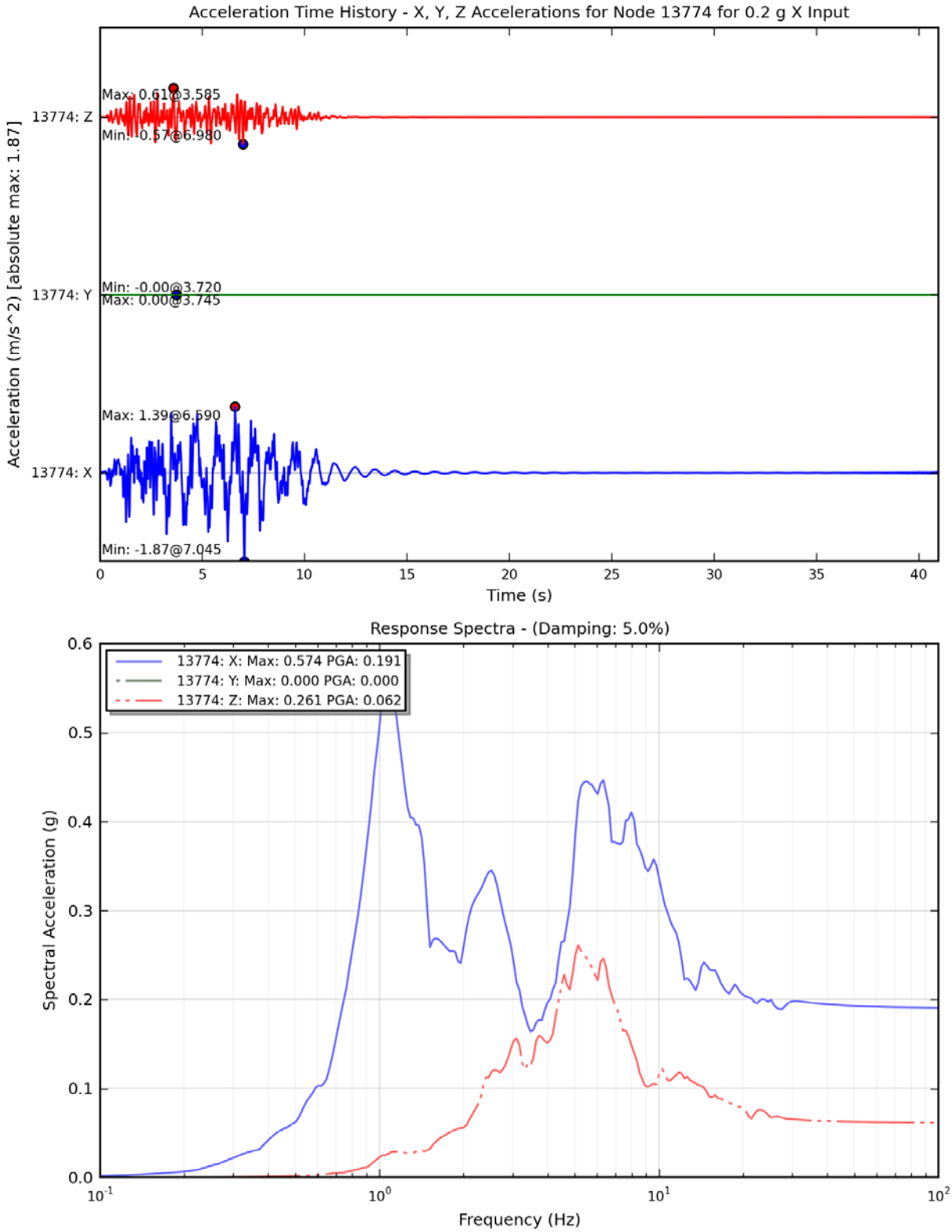

Figure 3-7 Response Acceleration Time Histories and ISRS at Node 13774 for X Input Motion (0.2 g)

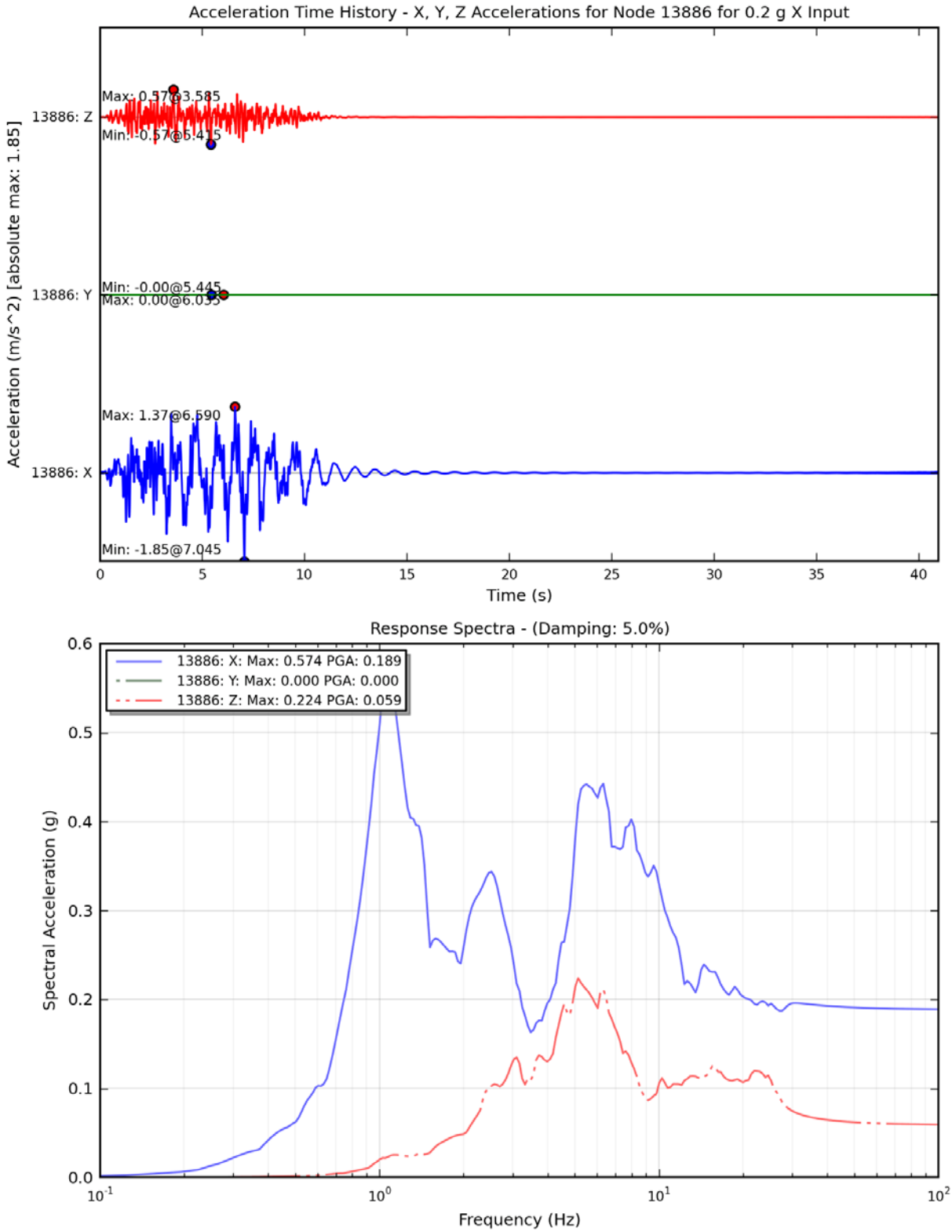

Figure 3-8 Response Acceleration Time Histories and ISRS at Node 13886 for X Input Motion (0.2 g)

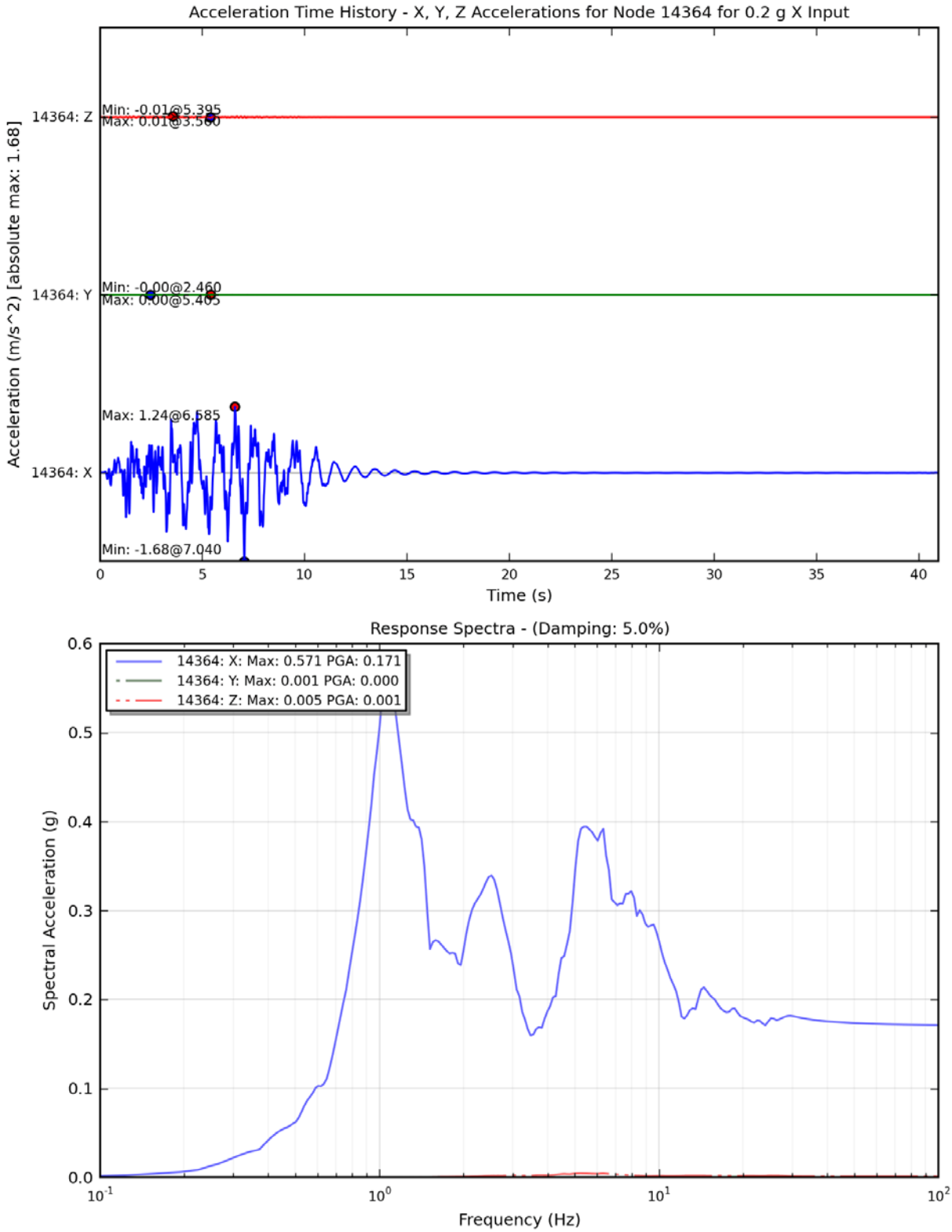

Figure 3-9 Response Acceleration Time Histories and ISRS at Node 14364 for X Input Motion (0.2 g)

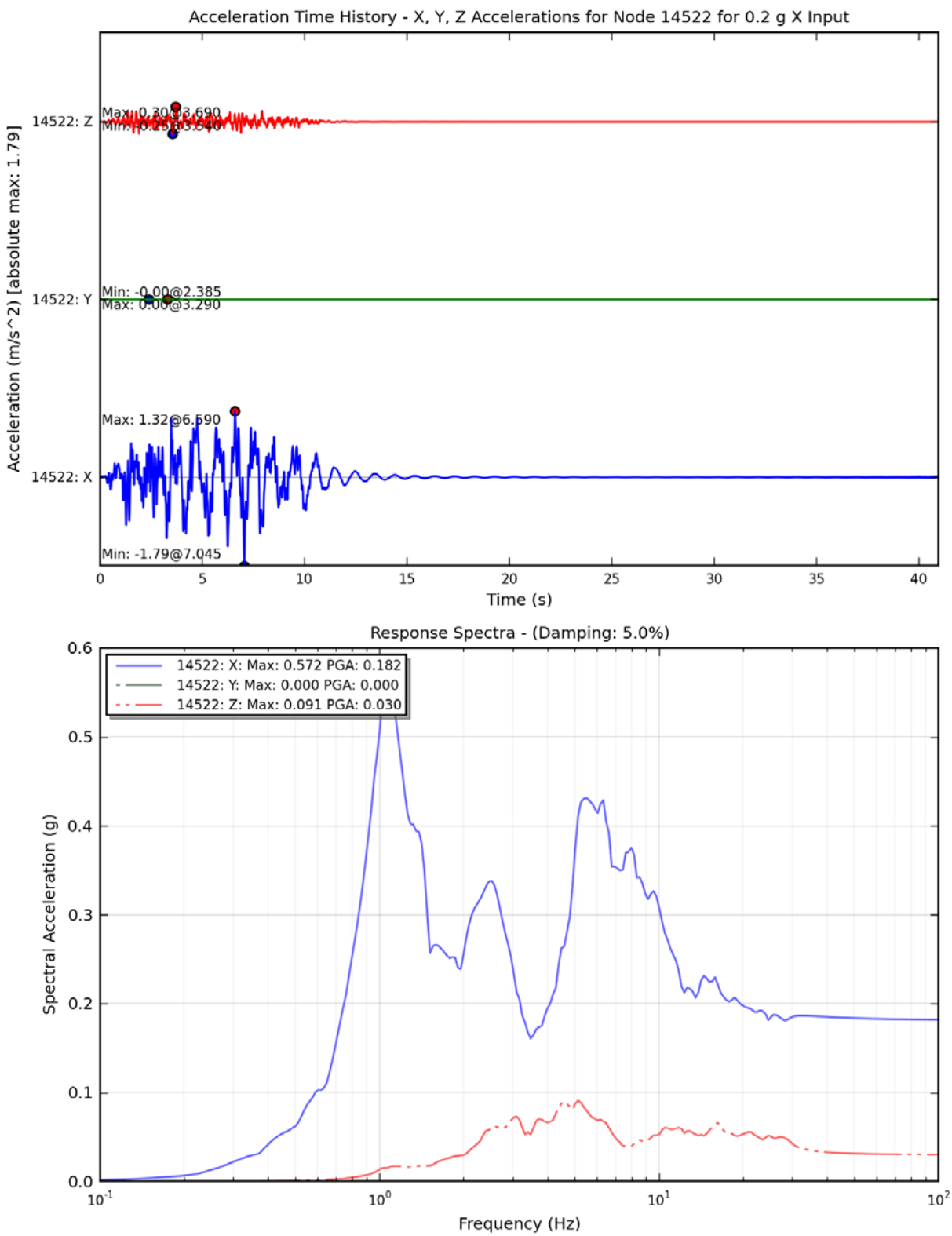

Figure 3-10 Response Acceleration Time Histories and ISRS at Node 14522 for X Input Motion (0.2 g)

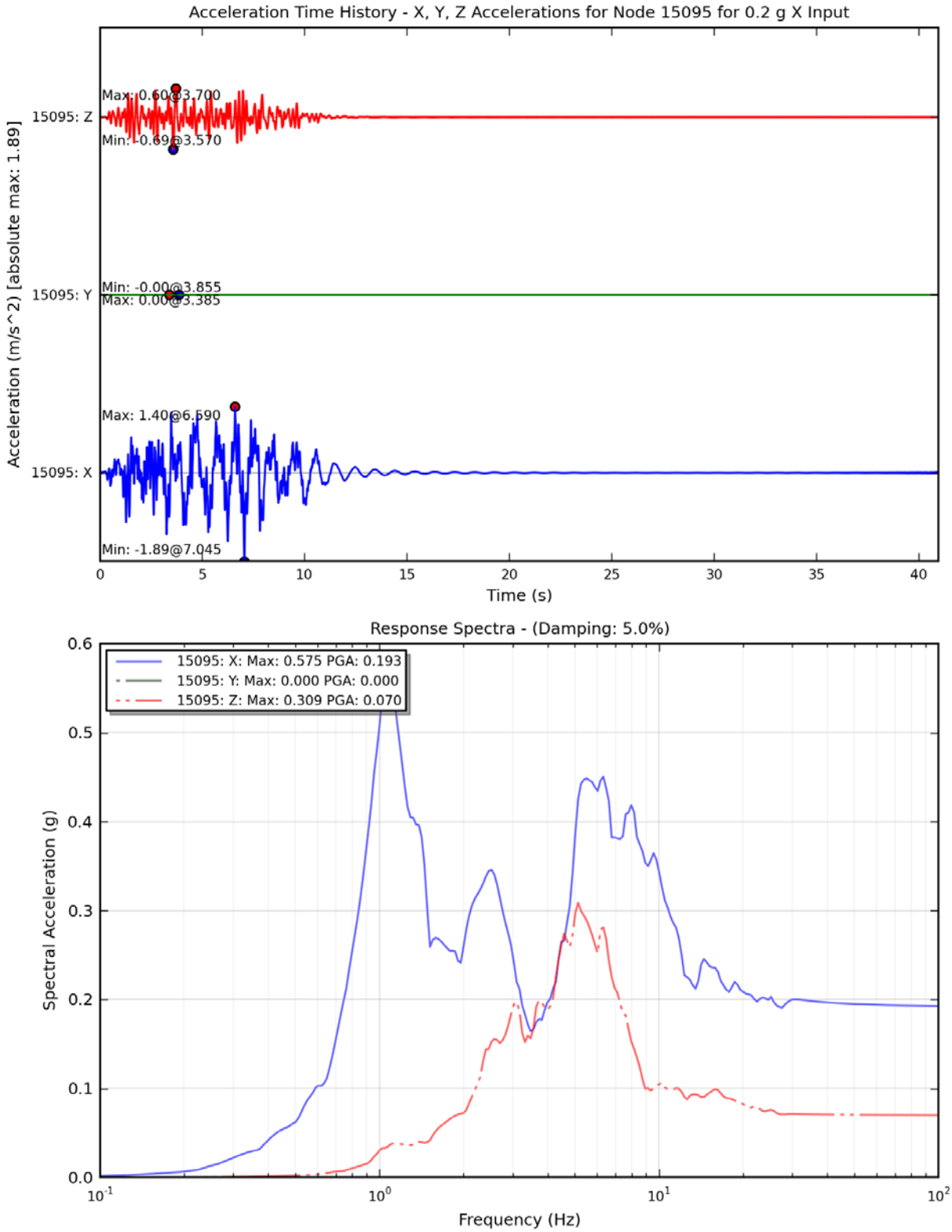

Figure 3-11 Response Acceleration Time Histories and ISRS at Node 15095 for X Input Motion (0.2 g)

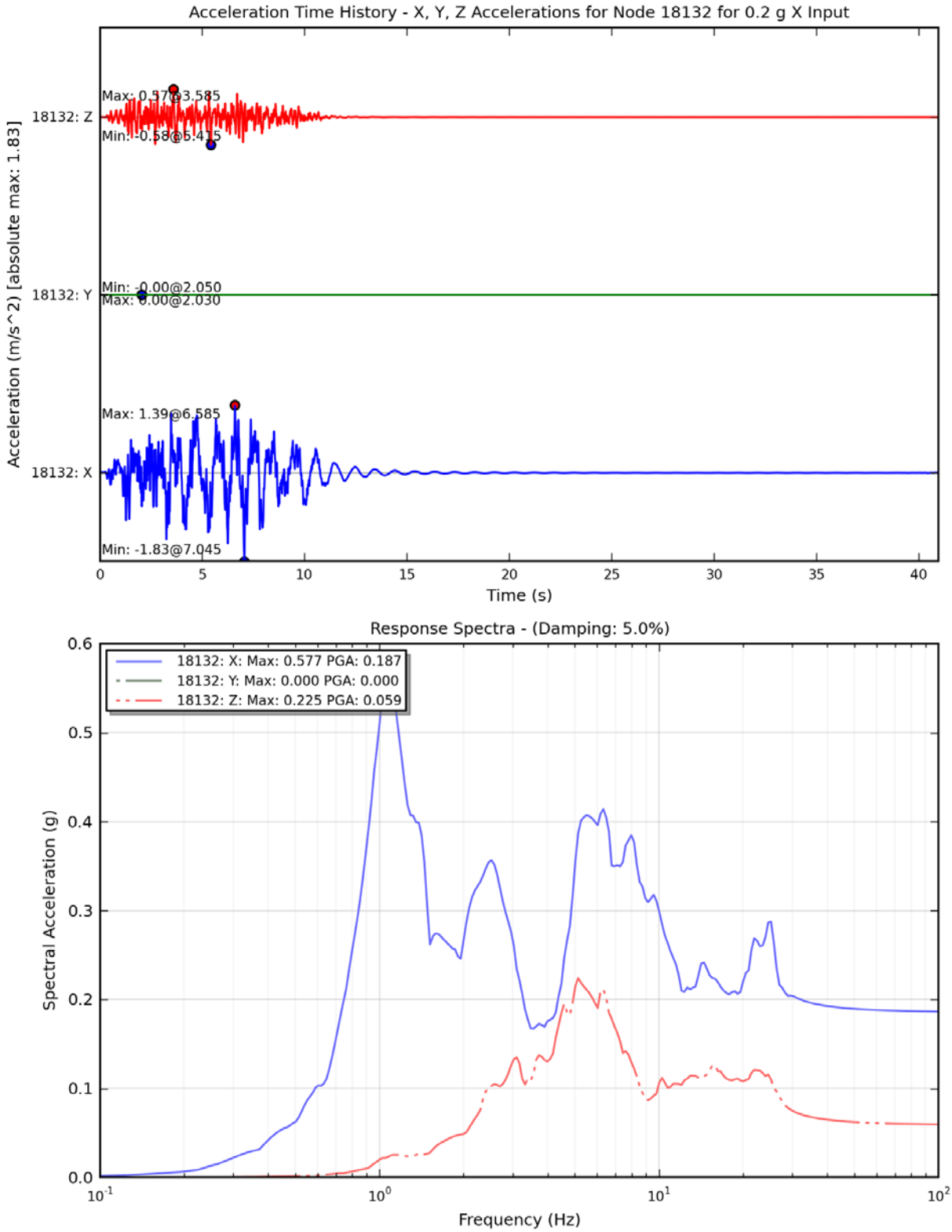

Figure 3-12 Response Acceleration Time Histories and ISRS at Node 18132 for X Input Motion (0.2 g)

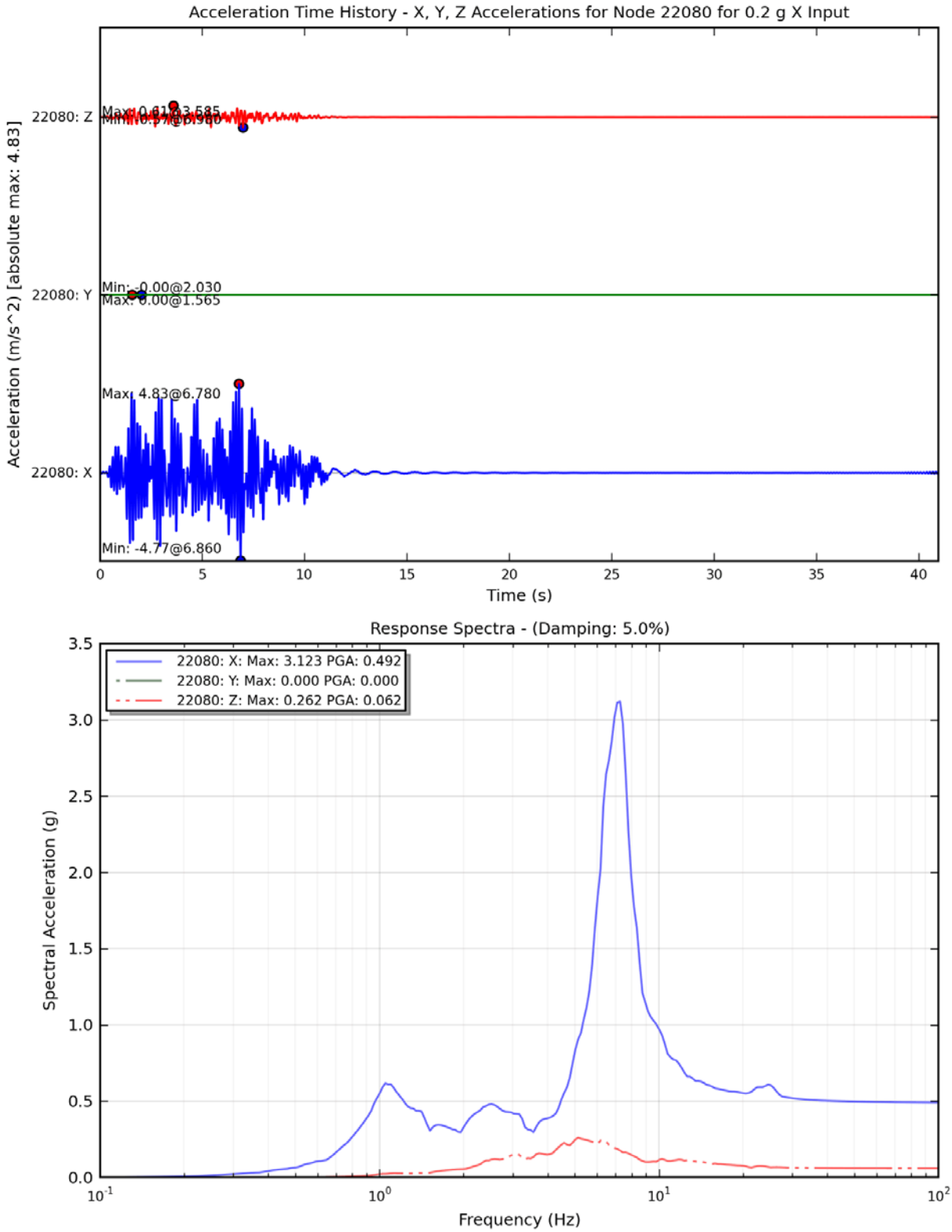

Figure 3-13 Response Acceleration Time Histories and ISRS at Node 22080 for X Input Motion (0.2 g)

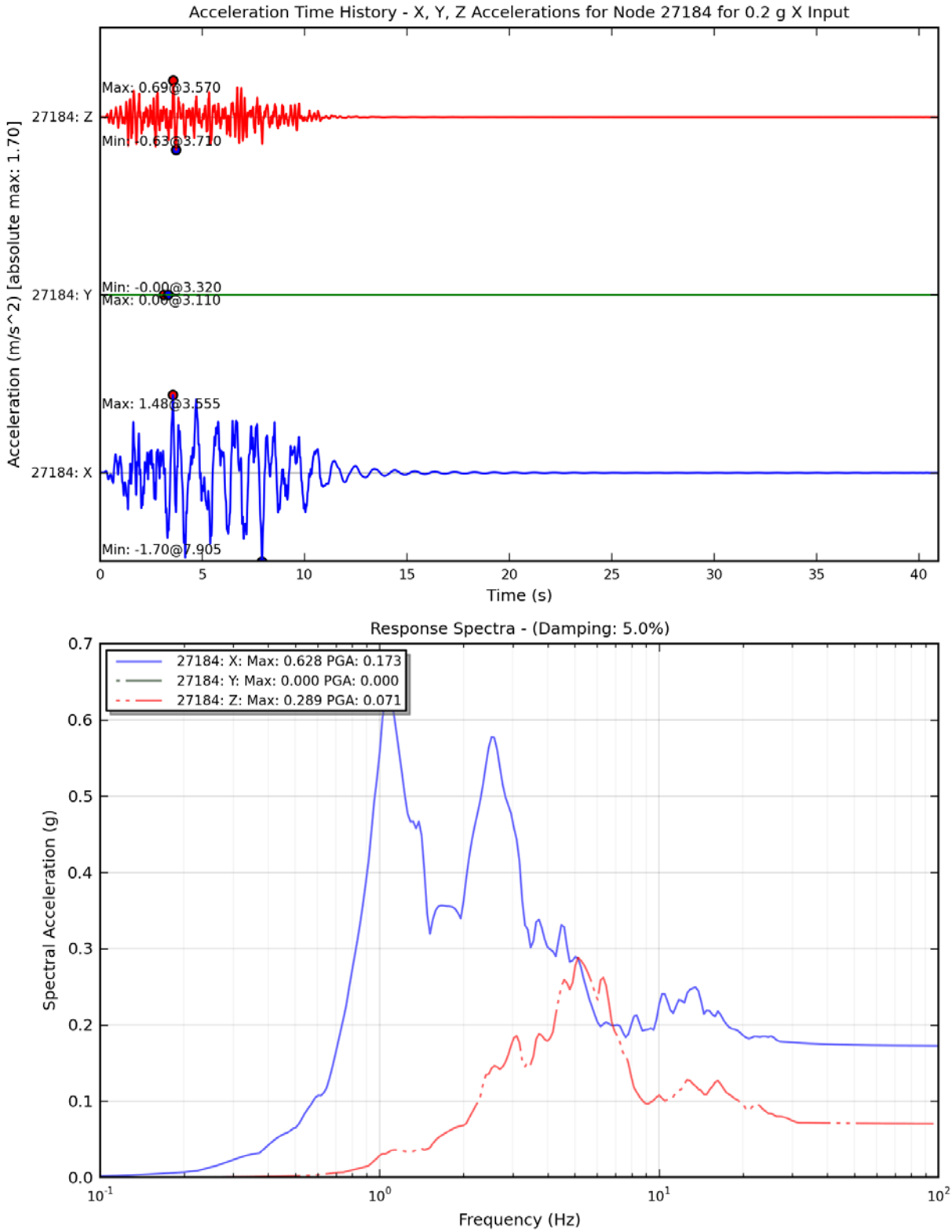

Figure 3-14 Response Acceleration Time Histories and ISRS at Node 27184 for X Input Motion (0.2 g)

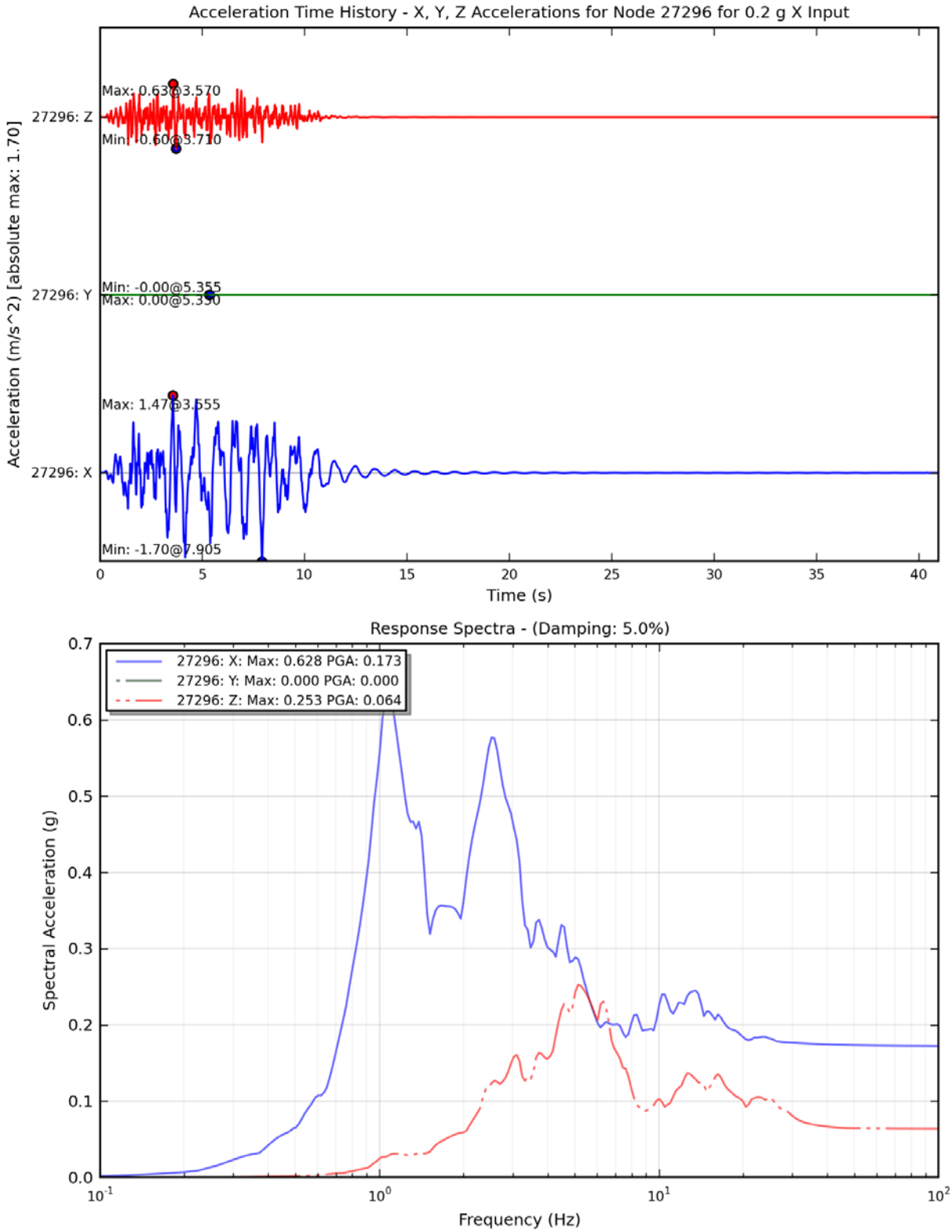

Figure 3-15 Response Acceleration Time Histories and ISRS at Node 27296 for X Input Motion (0.2 g)

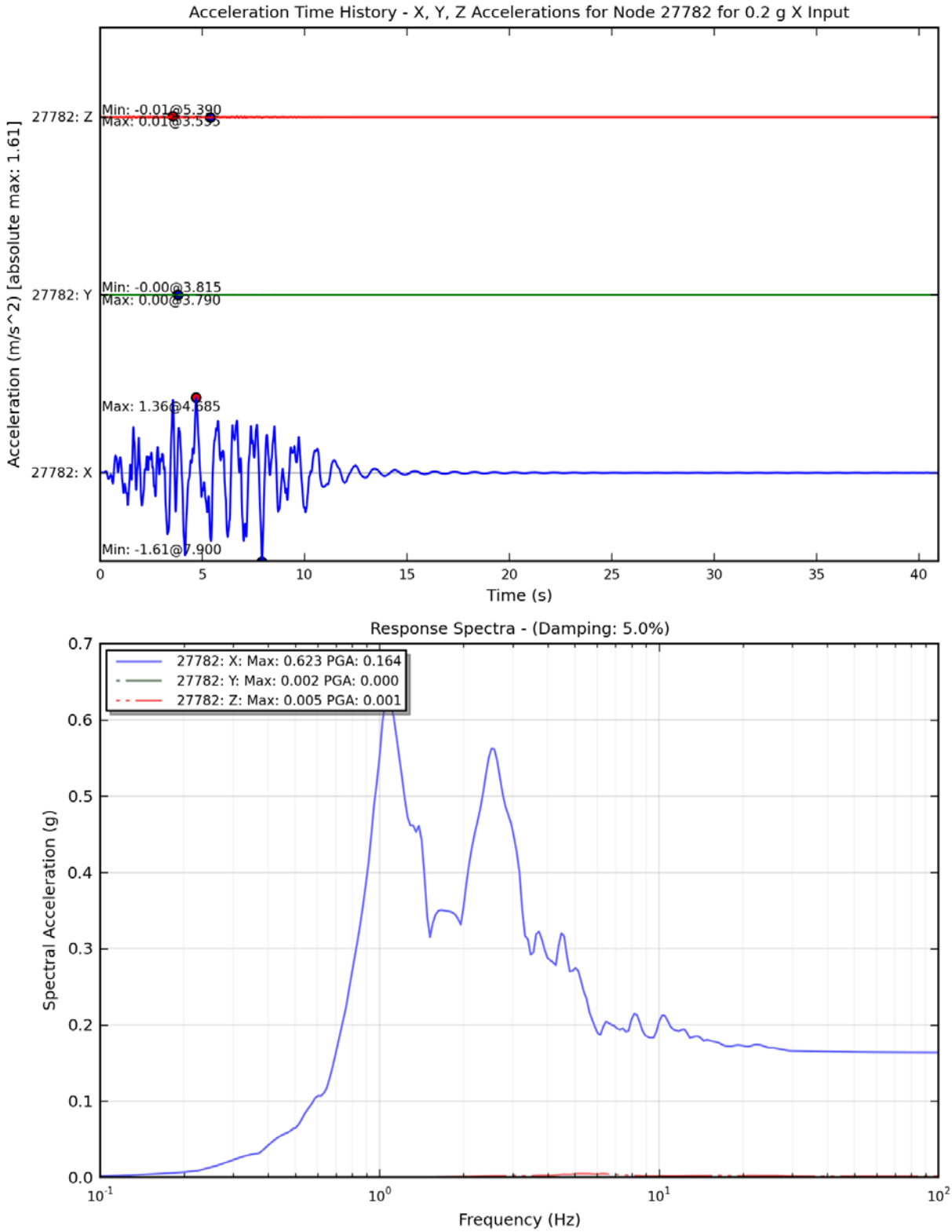

Figure 3-16 Response Acceleration Time Histories and ISRS at Node 27782 for X Input Motion (0.2 g)

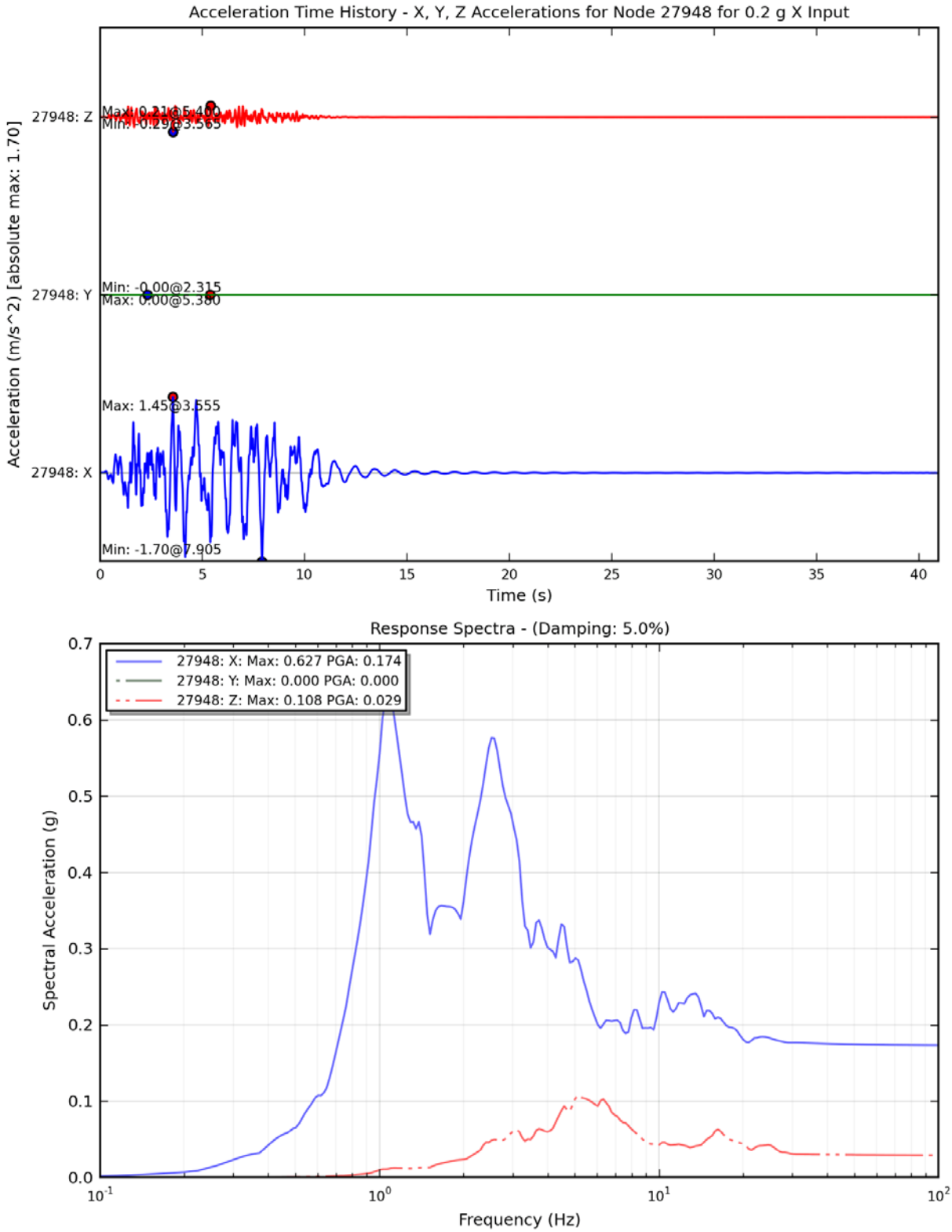

Figure 3-17 Response Acceleration Time Histories and ISRS at Node 27948 for X Input Motion (0.2 g)

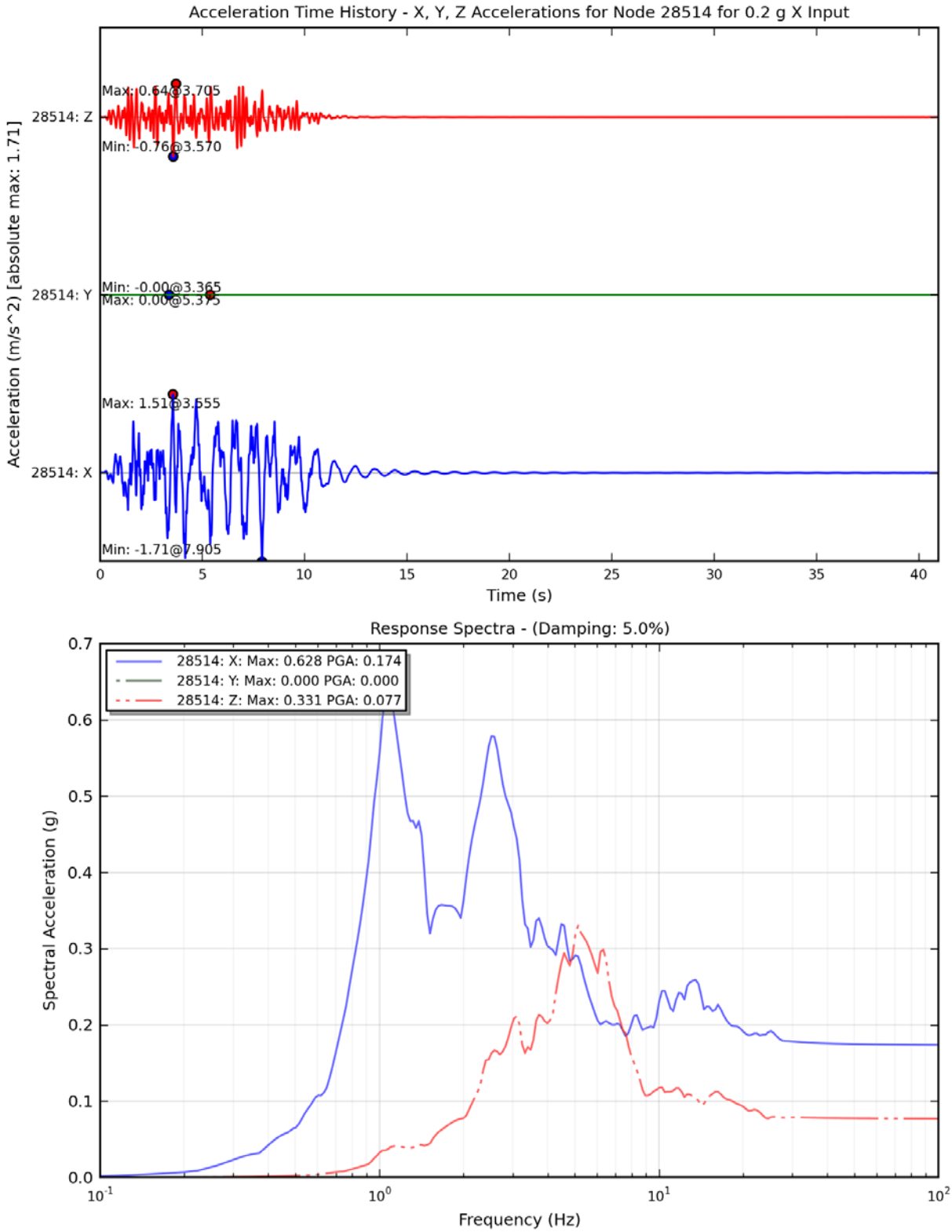

Figure 3-18 Response Acceleration Time Histories and ISRS at Node 28514 for X Input Motion (0.2 g)

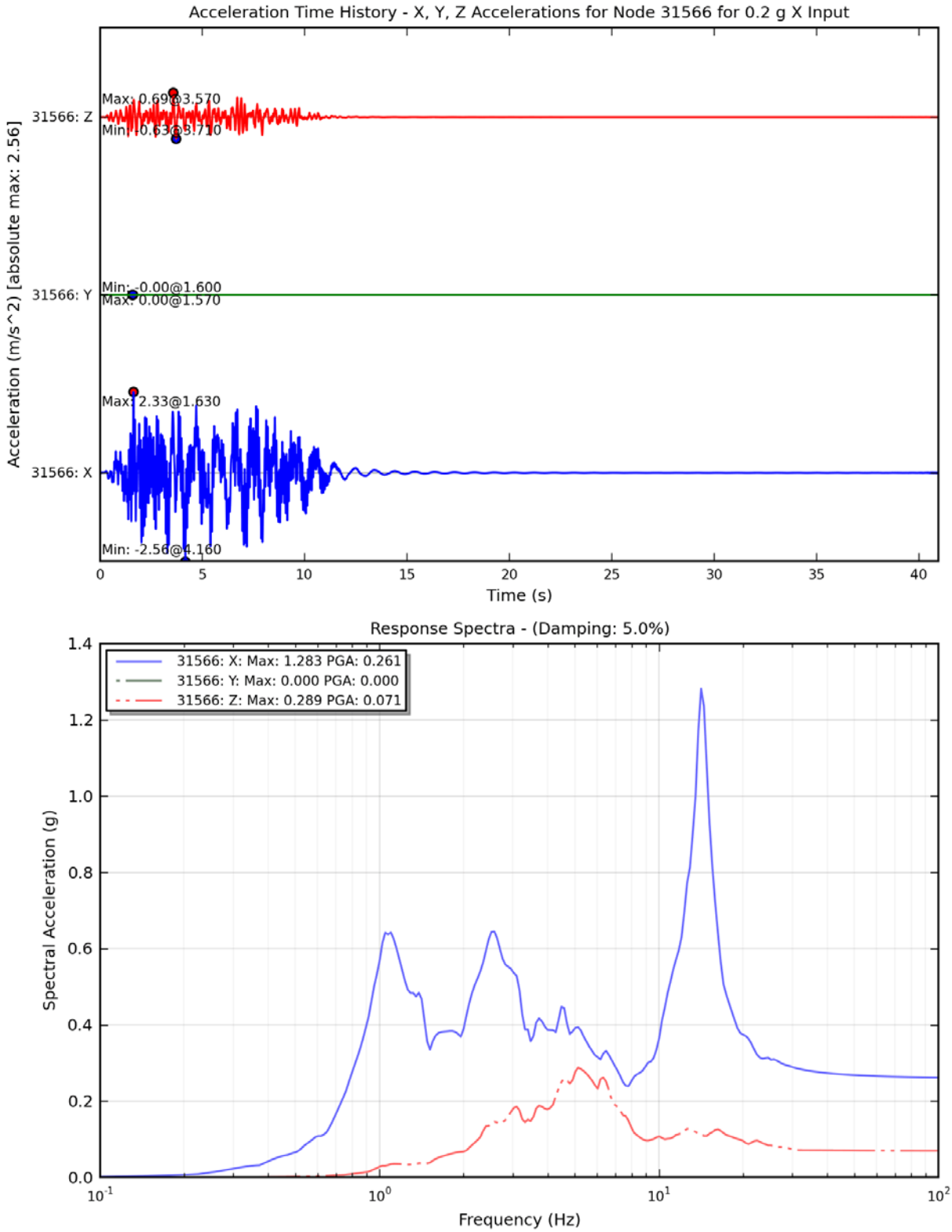

Figure 3-19 Response Acceleration Time Histories and ISRS at Node 31566 for X Input Motion (0.2 g)

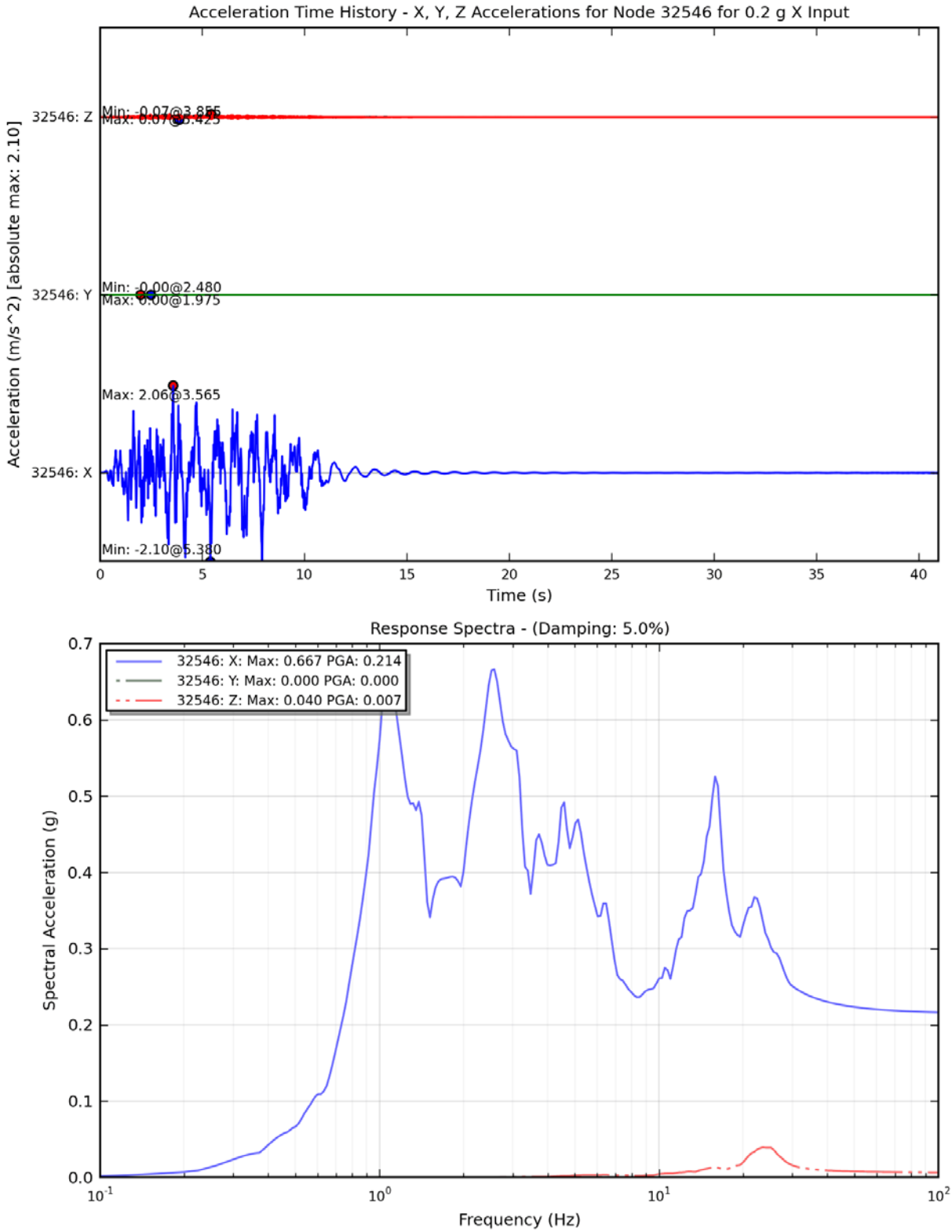

Figure 3-20 Response Acceleration Time Histories and ISRS at Node 32546 for X Input Motion (0.2 g)

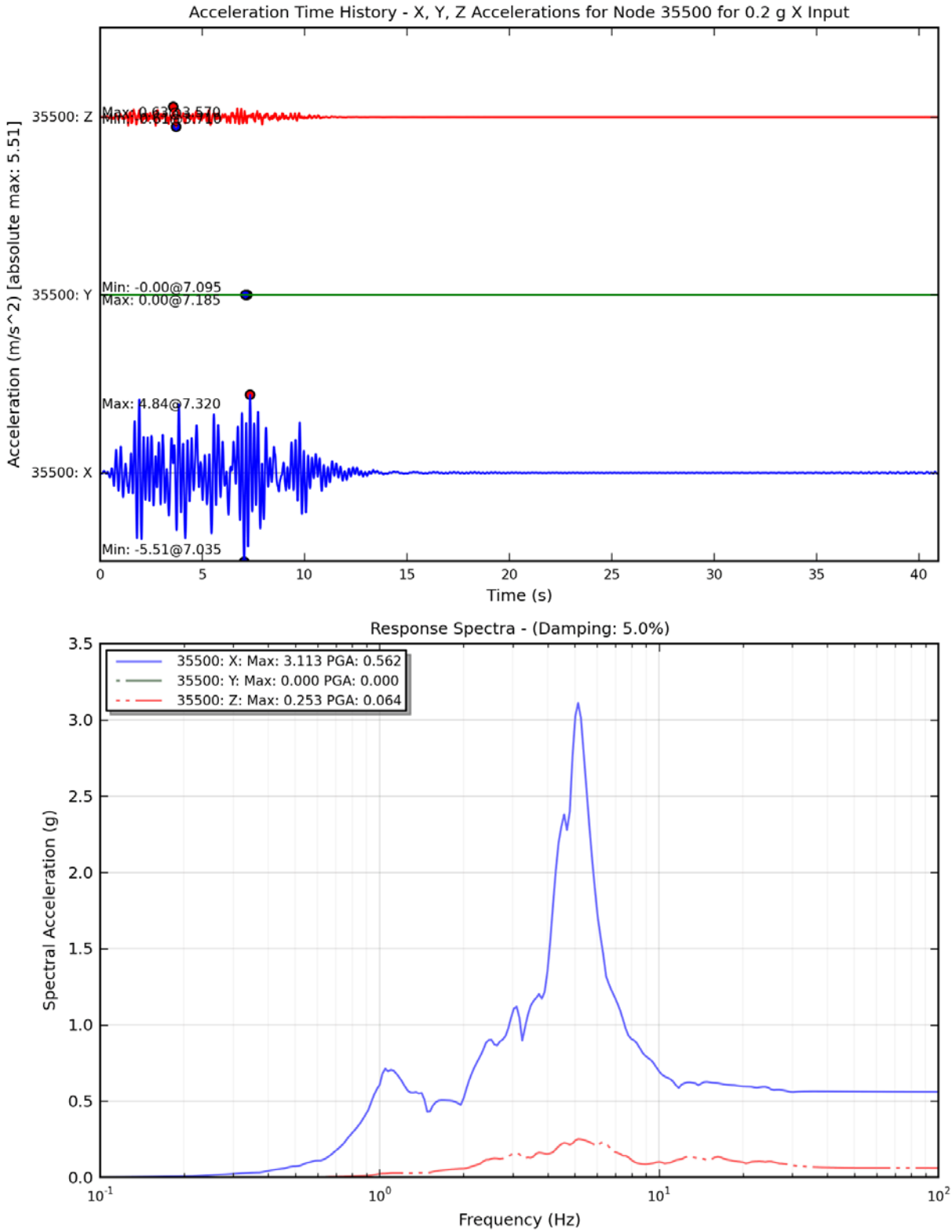

Figure 3-21 Response Acceleration Time Histories and ISRS at Node 35500 for X Input Motion (0.2 g)

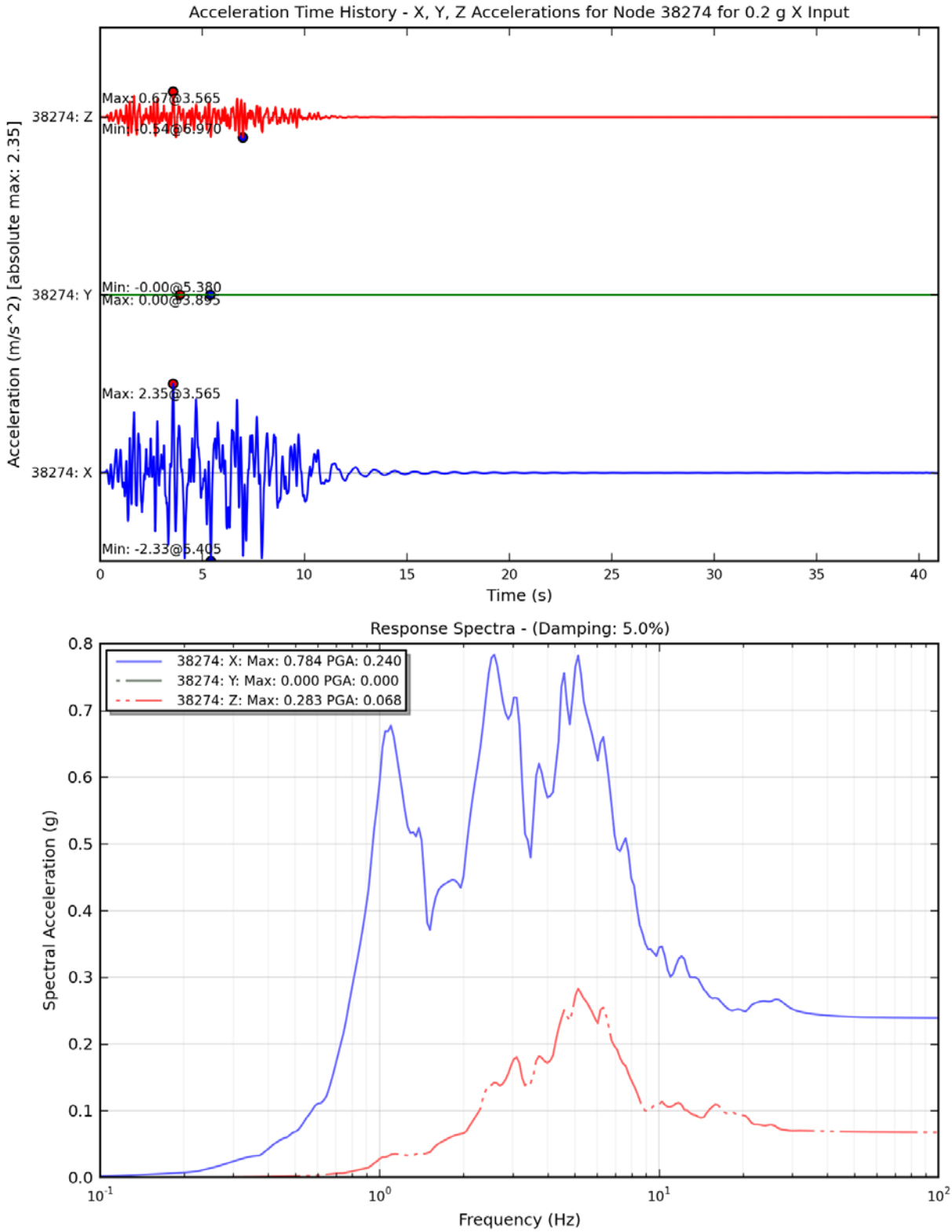

Figure 3-22 Response Acceleration Time Histories and ISRS at Node 38274 for X Input Motion (0.2 g)

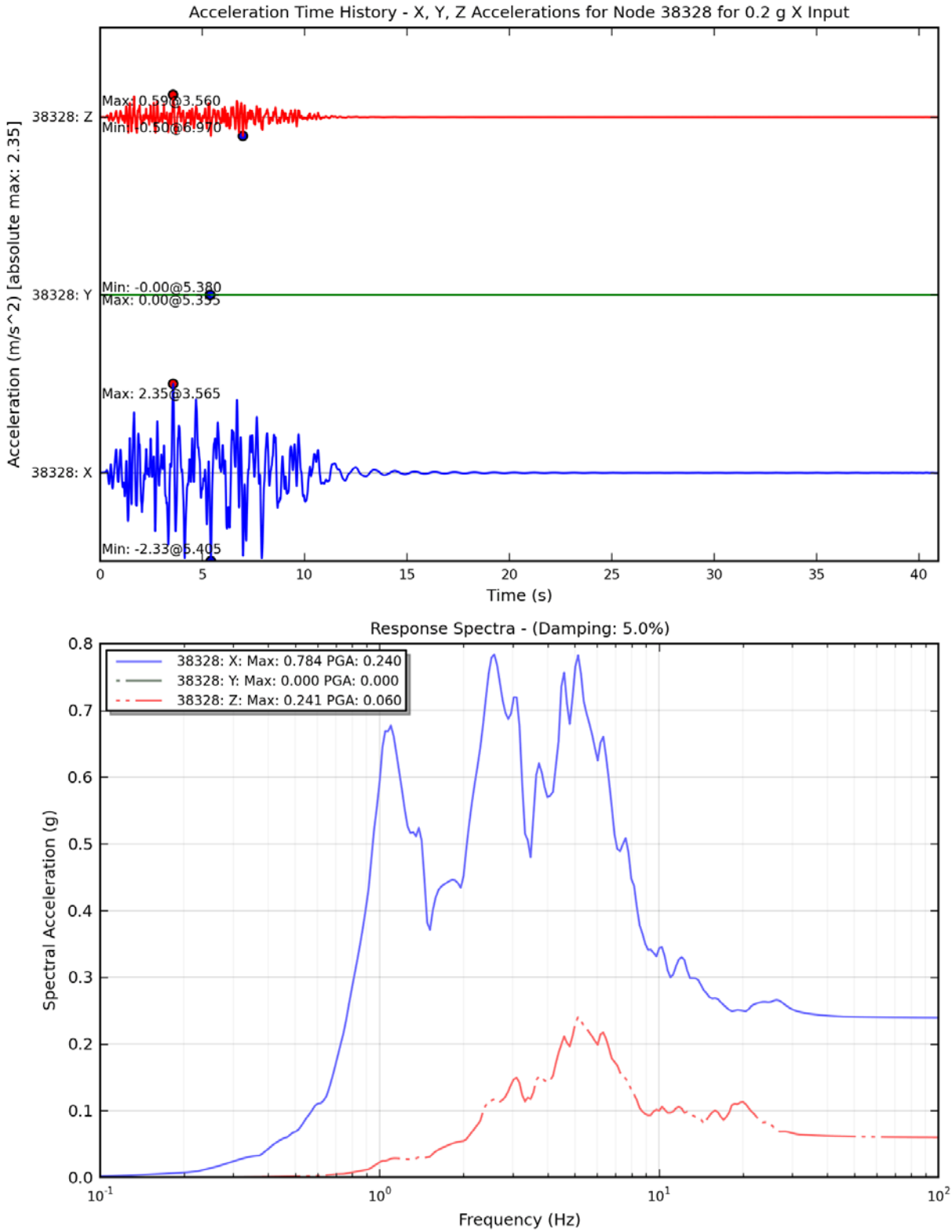

Figure 3-23 Response Acceleration Time Histories and ISRS at Node 38328 for X Input Motion (0.2 g)

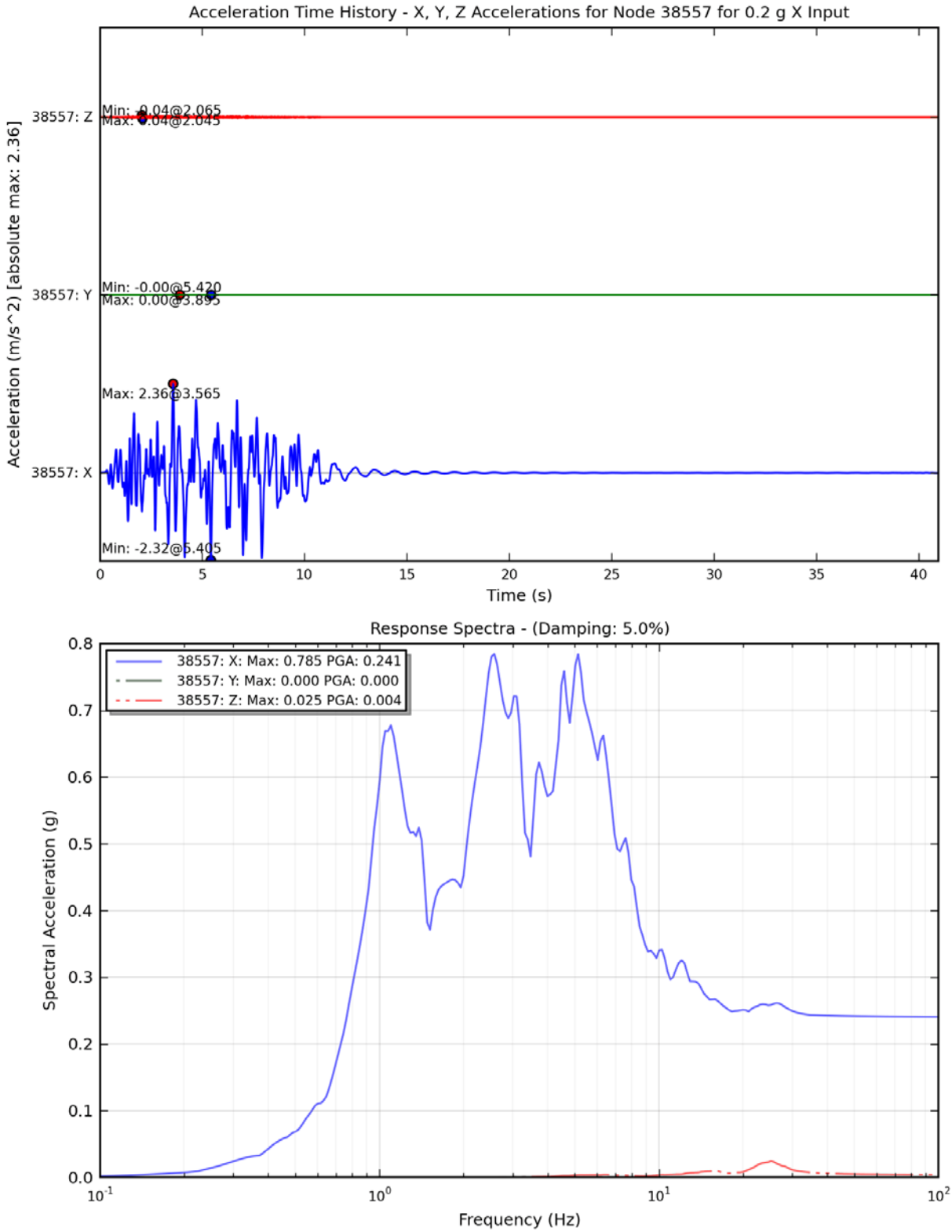

Figure 3-24 Response Acceleration Time Histories and ISRS at Node 38557 for X Input Motion (0.2 g)

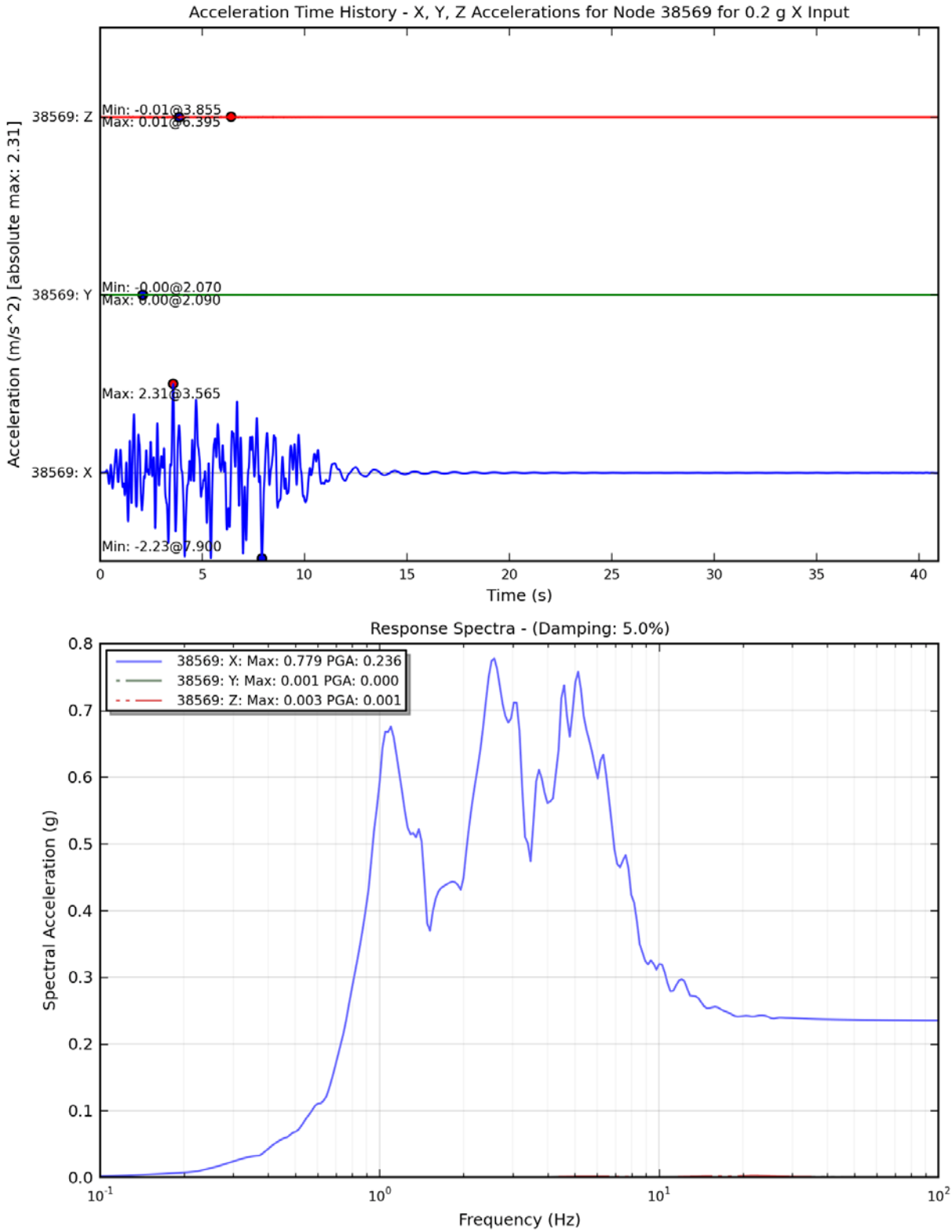

Figure 3-25 Response Acceleration Time Histories and ISRS at Node 38569 for X Input Motion (0.2 g)

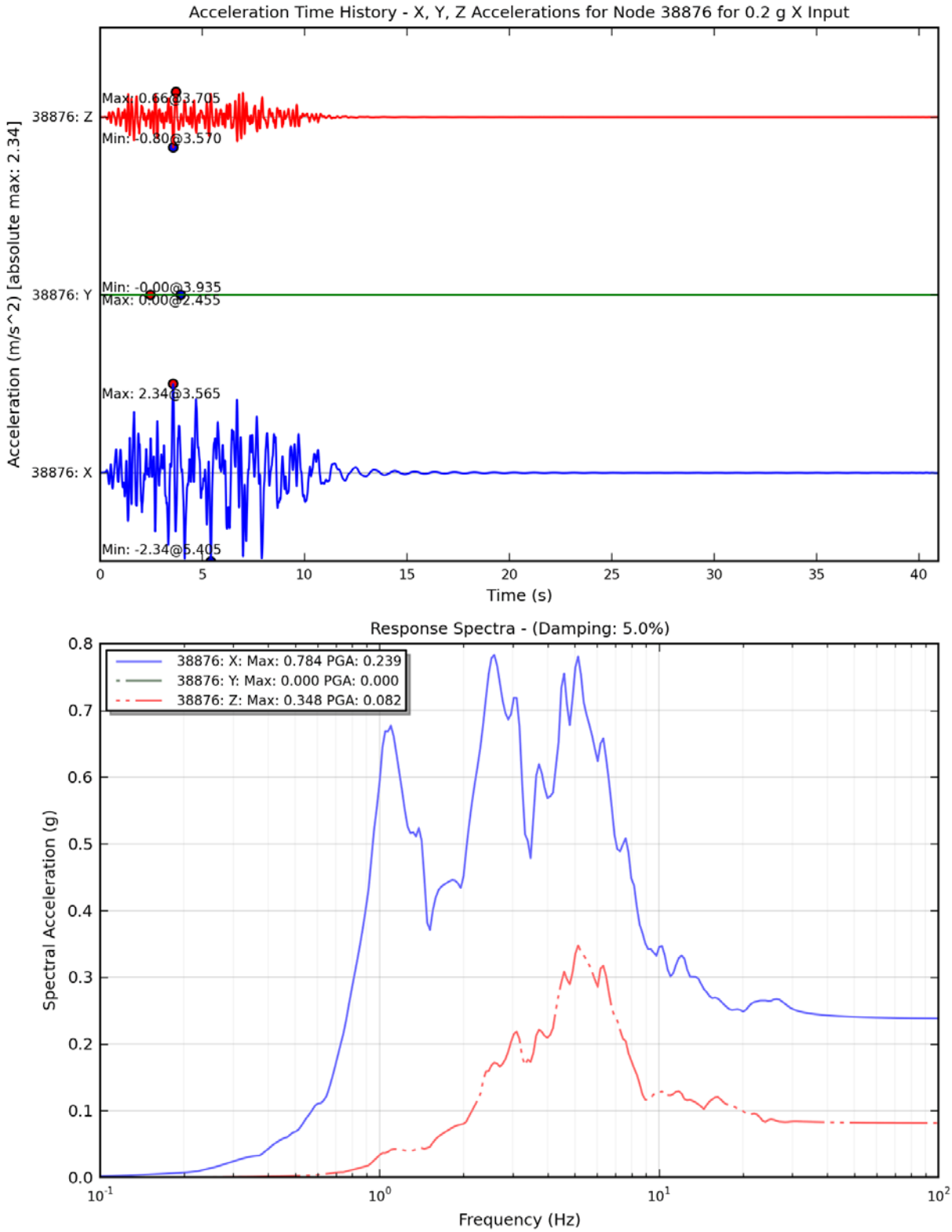

Figure 3-26 Response Acceleration Time Histories and ISRS at Node 38876 for X Input Motion (0.2 g)

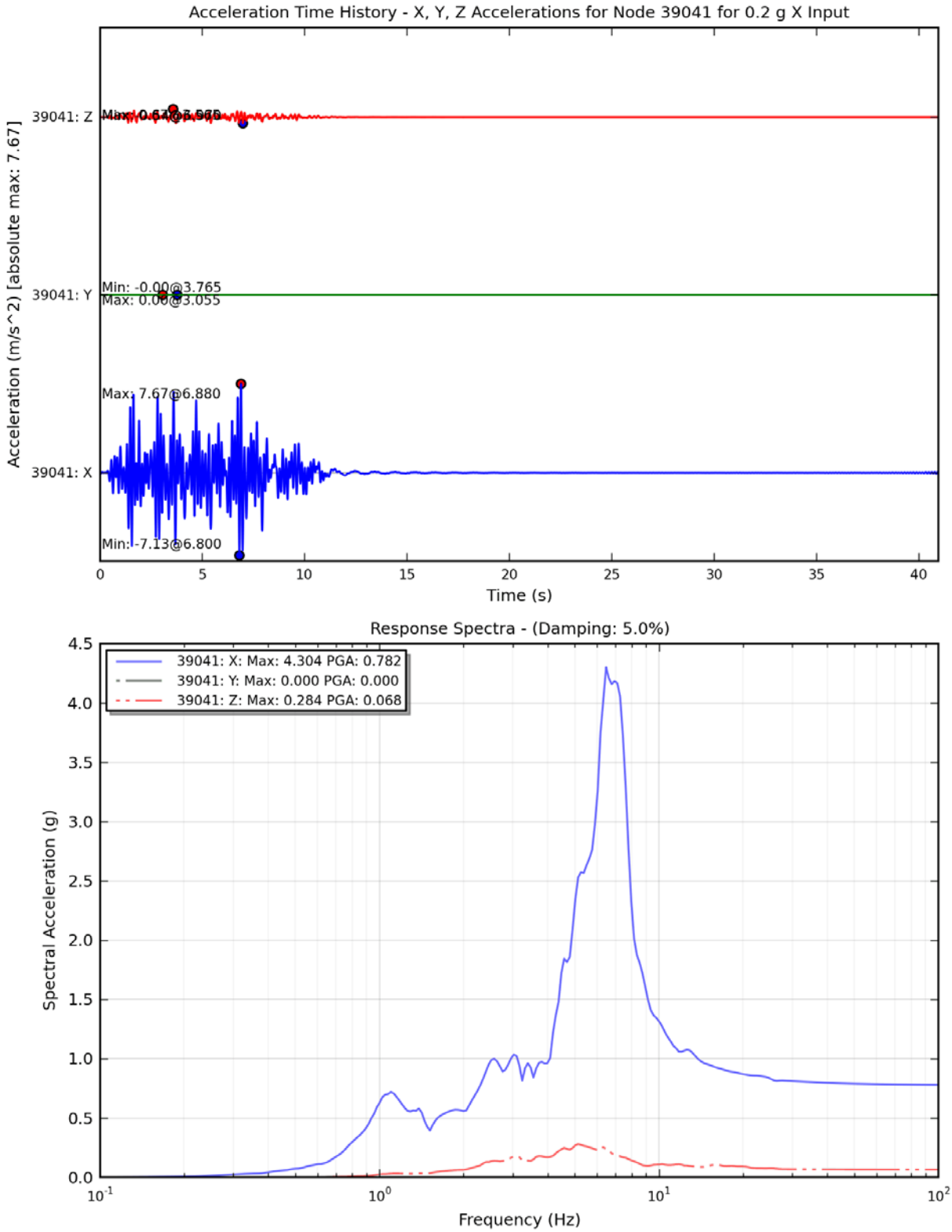

Figure 3-27 Response Acceleration Time Histories and ISRS at Node 39041 for X Input Motion (0.2 g)

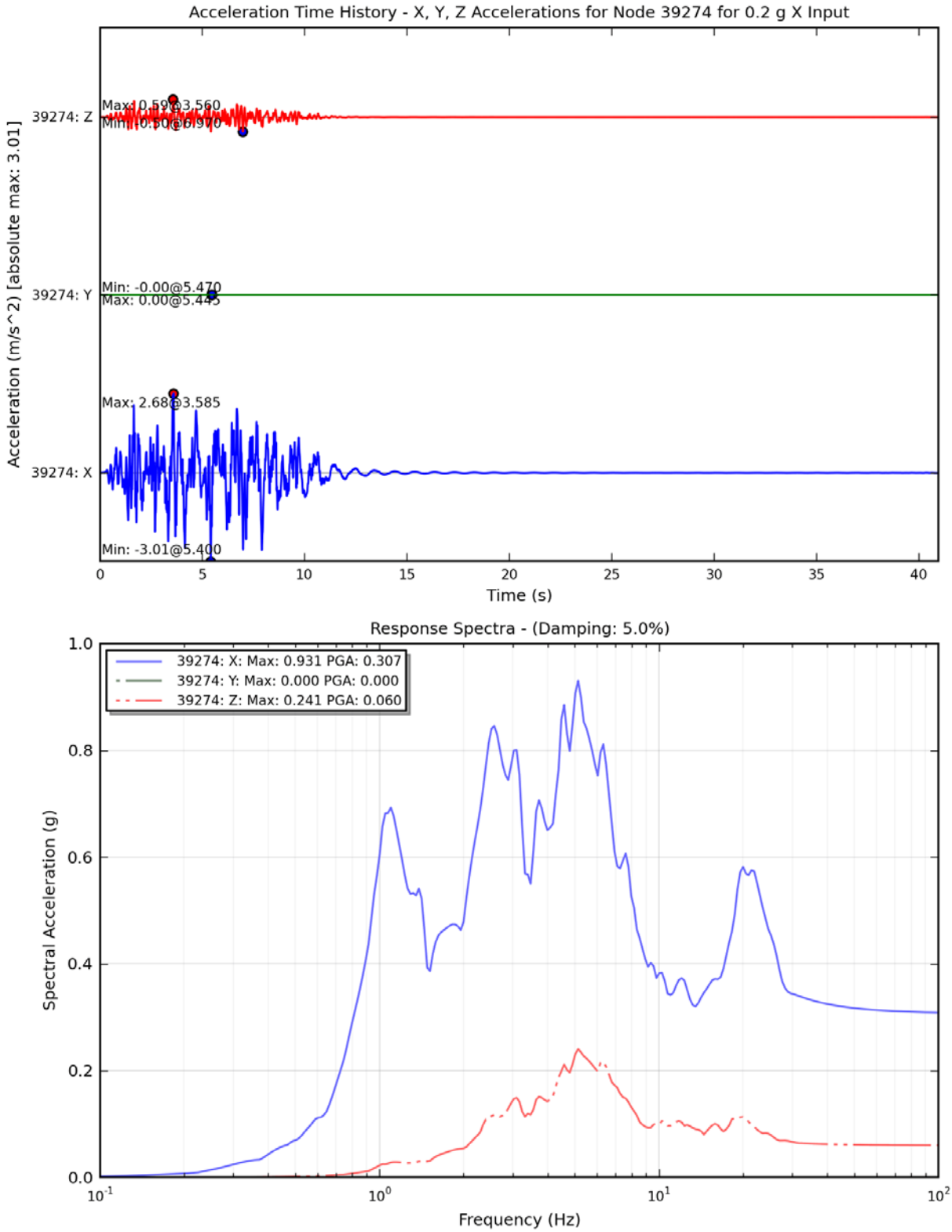

Figure 3-28 Response Acceleration Time Histories and ISRS at Node 39274 for X Input Motion (0.2 g)

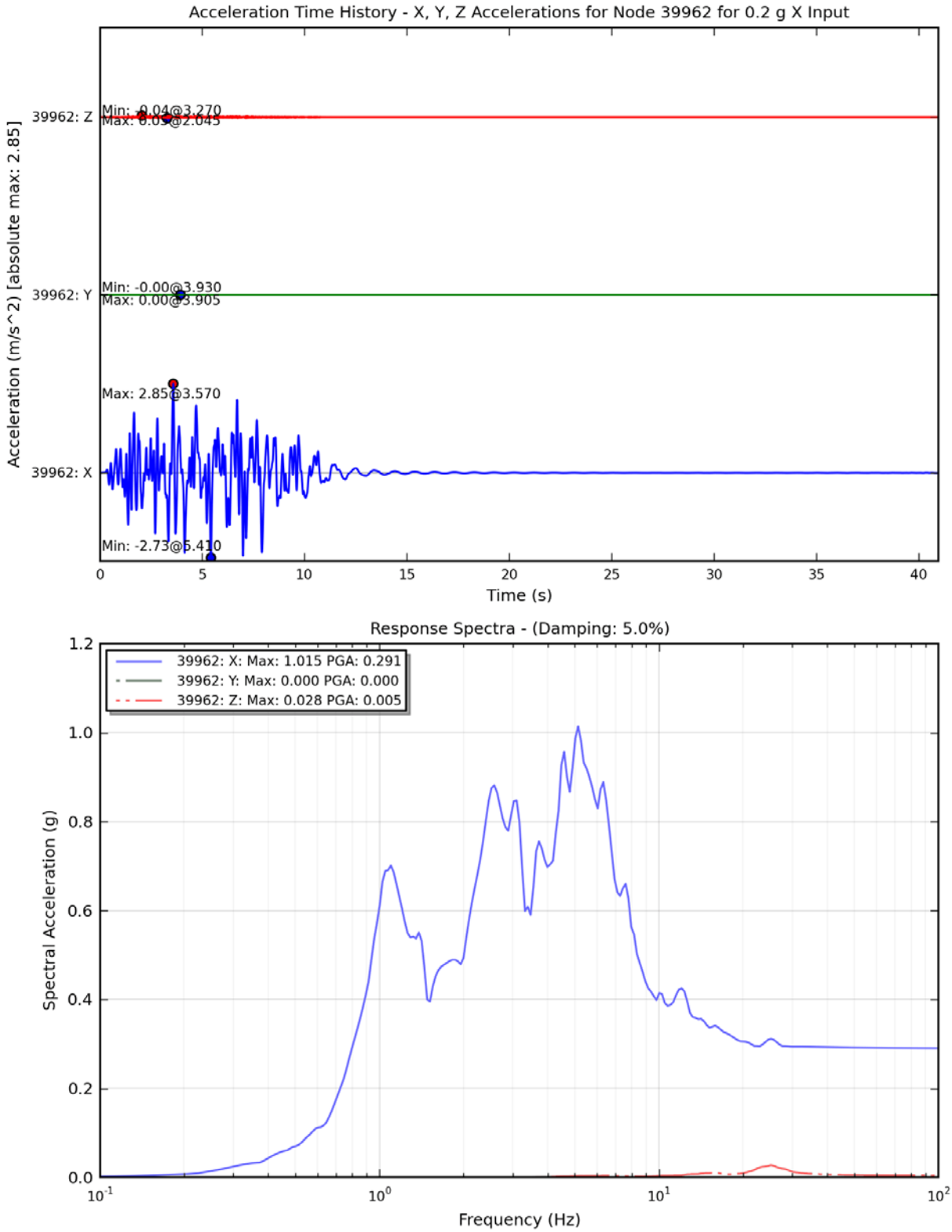

Figure 3-29 Response Acceleration Time Histories and ISRS at Node 39962 for X Input Motion (0.2 g)

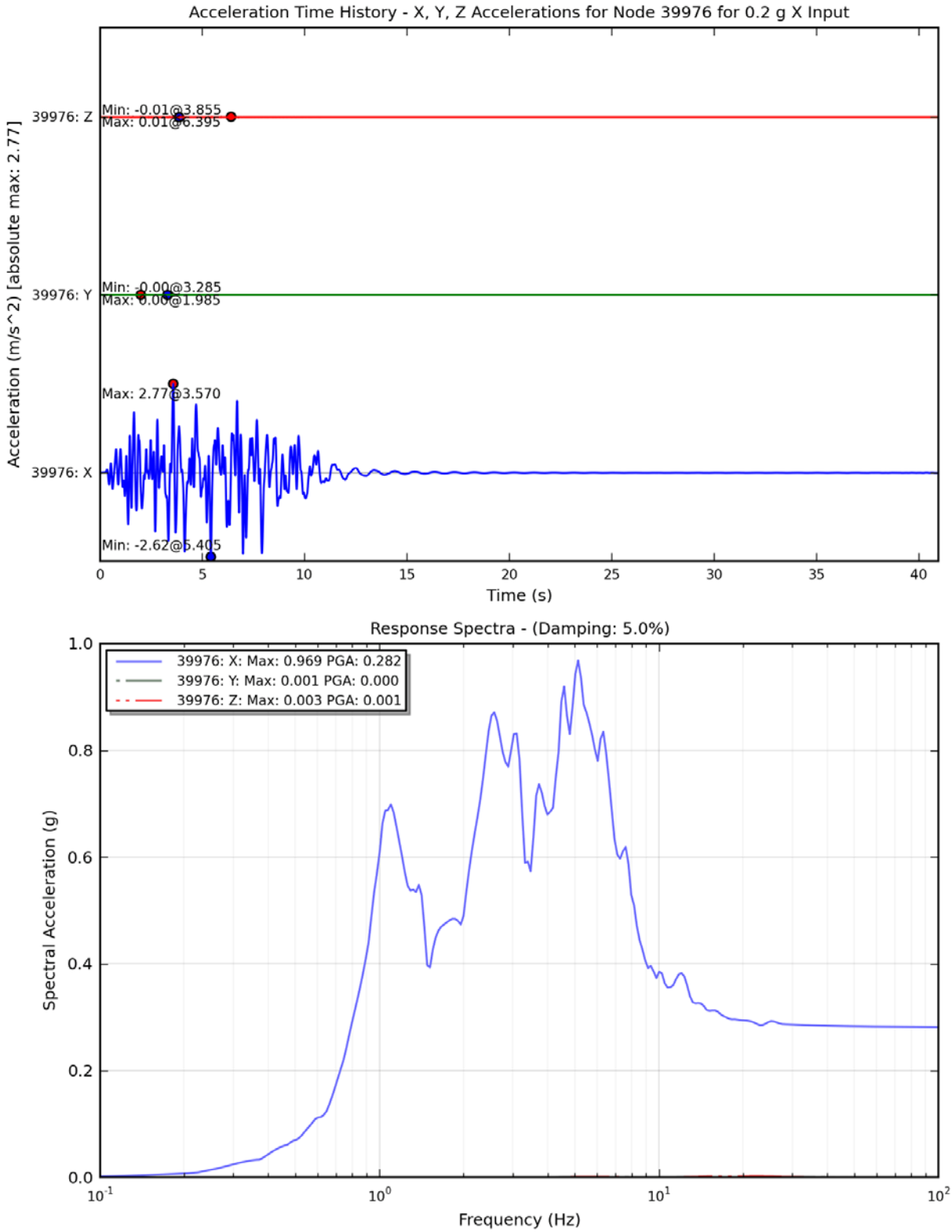

Figure 3-30 Response Acceleration Time Histories and ISRS at Node 39976 for X Input Motion (0.2 g)

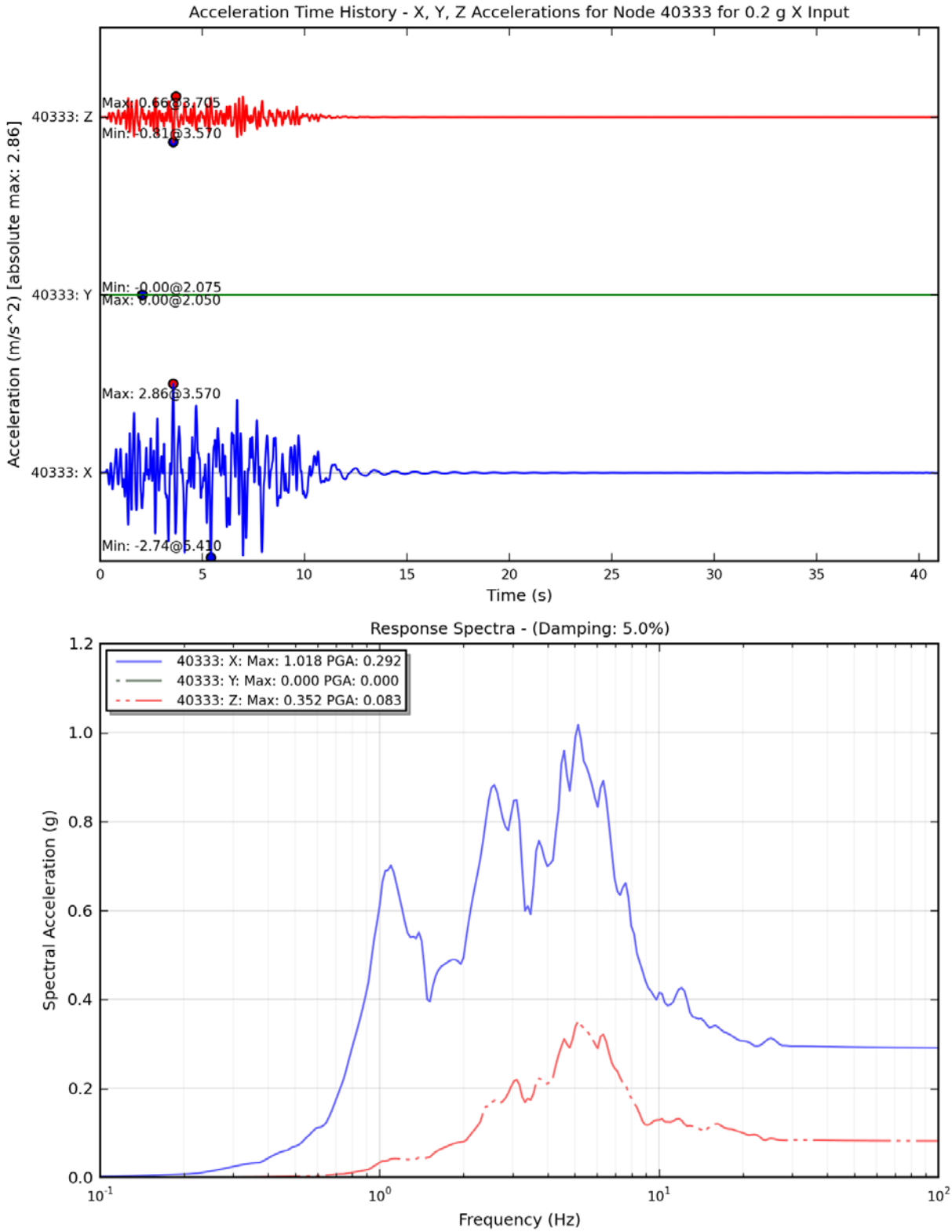

Figure 3-31 Response Acceleration Time Histories and ISRS at Node 40333 for X Input Motion (0.2 g)

3.3 Acceleration Time Histories and ISRS for the Z Directional Input Motion

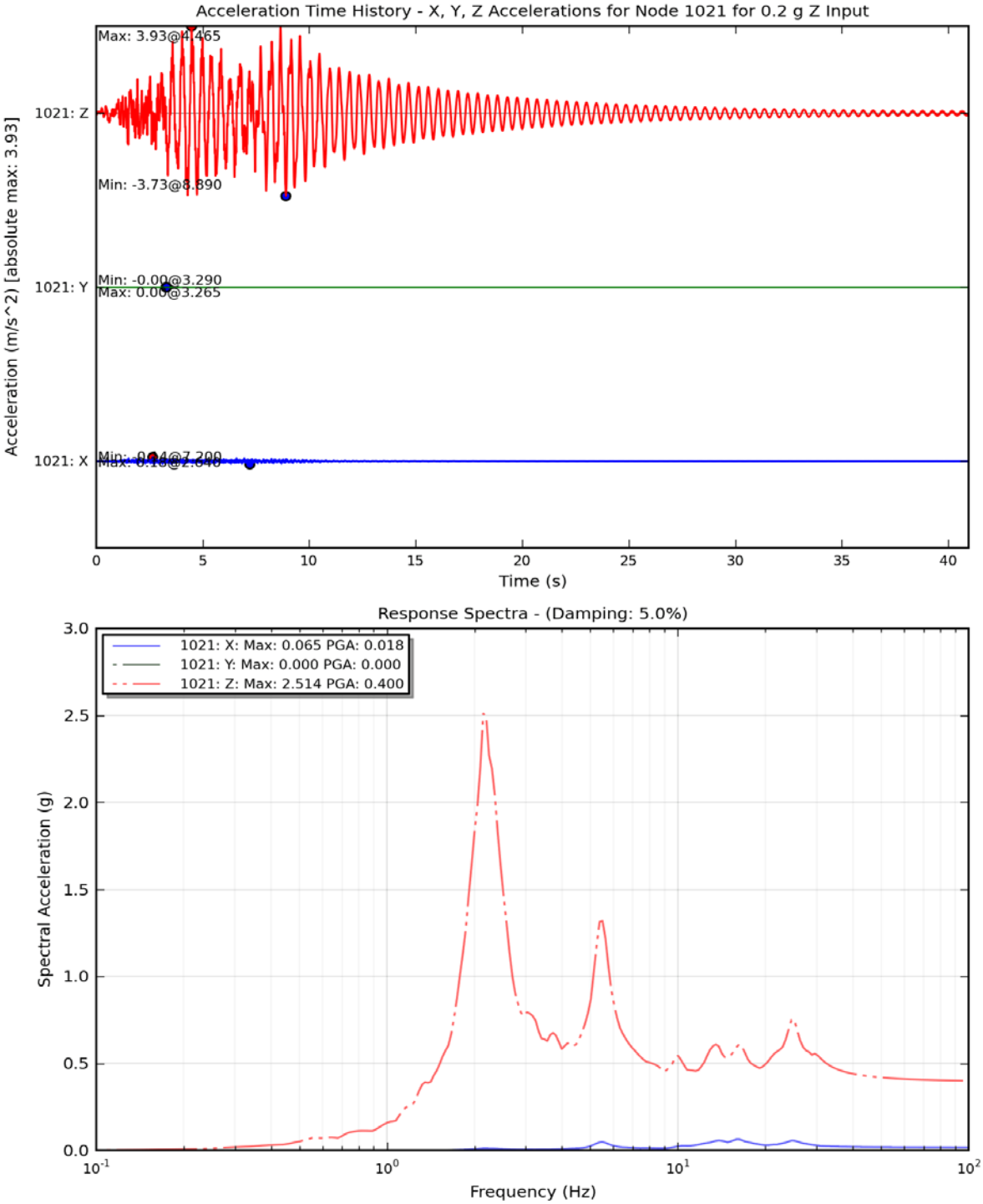

Figure 3-32 Response Acceleration Time Histories and ISRS at Node 1021 for Z Input Motion (0.2 g)

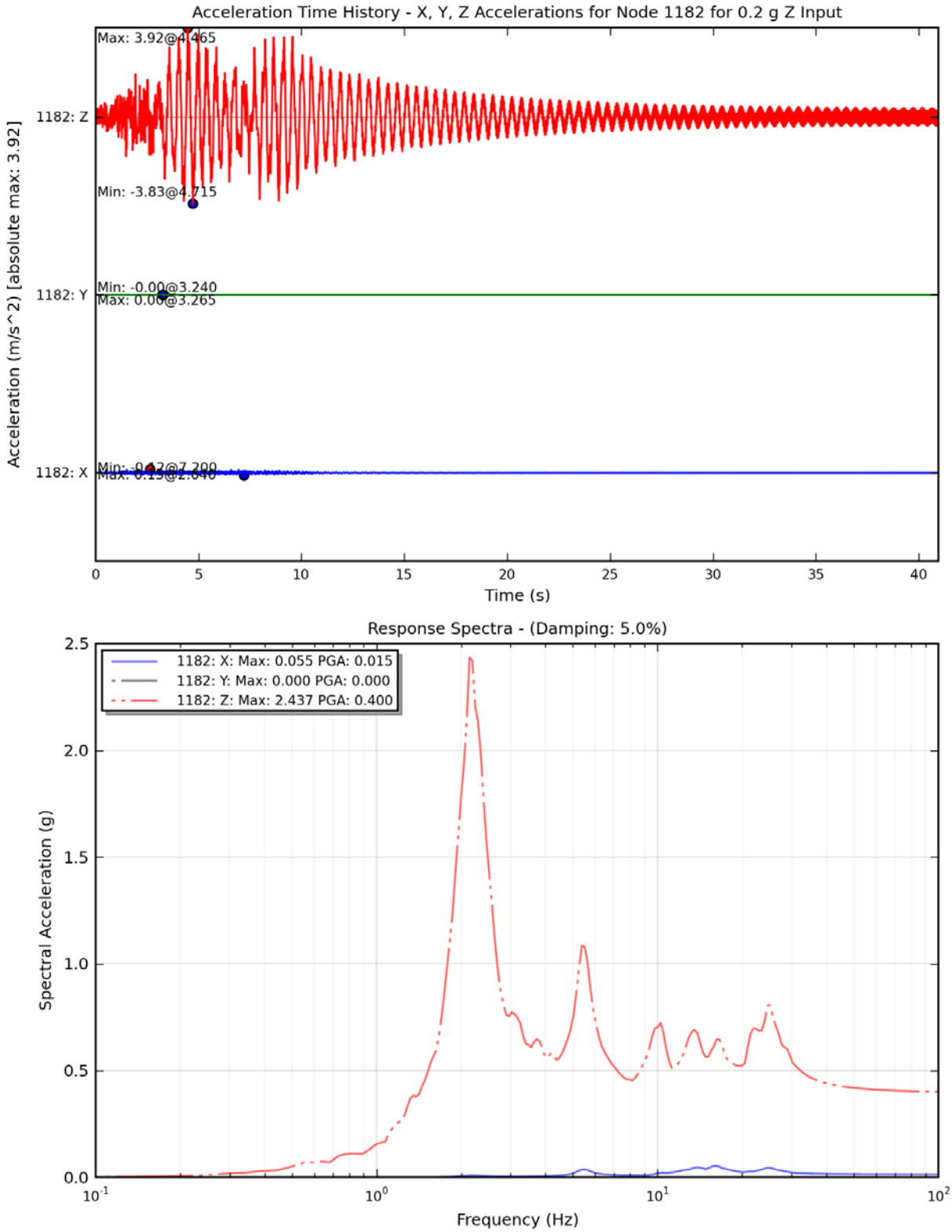

Figure 3-33 Response Acceleration Time Histories and ISRS at Node 1182 for Z Input Motion (0.2 g)

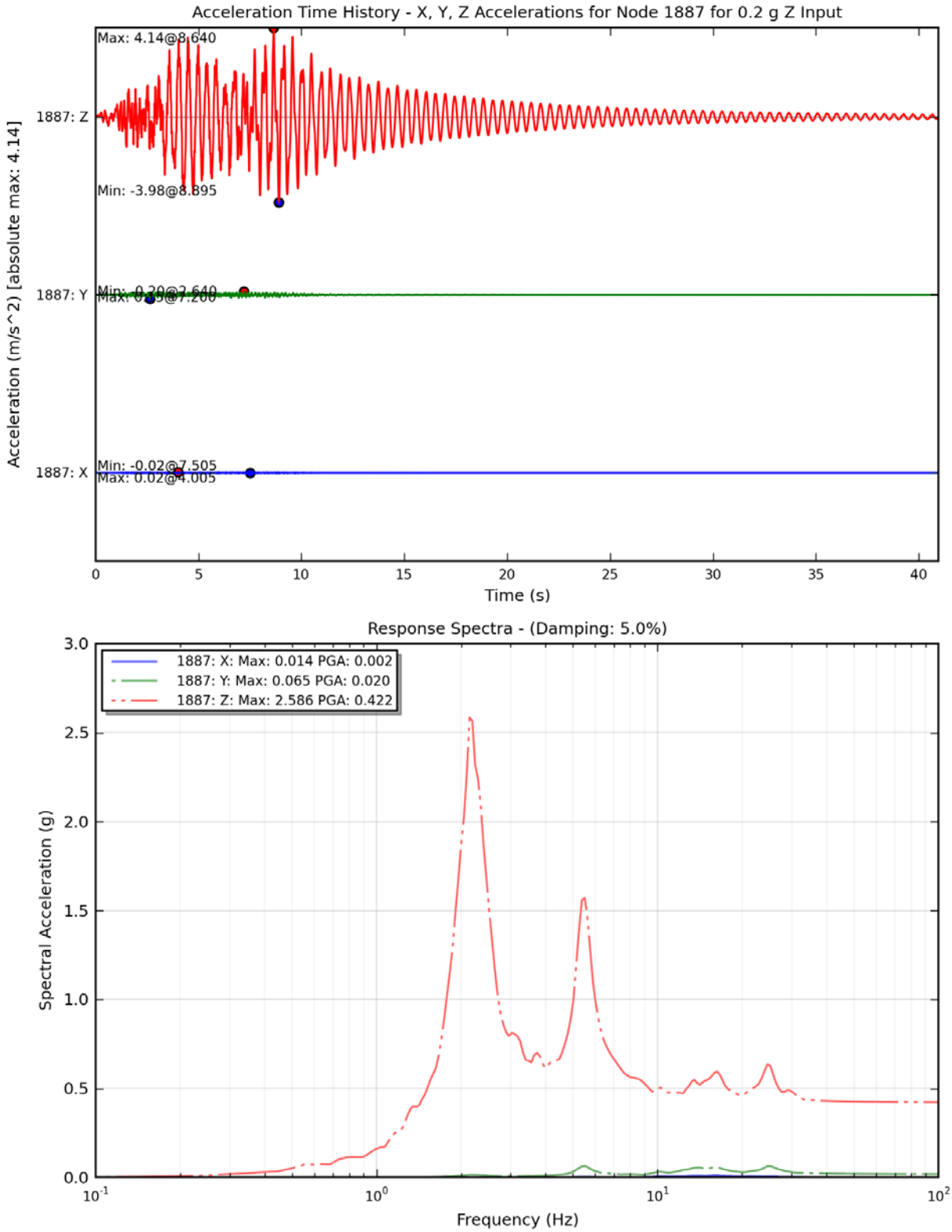

Figure 3-34 Response Acceleration Time Histories and ISRS at Node 1887 for Z Input Motion (0.2 g)

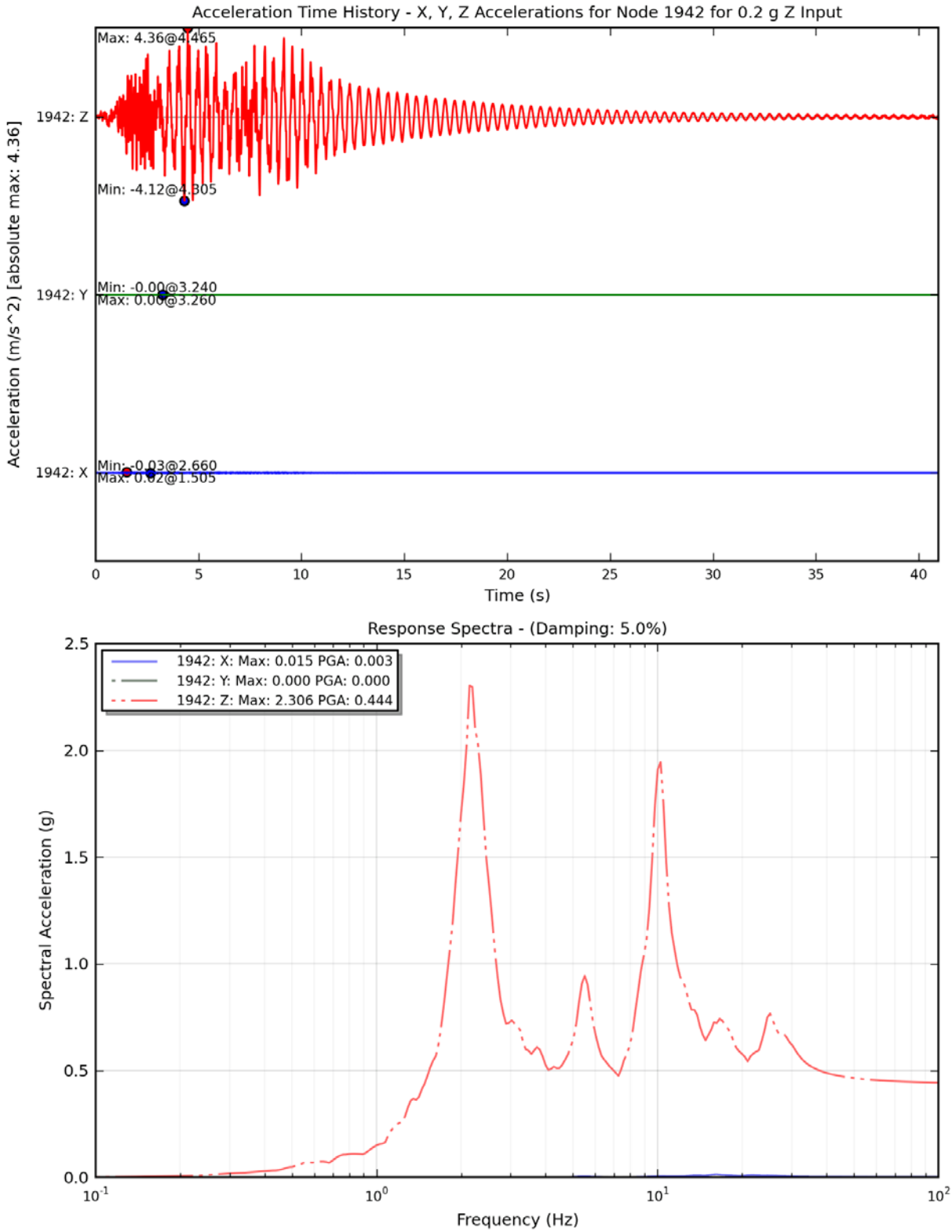

Figure 3-35 Response Acceleration Time Histories and ISRS at Node 1942 for Z Input Motion (0.2 g)

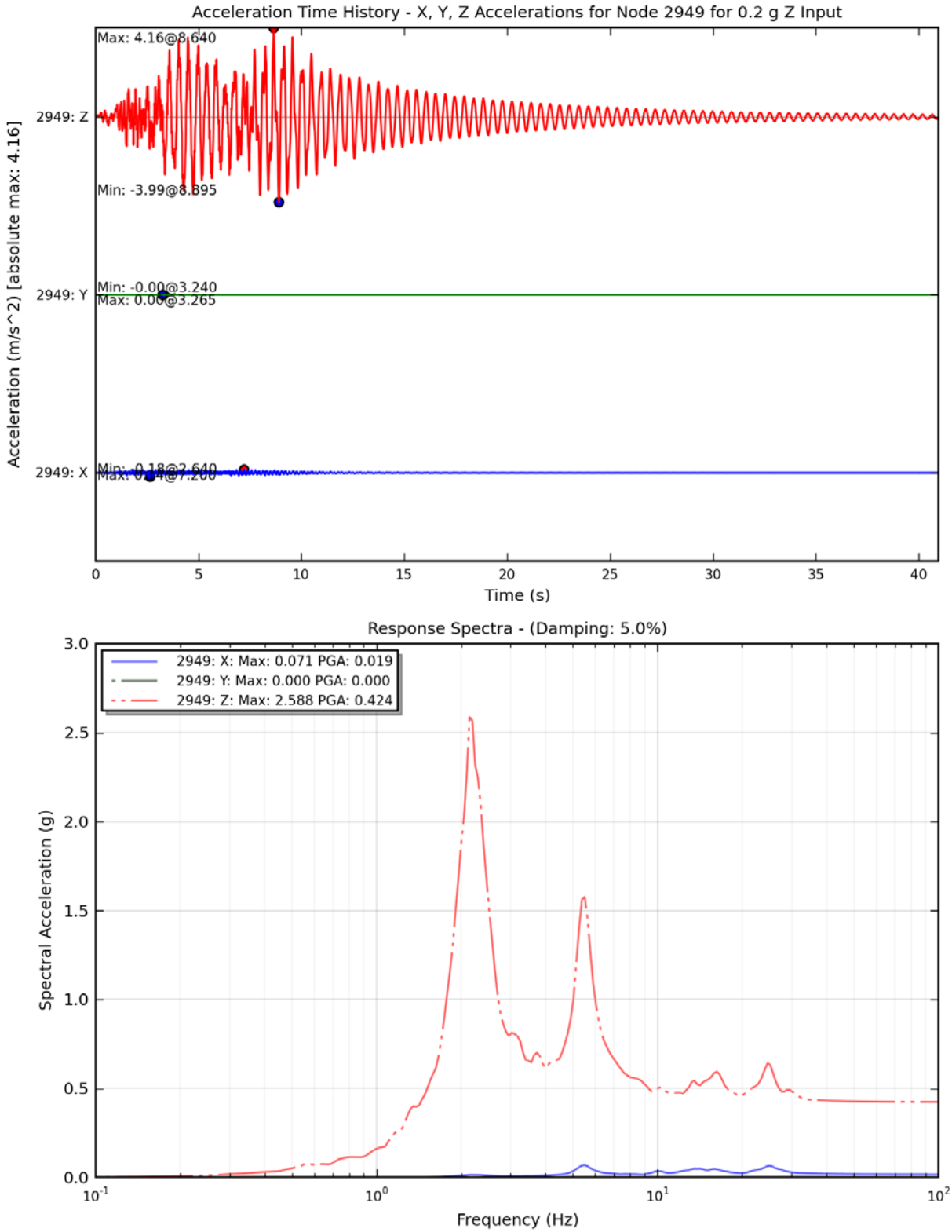

Figure 3-36 Response Acceleration Time Histories and ISRS at Node 2949 for Z Input Motion (0.2 g)

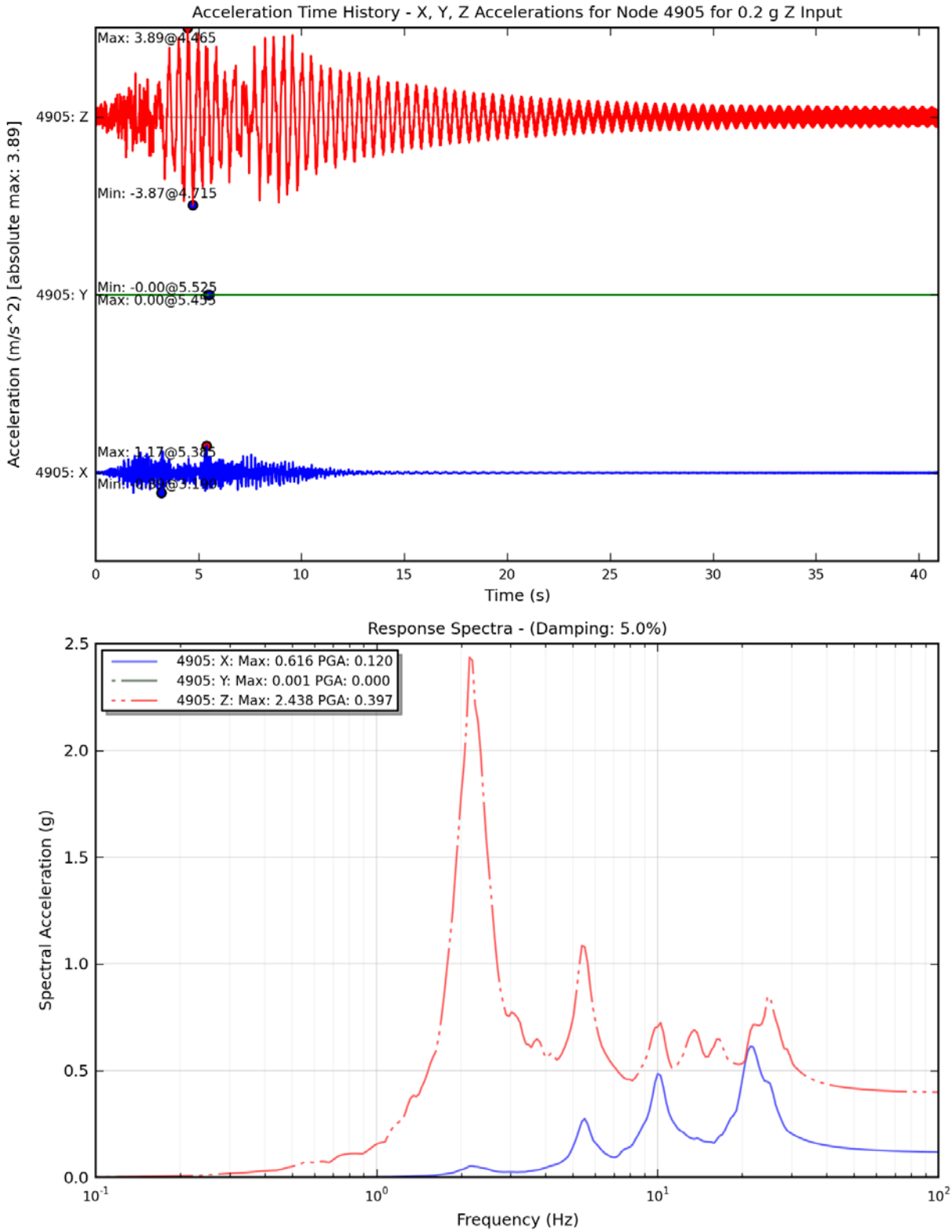

Figure 3-37 Response Acceleration Time Histories and ISRS at Node 4905 for Z Input Motion (0.2 g)

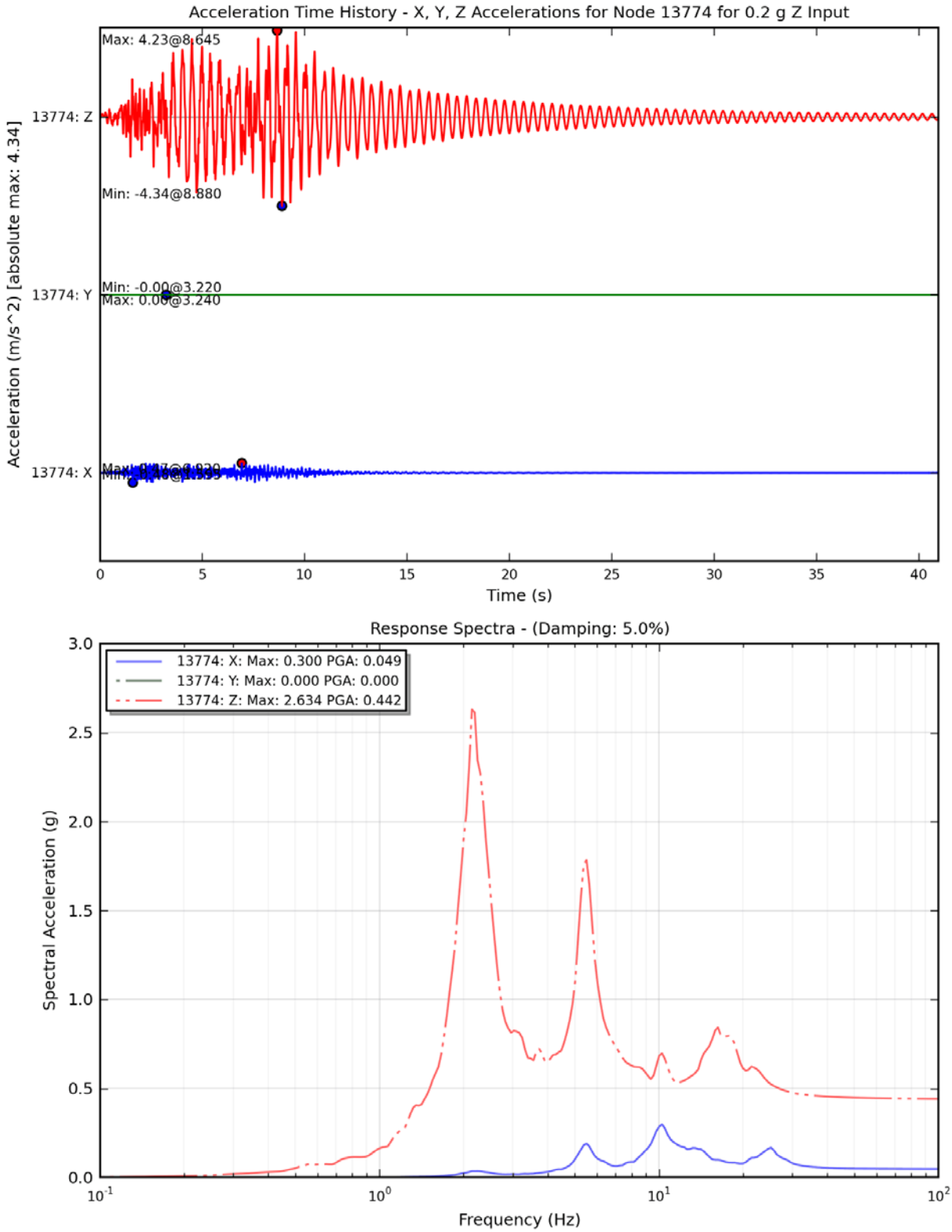

Figure 3-38 Response Acceleration Time Histories and ISRS at Node 13774 for Z Input Motion (0.2 g)

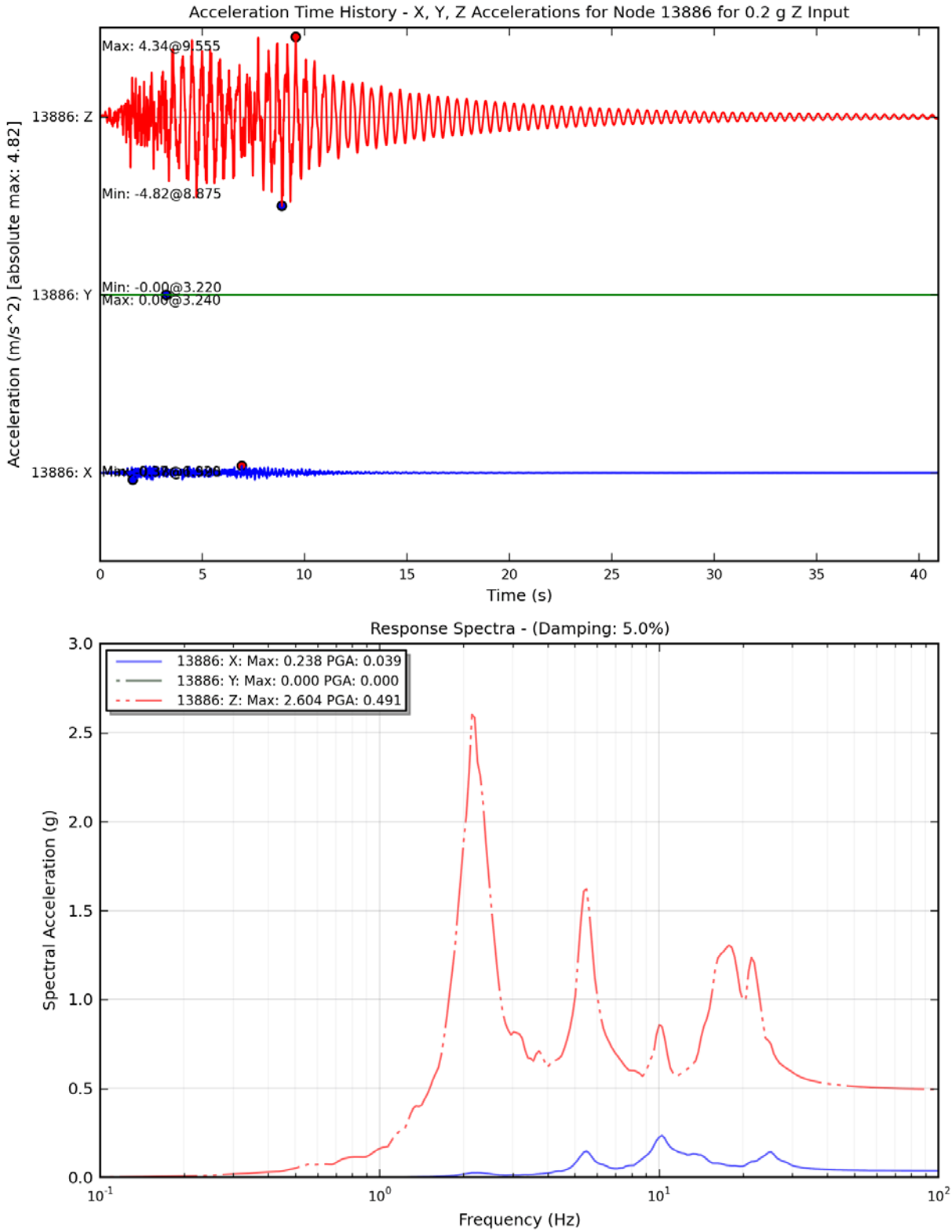

Figure 3-39 Response Acceleration Time Histories and ISRS at Node 13886 for Z Input Motion (0.2 g)

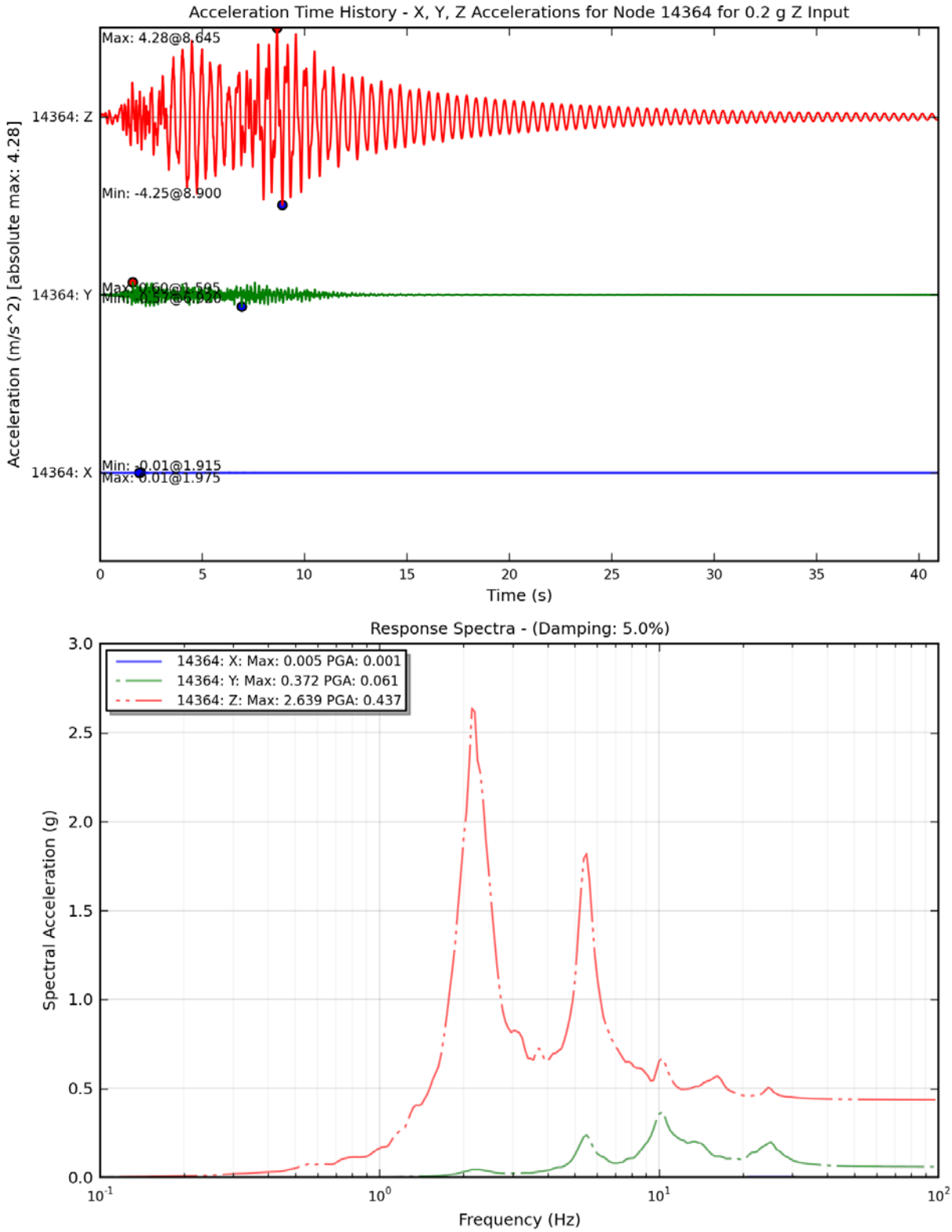

Figure 3-40 Response Acceleration Time Histories and ISRS at Node 14364 for Z Input Motion (0.2 g)

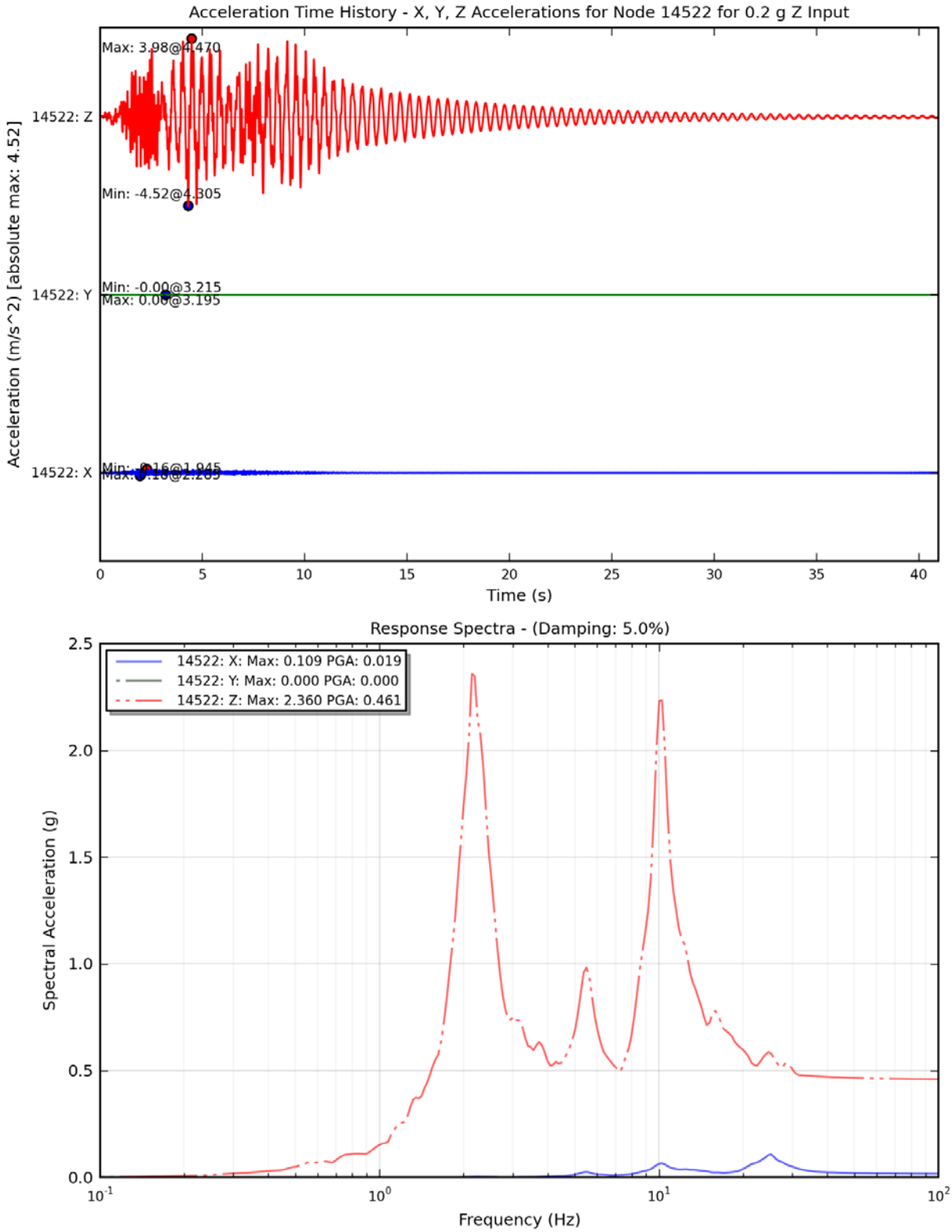

Figure 3-41 Response Acceleration Time Histories and ISRS at Node 14522 for Z Input Motion (0.2 g)

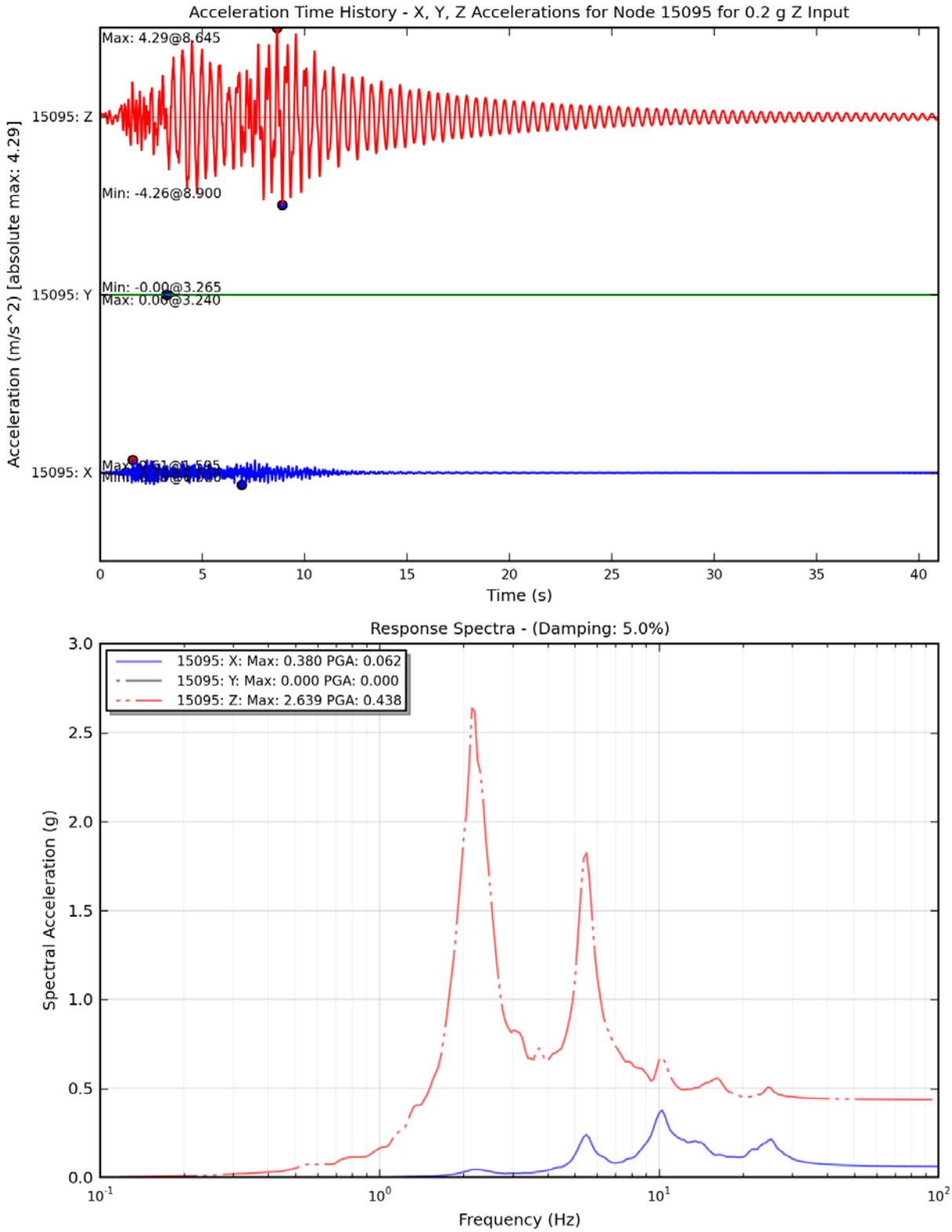

Figure 3-42 Response Acceleration Time Histories and ISRS at Node 15095 for Z Input Motion (0.2 g)

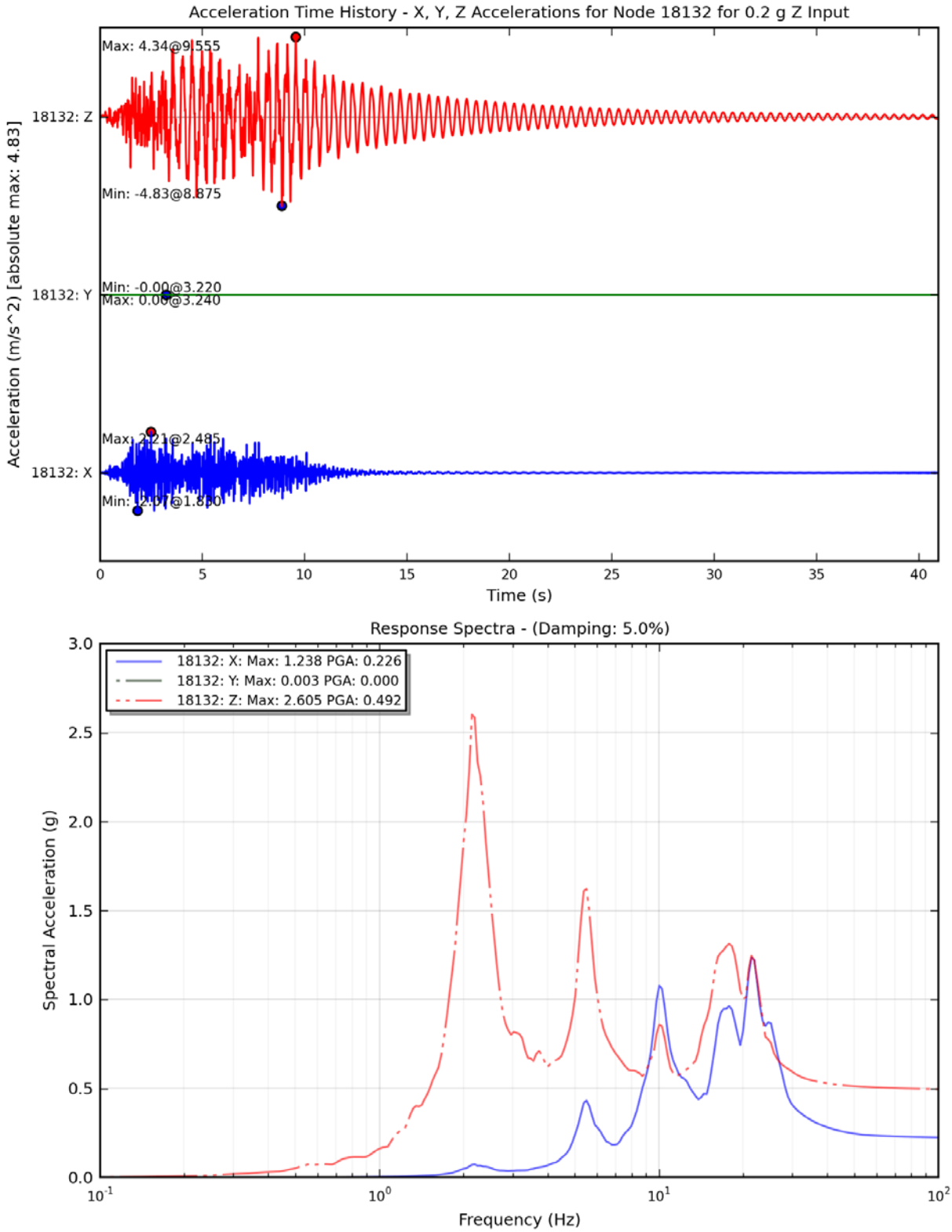

Figure 3-43 Response Acceleration Time Histories and ISRS at Node 18132 for Z Input Motion (0.2 g)

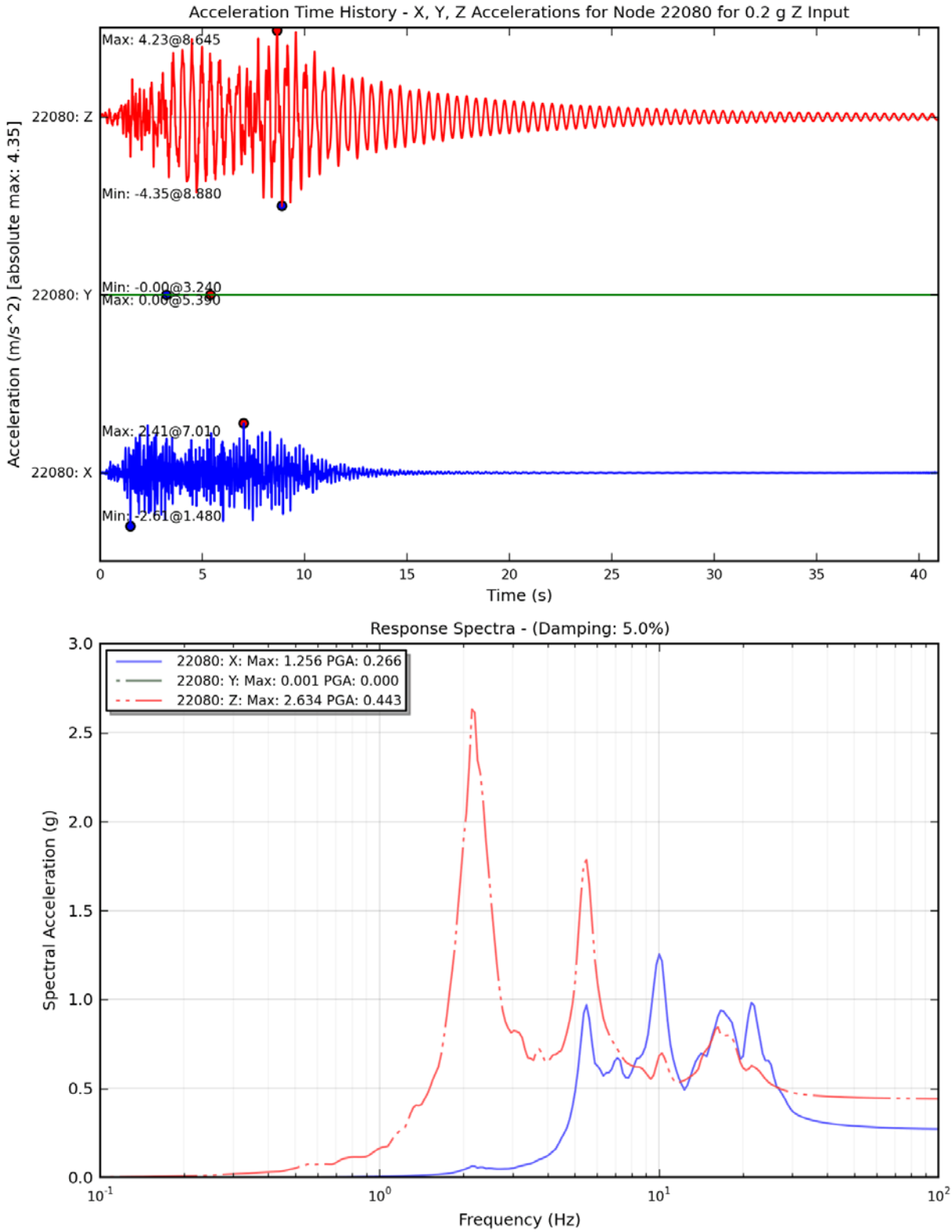

Figure 3-44 Response Acceleration Time Histories and ISRS at Node 22080 for Z Input Motion (0.2 g)

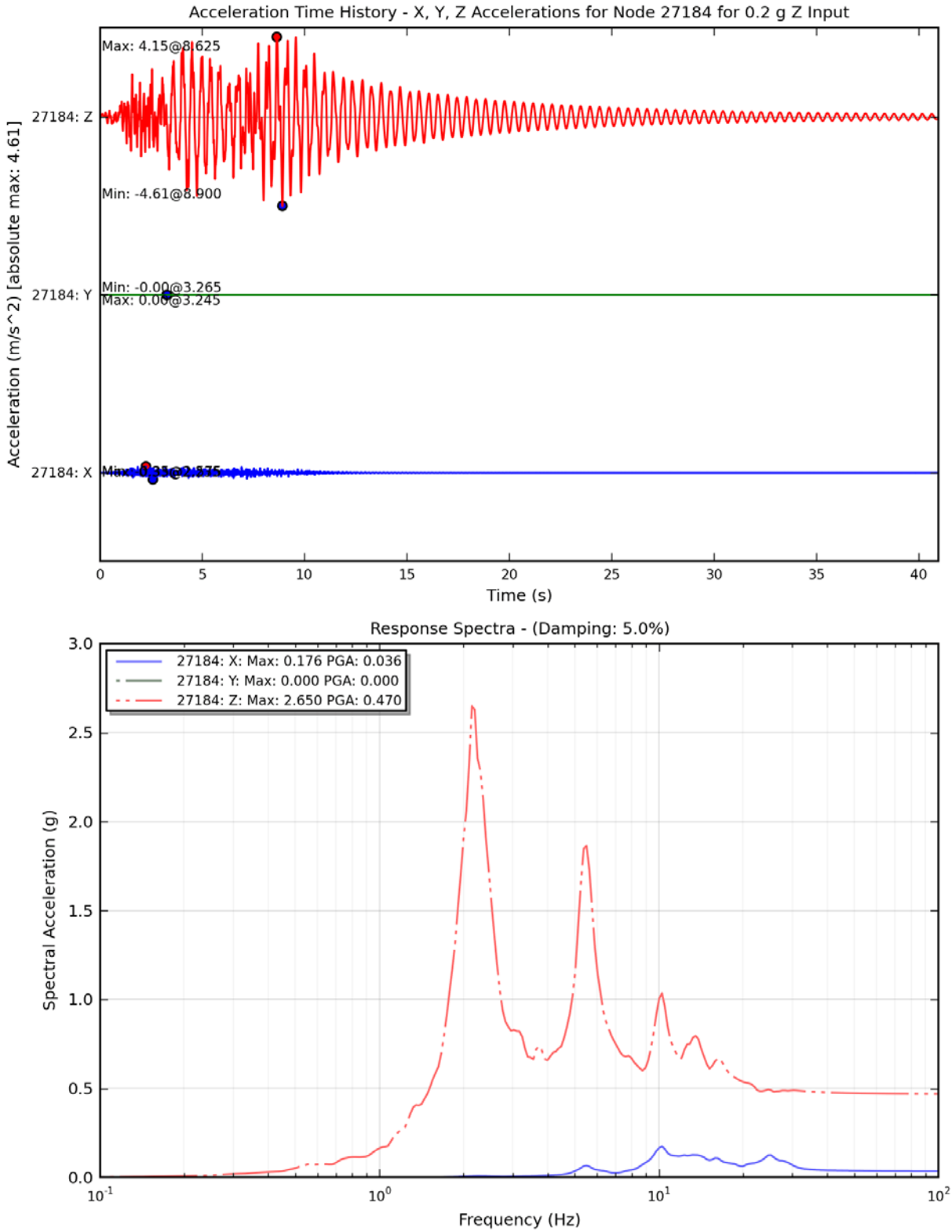

Figure 3-45 Response Acceleration Time Histories and ISRS at Node 27184 for Z Input Motion (0.2 g)

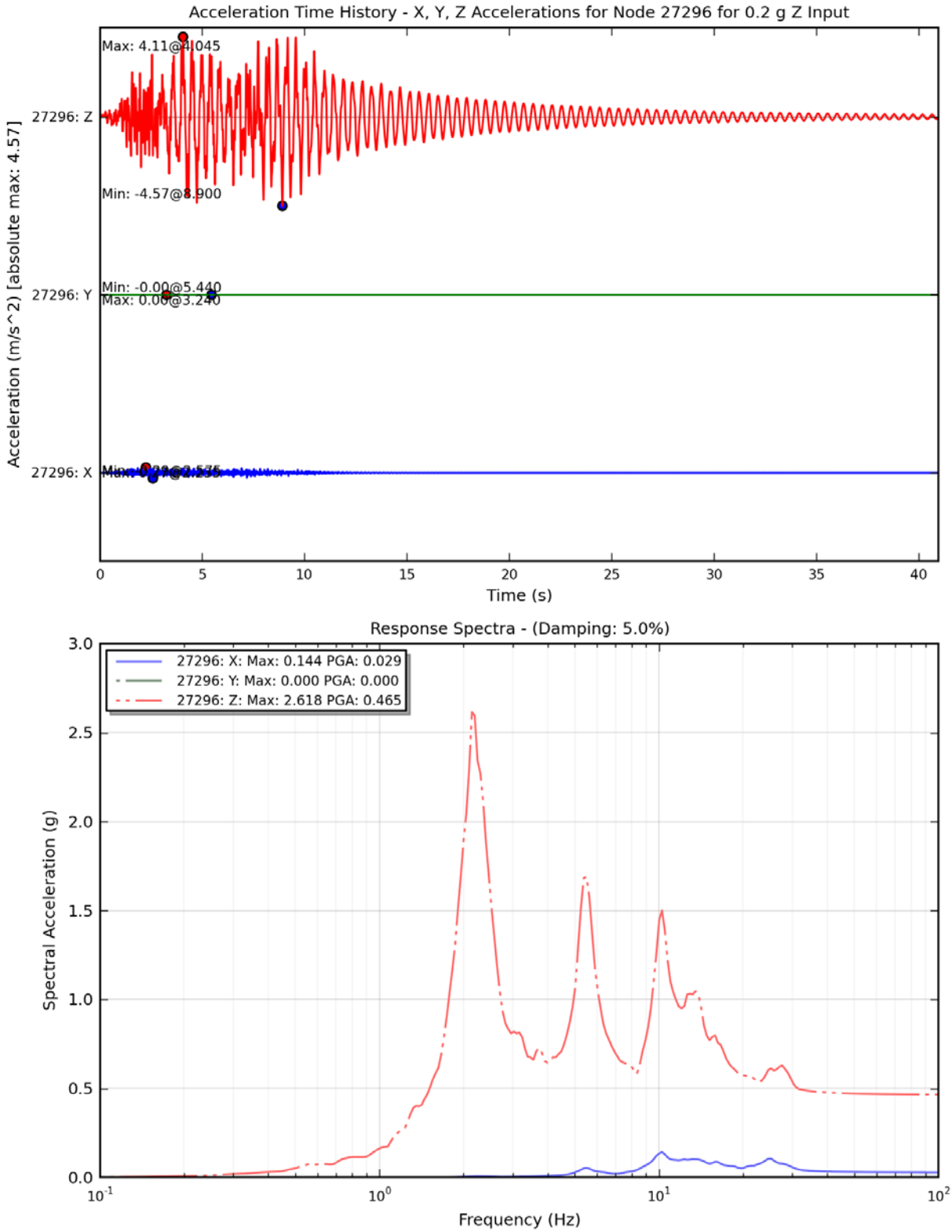

Figure 3-46 Response Acceleration Time Histories and ISRS at Node 27296 for Z Input Motion (0.2 g)

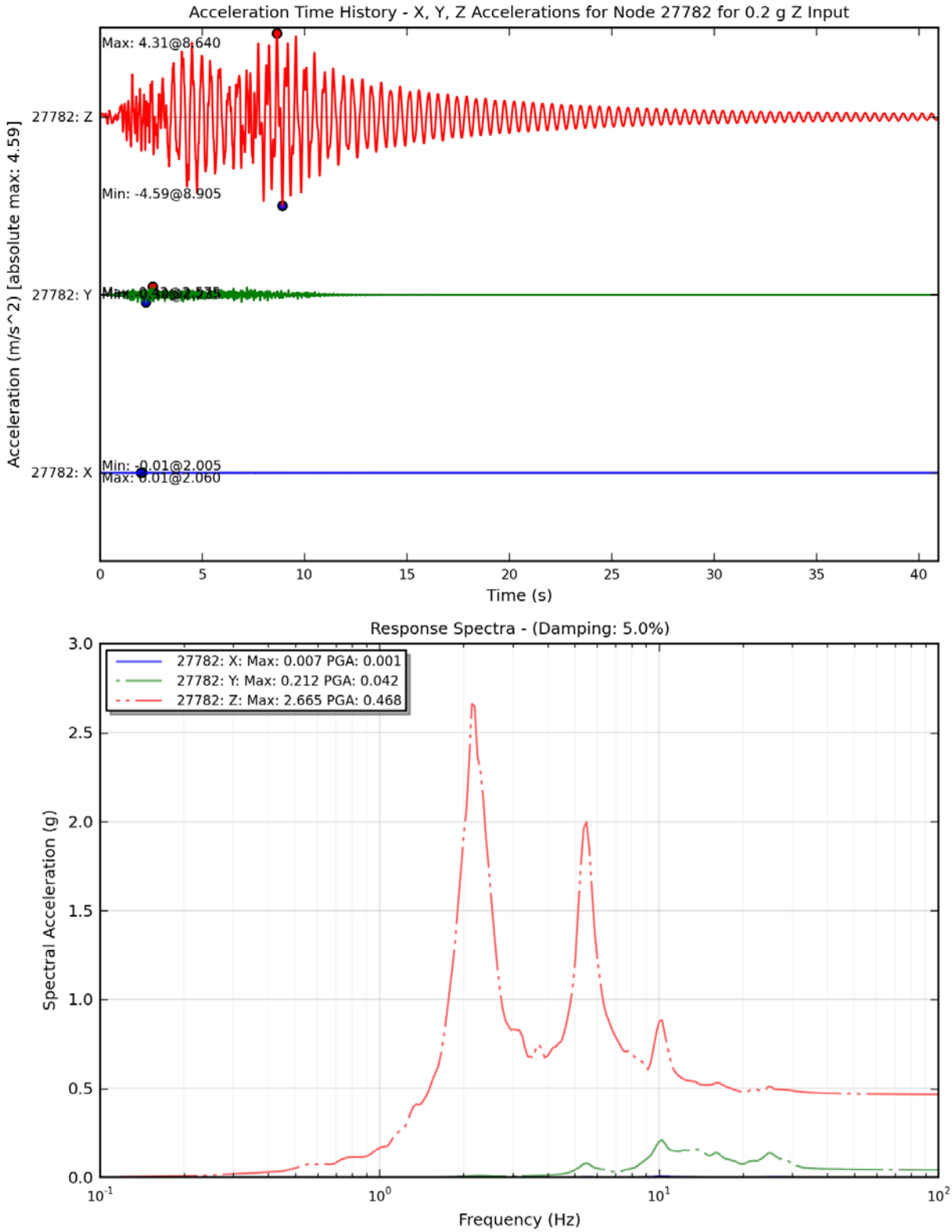

Figure 3-47 Response Acceleration Time Histories and ISRS at Node 27782 for Z Input Motion (0.2 g)

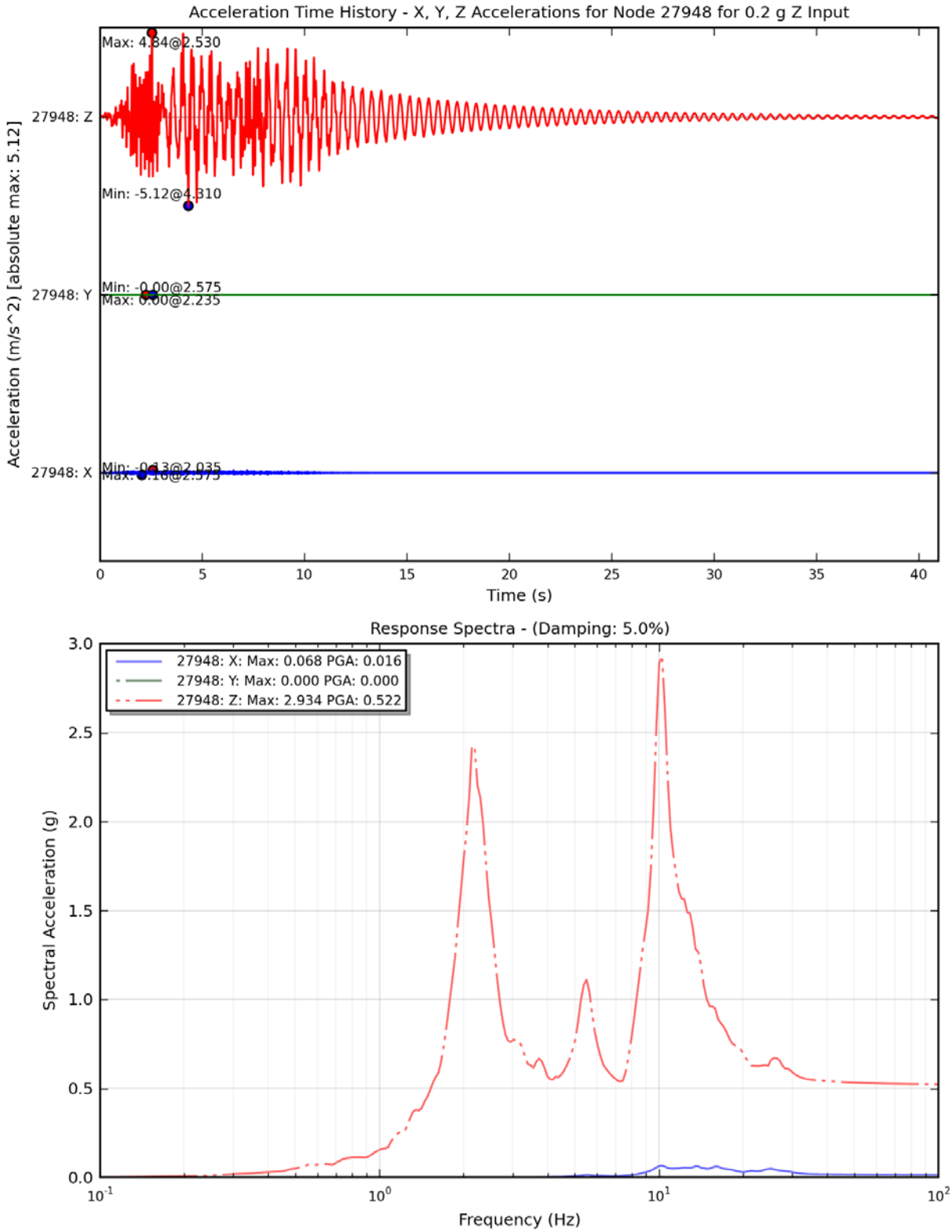

Figure 3-48 Response Acceleration Time Histories and ISRS at Node 27948 for Z Input Motion (0.2 g)

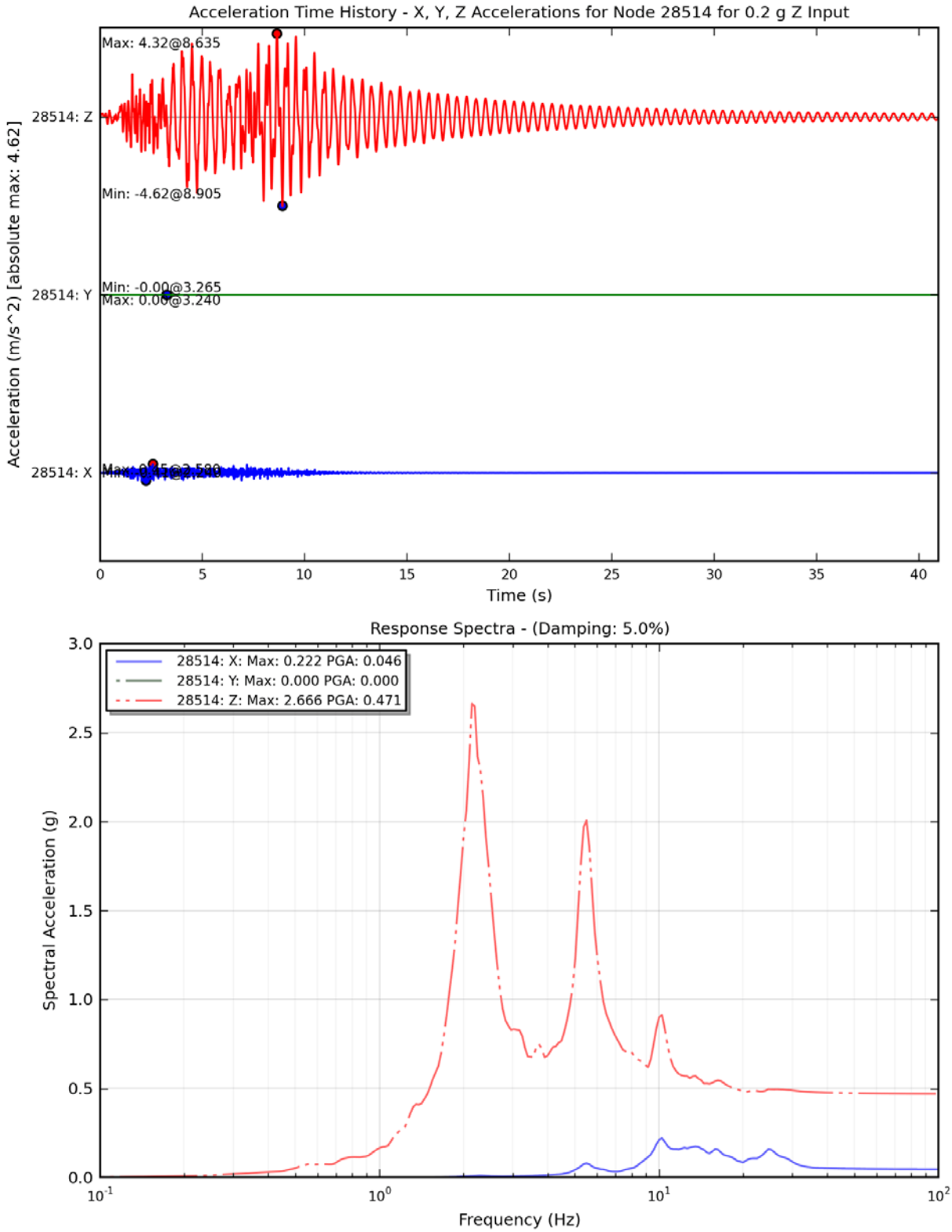

Figure 3-49 Response Acceleration Time Histories and ISRS at Node 28514 for Z Input Motion (0.2 g)

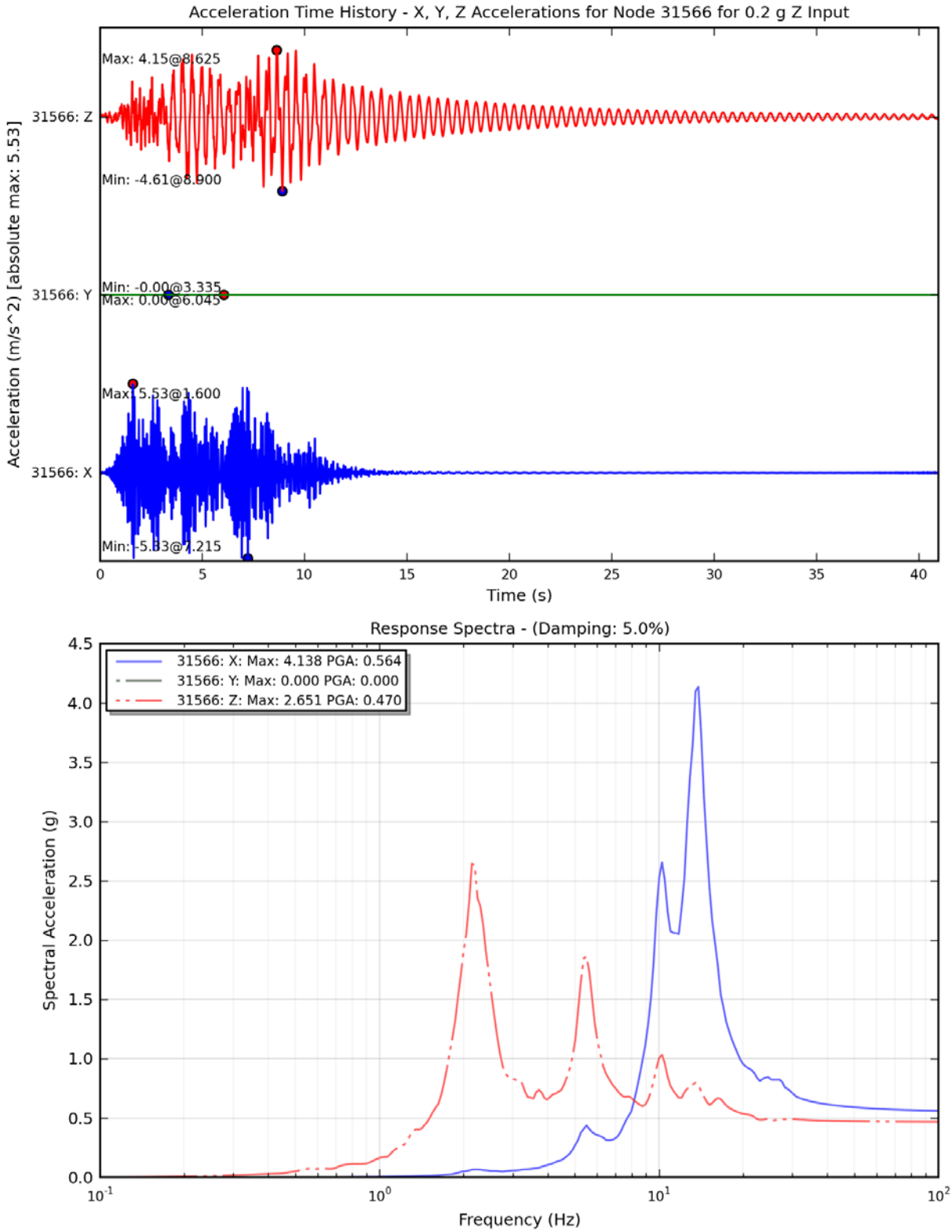

Figure 3-50 Response Acceleration Time Histories and ISRS at Node 31566 for Z Input Motion (0.2 g)

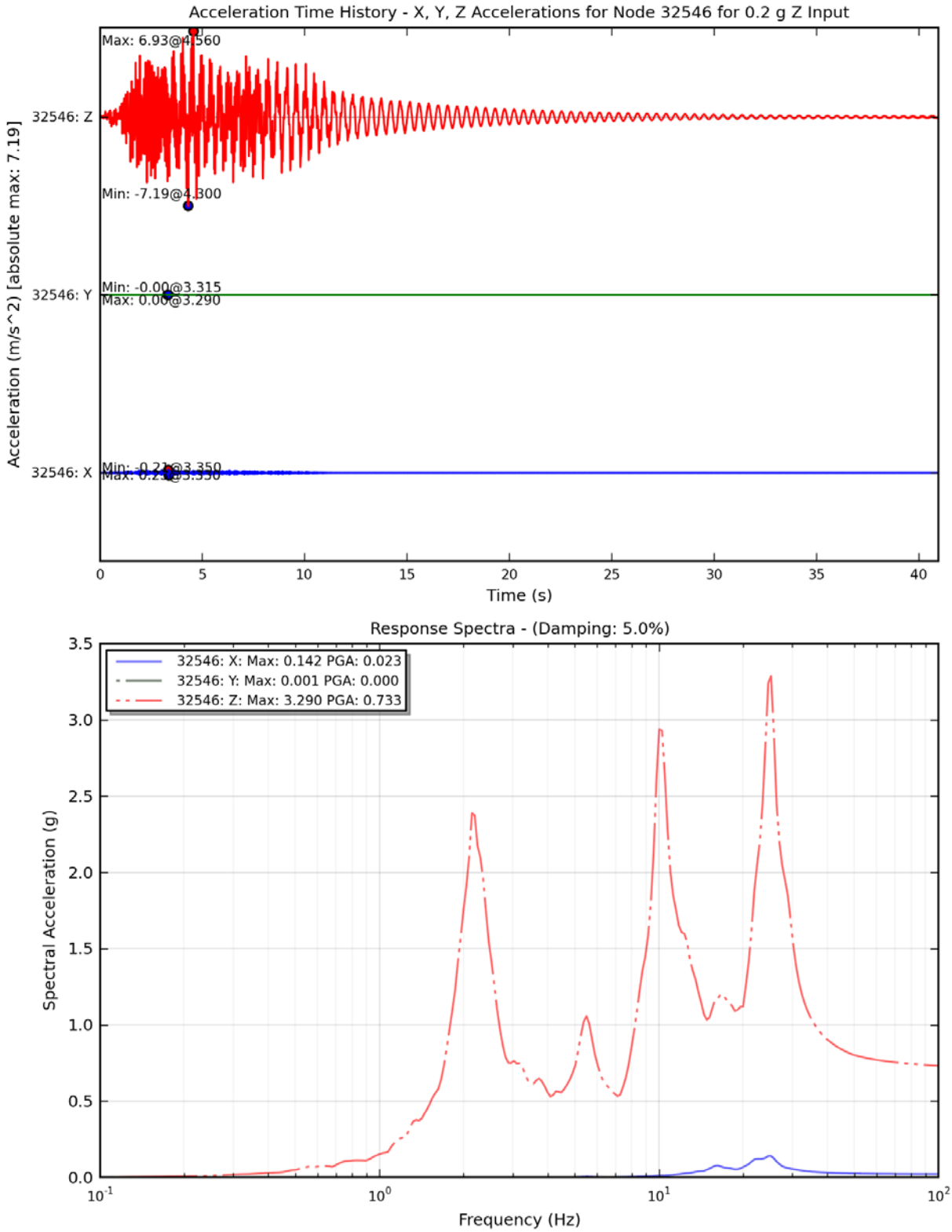

Figure 3-51 Response Acceleration Time Histories and ISRS at Node 32546 for Z Input Motion (0.2 g)

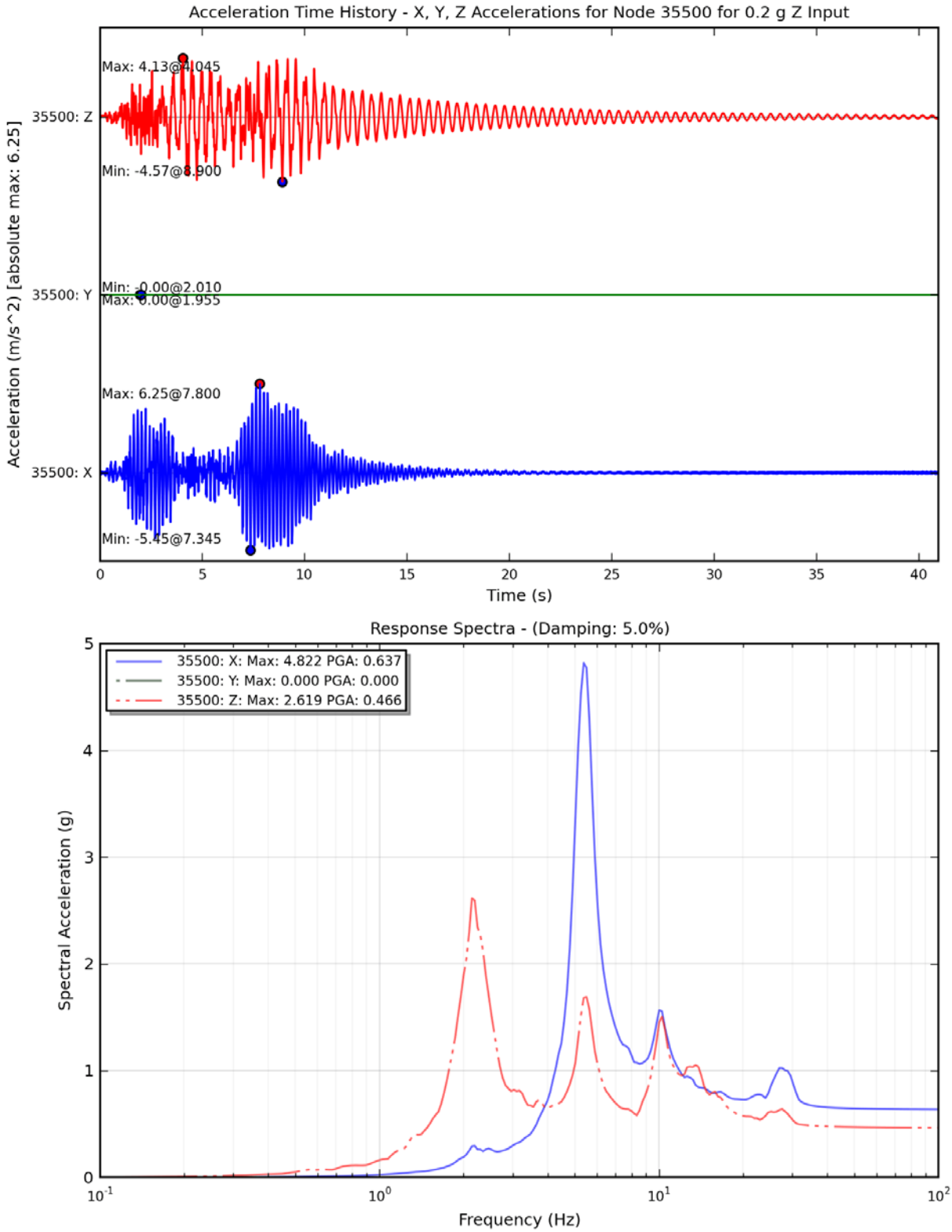

Figure 3-52 Response Acceleration Time Histories and ISRS at Node 35500 for Z Input Motion (0.2 g)

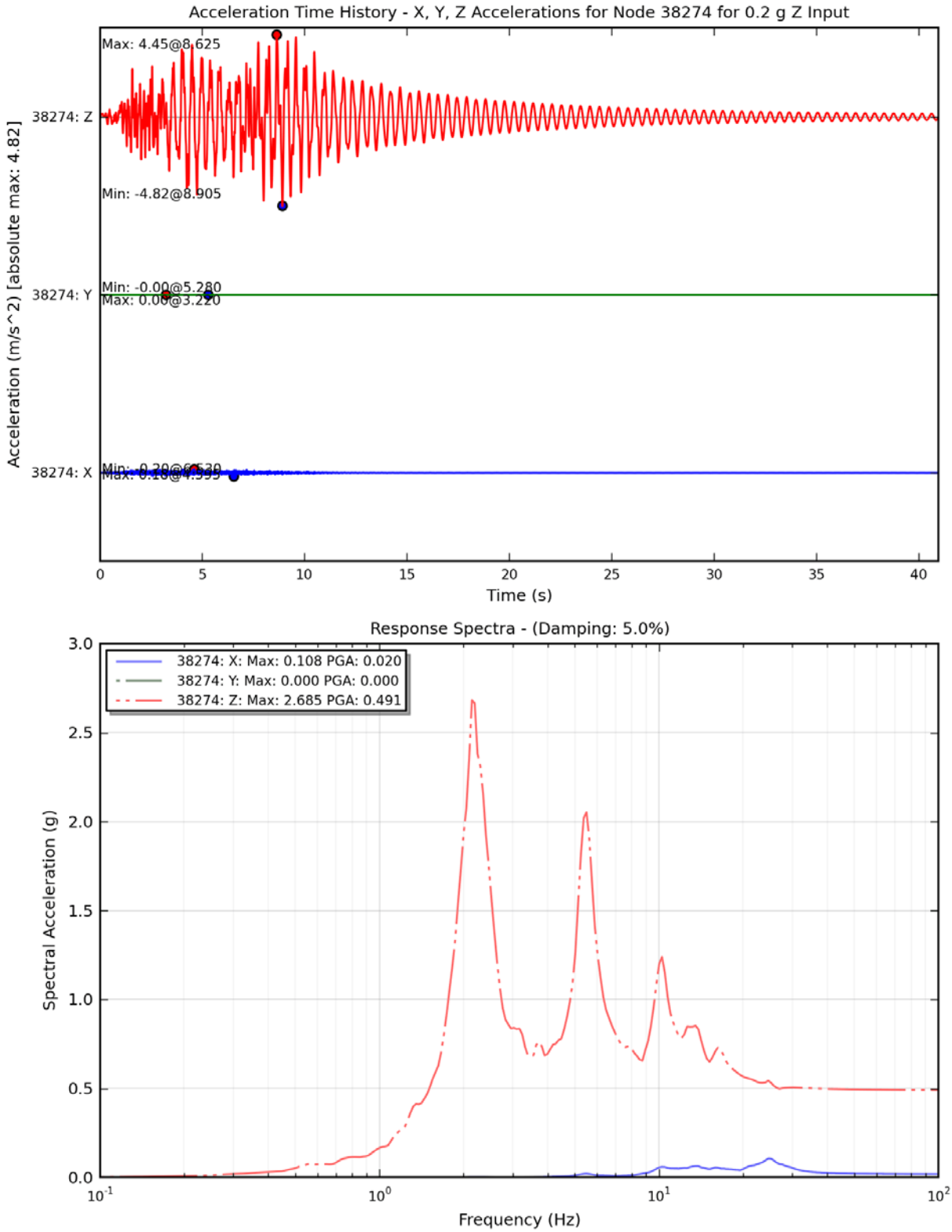

Figure 3-53 Response Acceleration Time Histories and ISRS at Node 38274 for Z Input Motion (0.2 g)

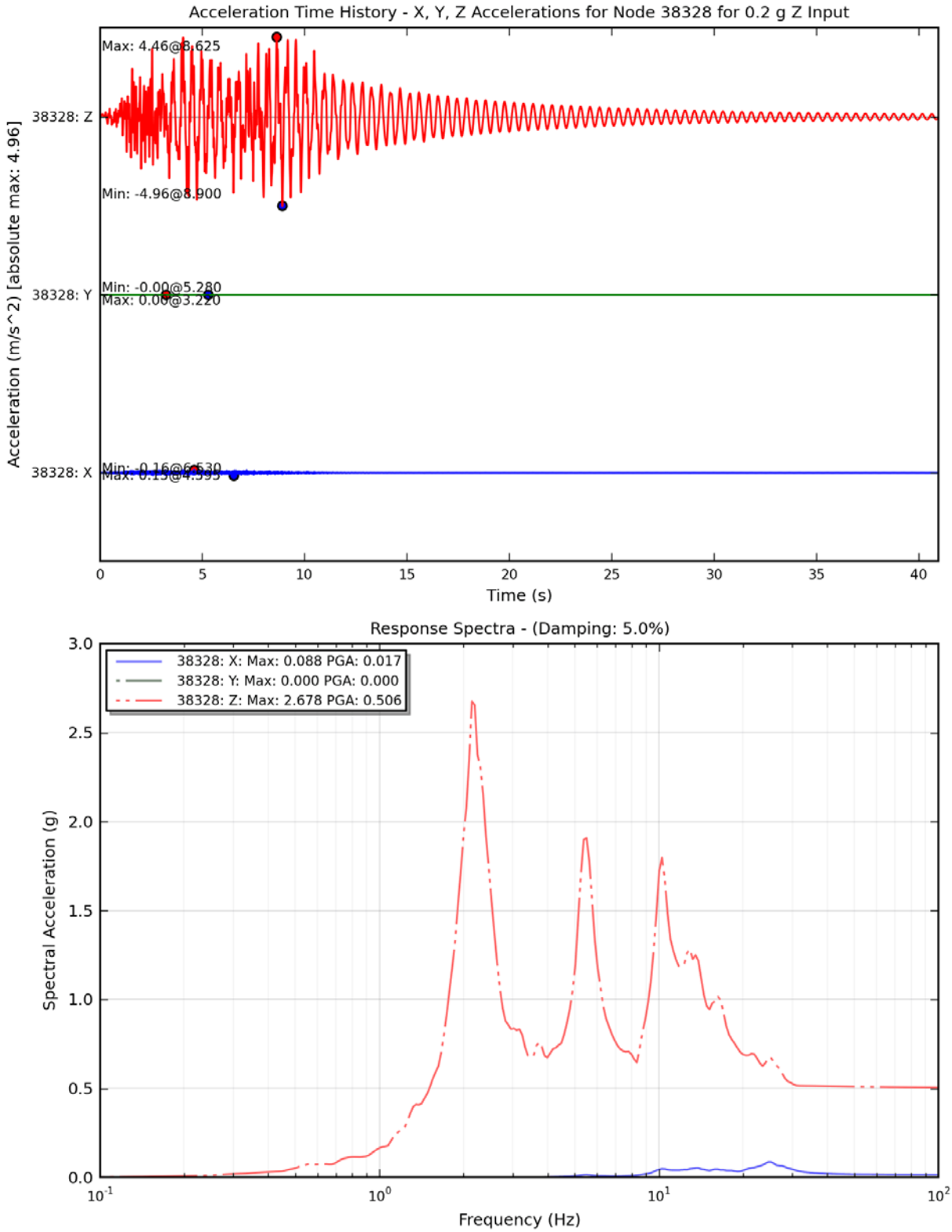

Figure 3-54 Response Acceleration Time Histories and ISRS at Node 38328 for Z Input Motion (0.2 g)

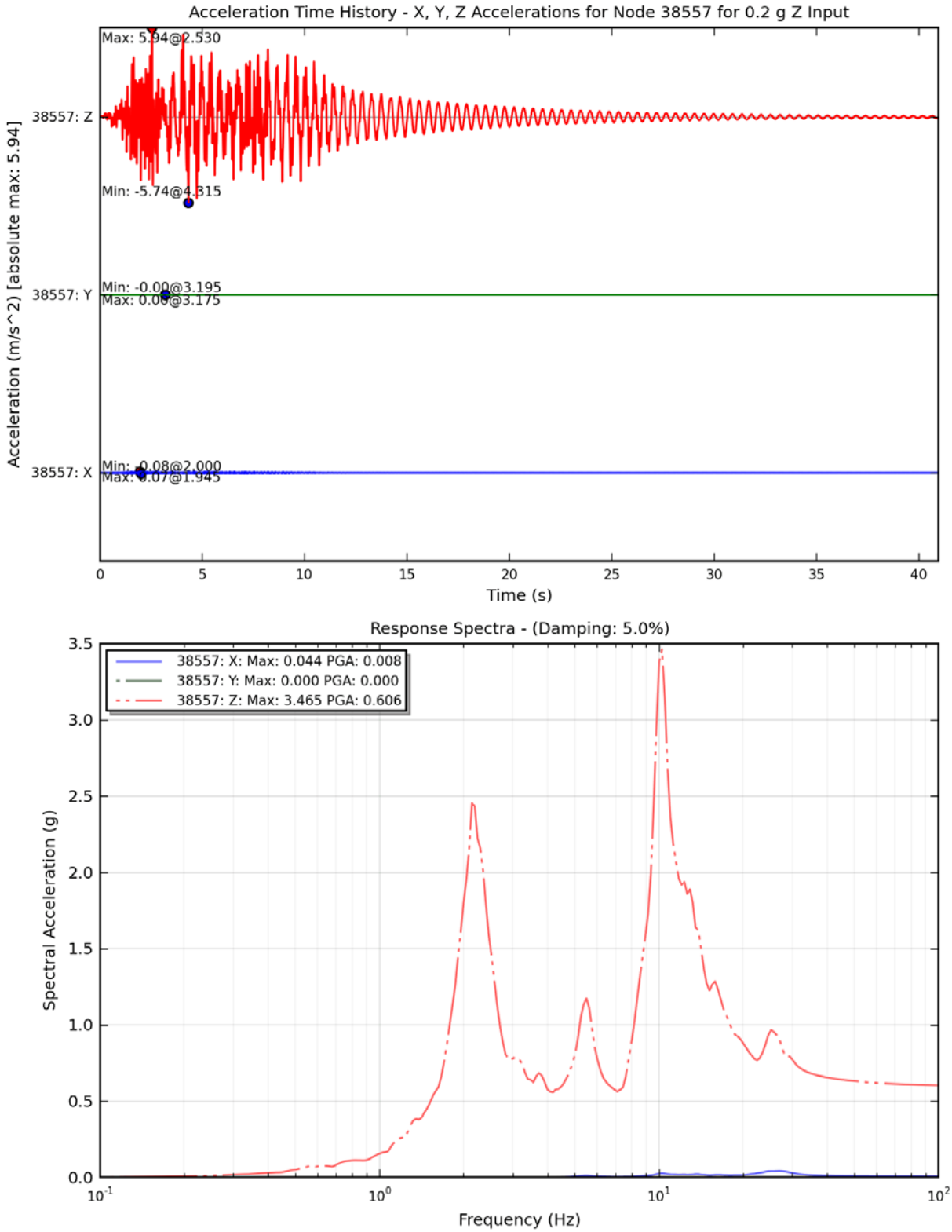

Figure 3-55 Response Acceleration Time Histories and ISRS at Node 38557 for Z Input Motion (0.2 g)

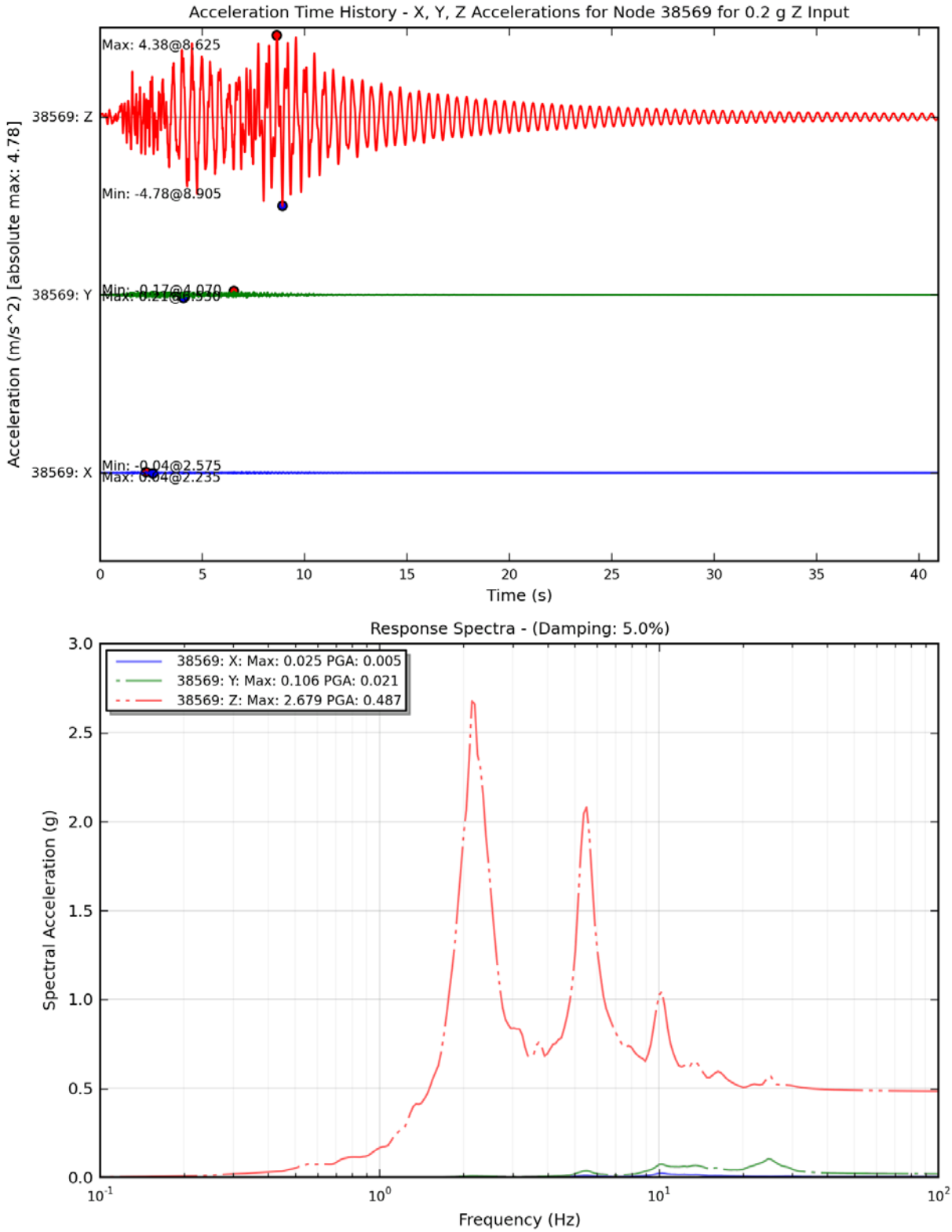

Figure 3-56 Response Acceleration Time Histories and ISRS at Node 38569 for Z Input Motion (0.2 g)

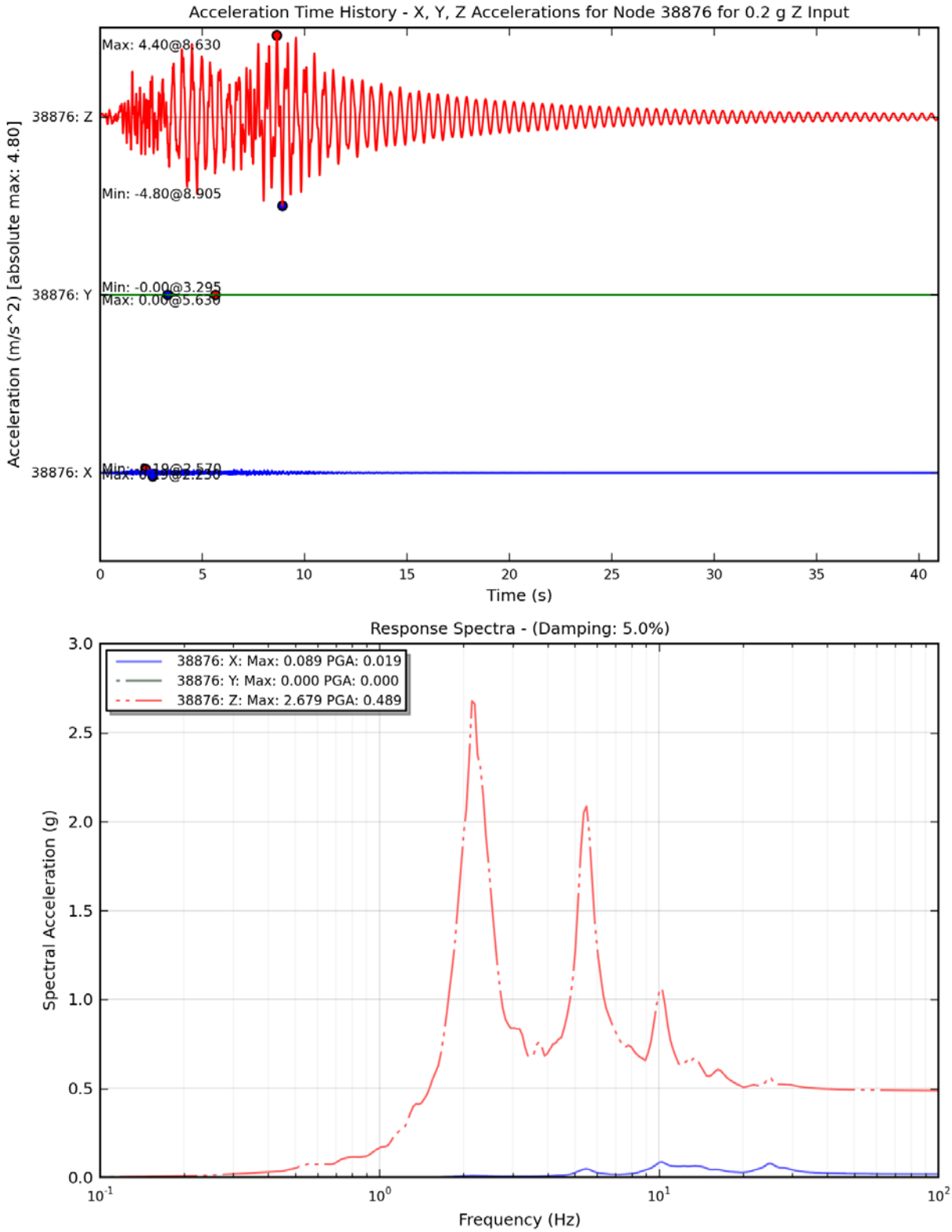

Figure 3-57 Response Acceleration Time Histories and ISRS at Node 38876 for Z Input Motion (0.2 g)

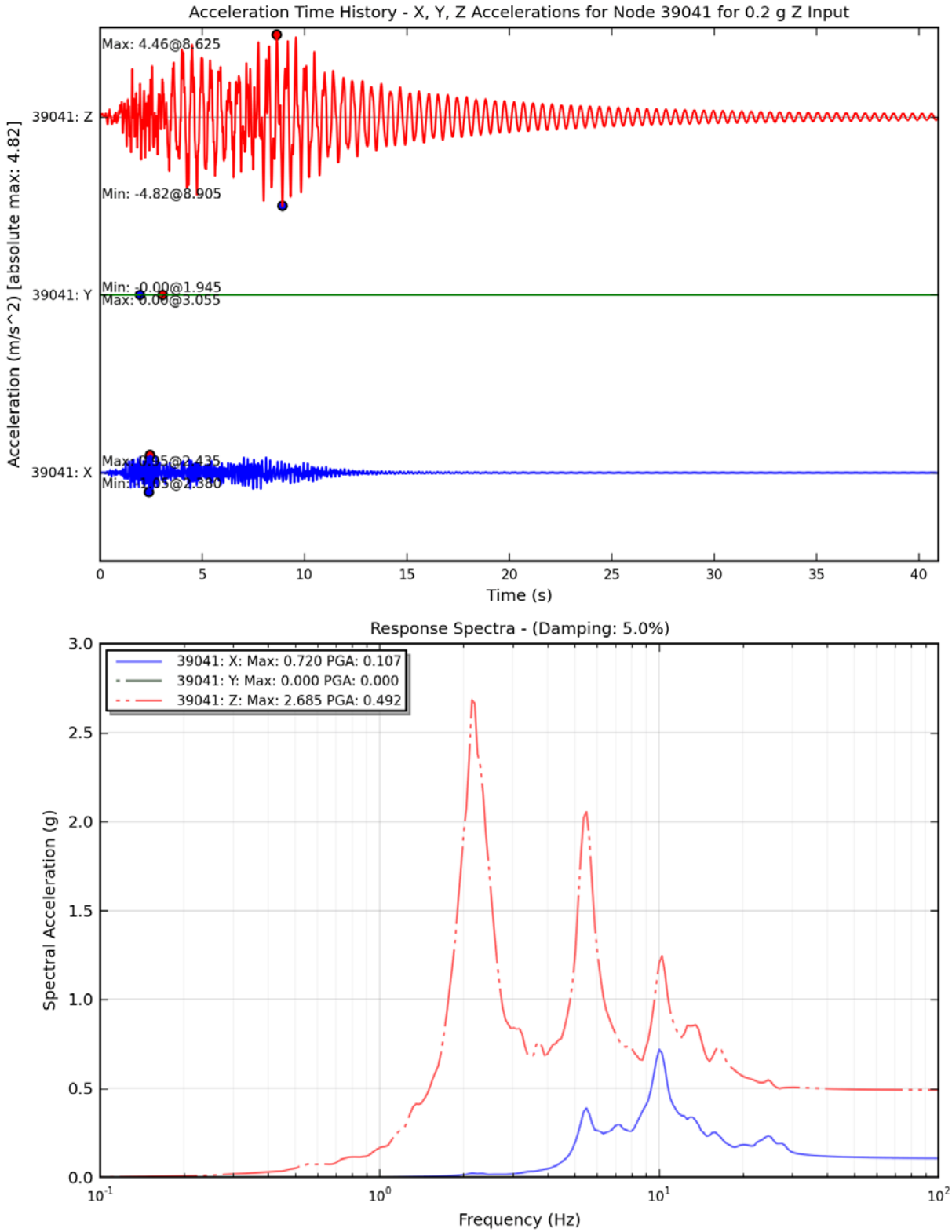

Figure 3-58 Response Acceleration Time Histories and ISRS at Node 39041 for Z Input Motion (0.2 g)

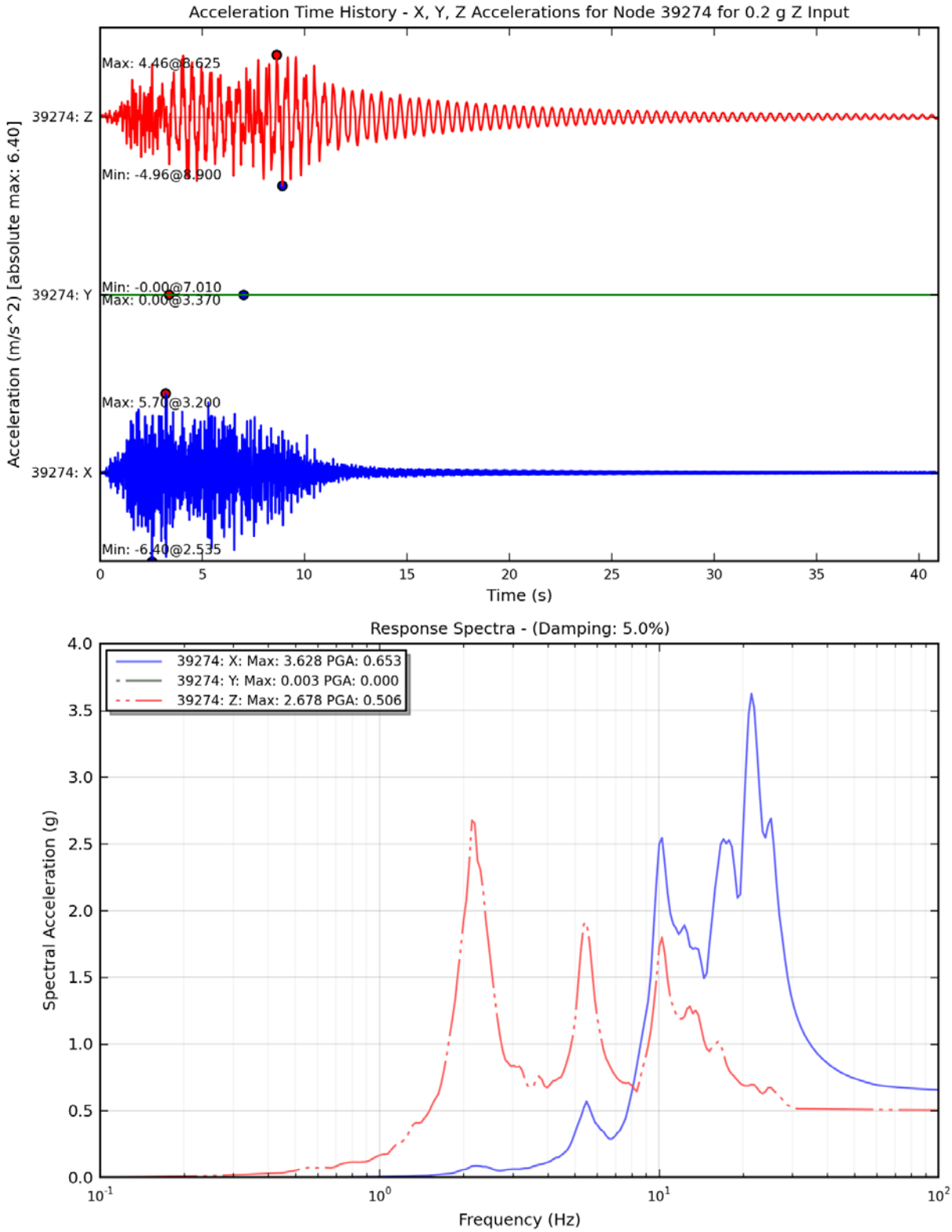

Figure 3-59 Response Acceleration Time Histories and ISRS at Node 39274 for Z Input Motion (0.2 g)

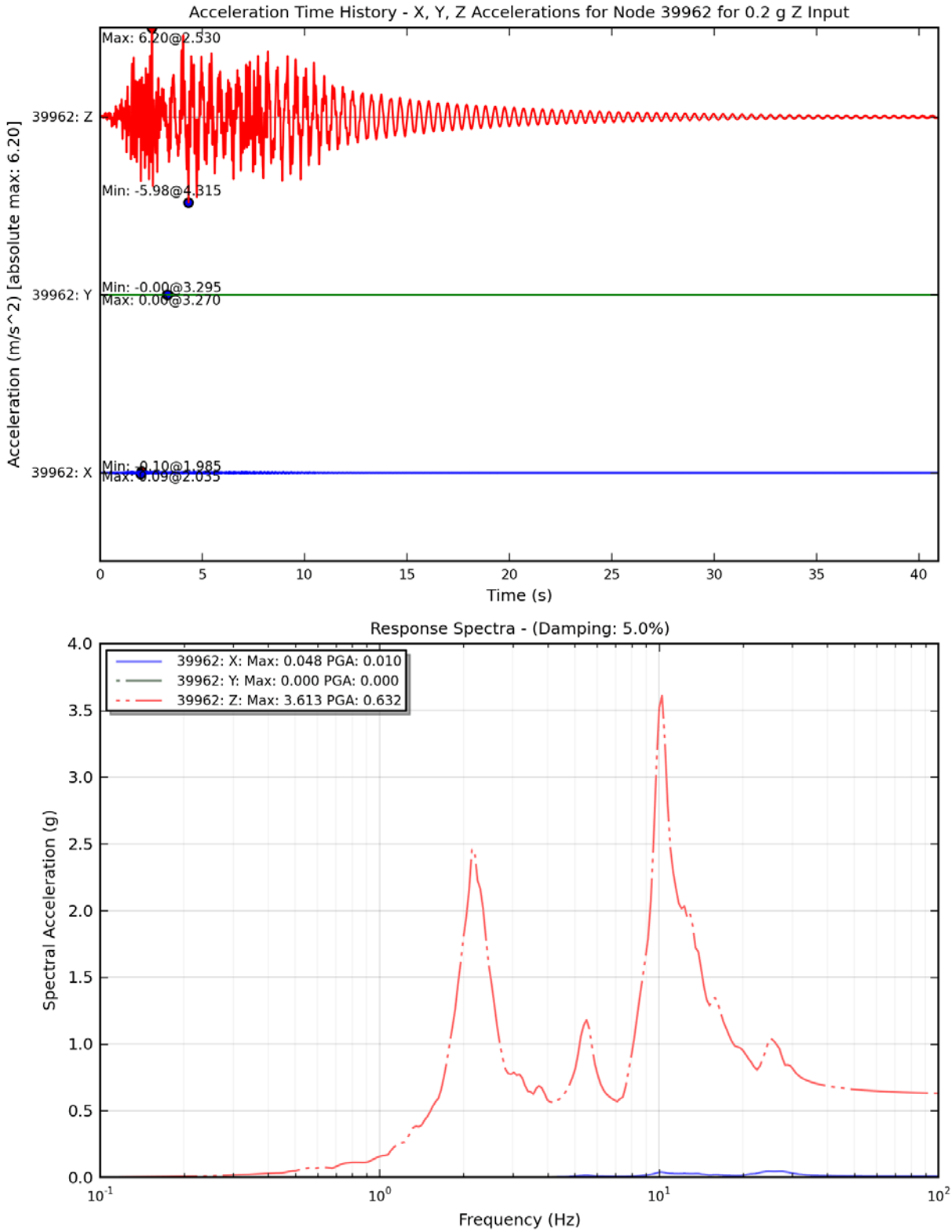

Figure 3-60 Response Acceleration Time Histories and ISRS at Node 39962 for Z Input Motion (0.2 g)

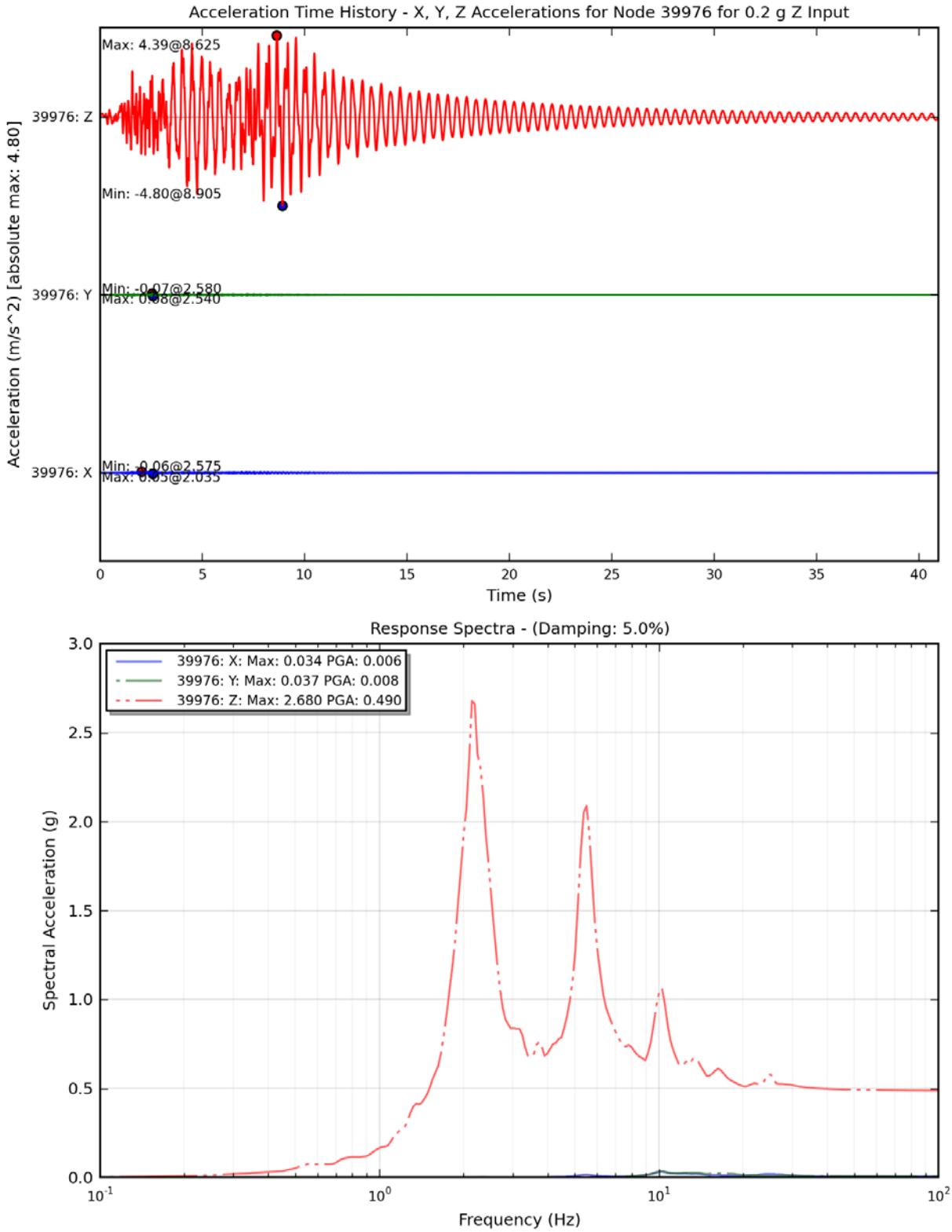

Figure 3-61 Response Acceleration Time Histories and ISRS at Node 39976 for Z Input Motion (0.2 g)

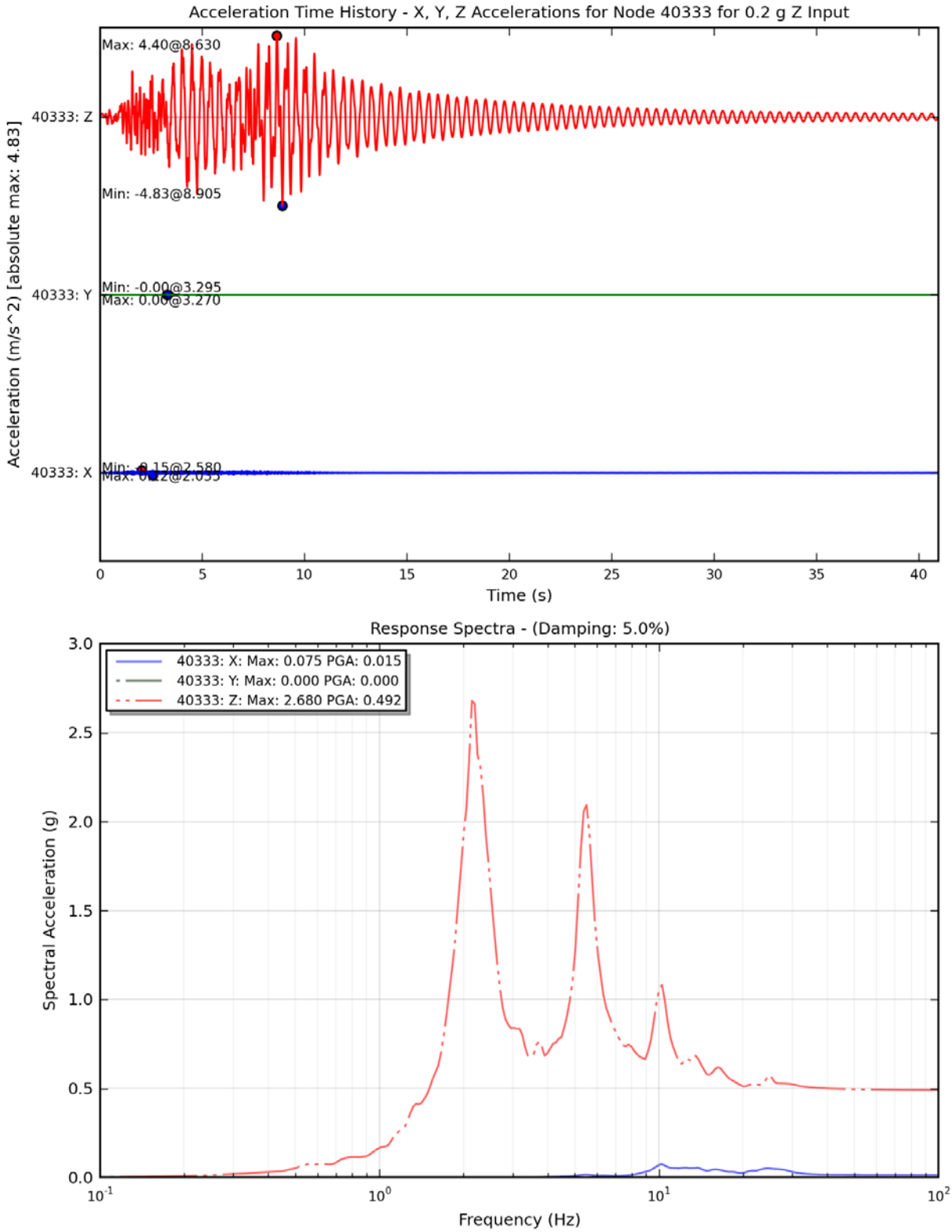

Figure 3-62 Response Acceleration Time Histories and ISRS at Node 40333 for Z Input Motion (0.2 g)

4 THE CASE OF 0.5 g

4.1 Summary of SASSI Results

This section describes the SASSI results for the case of a nominal bedrock peak acceleration of 0.5 g.

Section 4.2 includes acceleration time history and response spectral figures for the X directional input, while Section 4.3 includes figures for the Z directional input.

The acceleration time histories are output directly from the SASSI computer code. The ISRS were calculated outside of SASSI for each of these acceleration time histories, separately for the two input motions in the X and Z directions. All maximum acceleration values are rounded to the second decimal place. It should be noted that the input motion, used in both DIABLO and SASSI analyses, was not baseline-corrected, and neither were the response accelerations shown in this document. In addition, the acceleration time histories should not be integrated to obtain velocity or displacement time histories.

In summary, results are presented as follows:

Accelerations – Maximum values and time history plots
ISRS – Acceleration response spectra

The table and the footnotes were provided to BNL by LLNL in order for BNL to enter the SASSI results. All items in red denote SASSI node/element information. Where an "x" is presented in the table, the data is not available.

Table 4-1 SASSI Results for the Case of 0.5 g

Roof Slab			
Response Parameter (unit) & Location	**Response Parameter Value for**		**Remarks**
	X-Dir Input Motion	**Vertical (Z) Input Motion**	
Maximum[(1)] X, Y, Z-Directional Accelerations m/s^2) at Node xx near the center of Roof Slab	5.69 0.00 0.04	0.33 0.00 15.72	Node (EXODUS:4140, CUBIT:8789, SASSI-39962): Located (0.0,0.0,13.5)m
Maximum[(1)] X, Y, Z-Directional Displacements (m) at Node xx near the center of Roof Slab	x	x	Node (EXODUS:4140, CUBIT:8789, SASSI-39962): Located (0.0,0.0,13.5)m
Maximum[(1)] out-of-plane Bending Moment about X and Y axes (N-m/m) at Node xx near the center of the Roof Slab	x	x	Element (EXODUS:4452, CUBIT:9444, SASSI- (710, 8, 3)): Located (0.0,0.0,13.5)m
X, Y, Z-Directional Acceleration ISRSs (in 'g'unit) at Node xx near the center of Roof Slab	See figure for 39962	See figure for 39962	Node (EXODUS:4140, CUBIT:8789, SASSI-39962): Located (0.0,0.0,13.5)m
X, Y, Z-Directional Acceleration ISRSs (in 'g'unit) at Node xx and Node YY near the edges of Roof Slab	See figures for 40333 and 39976	See figures for 40333 and 39976	Node (EXODUS:3962, CUBIT:4922, SASSI-40333): Located (14.0,0.0,13.5)m Node (EXODUS:4145, CUBIT:1142, SASSI-39976): Located (0.0,14.0,13.5)m
Third Floor Slab			
Maximum[(1)] X, Y, Z-Directional Accelerations (m/s^2) at Node xx near the center of Slab	4.99 0.00 0.03	0.27 0.00 15.54	Node (EXODUS:3436, CUBIT:8193, SASSI-38557): Located (0.0, 0.0, 6.5) m
Maximum[(1)] X, Y, Z-Directional Displacements m) at Node xx near the center of Slab	x	x	Node (EXODUS:3436, CUBIT:8193, SASSI-38557): Located (0.0, 0.0, 6.5) m
Maximum[(1)] out-of-plane Bending Moment about X and Y axes N-m/m) at Node xx near the center of the Slab	x	x	Element (EXODUS:3258, CUBIT:8250, SASSI- (146, 7, 3)): Located (0.0, 0.0, 6.5) m
X, Y, Z-Directional Acceleration ISRSs (in 'g'unit) at Node xx near the center of Slab	See figure for 38557	See figure for 38557	Node (EXODUS:3436, CUBIT:8193, SASSI-38557): Located (0.0, 0.0, 6.5) m

X, Y, Z-Directional Acceleration ISRSs (in 'g'unit) at Node xx and Node YY near the edges of Slab	See figures for 38876 and 38569	See figures for 38876 and 38569	Node (EXODUS:3321, CUBIT:4747, SASSI-38876): Located (14.0,0.0,6.5)m Node (EXODU:3493, CUBIT:39, SASSI-38569): Located (0.0,14.0,6.5)m
Second Floor Slab			
Maximum[1] X, Y, Z-Directional Accelerations m/s^2) at Node xx near the center of Slab	3.61 0.00 0.50	0.32 0.00 13.49	Node (EXODUS:675, CUBIT:5718, SASSI-27948): Located (3.125, 0.0, -9.144)m
Maximum[1] X, Y, Z-Directional Displacements (m) at Node xx near the center of Slab	x	x	Node (EXODUS:675, CUBIT:5718, SASSI-27948): Located (3.125, 0.0, -9.144)m
Maximum[1] out-of-plane Bending Moment about X and Y axes (N-m/m) at Node xx near the center of the Slab	x	x	Element (EXODUS:2627, CUBIT:7619, SASSI- (65, 6, 3)): Located (3.125, 0.0, -9.144)m
X, Y, Z-Directional Acceleration ISRSs (in 'g'unit) at Node xx near the center of Slab	See figure for 27948	See figure for 27948	Node (EXODUS:675, CUBIT:5718, SASSI-27948): Located (3.125, 0.0, -9.144)m
X, Y, Z-Directional Acceleration ISRSs (in 'g'unit) at Node xx and Node YY near the edges of Slab	See figures for 28514 and 27782	See figures for 28514 and 27782	Node (EXODUS:2676, CUBIT:3872, SASSI-28514): Located (14.0,0.0,-9.144)m Node (EXODUS:2993, CUBIT:231, SASSI- 27782) Located (-0.1818,14.0,-9.144)m
First Floor Slab			
Maximum[1] X, Y, Z-Directional Accelerations m/s^2) at Node xx near the center of Slab	2.95 0.00 0.48	0.40 0.00 11.75	Node (EXODUS:435, CUBIT:5532, SASSI-14522): Located(3.125,0.0,-22.5552)m
Maximum[1] X, Y, Z-Directional Displacements (m) at Node xx near the center of Slab	x	x	Node (EXODUS:435, CUBIT:5532, SASSI-14522): Located(3.125,0.0,-22.5552)m
Maximum[1] out-of-plane Bending Moment about X and Y axes (N-m/m) at Node xx near the center of the Slab	x	x	Element (EXODUS:2224, CUBIT:7216, SASSI- (279, 5, 3)): Located(3.125,0.0,-22.5552)m

X, Y, Z-Directional Acceleration ISRSs (in 'g'unit) at Node xx near the center of Slab	See figure for 14522	See figure for 14522	Node (EXODUS:435, CUBIT:5532, SASSI-14522): Located(3.125,0.0,-22.5552)m
X, Y, Z-Directional Acceleration ISRSs (in 'g'unit) at Node xx and Node YY near the edges of Slab	See figures for 15095 and 14364	See figures for 15095 and 14364	Node (EXODUS:2055, CUBIT:4122, SASSI-15095): Located (14.00,0.0,-22.5552) Node (EXODUS:2363, CUBIT:486, SASSI- 14364): Located(-0.1818,14.0,-22.5552)
Base Mat			
Maximum[(1)] X, Y, Z-Directional Accelerations (m/s^2) at Node xx near the center of Slab	3.90 0.00 0.02	0.09 0.00 12.09	Node (EXODUS:1319, CUBIT:6413, New basemat 9828, SASSI- 1942): Located (0.0,0.0,-34.5)
Maximum[(1)] X, Y, Z-Directional Displacements (m) at Node xx near the center of Slab	x	x	Node (EXODUS:1319, CUBIT:6413, New basemat 9828, SASSI- 1942): Located (0.0,0.0,-34.5)
Maximum[(1)] out-of-plane Bending Moment about X and Y axes (N-m/m) at Node xx near the center of the Slab	x	x	Element (EXODUS:1299, CUBIT:6413, New basemat 19363 (+X+Y to node 9828), SASSI- (351, 4, 3)): Located (0.0,0.0,-34.5)
X, Y, Z-Directional Acceleration ISRSs (in 'g'unit) at Node xx near the center of Slab	See figure for 1942	See figure for 1942	Node (EXODUS:1319, CUBIT:6413, New basemat 9828, SASSI- 1942): Located (0.0,0.0,-34.5)
X, Y, Z-Directional Acceleration ISRSs (in 'g'unit) at Node xx and Node YY near the edges of Slab	See figures for 2949 And 1887	See figures for 2949 And 1887	Node (EXODUS:1384, CUBIT:4447, SASSI- 2949): Located (14,0.0,-34.5)m Node (EXODUS:1700, CUBIT:835, SASSI- 1887): Located (0.909,14.0,-34.5)m
Reactor Vessel and Supports			
Maximum[(1)] X, Y, Z-Directional Displacements (m) at Node xx near the top Cover Plate of the Reactor Vessel	x	x	Node (EXODUS:27, CUBIT:5122, SASSI-32546): Located (0.0,0.0,-4.5)m

Maximum[1] out-of-plane Bending Moments about X and Y axes (N-m/m) at Node xx near the top Cover Plate of the Reactor Vessel	x	x	Element (EXODUS:14, CUBIT:5006, SASSI- (14, 1, 3)): Located (0.0,0.0,-4.5)m
Maximum[1] out-of-plane Bending Moments about X and Y axes (N-m/m) at Node xx of the Reactor Support Ring Plate		x	Element (EXODUS:4460, CUBIT:9452, SASSI- (2, 9, 3)): Located (2.0,0.0,-20.5)m Element (EXODUS:4486. CUBIT:9478, SASSI- (28, 9, 3)): Located (0.0,2.0,-20.5)m
Reactor Building Walls			
Maximum out-of-plane bending moments about X and Y axes (N-m/m) at Elev XX (4 Nodes, one in each wall near the center)	x	x	Elevation 1 Element (EXODUS:4503, CUBIT:13), SASSI- (13, 10, 3) located: (0.0,14.0,0.0)m Element(EXODUS: 8351, CUBIT:3861), SASSI- (3861, 10, 3) Located: (14.0,0.0,0.0) Element (EXODUS:5751, CUBIT:1261) , SASSI- (1261, 10, 3) Located: (0.0, -14.0,0.0)m Element(EXODUS: 6999, CUBIT:2509) SASSI- (2509, 10, 3) Located: (-14.0, 0.0, 0.0)m Elevation 2 Element (EXODUS:7571, CUBIT:3081), SASSI- (3081, 10, 3) Located: (-14.0,0.0, -16.36541)m Element (EXODUS:6323, CUBIT:1833) SASSI- (1833, 10, 3) Located: (-0.1818, -14.00, -16.36541)m Element (EXODUS:8637, CUBIT:4147), SASSI- (4147, 10, 3)Located: (14.00, 0.0, -16.36541)m Element (EXODUS:5075, CUBIT:585) SASSI- (585, 10, 3): Located: (-0.1818, 14.00, -16.36541)m

Maximum soil pressure in X and Y direction (in psi Pa) at 4 Nodes, one in each outer wall near the center	x	x	Elevation 1 Element(EXODUS: 8351, CUBIT:3861) StructSoil: 24702, SASSI-(900, 101, 1) Located: (14.0,0.0,0.0) Element Element(EXODUS: 6999, CUBIT:2509) Located: (-14.0, 0.0, 0.0)m Elevation 2 Element (EXODUS:7571, CUBIT:3081) StructSoil: 22828, SASSI-(1060, 102, 1) Located: (-14.0,0.0, -16.36541)m Element (EXODUS:6323, CUBIT:1833) StructSoil: 22282, SASSI-(514, 102, 1) Located: (-0.1818, -14.00, -16.36541)m Element (EXODUS:8637, CUBIT:4147) StructSoil: 22321, SASSI-(553, 102, 1) Located: (14.00, 0.0, -16.36541)m Element (EXODUS:5075, CUBIT:585): StructSoil: 22516, SASSI-(748, 102, 1) Located: (-0.1818, 14.00, -16.36541)m

Maximum in-plane shear stress(Pa) in the reactor building X and Y-Dir outer walls at 8 Nodes, two in each outer wall (one near the center, one near the edge)			Set 1 Element (EXODUS:5544, CUBIT:1054) SASSI- (1054, 10, 3) Located: (-0.1818,14.00,-34.5) Element (EXODUS:5554, CUBIT:1064) SASSI- (1064, 10, 3) Located: (10.7272,14.00,-34.5) Set 2 Element (EXODUS:9106, CUBIT:4616) SASSI- (4616, 10, 3) Located: (14.00, 0.0, -34.5) Element (EXODUS:9116, CUBIT:4626) SASSI- (4626, 10, 3) Located: (14.00,-10.7692,-34.5) Set 3 Element (EXODUS:6791, CUBIT:2301) SASSI- (2301, 10, 3) Located: (-0.1818,-14.00,-34.5) Element (EXODUS:6781, CUNIT:2291) SASSI- (2291, 10, 3) Located: (-11.00, -14.00,-34.5) Set 4 Element (EXODUS:8039, CUBIT:3549) SASSI- (3549, 10, 3) Located: (-14.00, 0.0, -34.5)
Lumped-Mass Stick Models			

X, Y, Z-Directional Acceleration ISRSs (in 'g'unit) at the top and the bottom node of each stick	See figures for the ISRSs for these nodes.	See figures for the ISRSs for these nodes.	Node EXODUS 1893, Cubit 9396 Node EXODUS 1330, Cubit 9400 Node EXODUS 2554, Cubit 9404 Node EXODUS 2001, Cubit 9420 Node EXODUS 3163, Cubit 9428 Node EXODUS 2674, Cubit 9436 Node EXODUS 3830, Cubit 9452 Node EXODUS 3619, Cubit 9456 See the following for beam bottom and top Node CUBIT 6918, Cubit 9396 SASSI-1021, 4904 Node CUBIT 6426, 9400 SASSI- 1182, 4905 Node CUBIT 7475, 9404 SASSI-13774, 22080 Node CUBIT 6993, 9420 SASSI-13886, 18132 Node CUBIT 7980, 9428 SASSI-27184, 31566 Node CUBIT 7550, 9436 SASSI-27296, 35500 Node CUBIT 8543, 9452 SASSI-38274, 39041 Node CUBIT 8338, 9456 SASSI-38328, 39274
Maximum Accelerations (m/s^2) at the top and bottom nodes of each "stick."	3.91 17.72	11.07 11.74	CUBIT 6918, 9396 SASSI-1021, 4904
	3.91 6.30	11.54 11.57	CUBIT 6426, 9400 SASSI- 1182, 4905
	2.93 7.78	12.17 12.18	CUBIT 7475, 9404 SASSI-13774, 22080

	2.94 2.71	12.70 12.73	CUBIT 6993, 9420 SASSI-13886, 18132
	3.61 4.60	12.59 12.60 17.45 (X, 31566; This denotes that the response in X direction is larger than the response in the Z direction*)	CUBIT 7980, 9428 SASSI-27184, 31566
	3.60 7.86	13.86 13.94 18.25 (X, 35500; see * above)	CUBIT 7550, 9436 SASSI-27296, 35500
	4.99 9.31	12.63 12.65	CUBIT 8543, 9452 SASSI-38274, 39041
	4.99 5.62	13.90 13.91 22.21 (X, 39274; see * above)	CUBIT 8338, 9456 SASSI-38328, 39274

Notes:

(1) The term "Maximum" is used to mean the maximum considering the entire time period for which the time-history analysis was performed.

4.2 Acceleration Time Histories and ISRS for the X Directional Input Motion

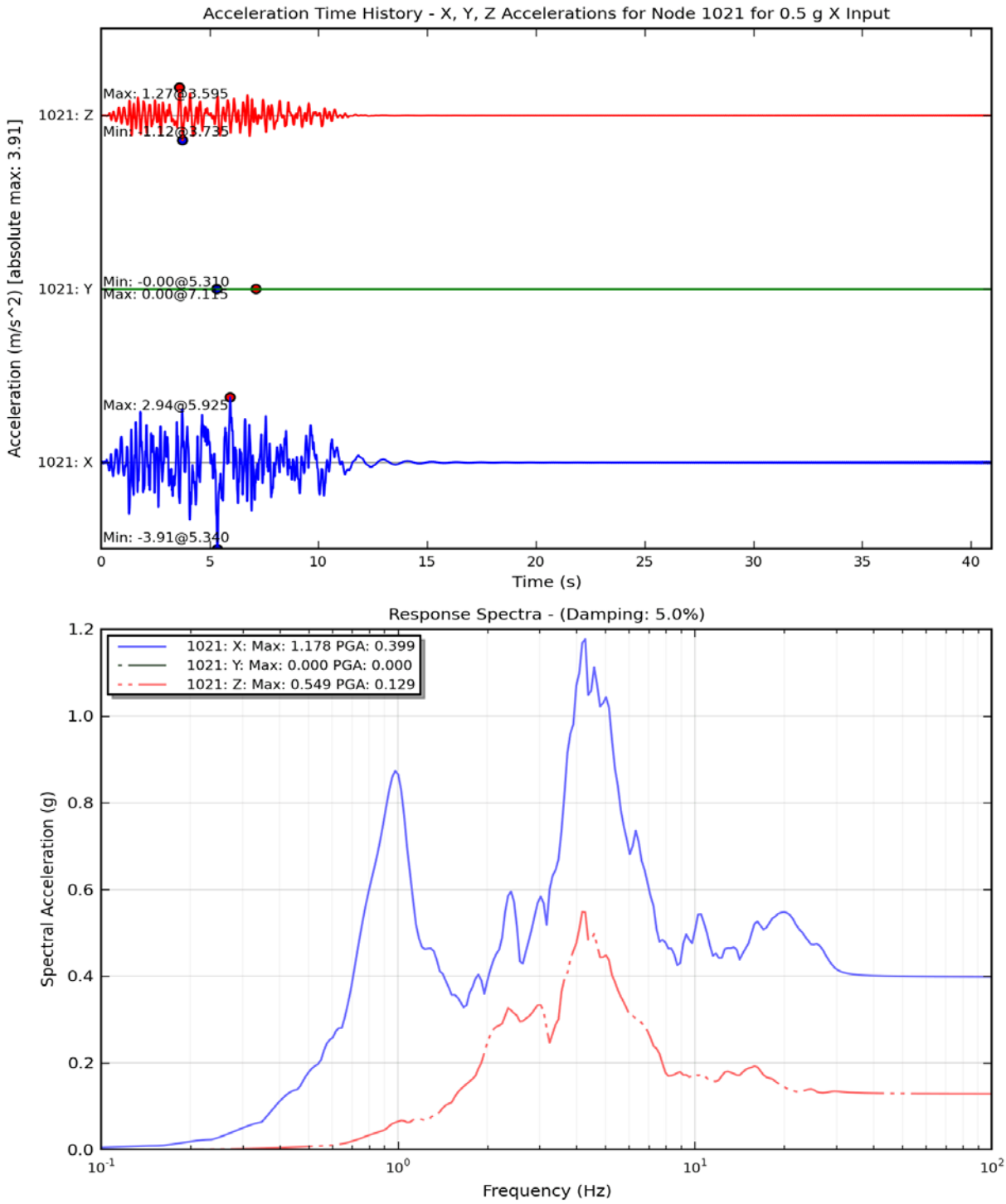

Figure 4-1 Response Acceleration Time Histories and ISRS at Node 1021 for X Input Motion (0.5 g)

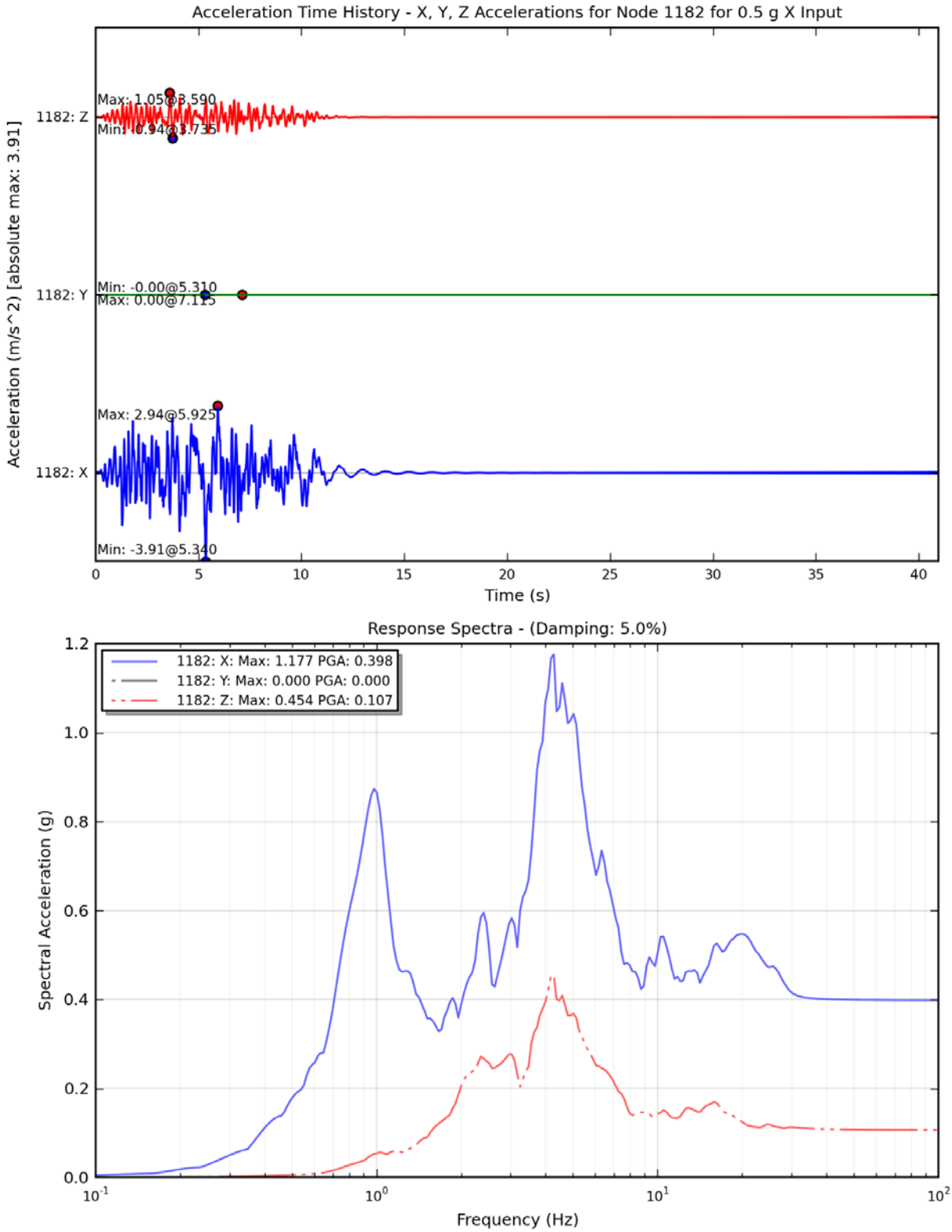

Figure 4-2 Response Acceleration Time Histories and ISRS at Node 1182 for X Input Motion (0.5 g)

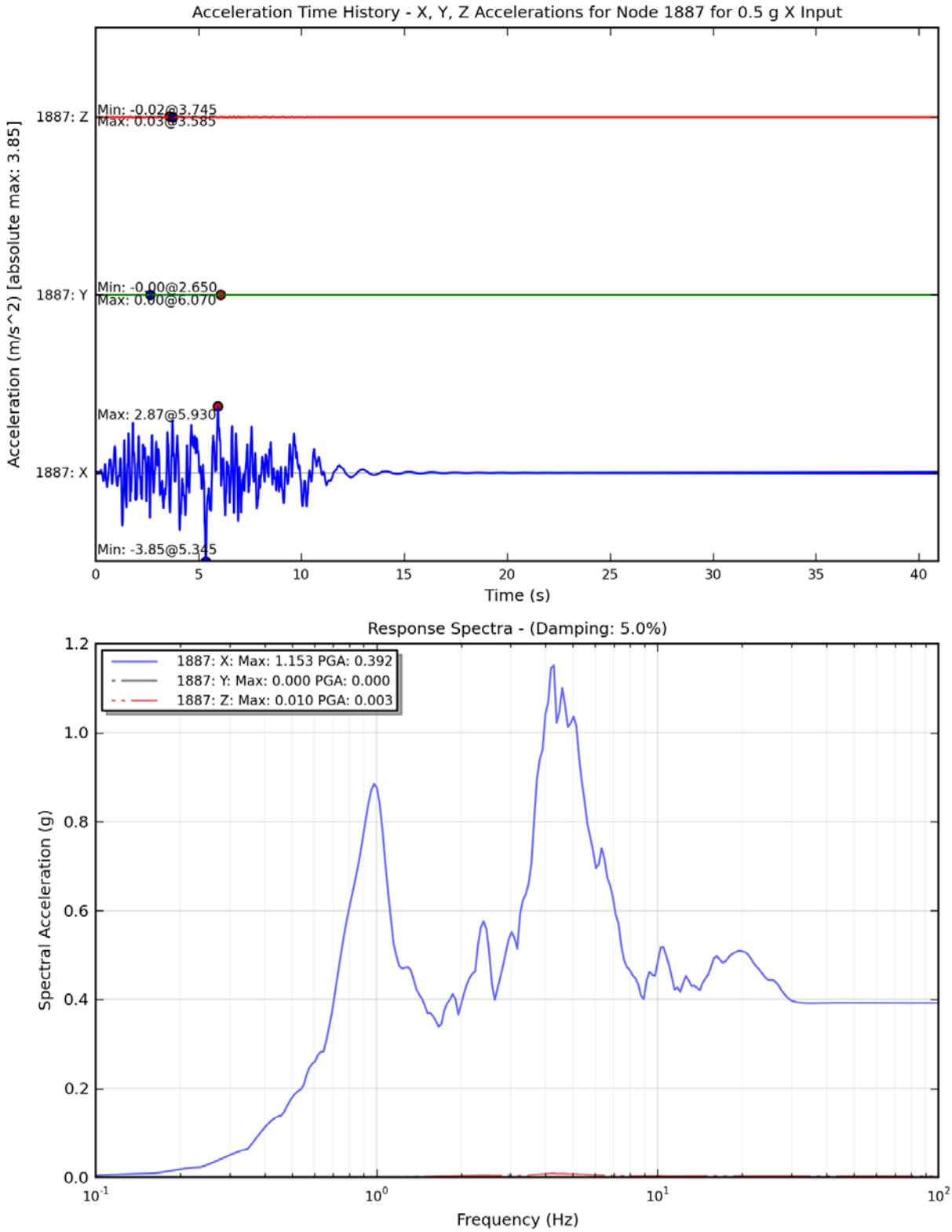

Figure 4-3 Response Acceleration Time Histories and ISRS at Node 1887 for X Input Motion (0.5 g)

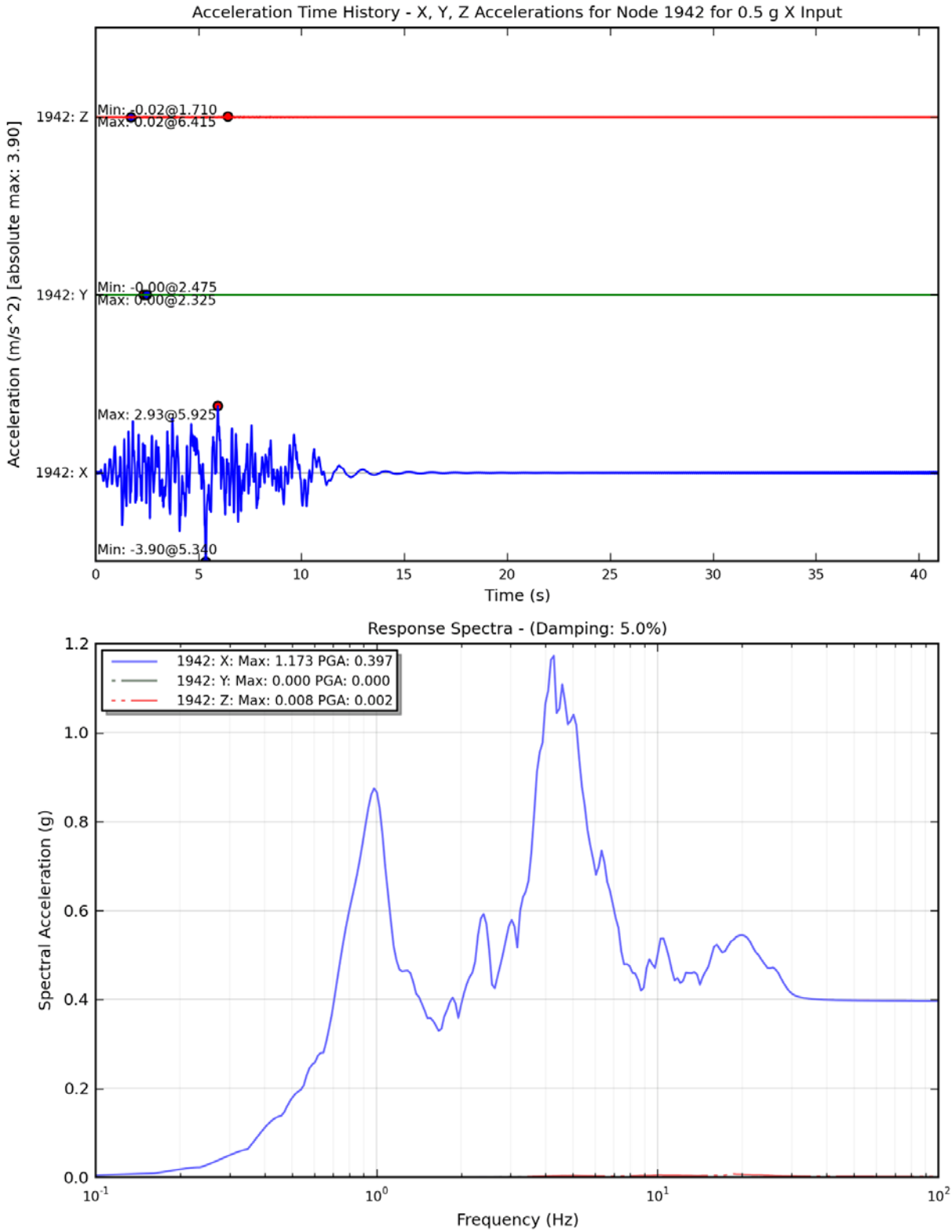

Figure 4-4 Response Acceleration Time Histories and ISRS at Node 1942 for X Input Motion (0.5 g)

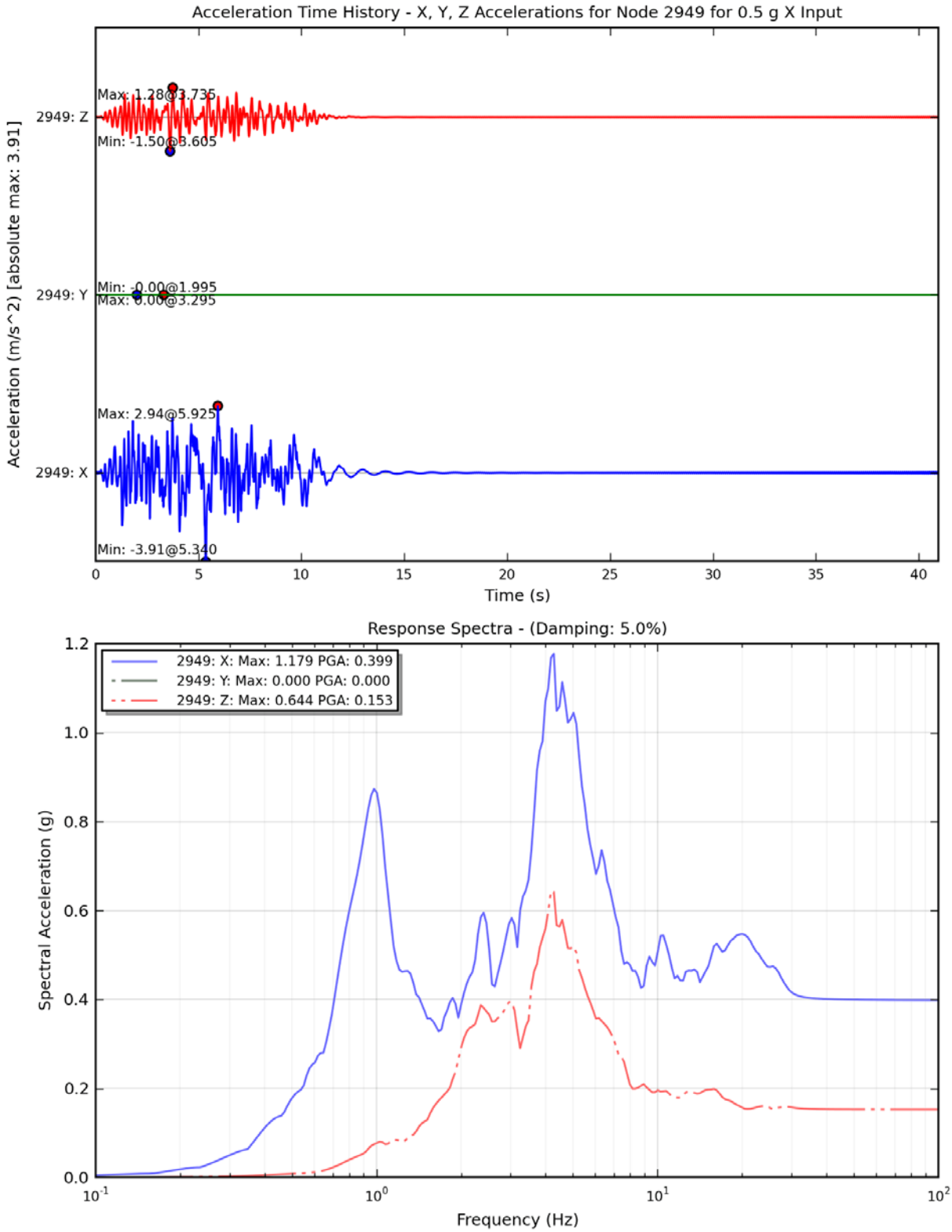

Figure 4-5 Response Acceleration Time Histories and ISRS at Node 2949 for X Input Motion (0.5 g)

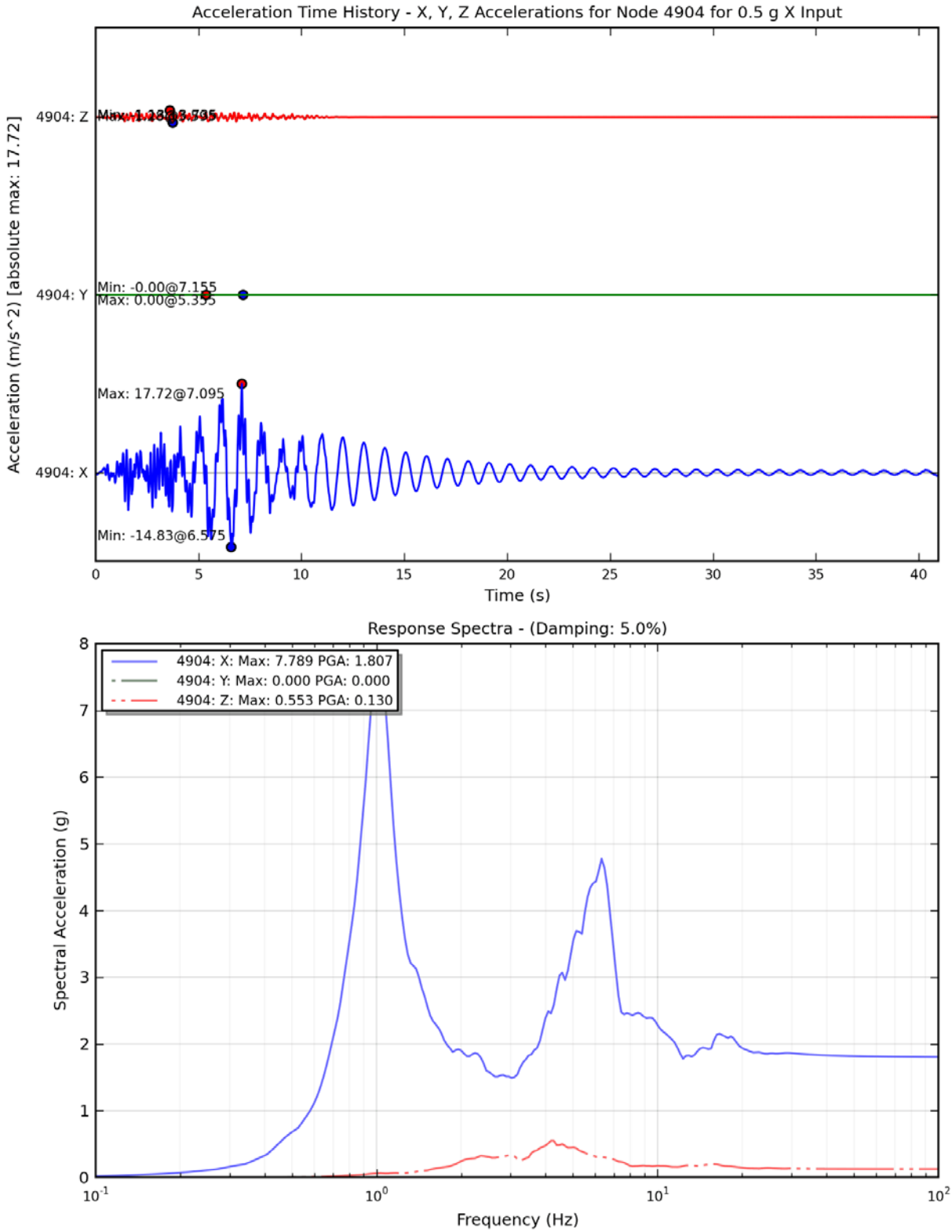

Figure 4-6 Response Acceleration Time Histories and ISRS at Node 4904 for X Input Motion (0.5 g)

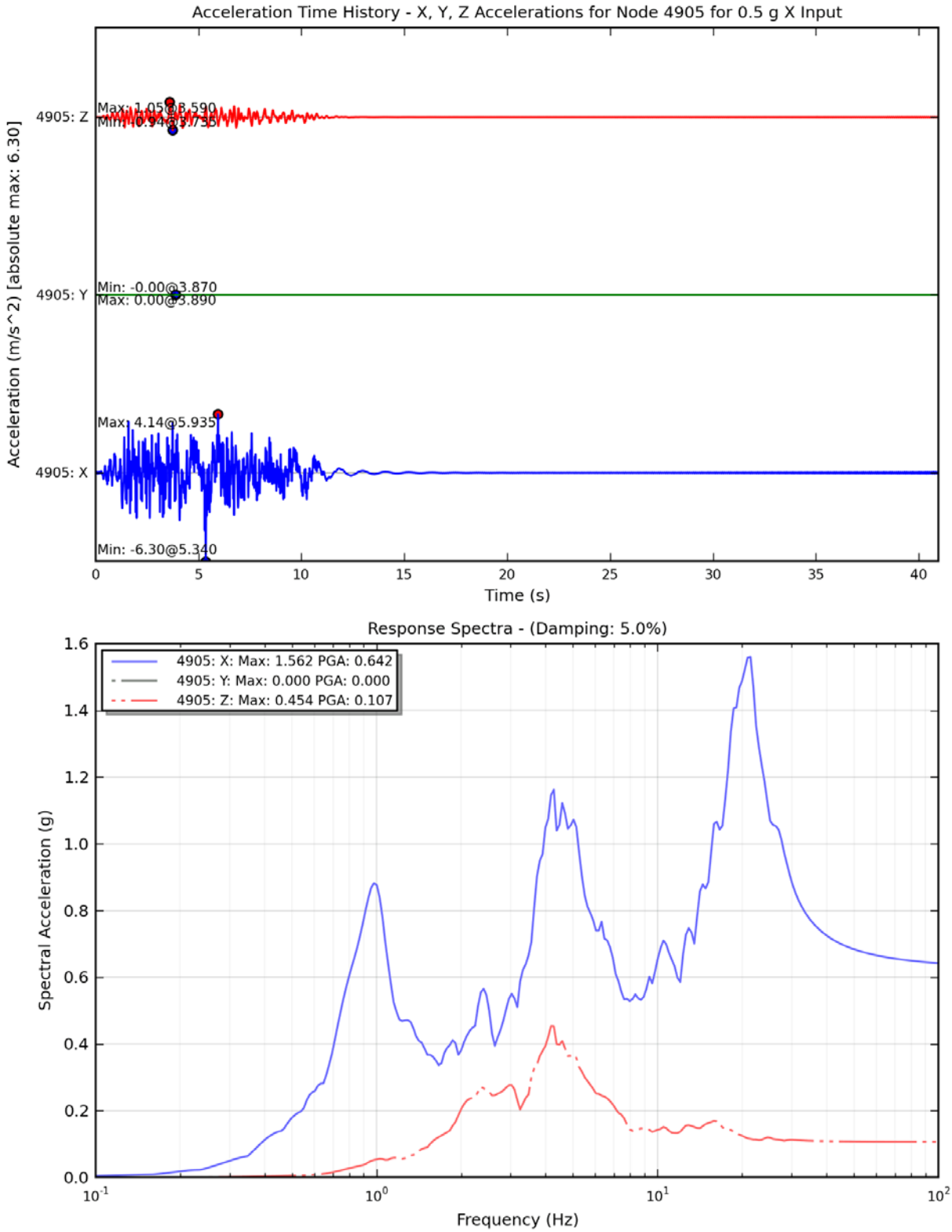

Figure 4-7 Response Acceleration Time Histories and ISRS at Node 4905 for X Input Motion (0.5 g)

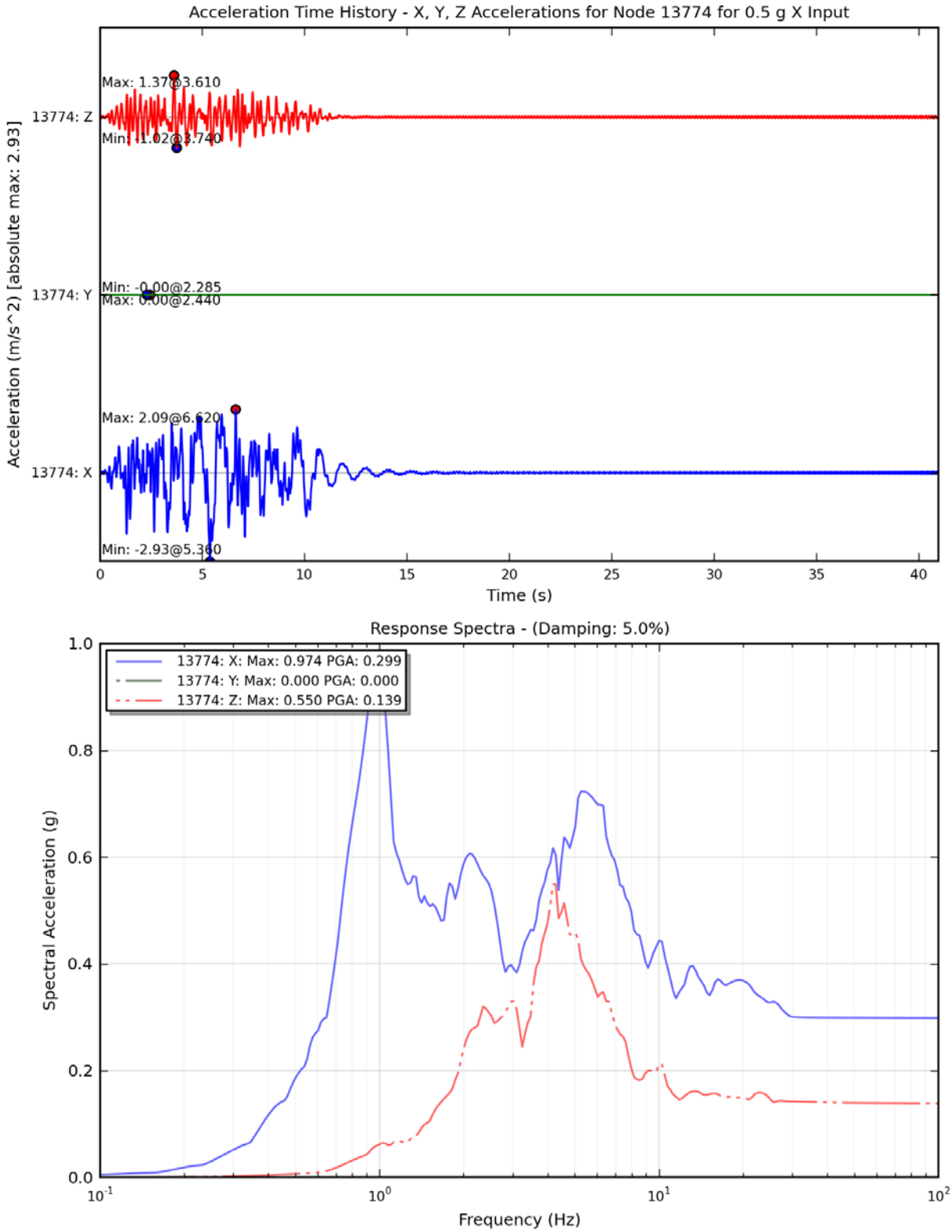

Figure 4-8 Response Acceleration Time Histories and ISRS at Node 13774 for X Input Motion (0.5 g)

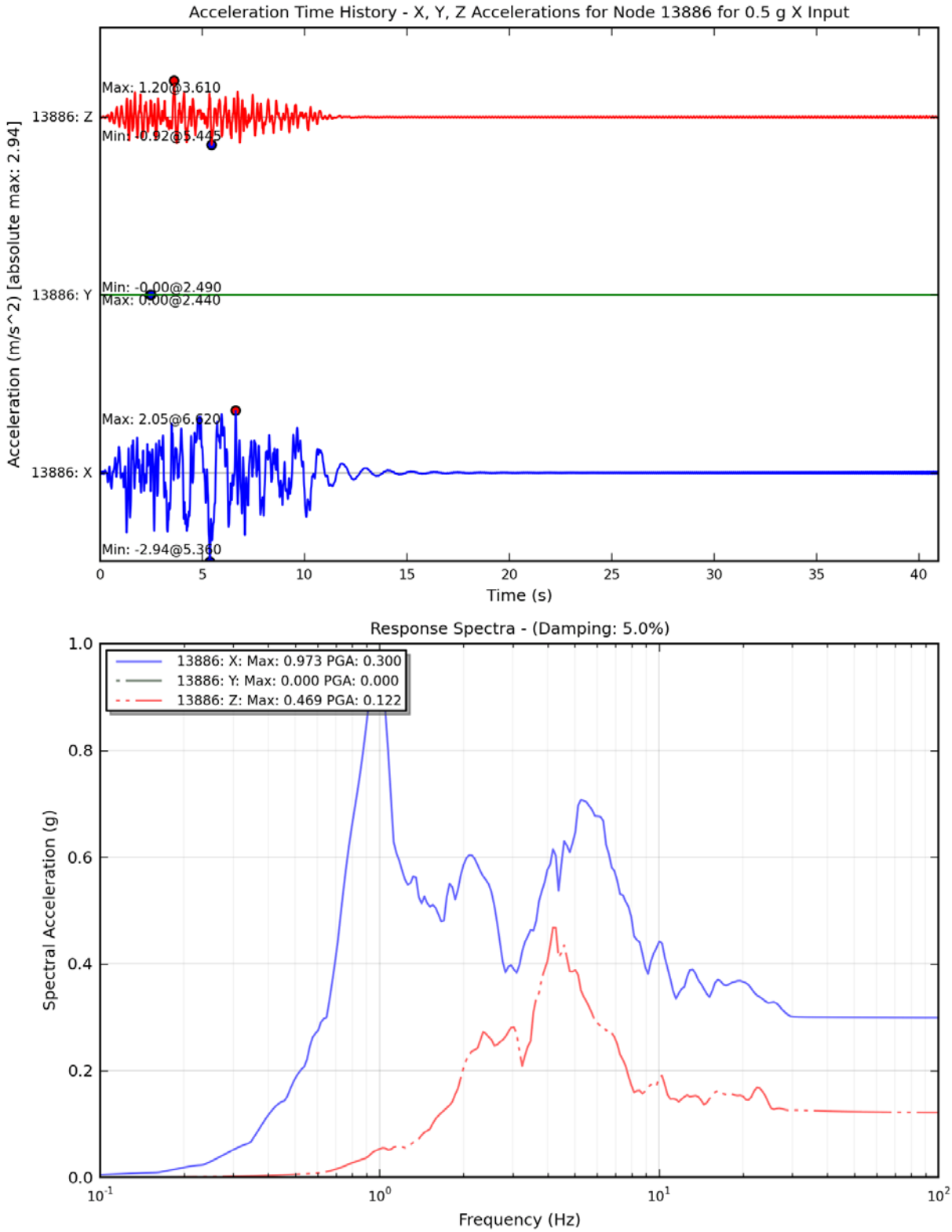

Figure 4-9 Response Acceleration Time Histories and ISRS at Node 13886 for X Input Motion (0.5 g)

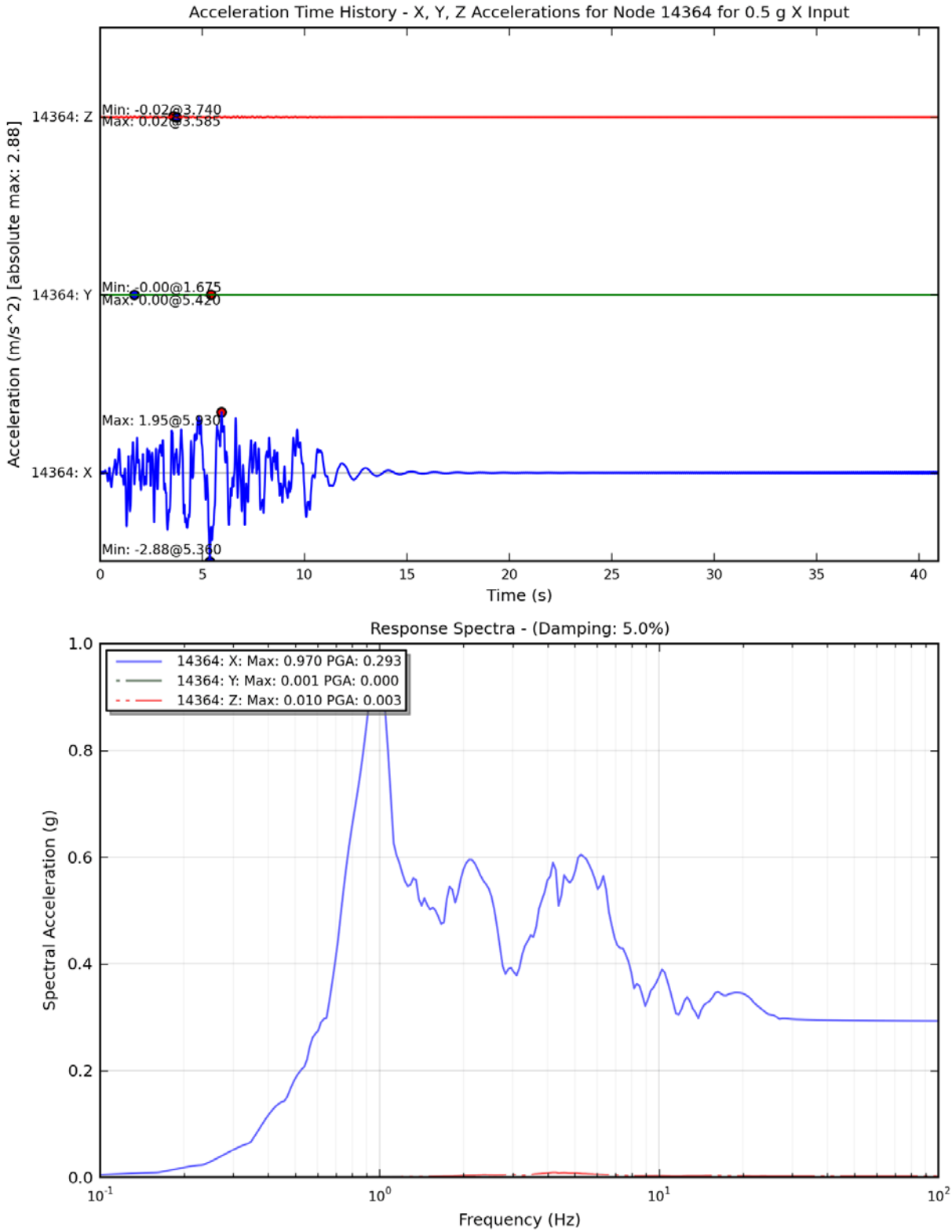

Figure 4-10 Response Acceleration Time Histories and ISRS at Node 14364 for X Input Motion (0.5 g)

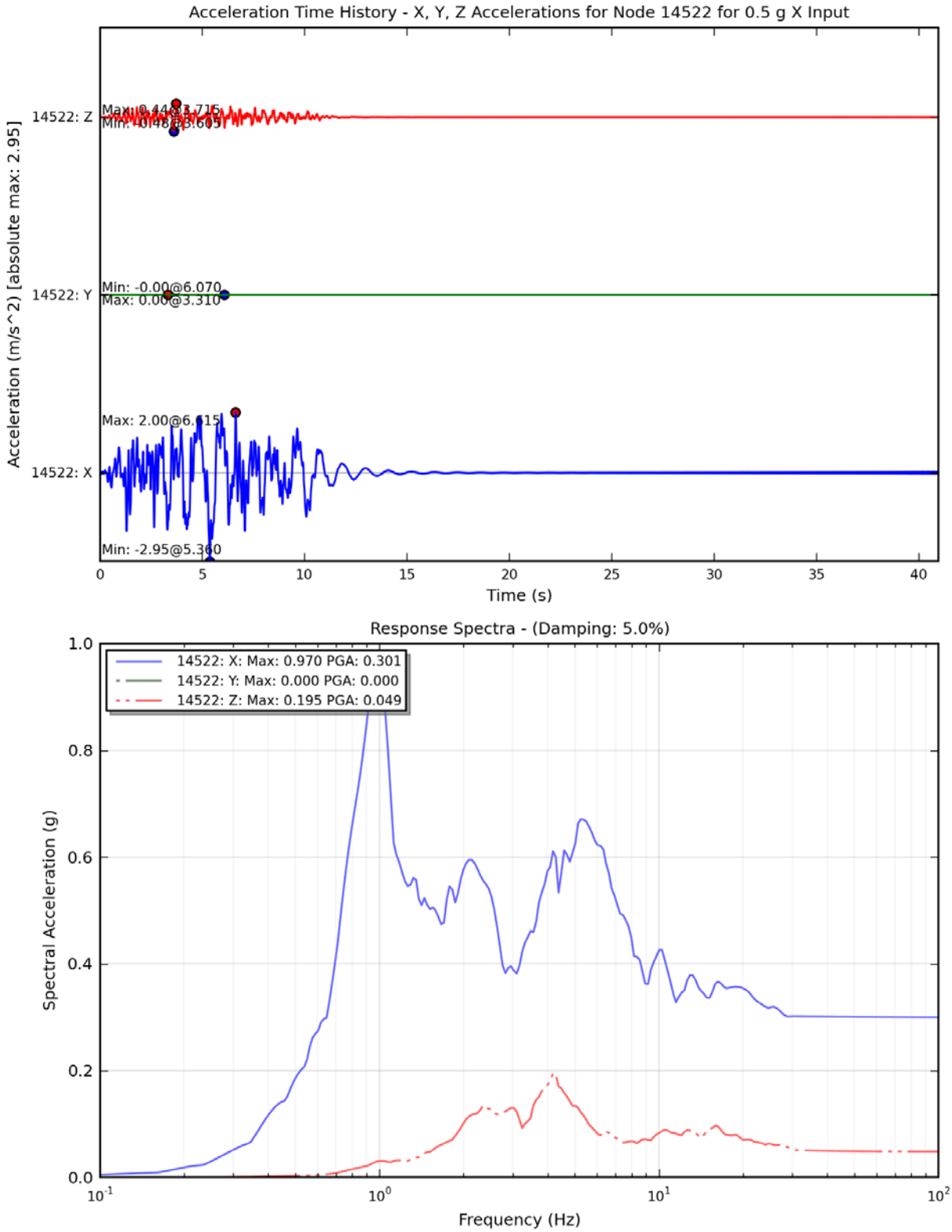

Figure 4-11 Response Acceleration Time Histories and ISRS at Node 14522 for X Input Motion (0.5 g)

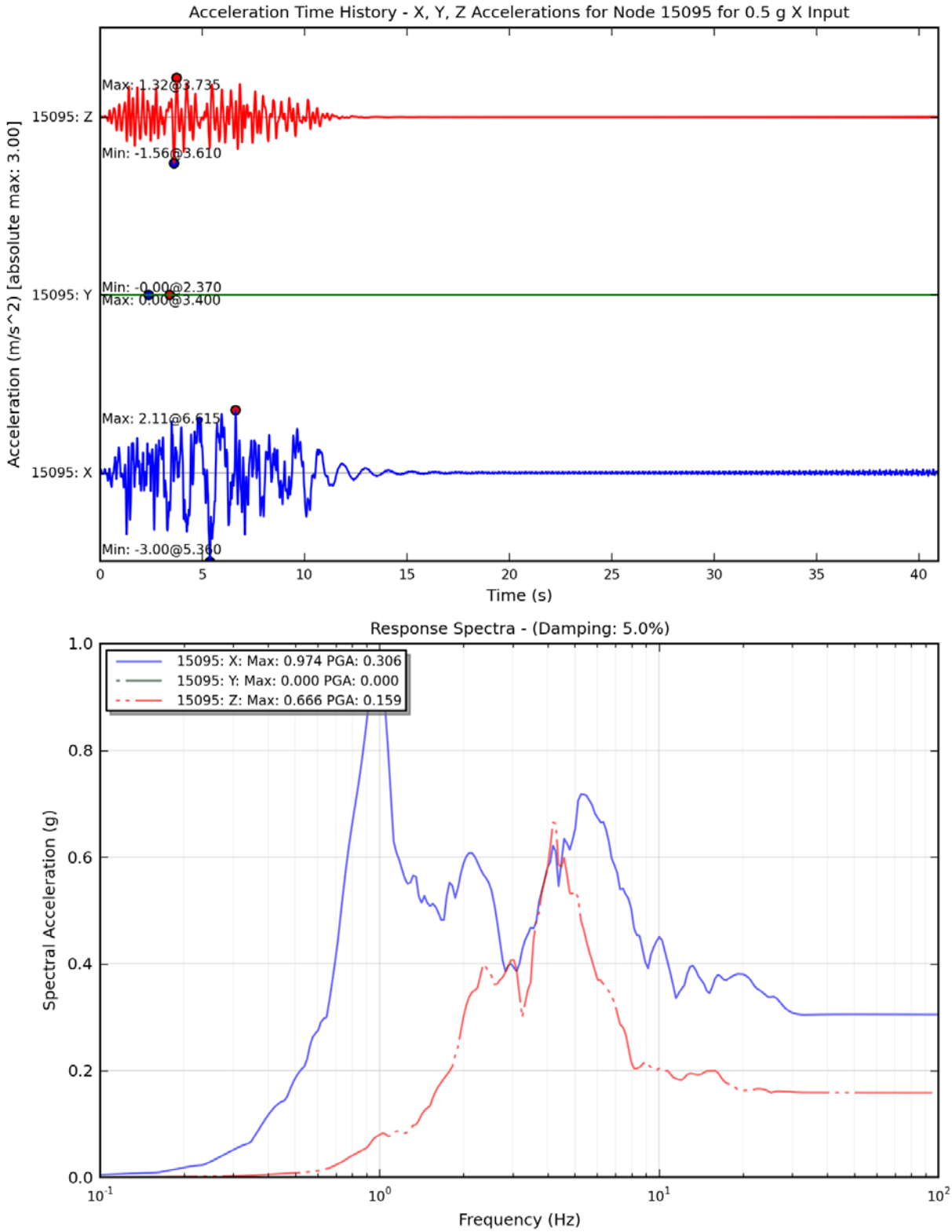

Figure 4-12 Response Acceleration Time Histories and ISRS at Node 15095 for X Input Motion (0.5 g)

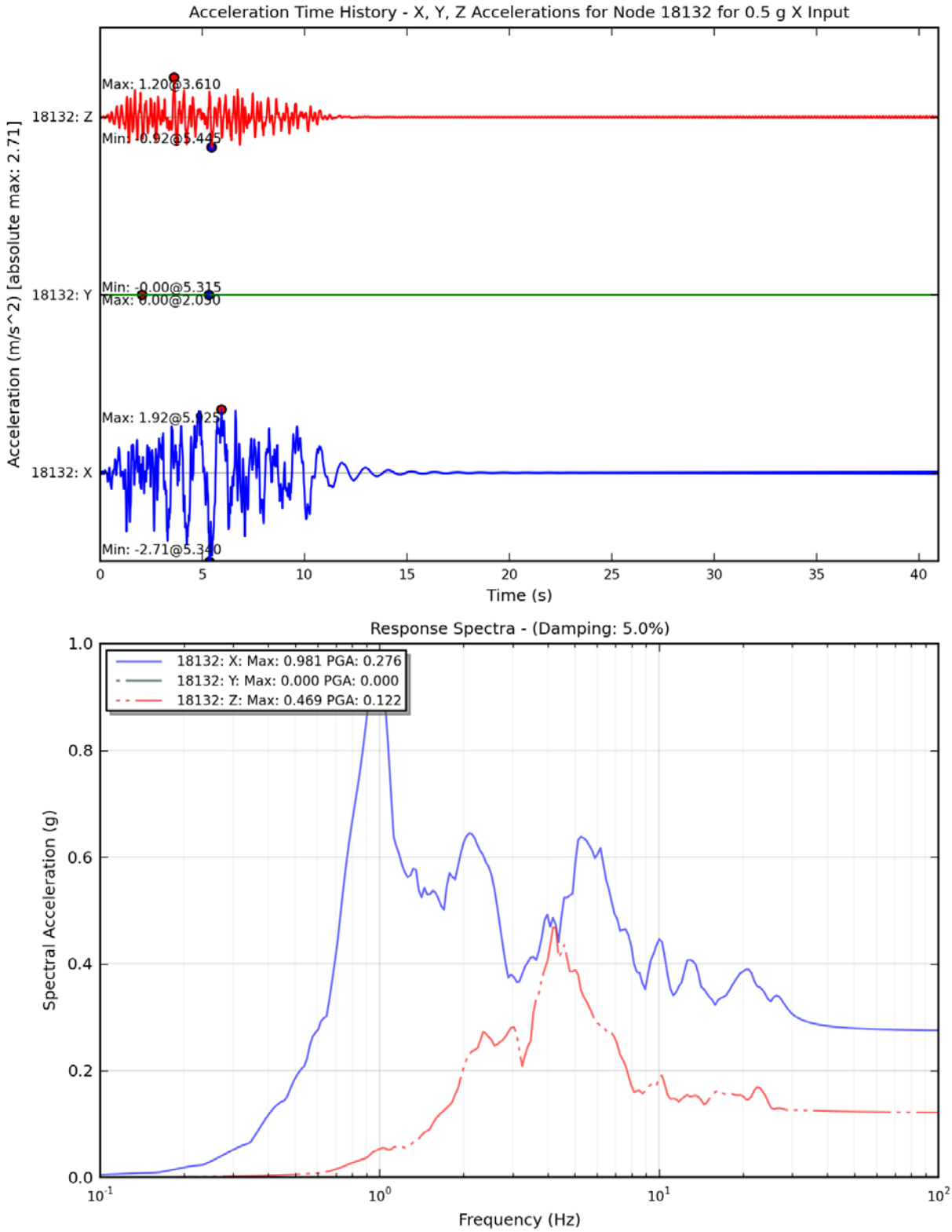

Figure 4-13 Response Acceleration Time Histories and ISRS at Node 18132 for X Input Motion (0.5 g)

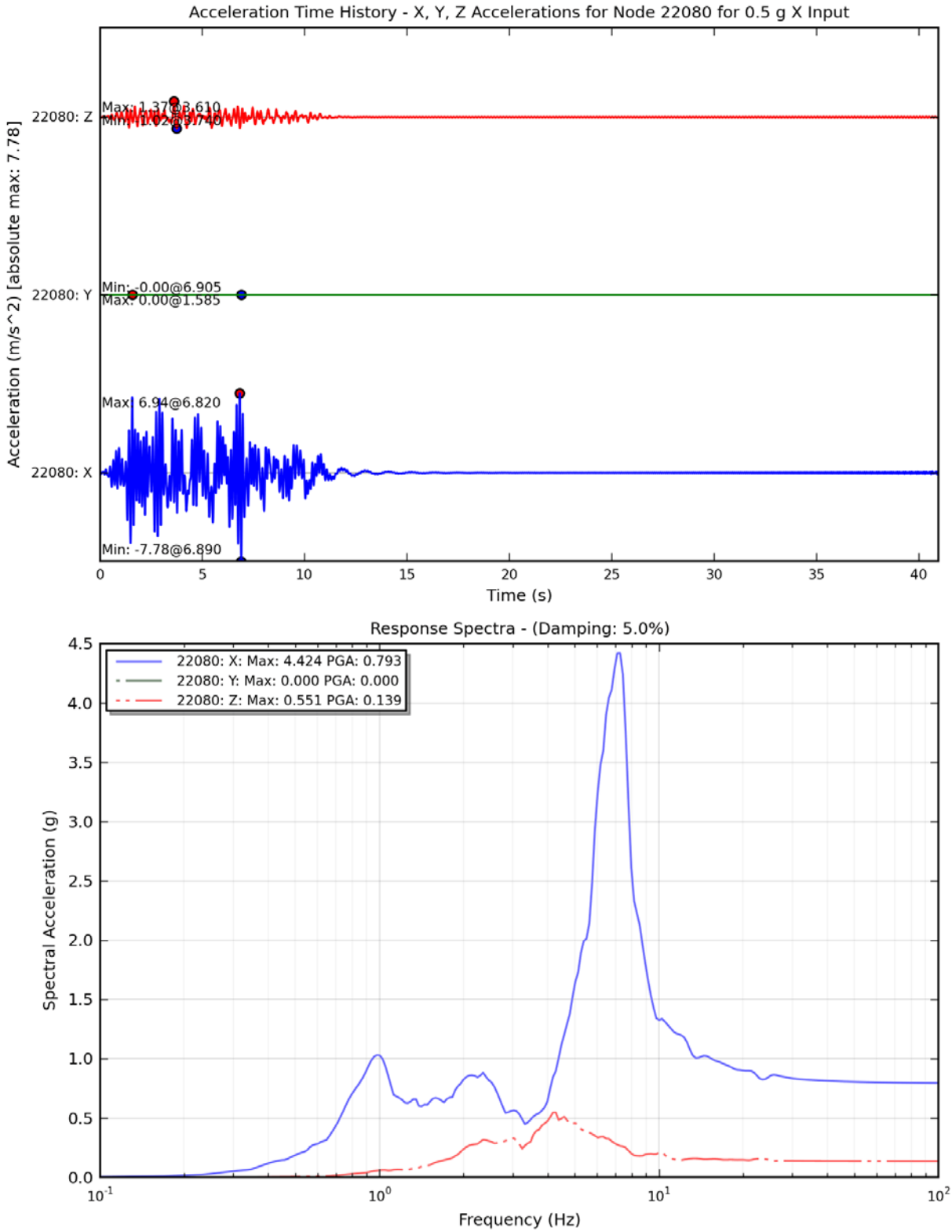

Figure 4-14 Response Acceleration Time Histories and ISRS at Node 22080 for X Input Motion (0.5 g)

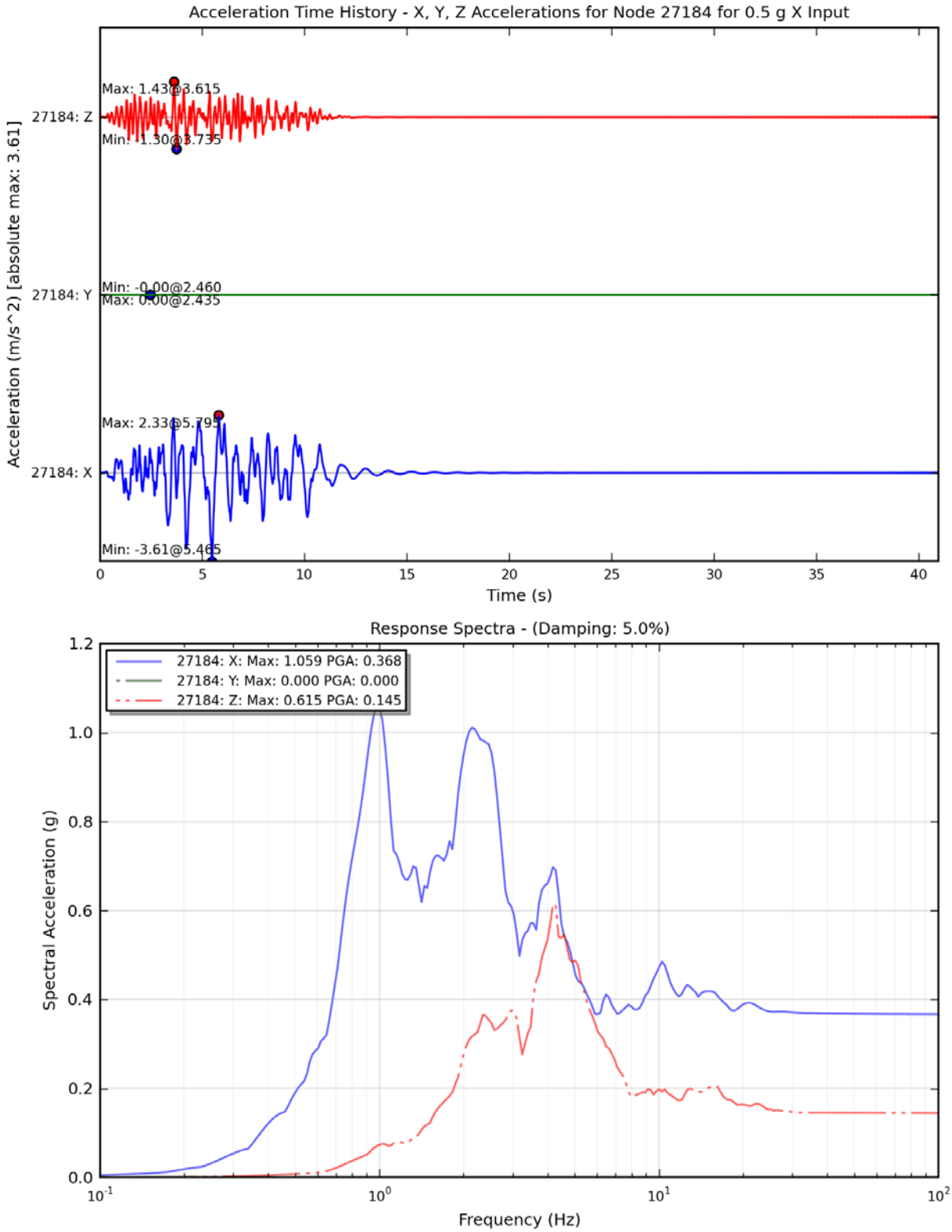

Figure 4-15 Response Acceleration Time Histories and ISRS at Node 27184 for X Input Motion (0.5 g)

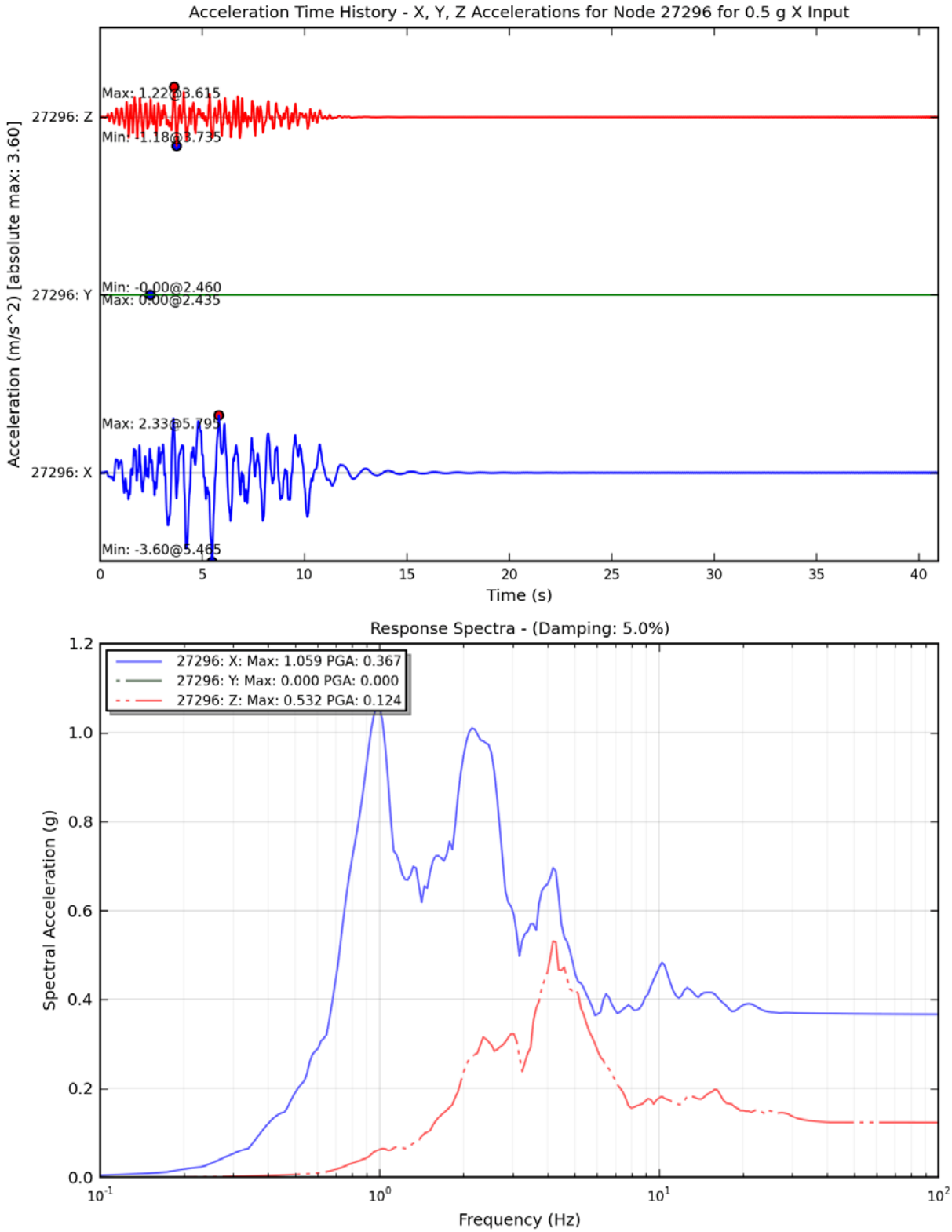

Figure 4-16 Response Acceleration Time Histories and ISRS at Node 27296 for X Input Motion (0.5 g)

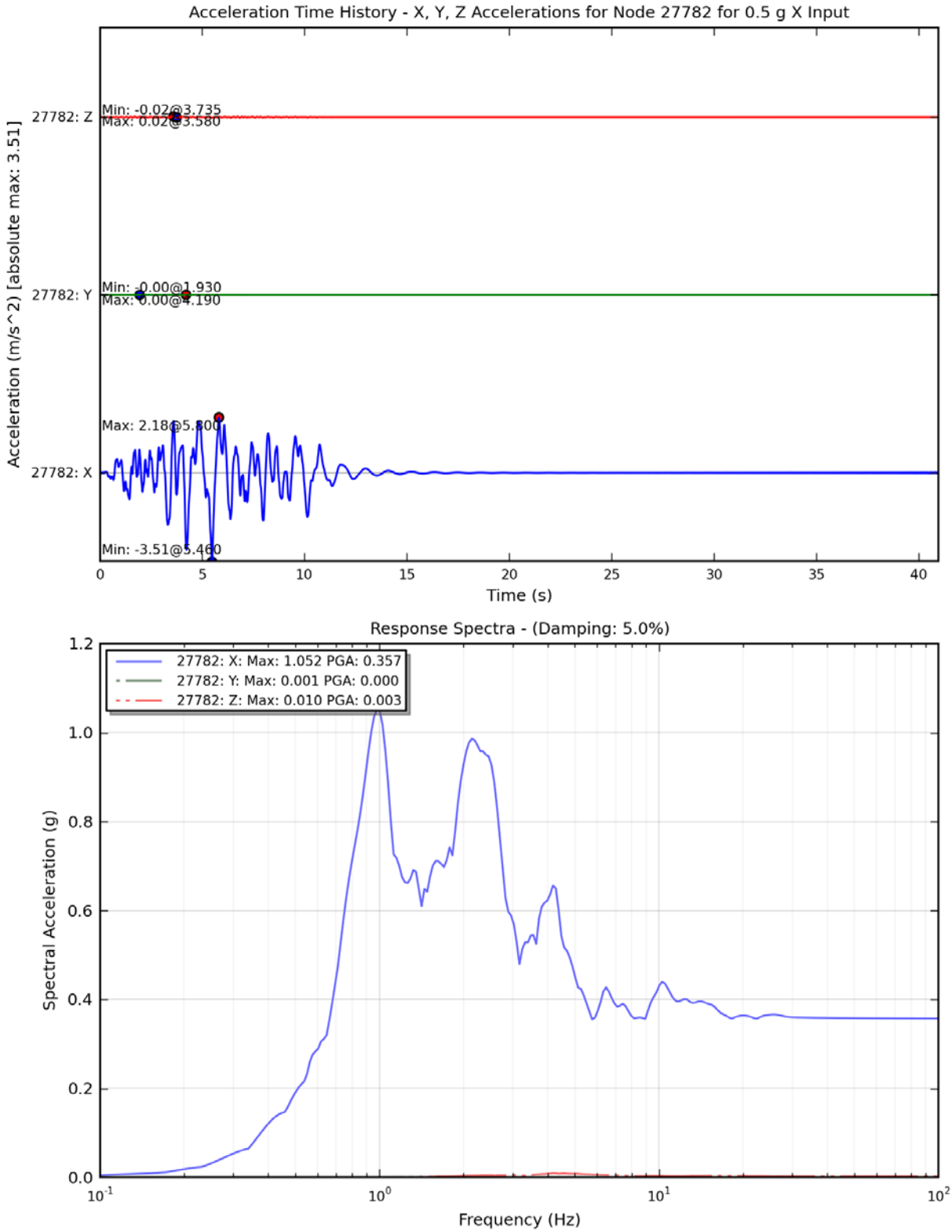

Figure 4-17 Response Acceleration Time Histories and ISRS at Node 27782 for X Input Motion (0.5 g)

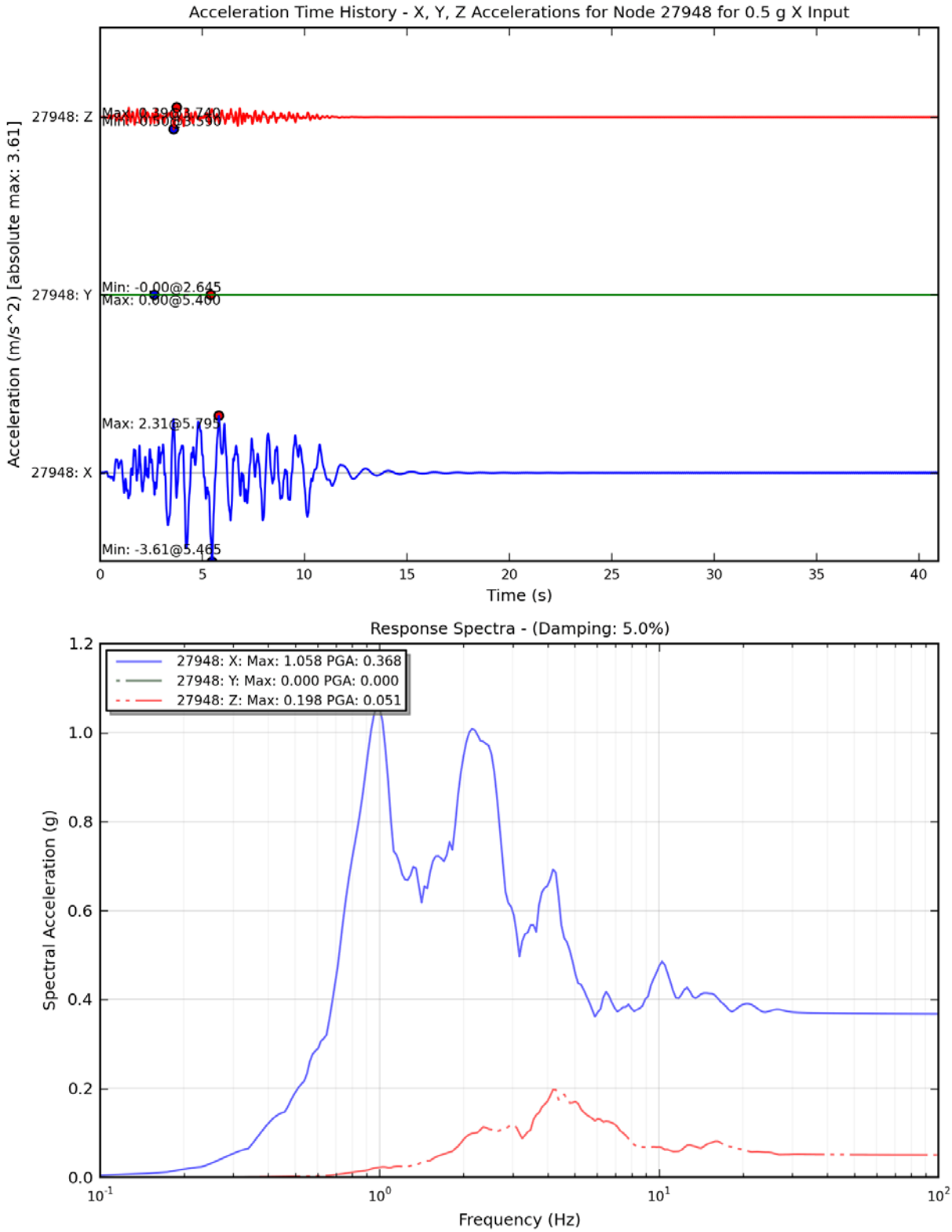

Figure 4-18 Response Acceleration Time Histories and ISRS at Node 27948 for X Input Motion (0.5 g)

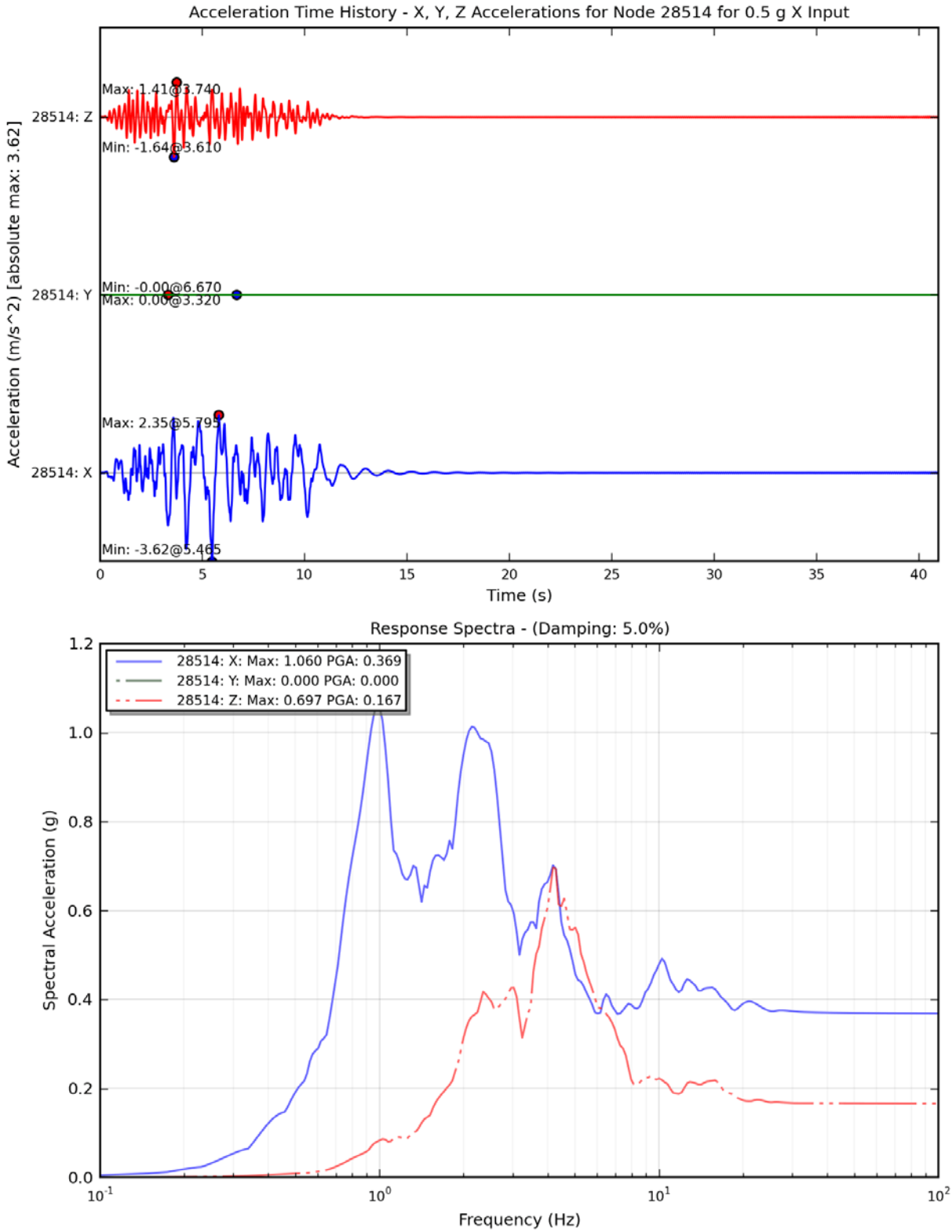

Figure 4-19 Response Acceleration Time Histories and ISRS at Node 28514 for X Input Motion (0.5 g)

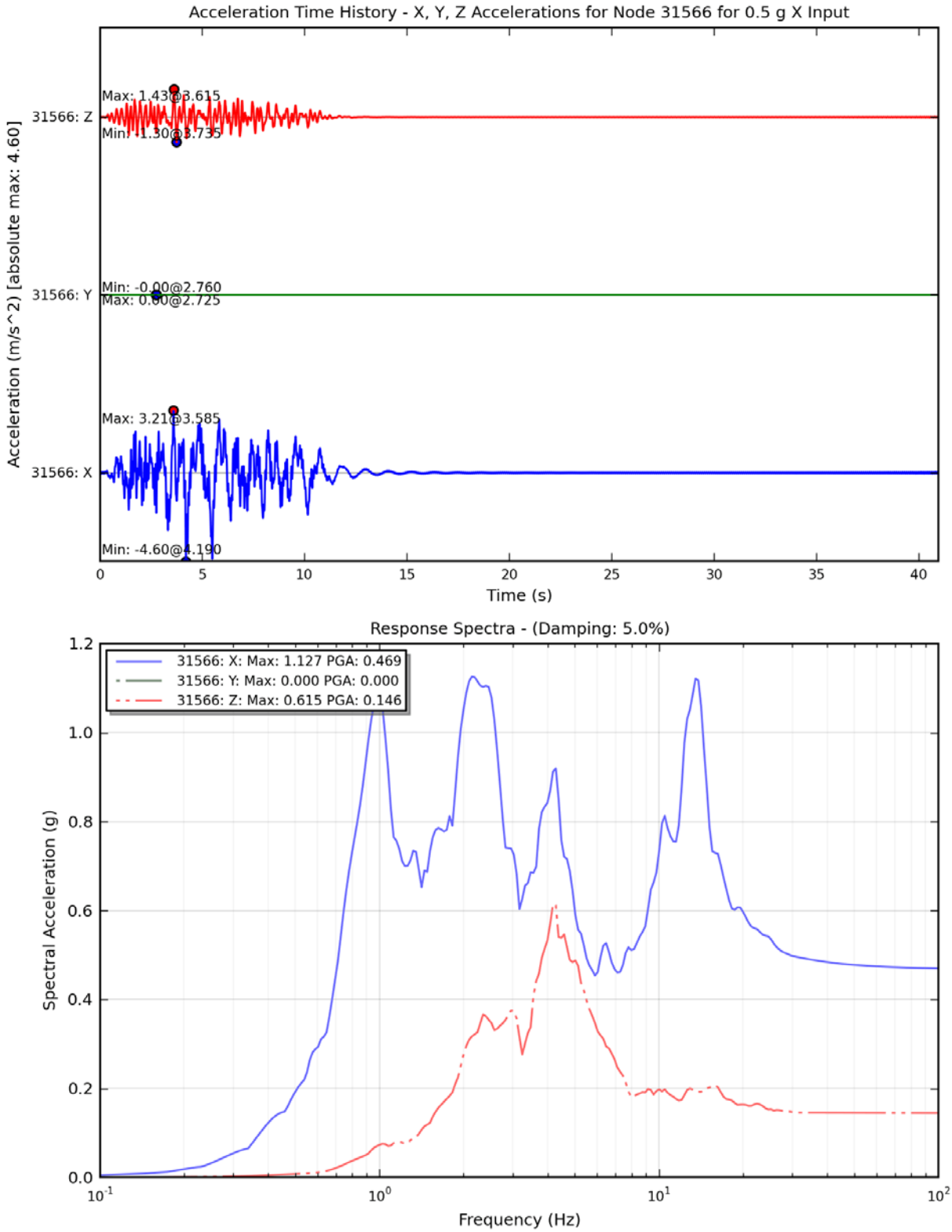

Figure 4-20 Response Acceleration Time Histories and ISRS at Node 31566 for X Input Motion (0.5 g)

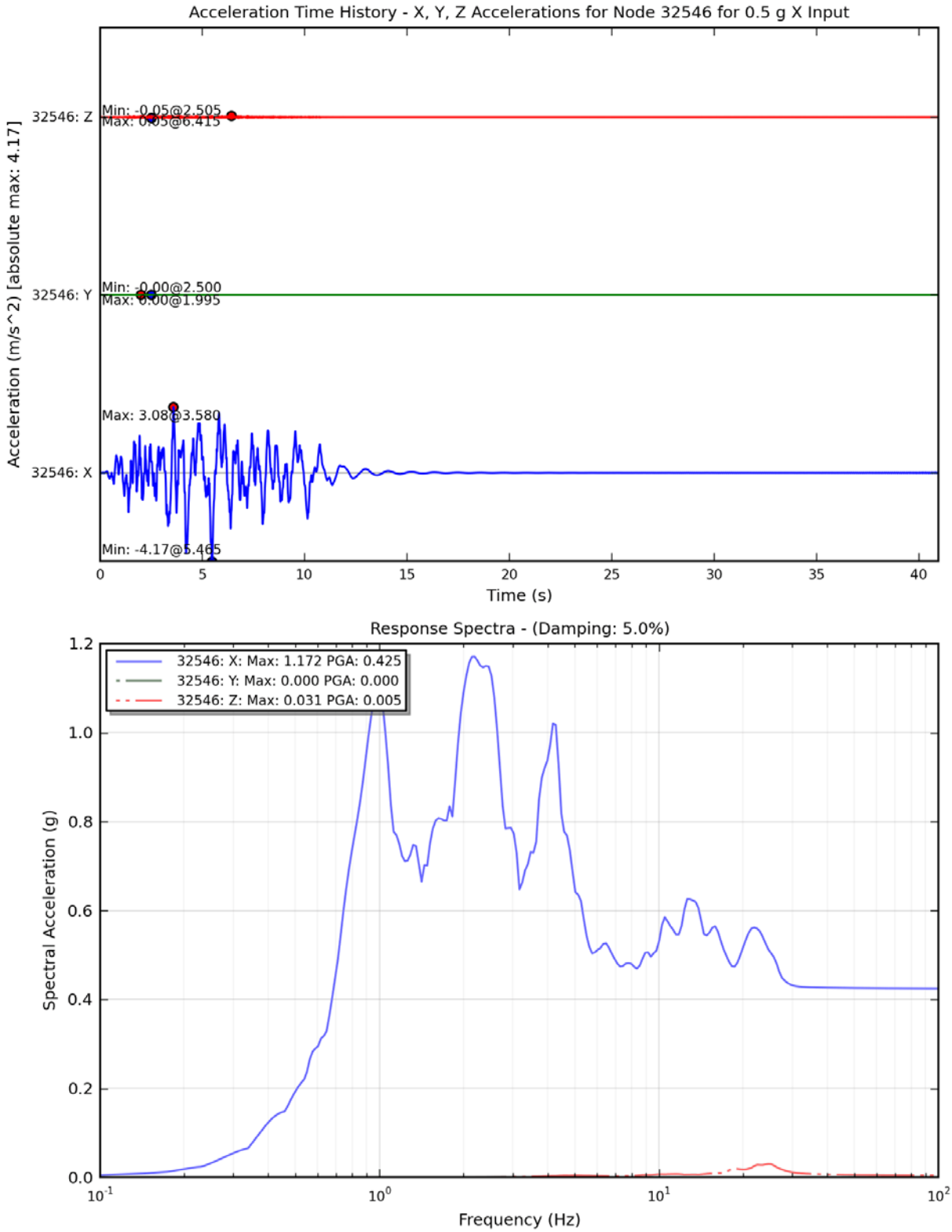

Figure 4-21 Response Acceleration Time Histories and ISRS at Node 32546 for X Input Motion (0.5 g)

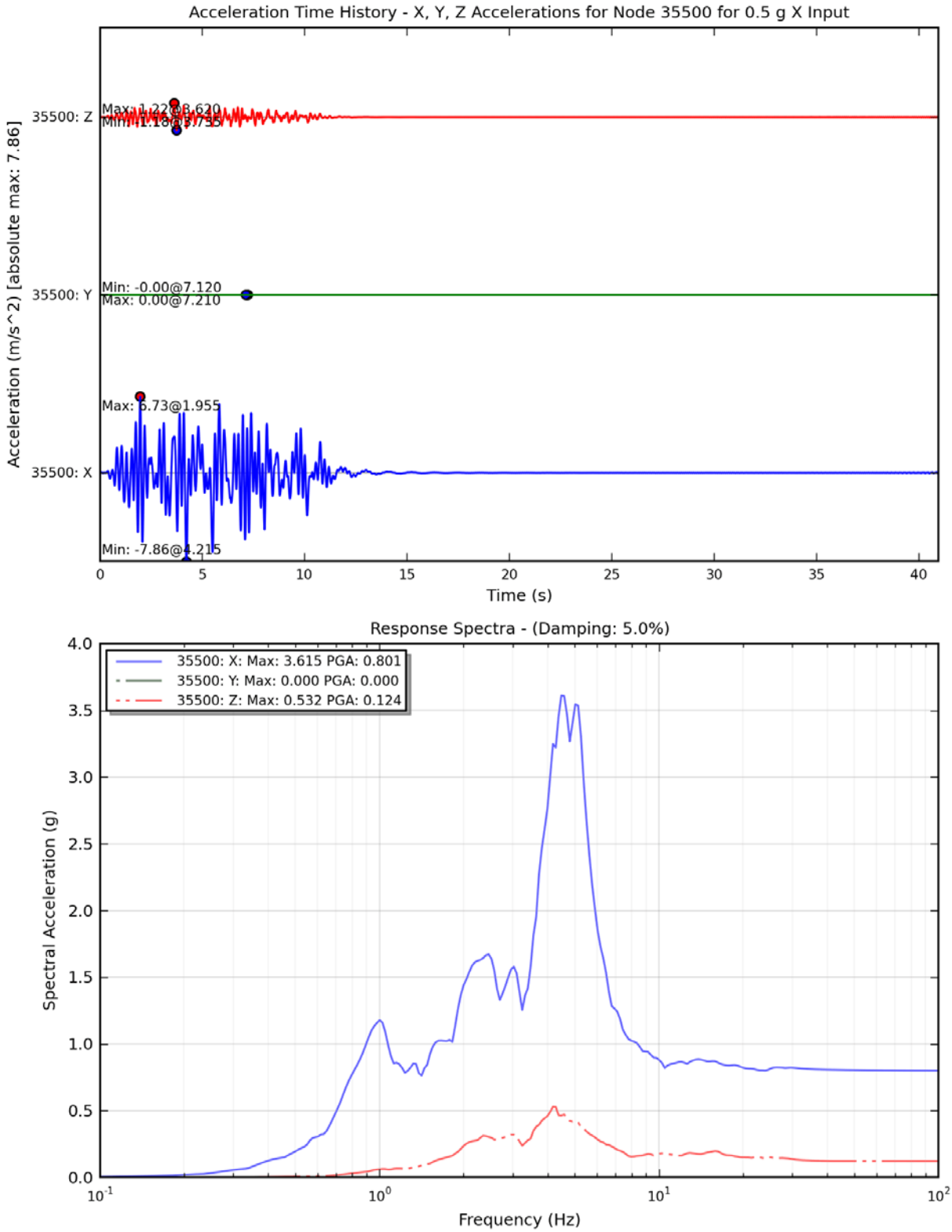

Figure 4-22 Response Acceleration Time Histories and ISRS at Node 35500 for X Input Motion (0.5 g)

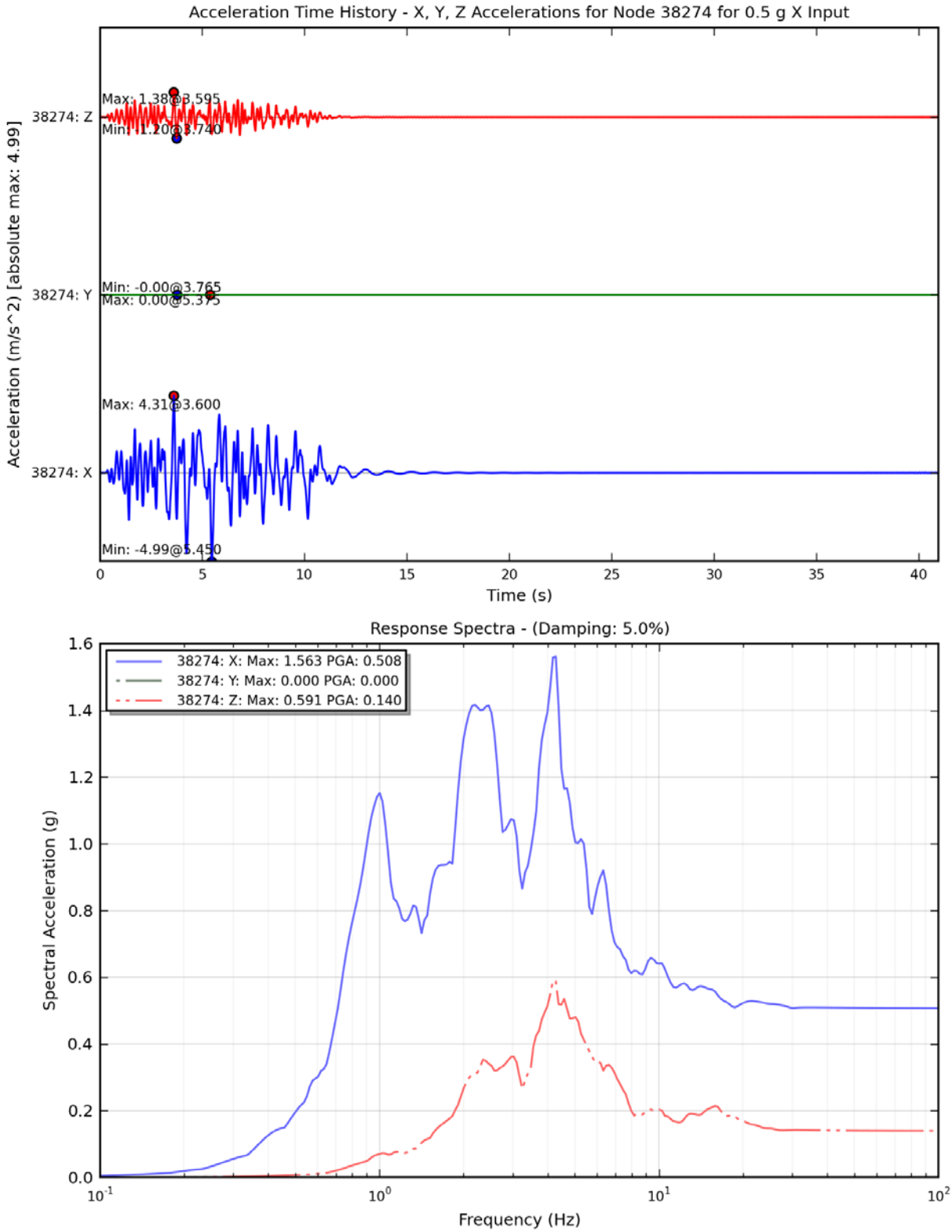

Figure 4-23 Response Acceleration Time Histories and ISRS at Node 38274 for X Input Motion (0.5 g)

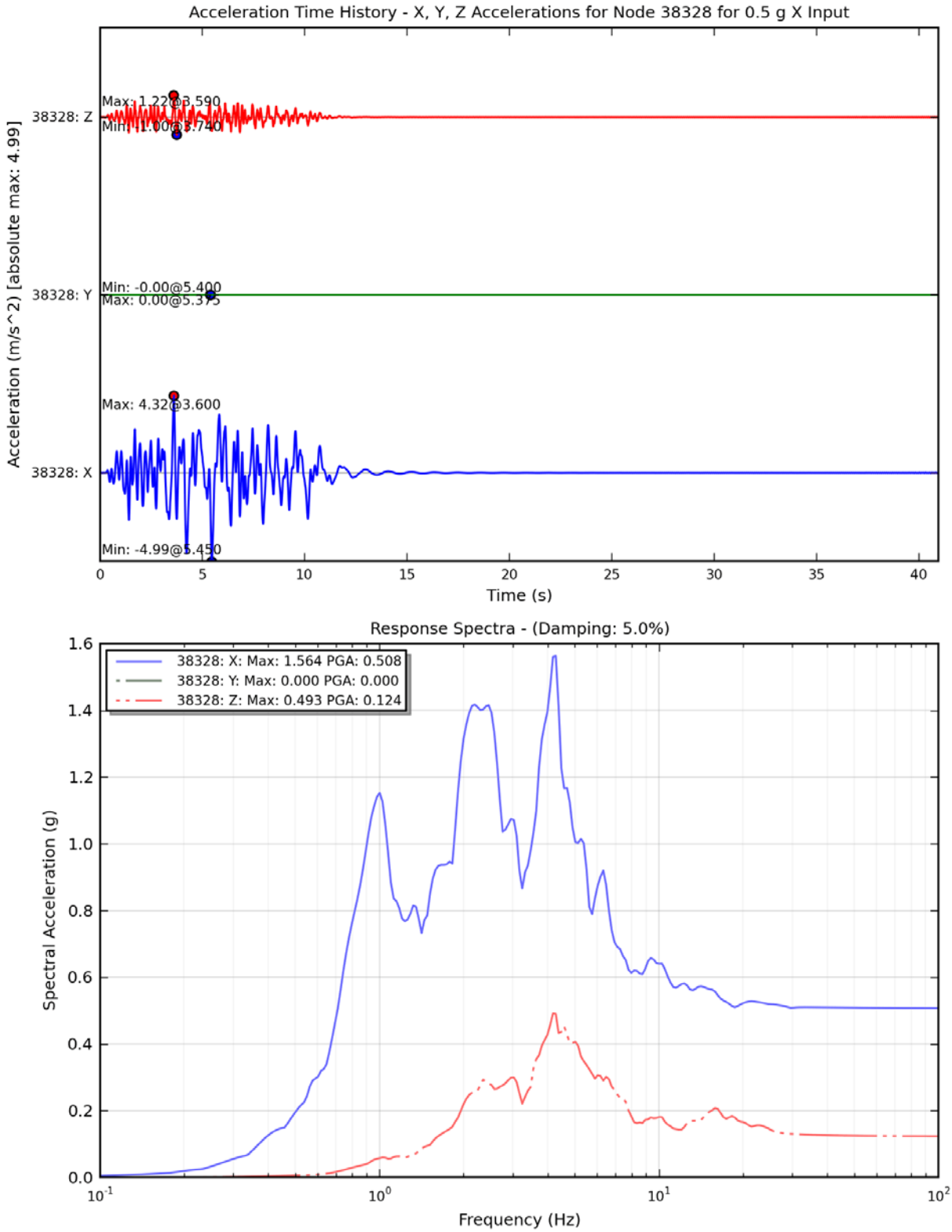

Figure 4-24 Response Acceleration Time Histories and ISRS at Node 38328 for X Input Motion (0.5 g)

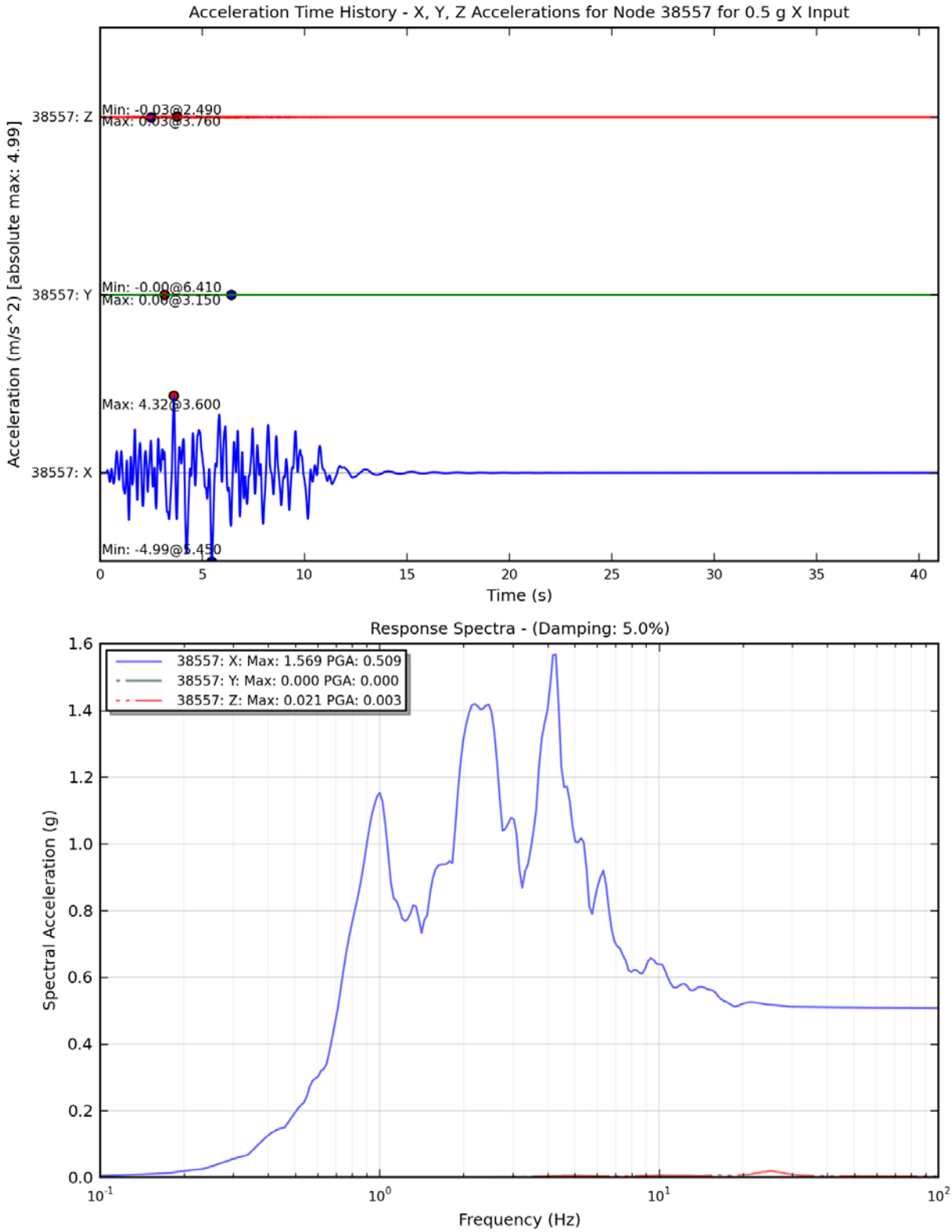

Figure 4-25 Response Acceleration Time Histories and ISRS at Node 38557 for X Input Motion (0.5 g)

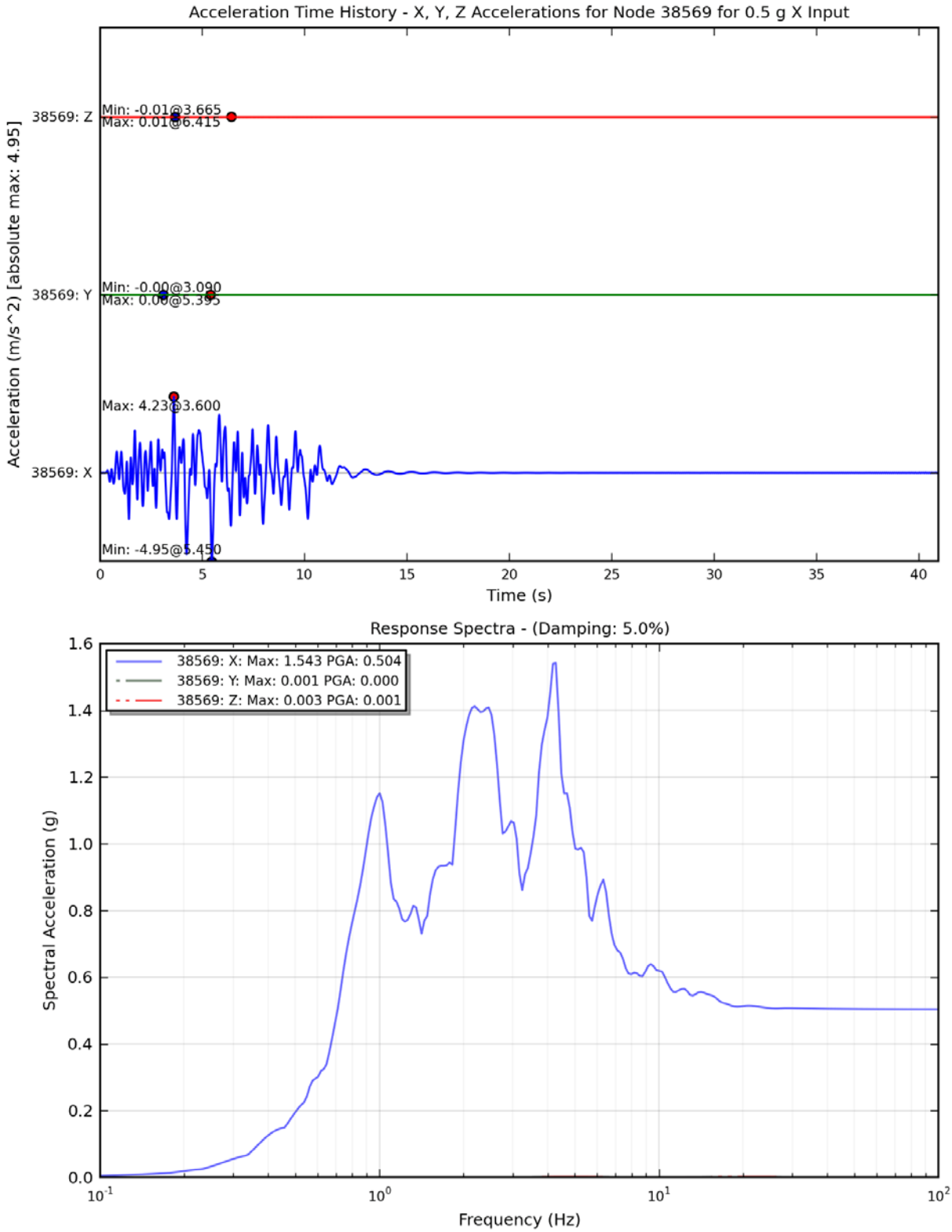

Figure 4-26 Response Acceleration Time Histories and ISRS at Node 38569 for X Input Motion (0.5 g)

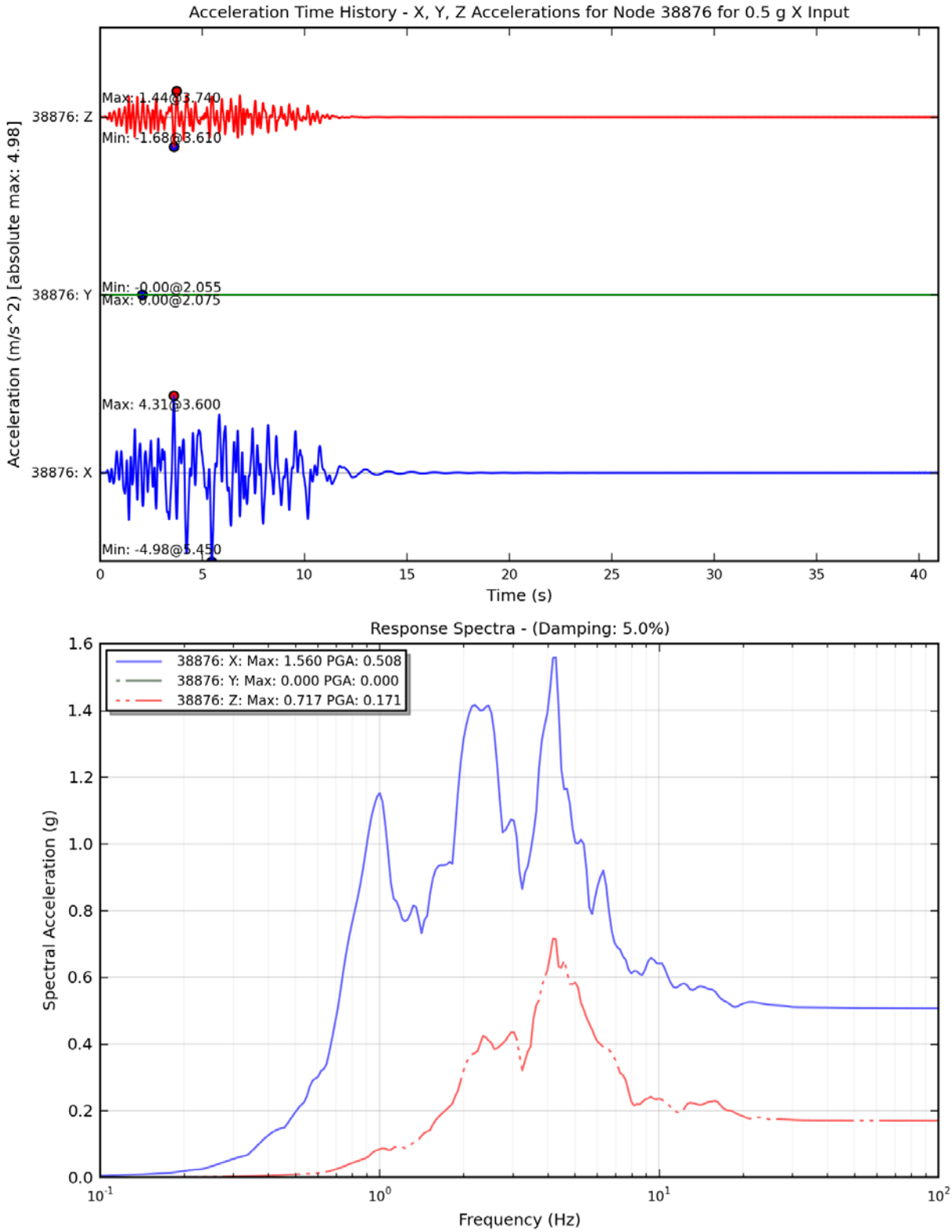

Figure 4-27 Response Acceleration Time Histories and ISRS at Node 38876 for X Input Motion (0.5 g)

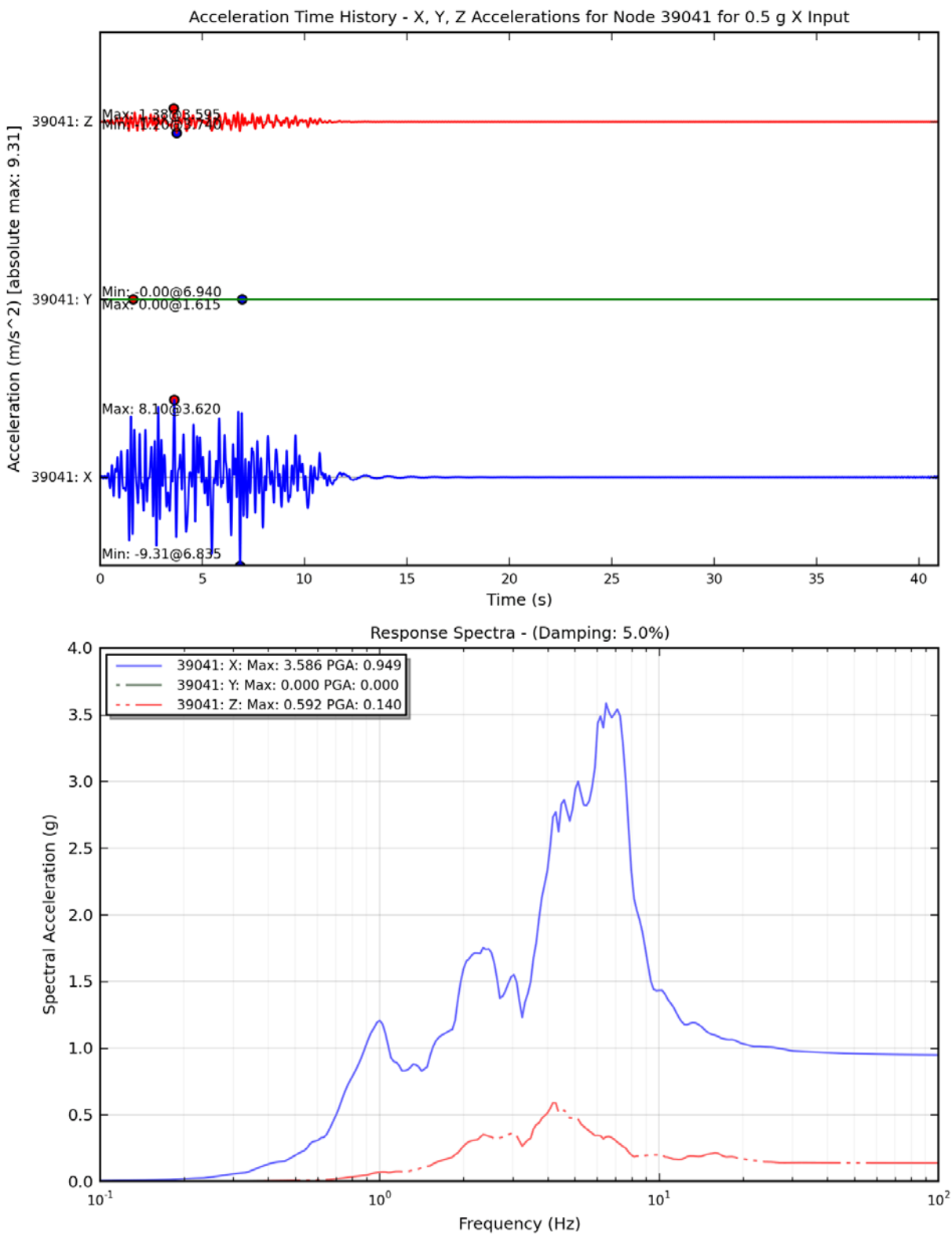

Figure 4-28 Response Acceleration Time Histories and ISRS at Node 39041 for X Input Motion (0.5 g)

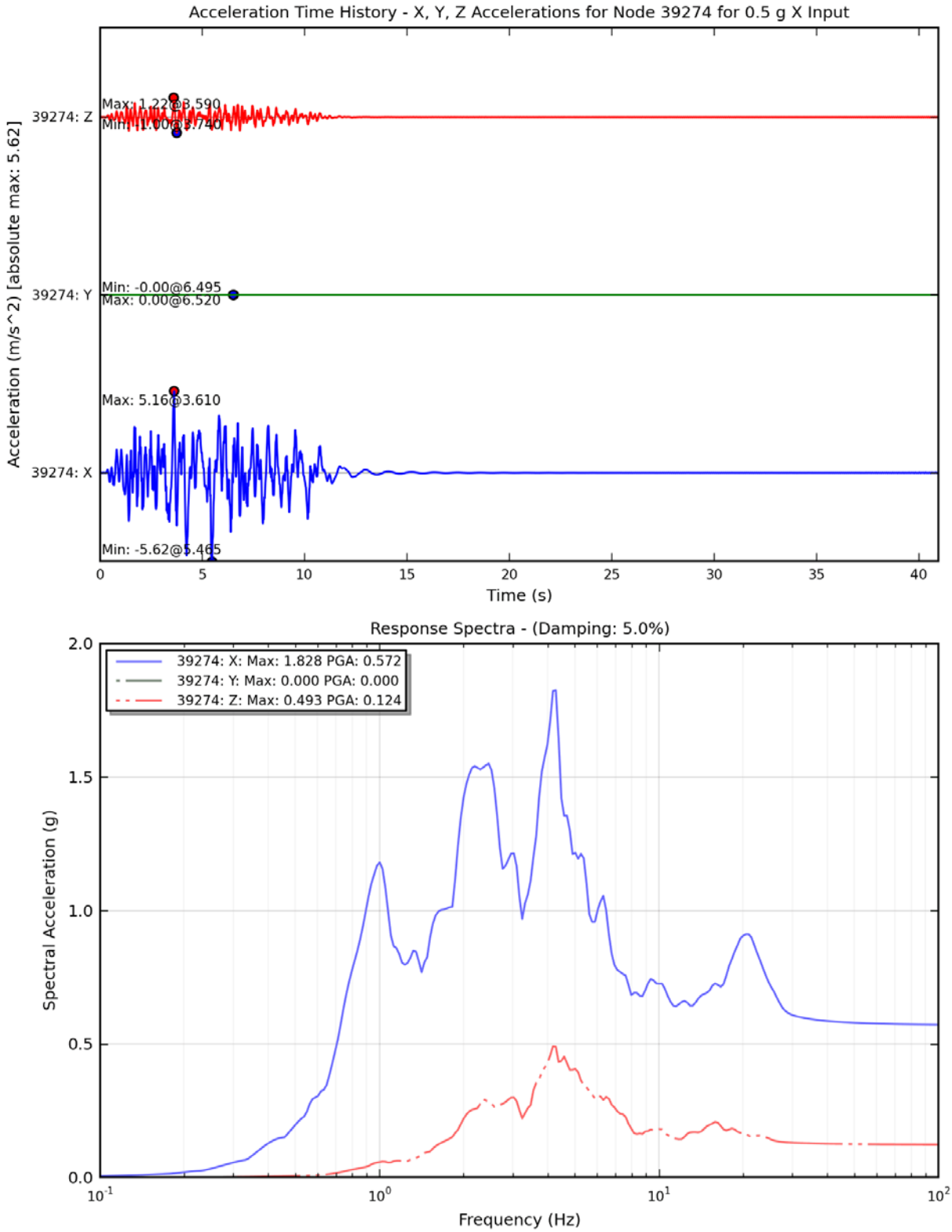

Figure 4-29 Response Acceleration Time Histories and ISRS at Node 39274 for X Input Motion (0.5 g)

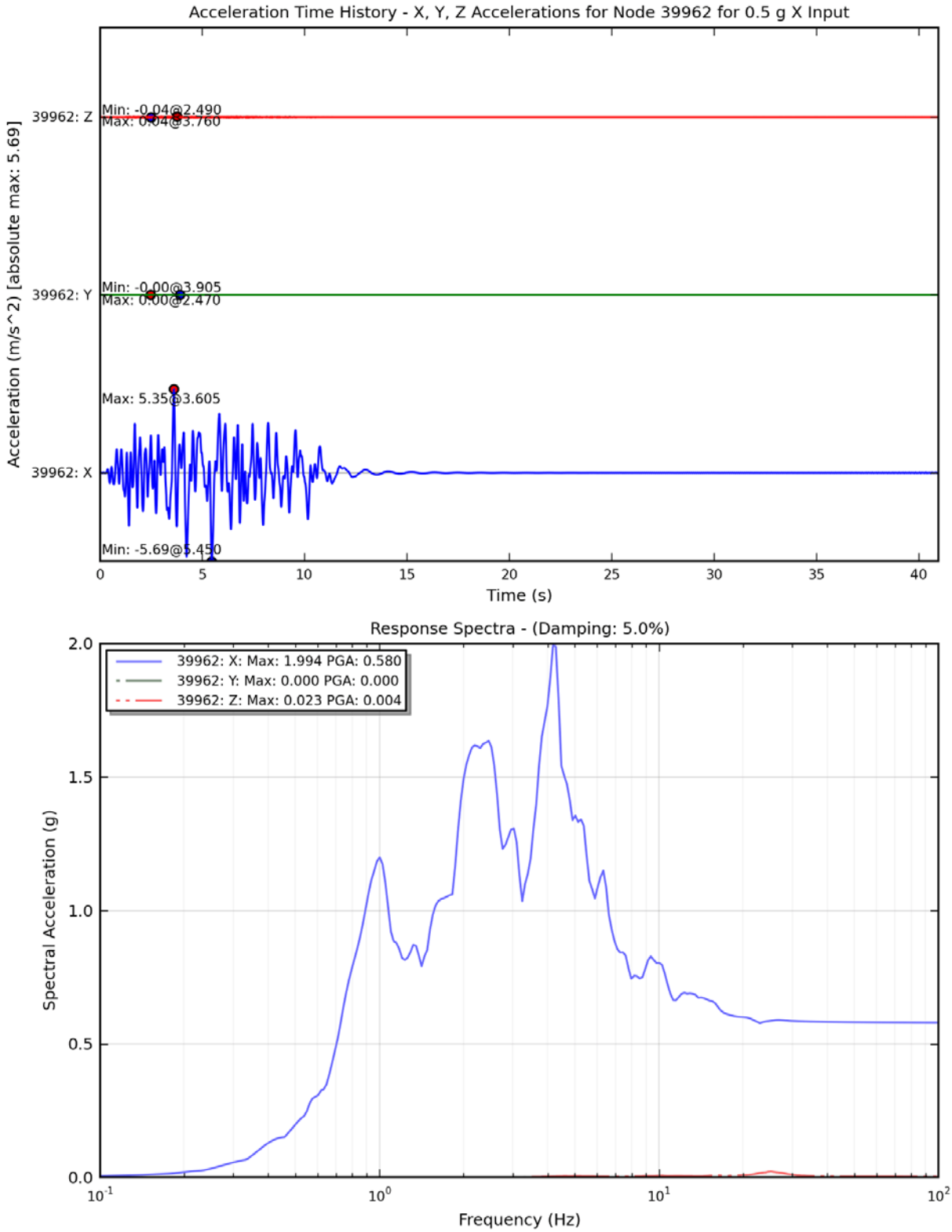

Figure 4-30 Response Acceleration Time Histories and ISRS at Node 39962 for X Input Motion (0.5 g)

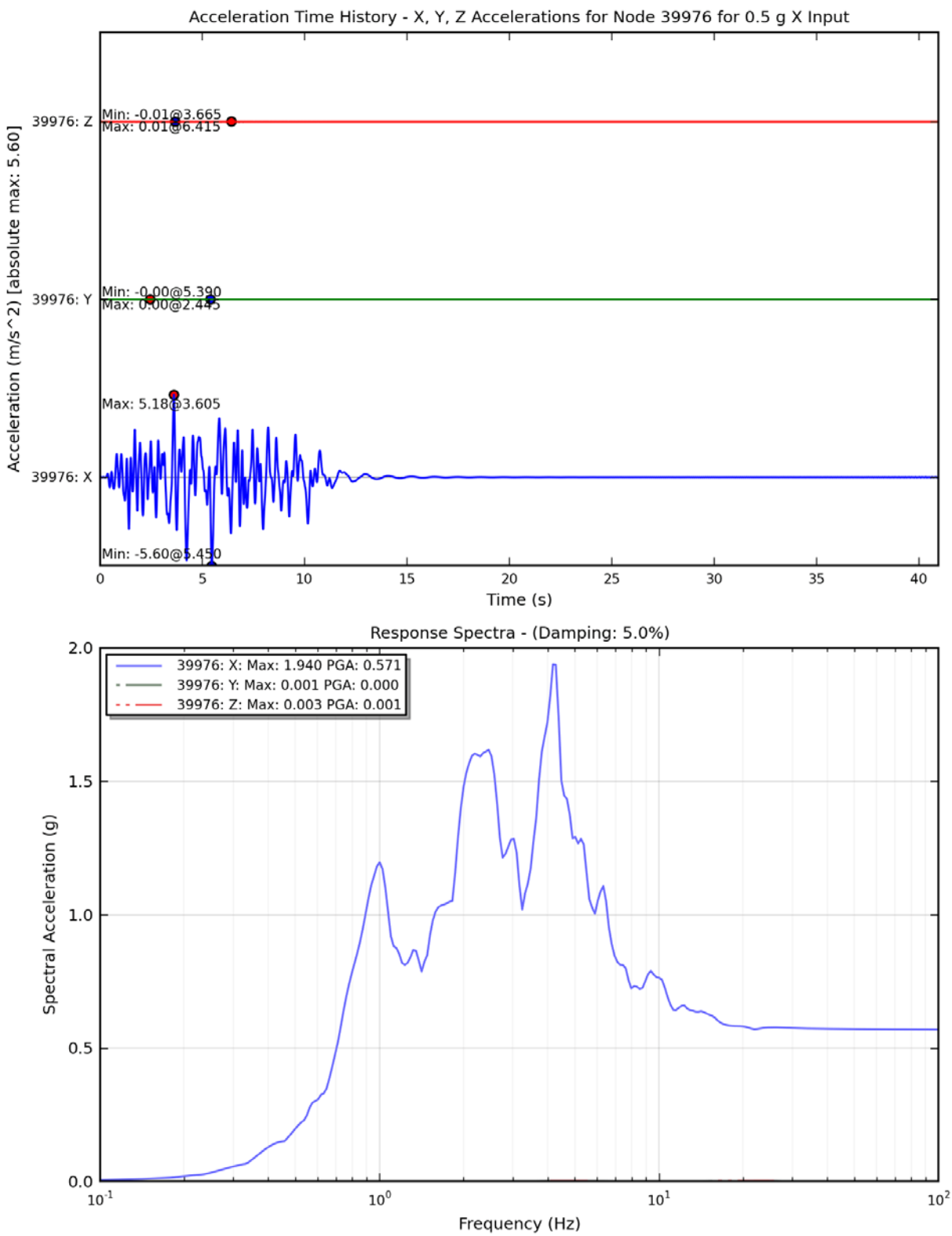

Figure 4-31 Response Acceleration Time Histories and ISRS at Node 39976 for X Input Motion (0.5 g)

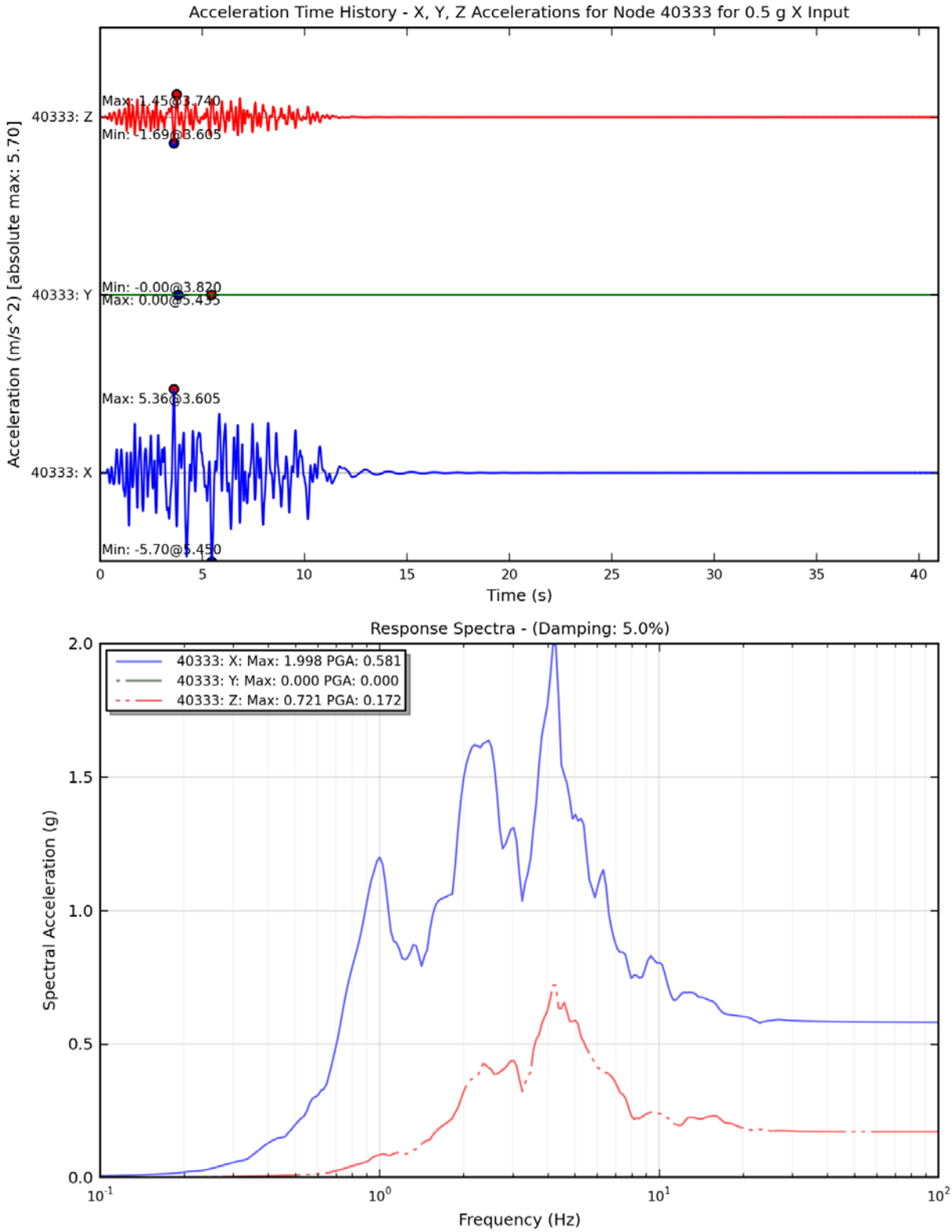

Figure 4-32 Response Acceleration Time Histories and ISRS at Node 40333 for X Input Motion (0.5 g)

4.3 Acceleration Time Histories and ISRS for the Z Directional Input Motion

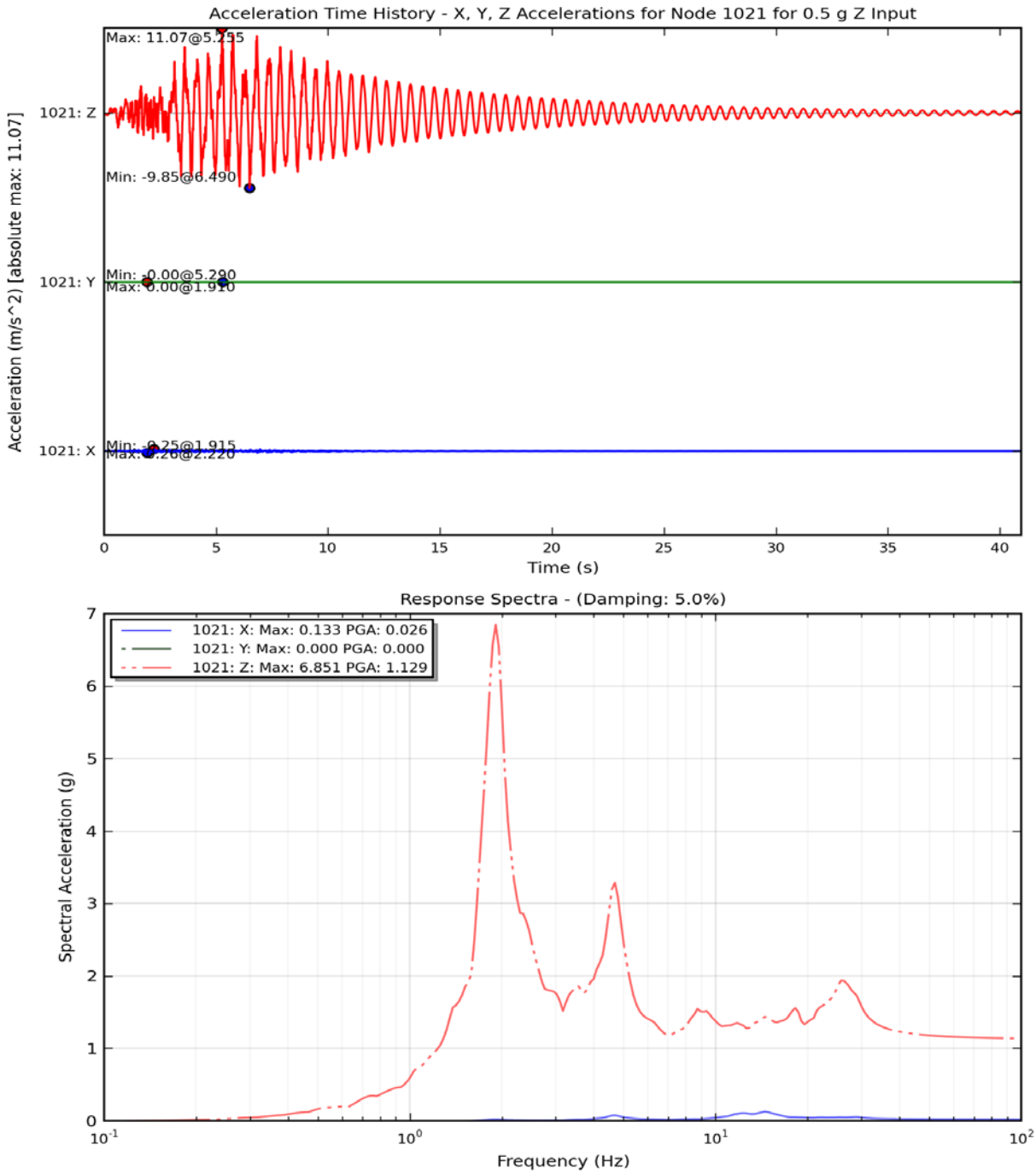

Figure 4-33 Response Acceleration Time Histories and ISRS at Node 1021 for Z Input Motion (0.5 g)

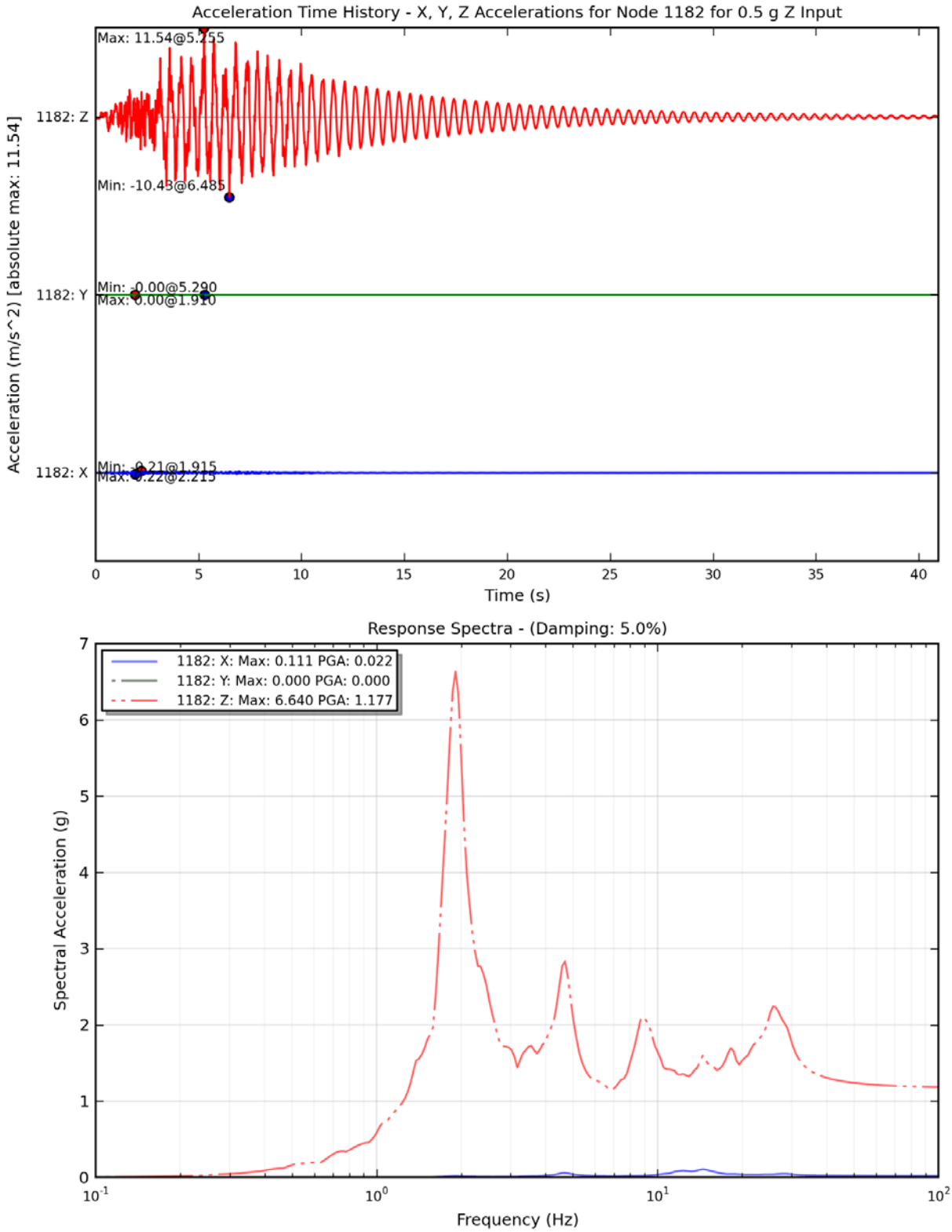

Figure 4-34 Response Acceleration Time Histories and ISRS at Node 1182 for Z Input Motion (0.5 g)

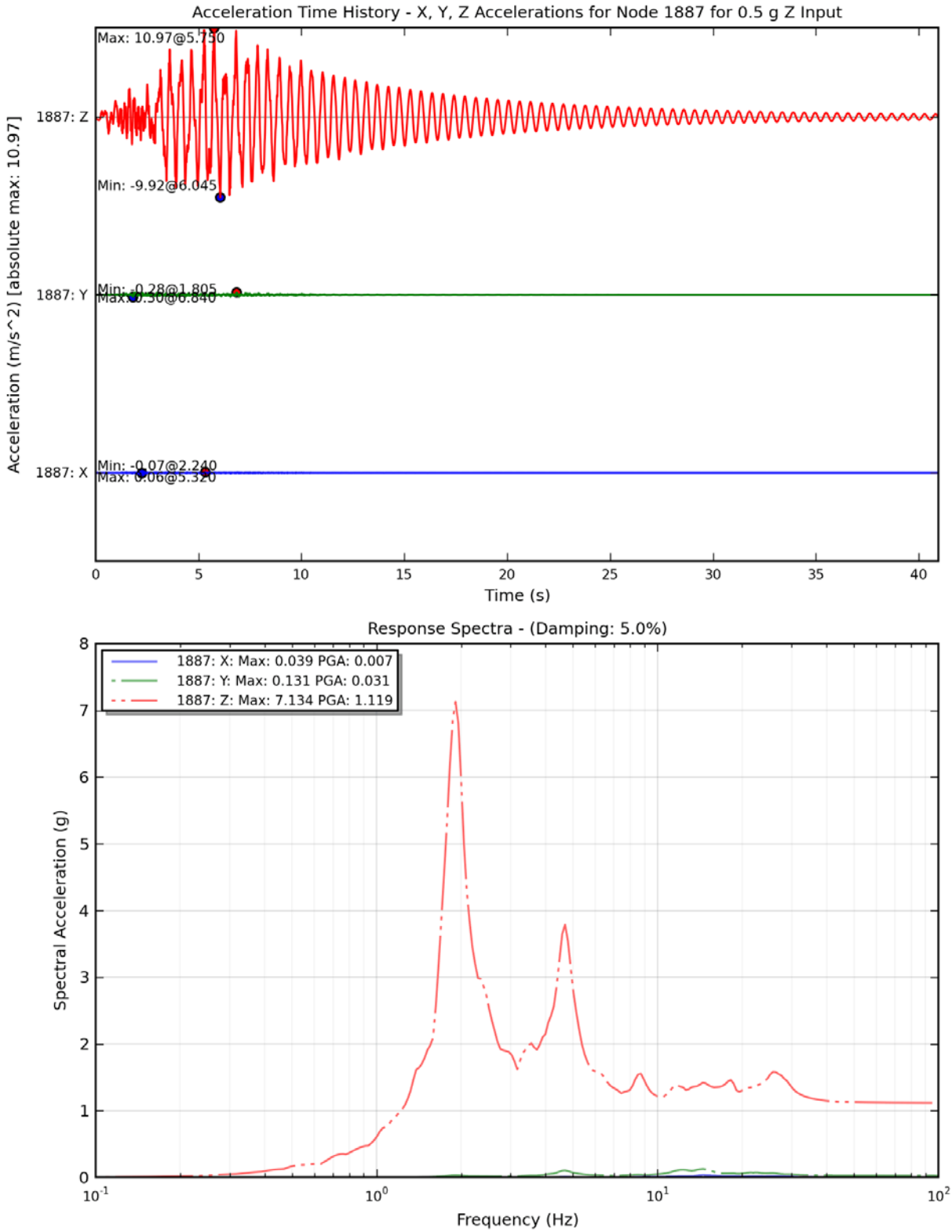

Figure 4-35 Response Acceleration Time Histories and ISRS at Node 1887 for Z Input Motion (0.5 g)

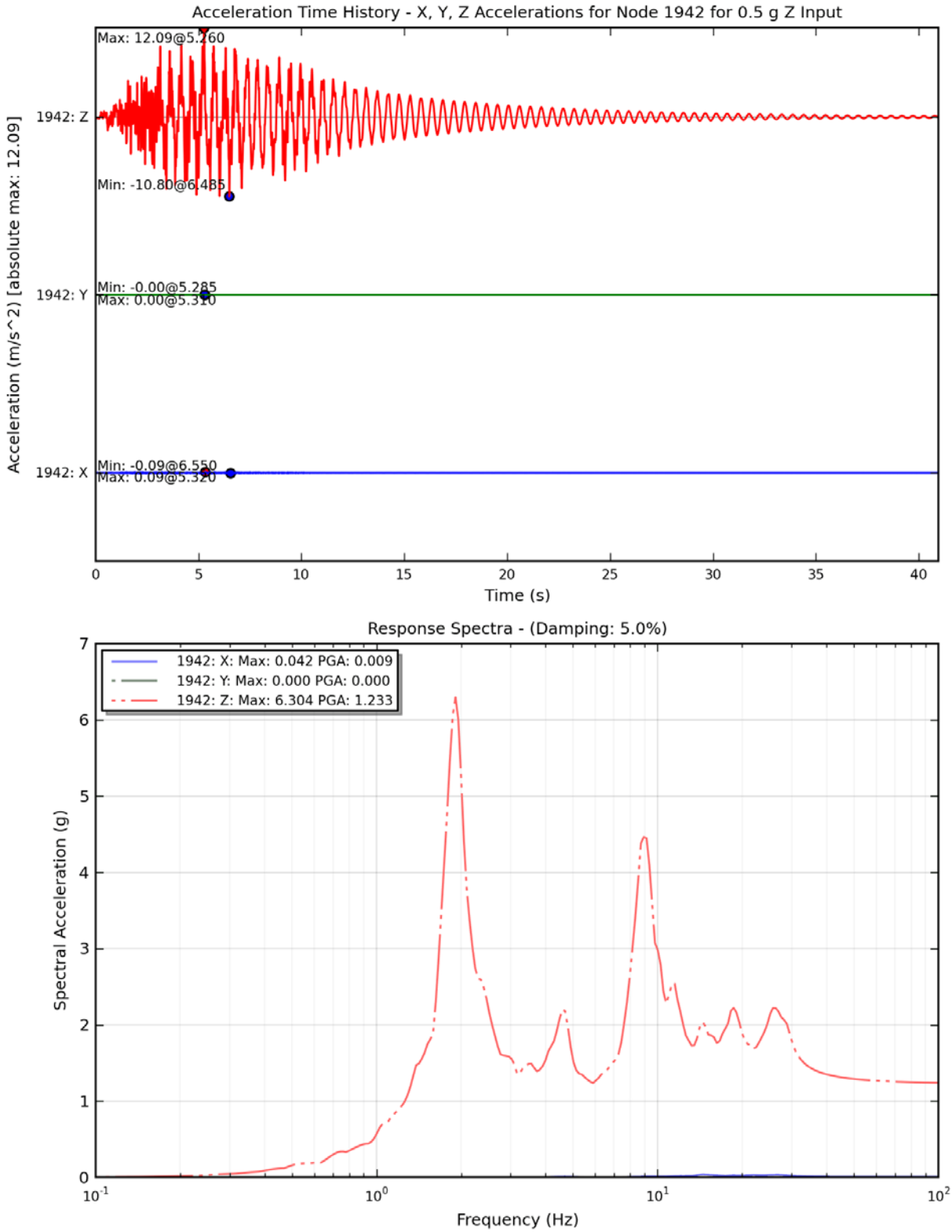

Figure 4-36 Response Acceleration Time Histories and ISRS at Node 1942 for Z Input Motion (0.5 g)

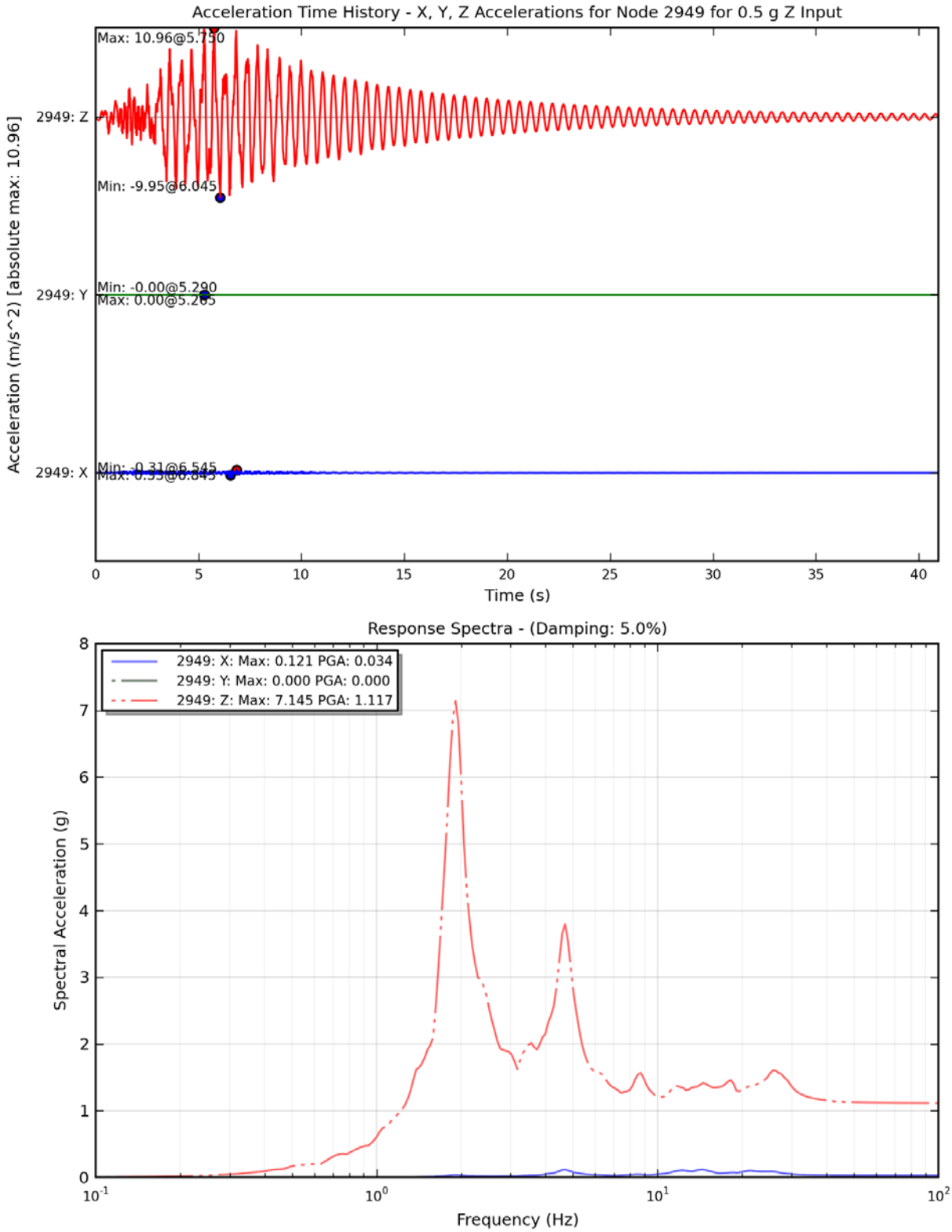

Figure 4-37 Response Acceleration Time Histories and ISRS at Node 2949 for Z Input Motion (0.5 g)

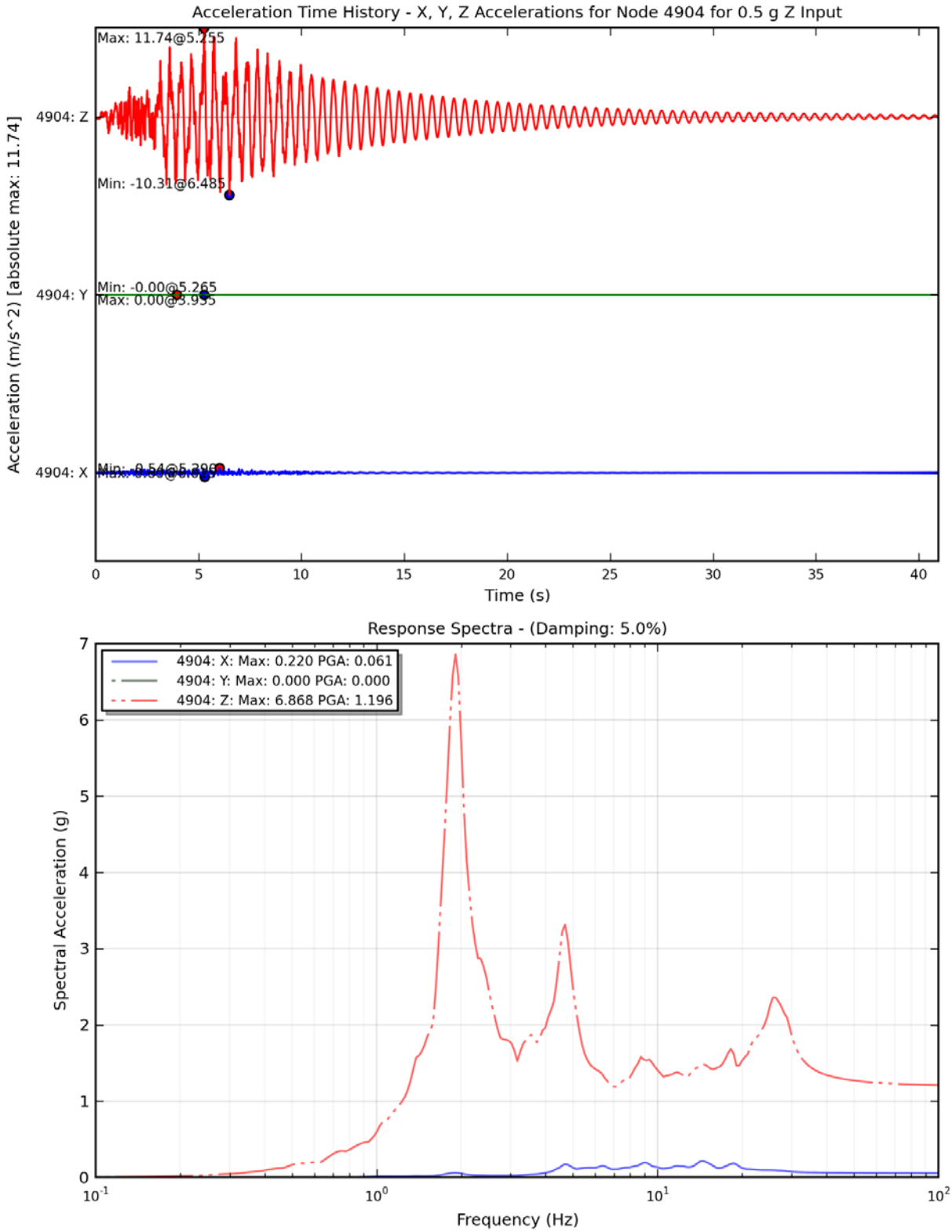

Figure 4-38 Response Acceleration Time Histories and ISRS at Node 4904 for Z Input Motion (0.5 g)

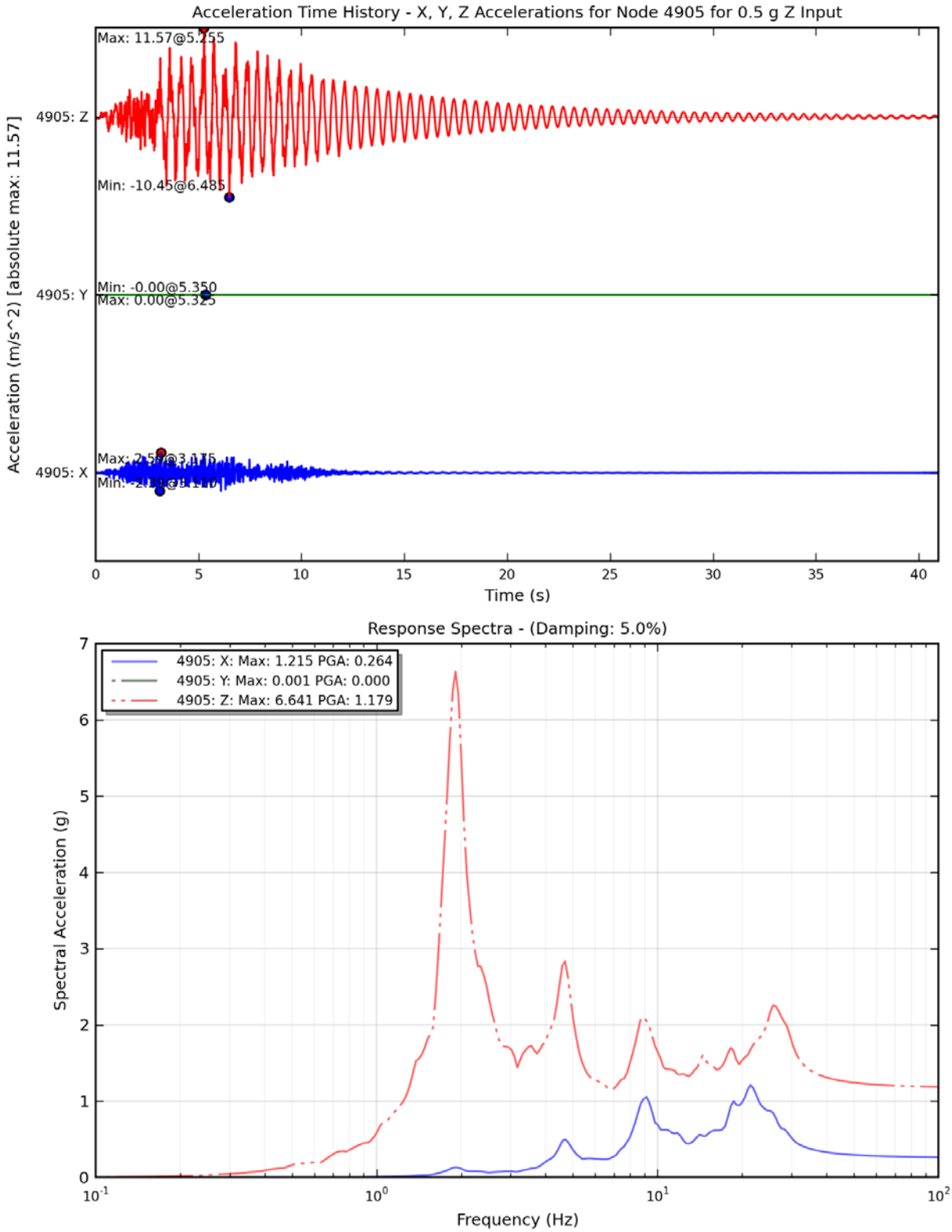

Figure 4-39 Response Acceleration Time Histories and ISRS at Node 4905 for Z Input Motion (0.5 g)

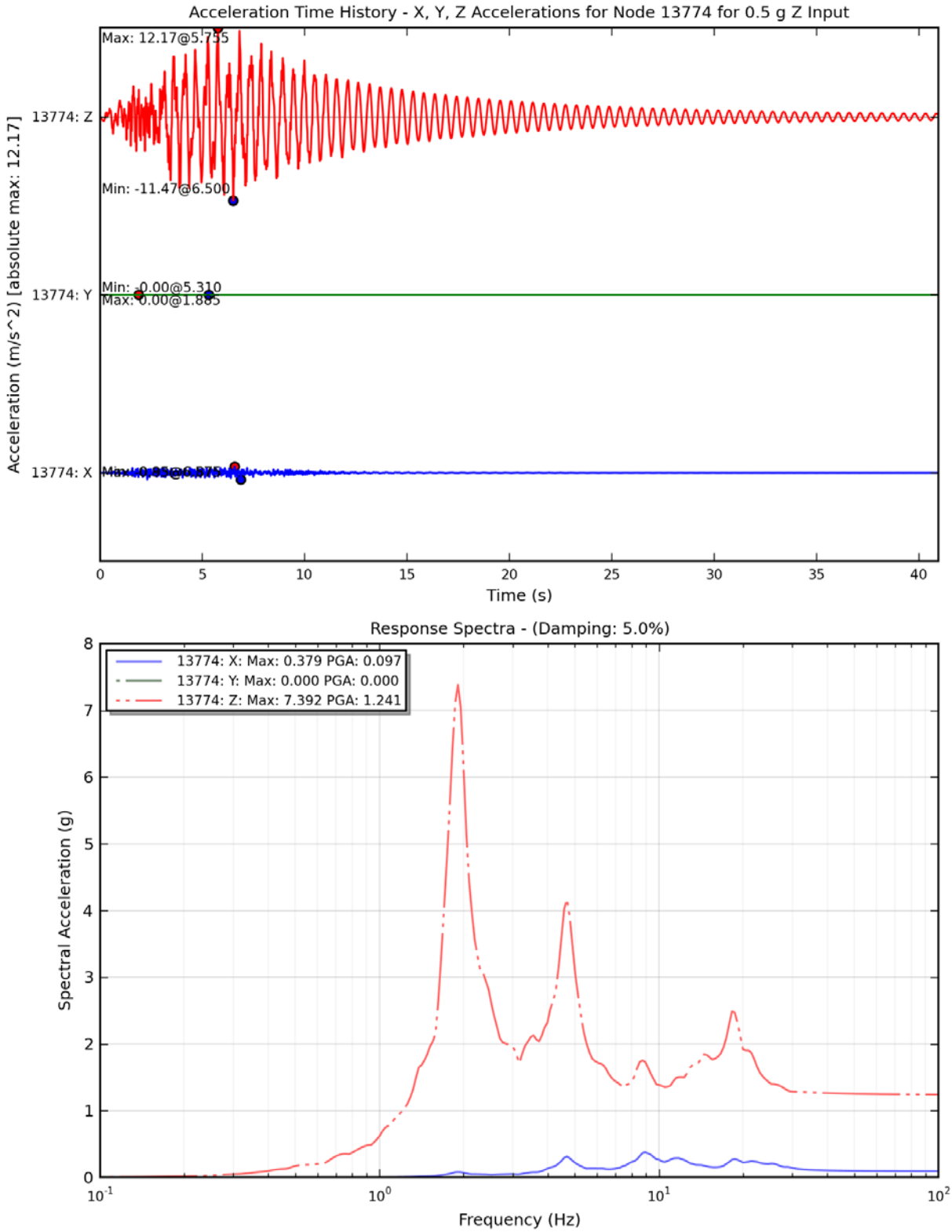

Figure 4-40 Response Acceleration Time Histories and ISRS at Node 13774 for Z Input Motion (0.5 g)

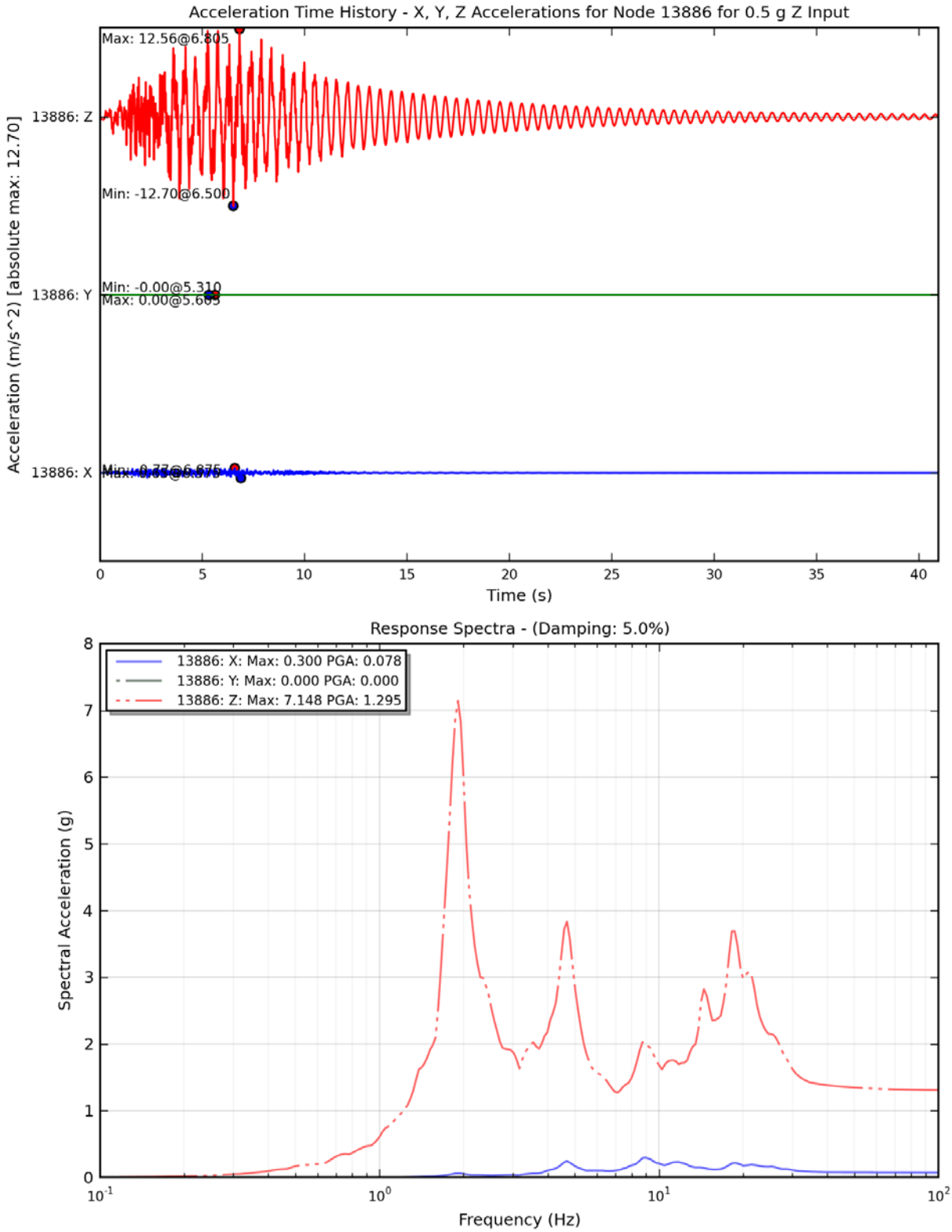

Figure 4-41 Response Acceleration Time Histories and ISRS at Node 13886 for Z Input Motion (0.5 g)

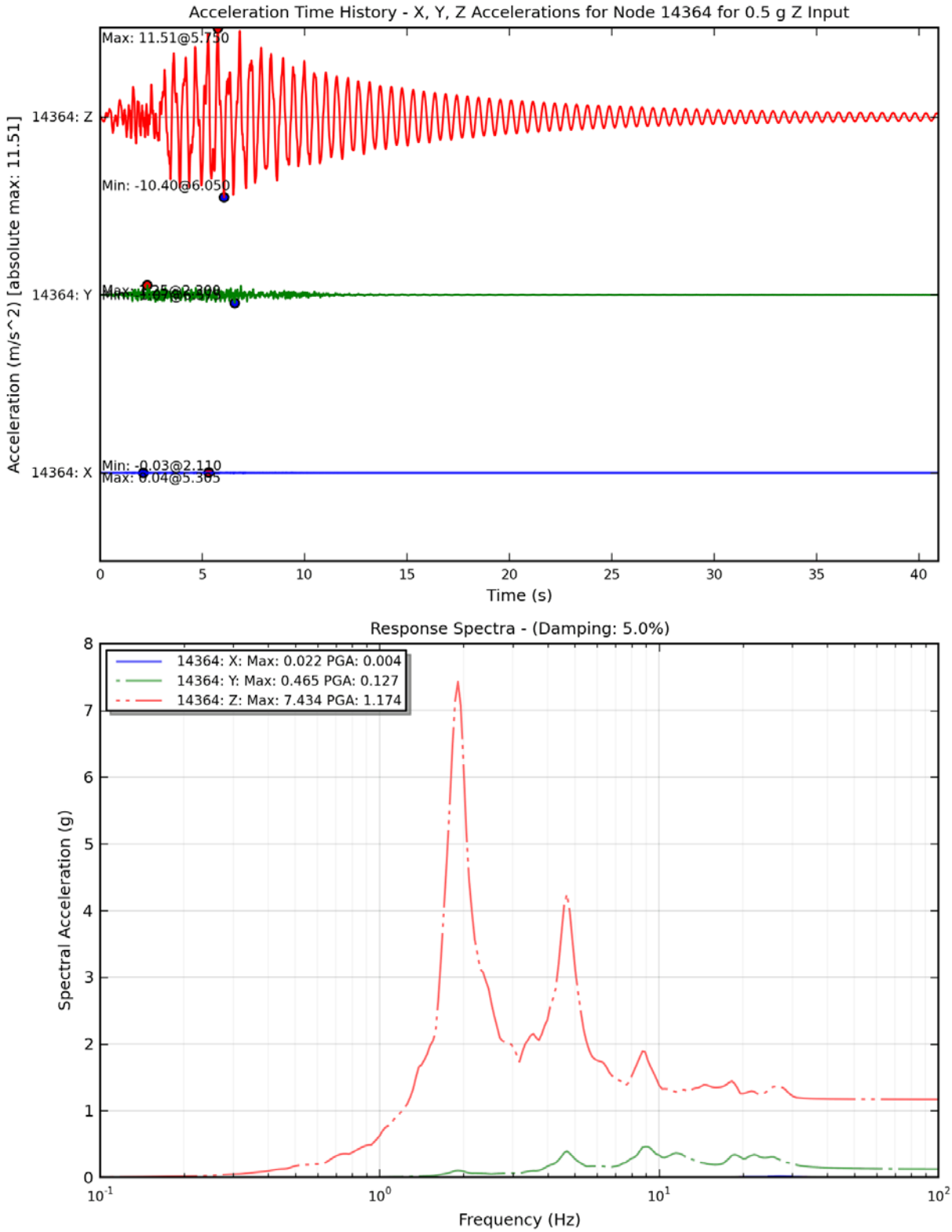

Figure 4-42 Response Acceleration Time Histories and ISRS at Node 14364 for Z Input Motion (0.5 g)

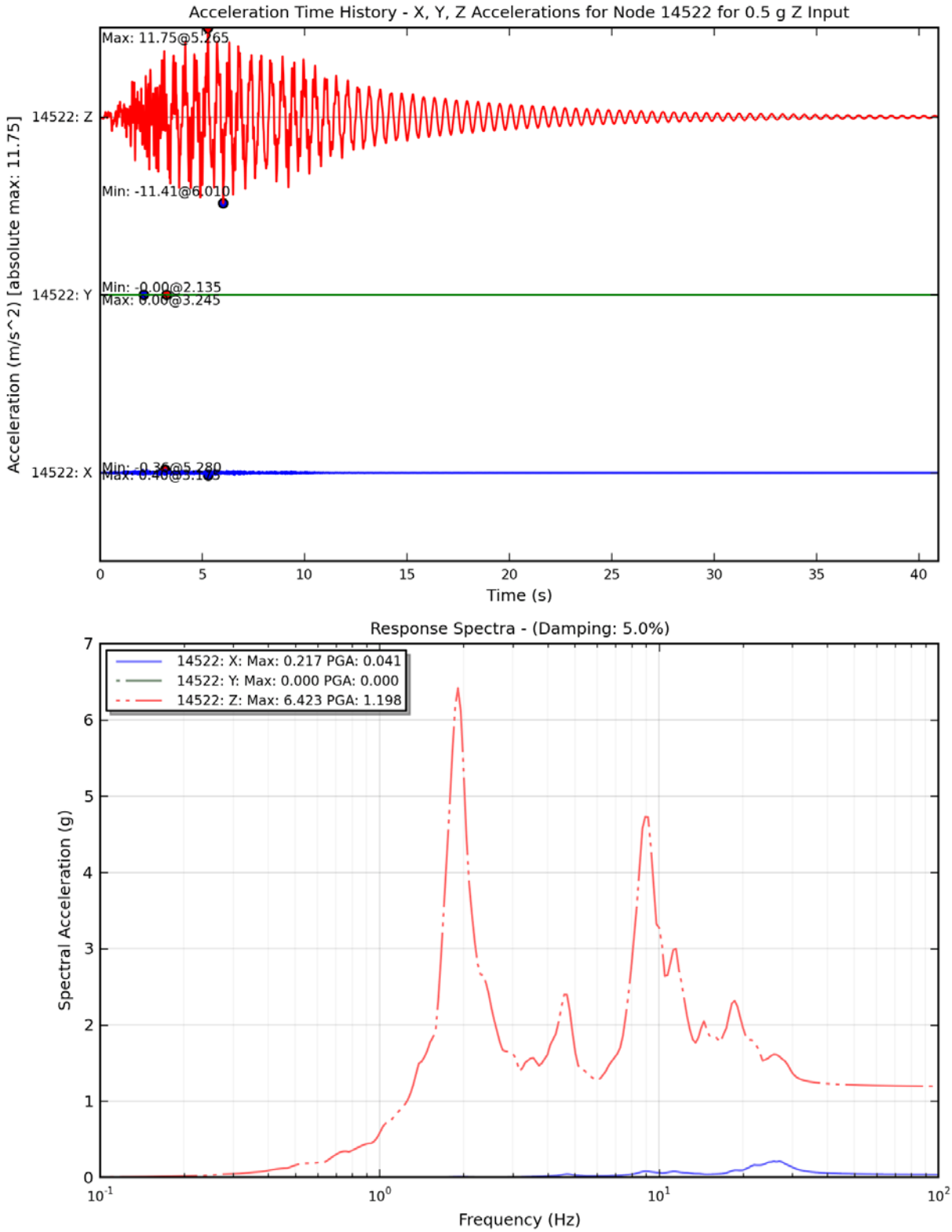

Figure 4-43 Response Acceleration Time Histories and ISRS at Node 14522 for Z Input Motion (0.5 g)

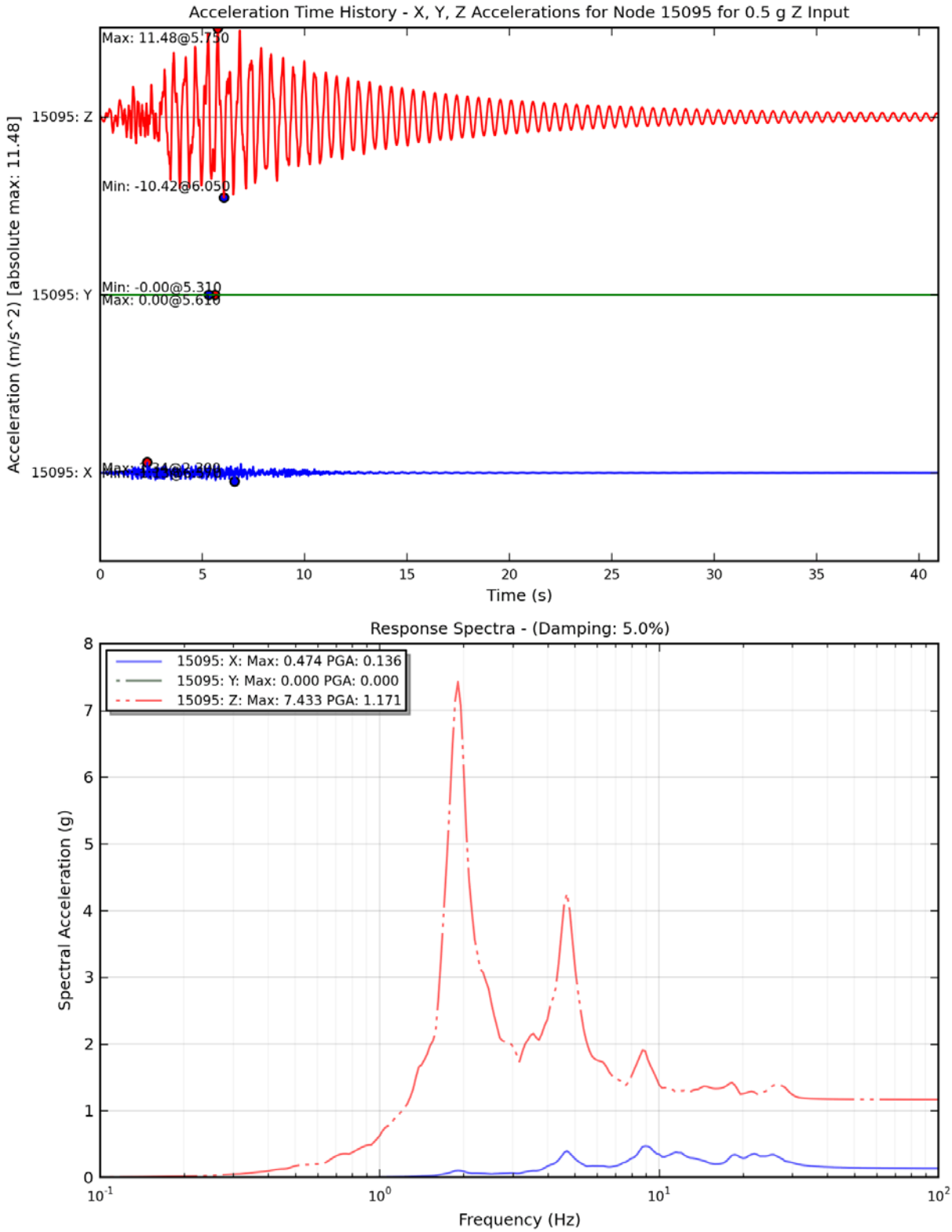

Figure 4-44 Response Acceleration Time Histories and ISRS at Node 15095 for Z Input Motion (0.5 g)

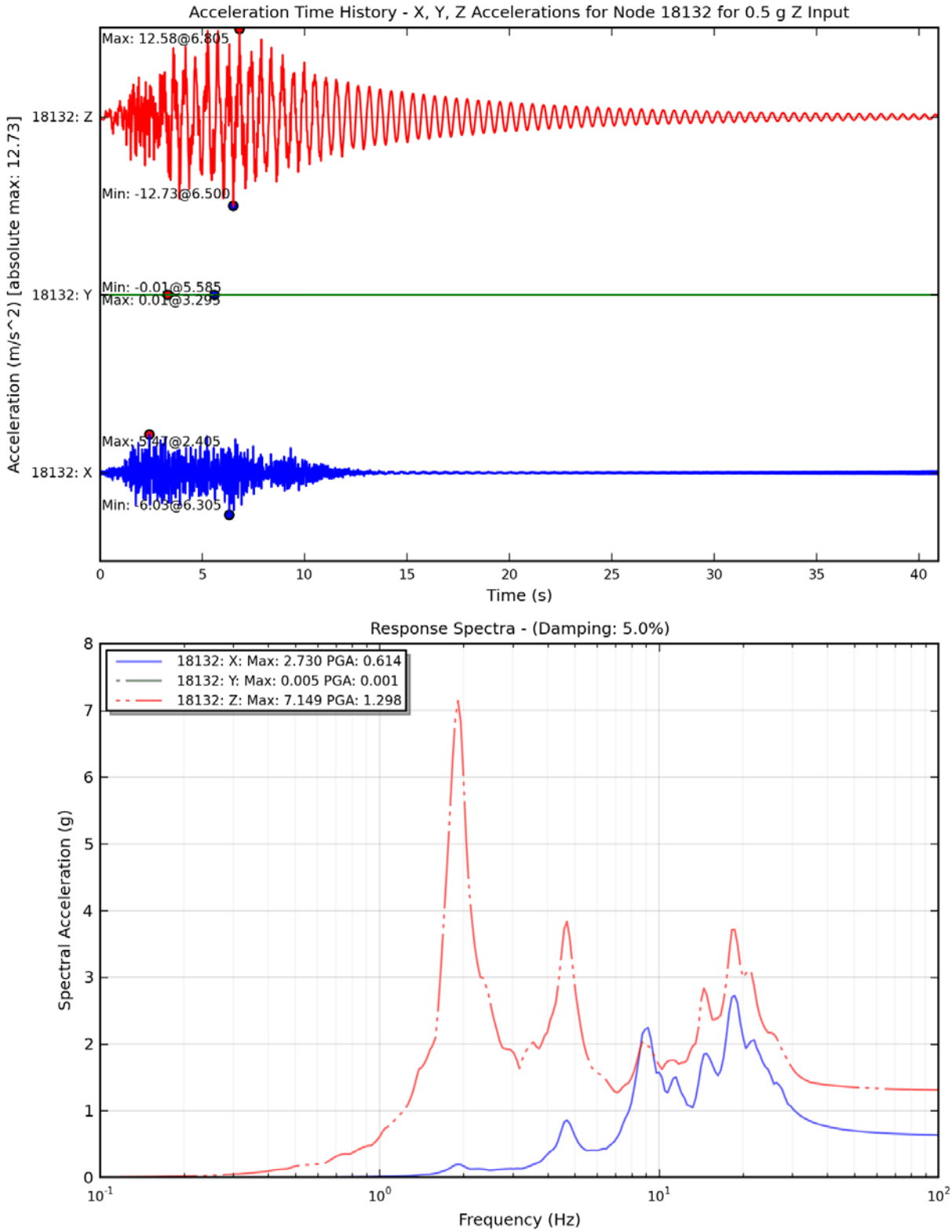

Figure 4-45 Response Acceleration Time Histories and ISRS at Node 18132 for Z Input Motion (0.5 g)

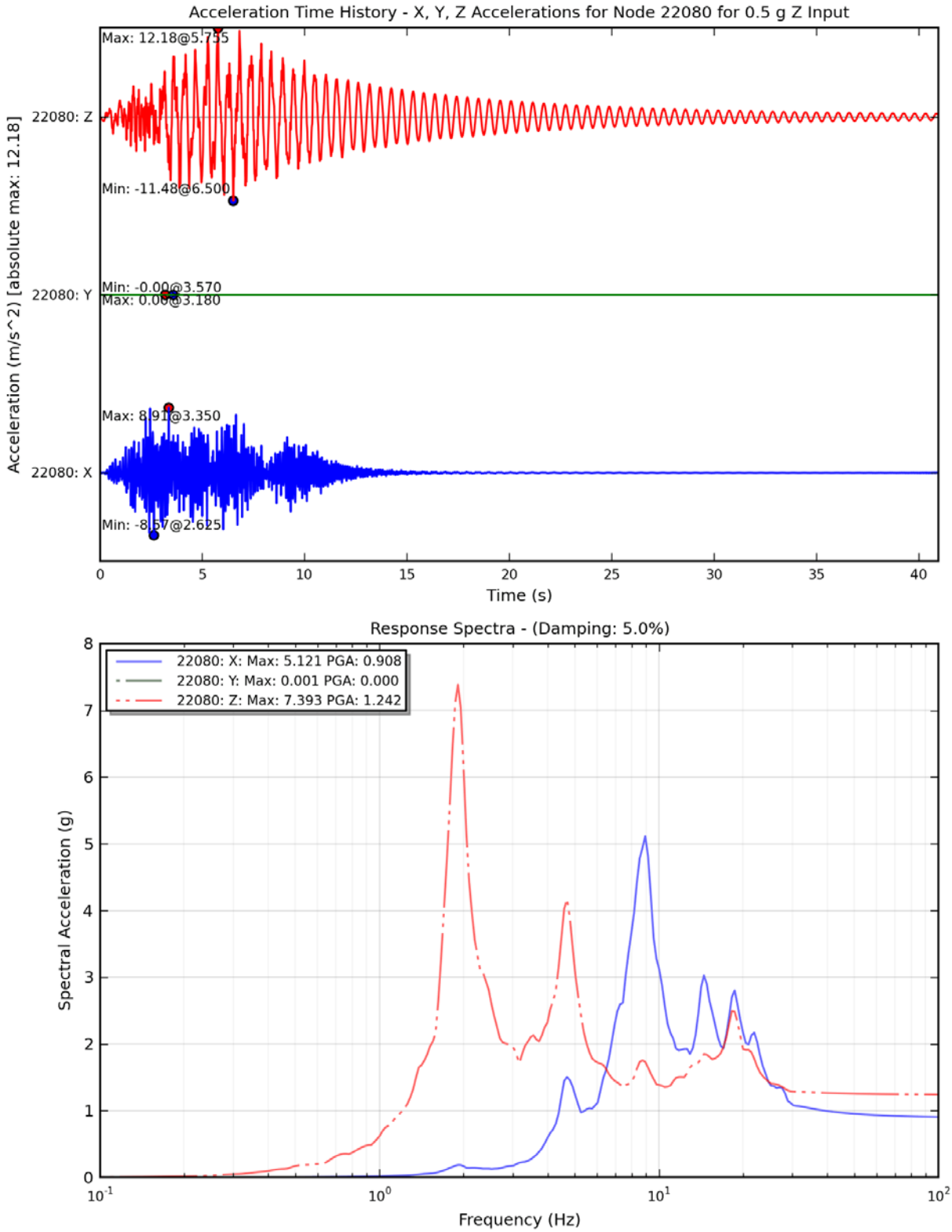

Figure 4-46 Response Acceleration Time Histories and ISRS at Node 22080 for Z Input Motion (0.5 g)

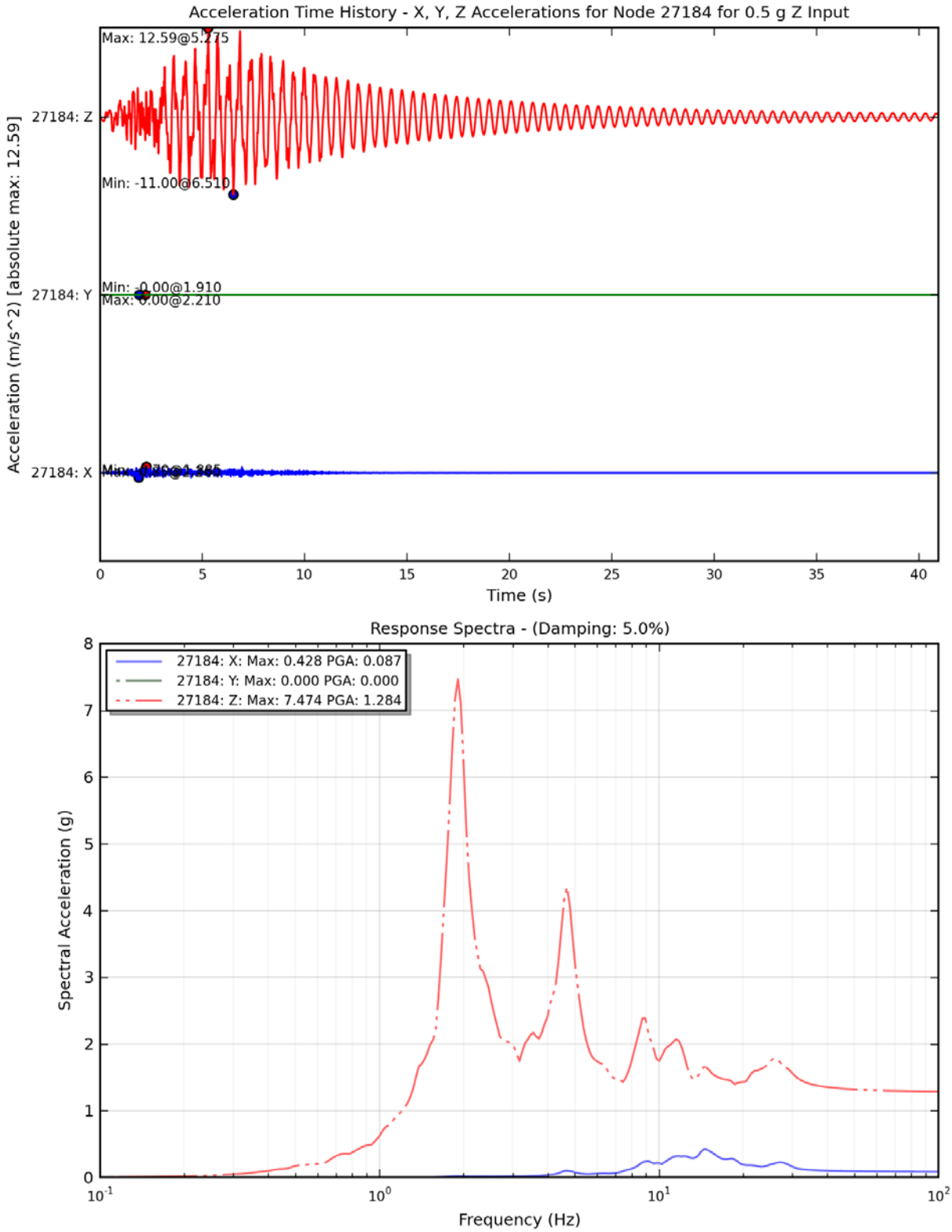

Figure 4-47 Response Acceleration Time Histories and ISRS at Node 27184 for Z Input Motion (0.5 g)

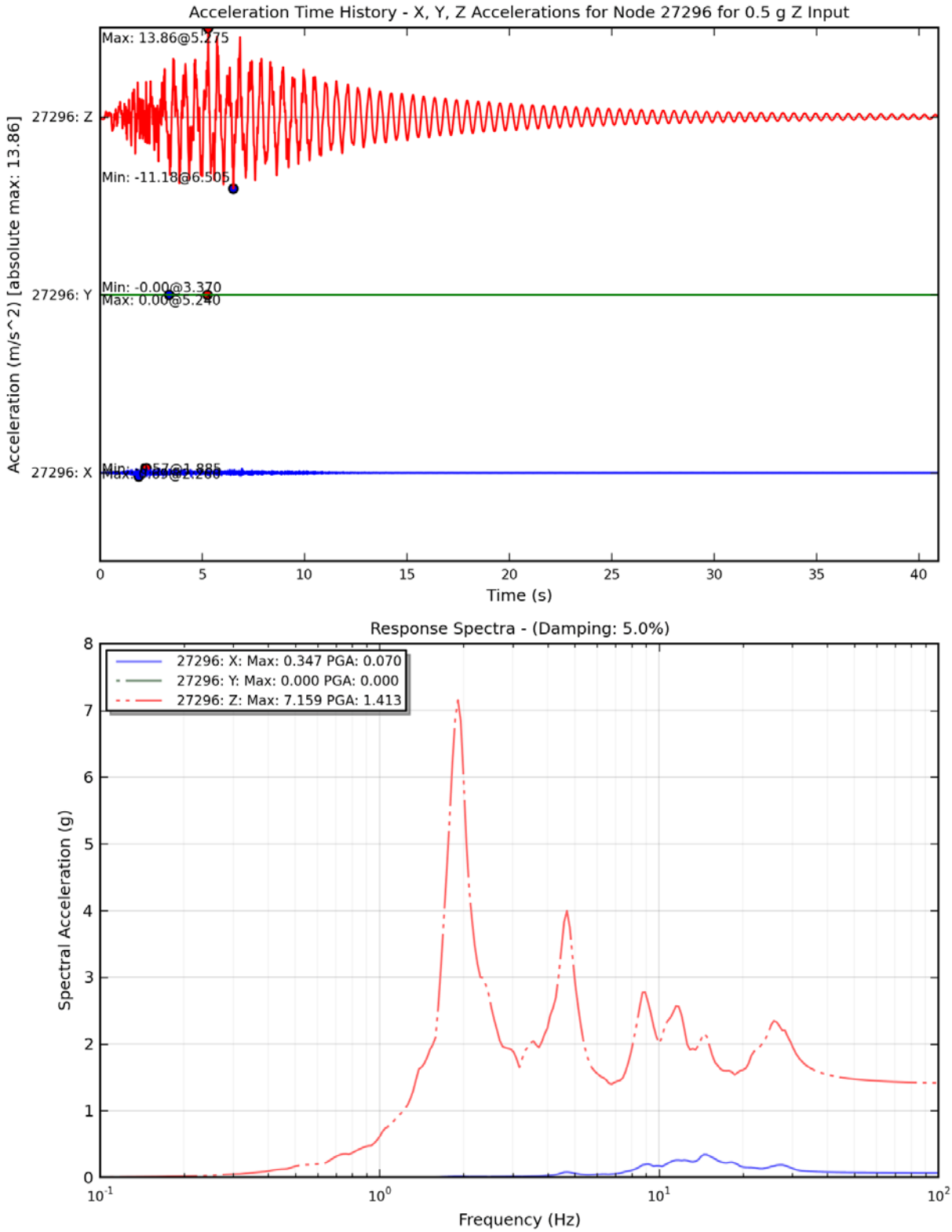

Figure 4-48 Response Acceleration Time Histories and ISRS at Node 27296 for Z Input Motion (0.5 g)

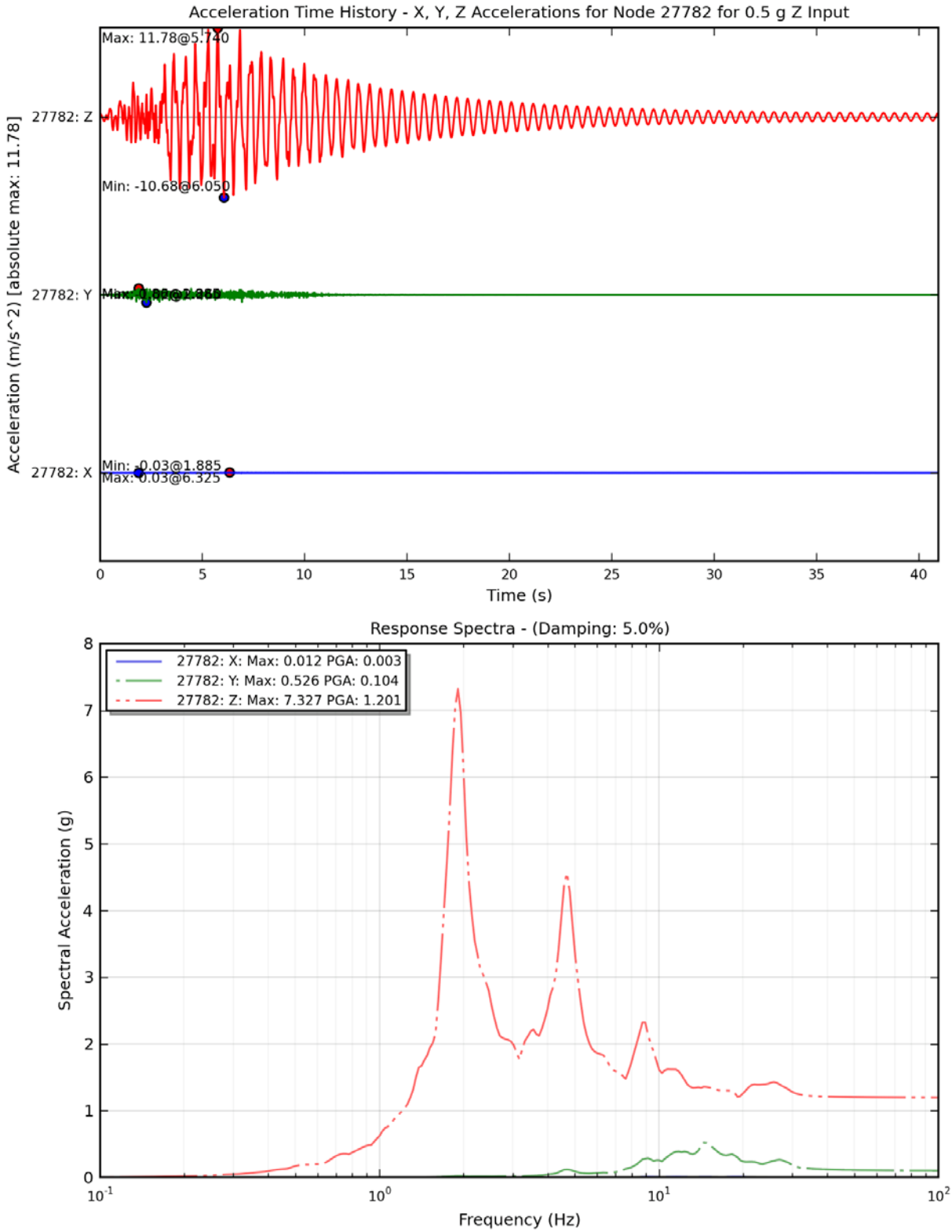

Figure 4-49 Response Acceleration Time Histories and ISRS at Node 27782 for Z Input Motion (0.5 g)

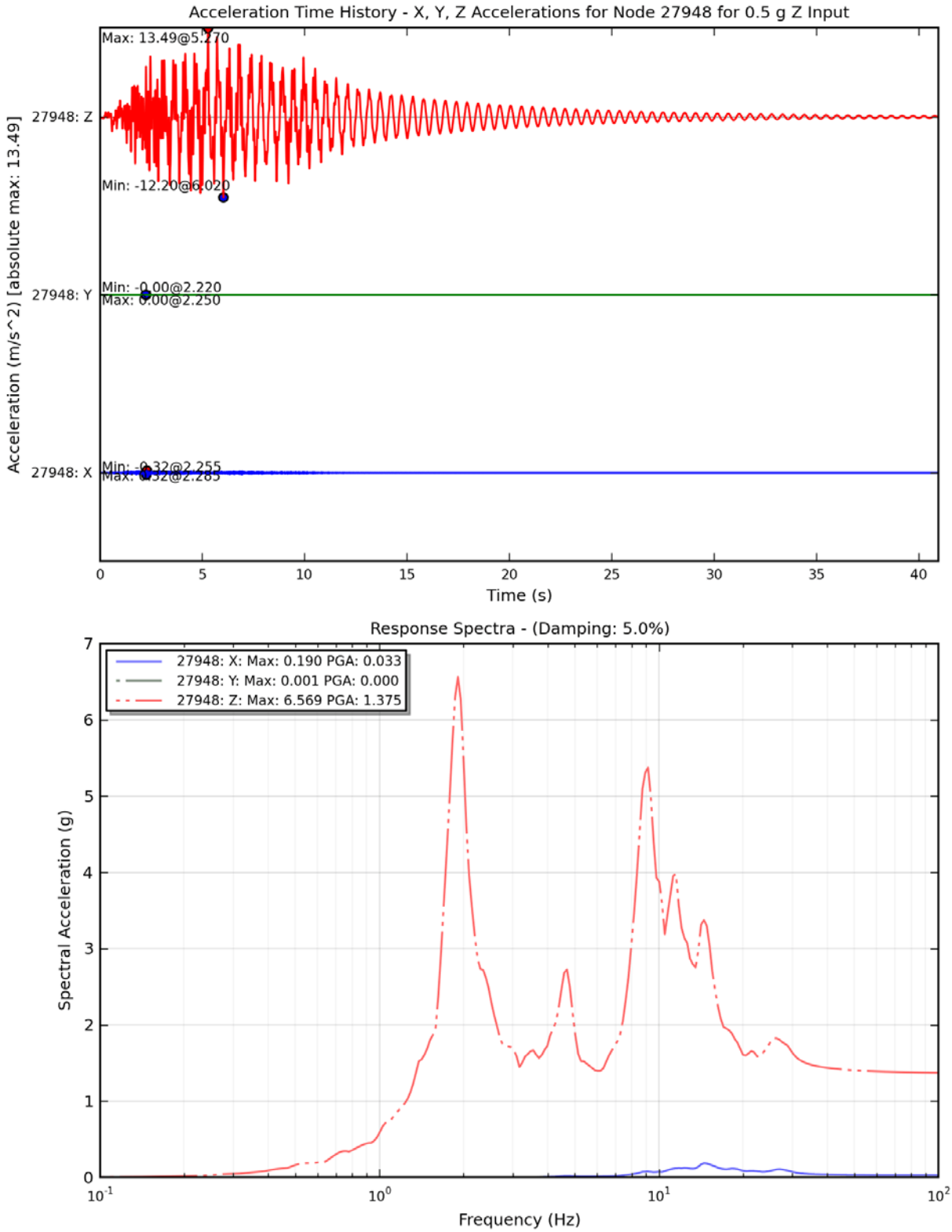

Figure 4-50 Response Acceleration Time Histories and ISRS at Node 27948 for Z Input Motion (0.5 g)

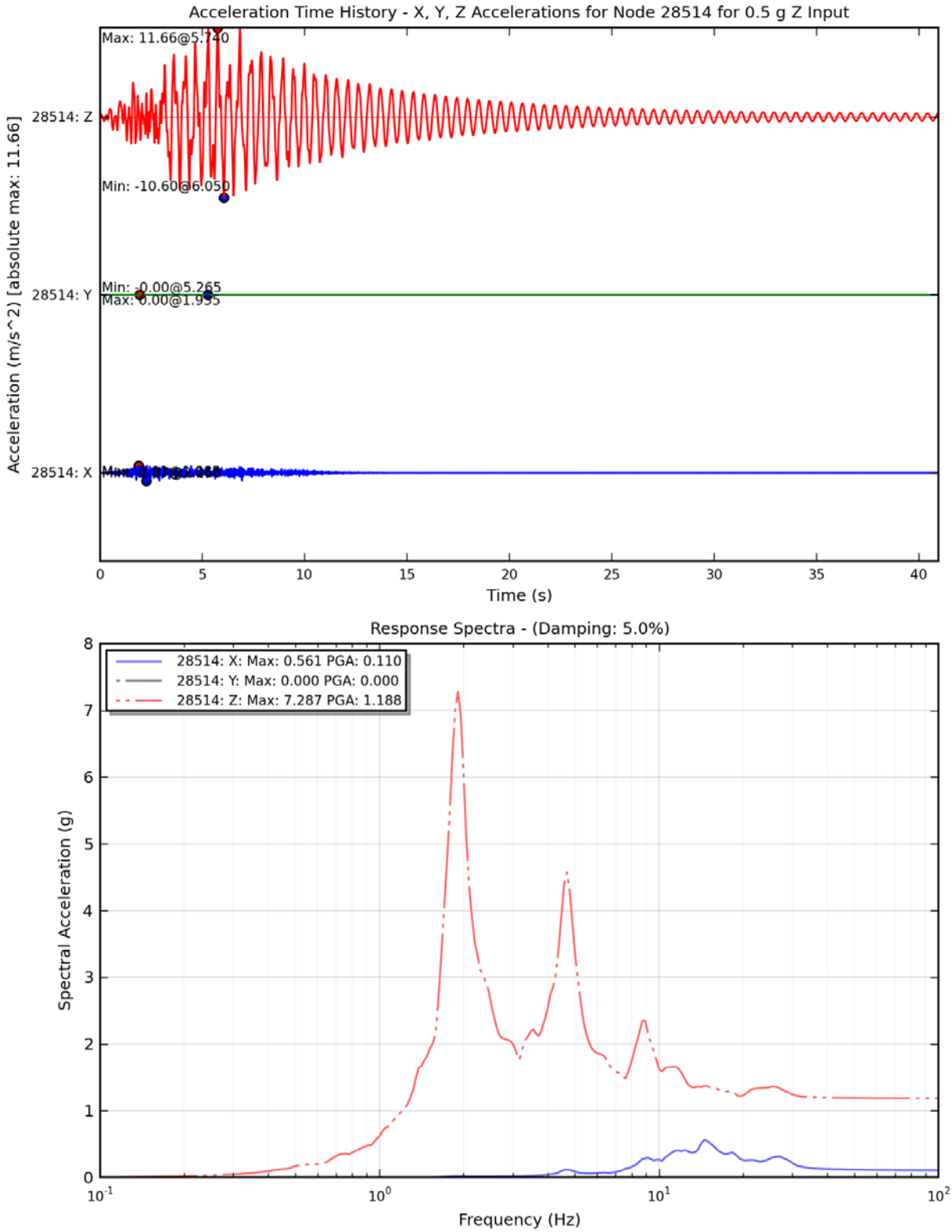

Figure 4-51 Response Acceleration Time Histories and ISRS at Node 28514 for Z Input Motion (0.5 g)

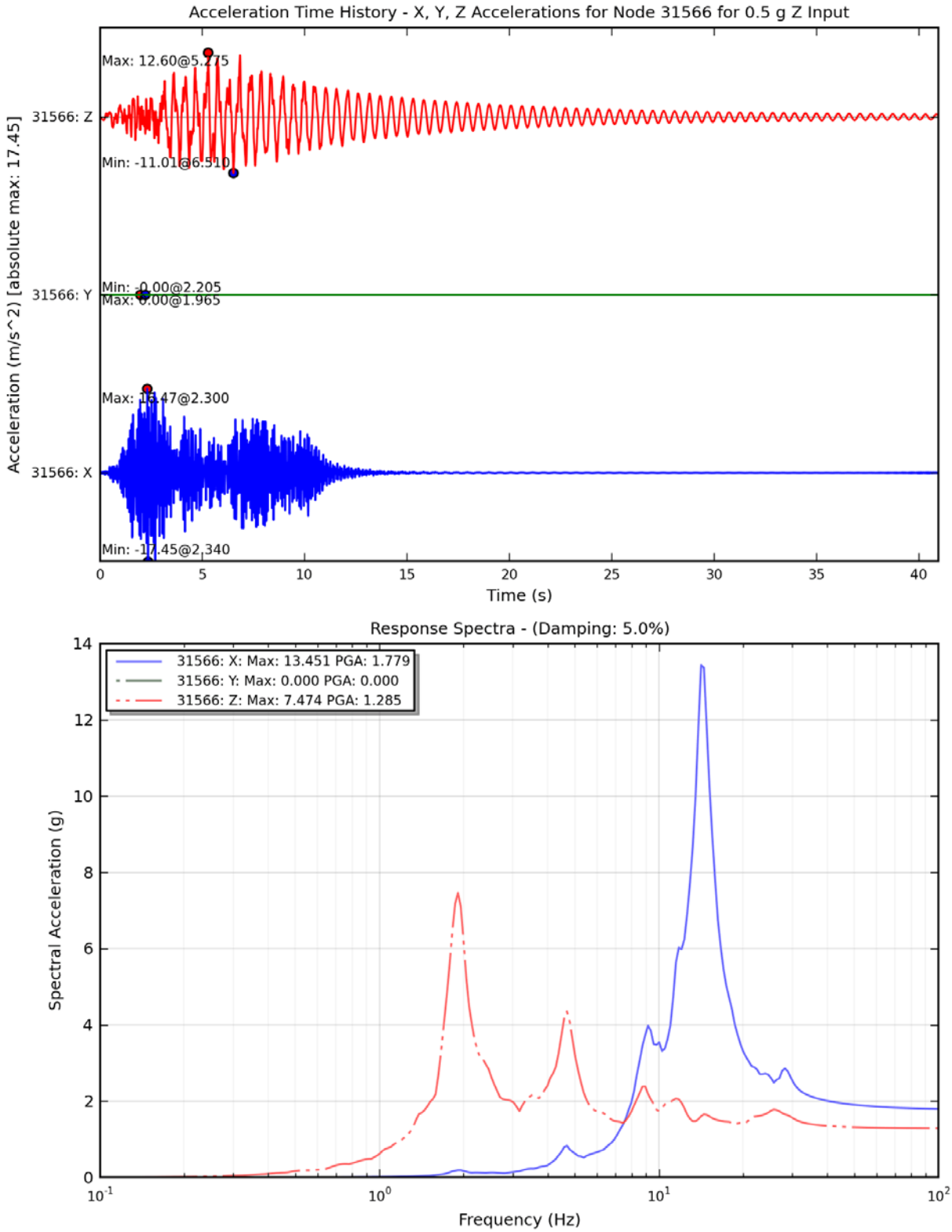

Figure 4-52 Response Acceleration Time Histories and ISRS at Node 31566 for Z Input Motion (0.5 g)

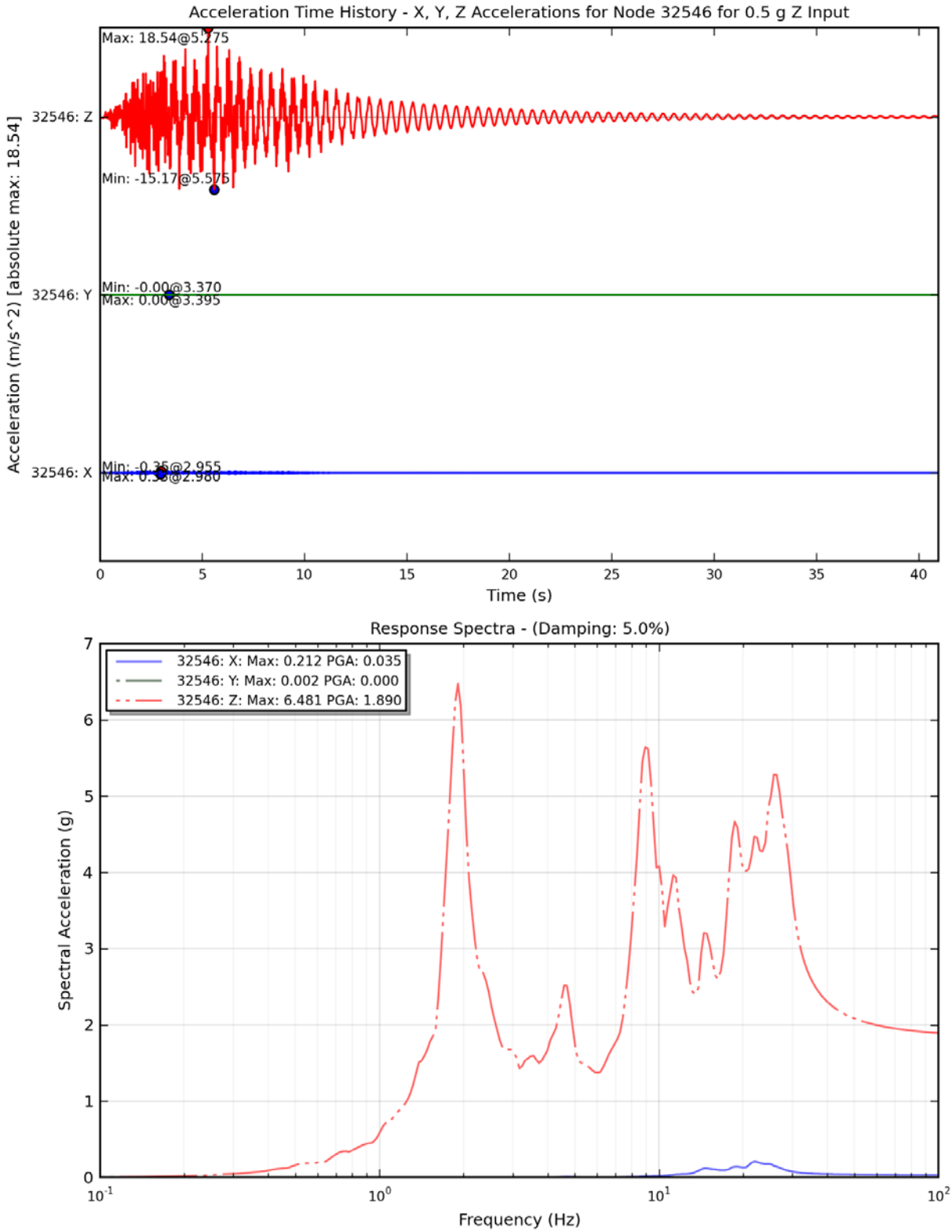

Figure 4-53 Response Acceleration Time Histories and ISRS at Node 32546 for Z Input Motion (0.5 g)

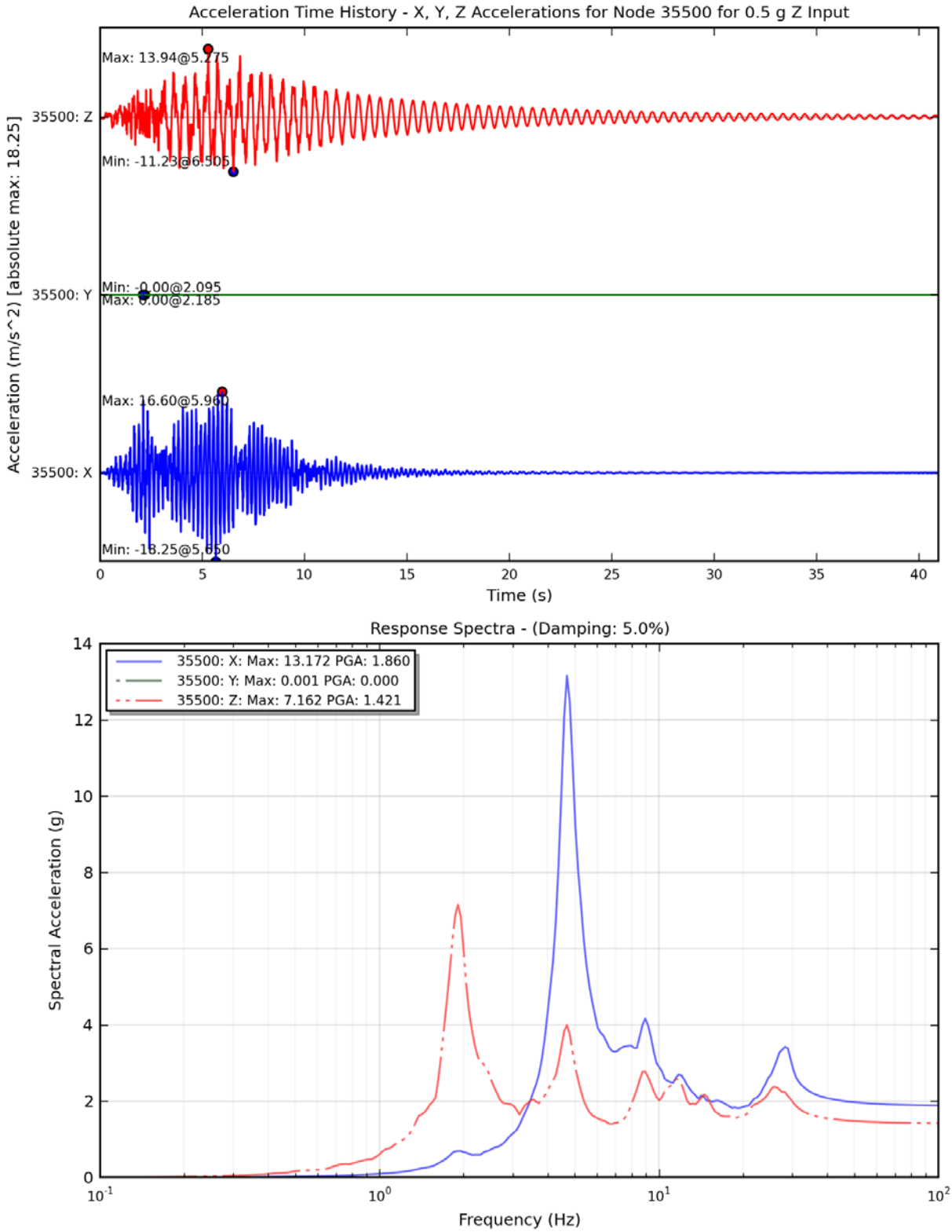

Figure 4-54 Response Acceleration Time Histories and ISRS at Node 35500 for Z Input Motion (0.5 g)

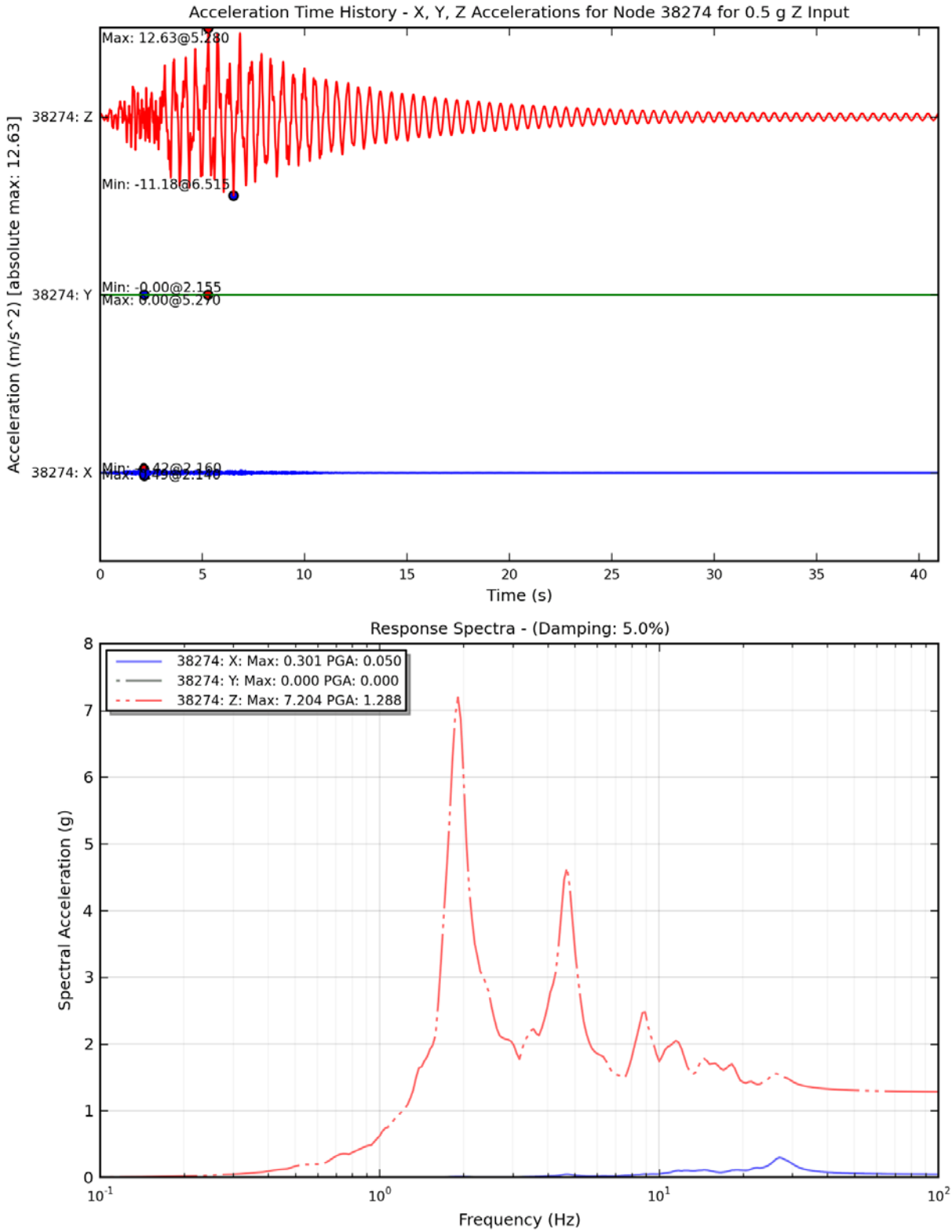

Figure 4-55 Response Acceleration Time Histories and ISRS at Node 38274 for Z Input Motion (0.5 g)

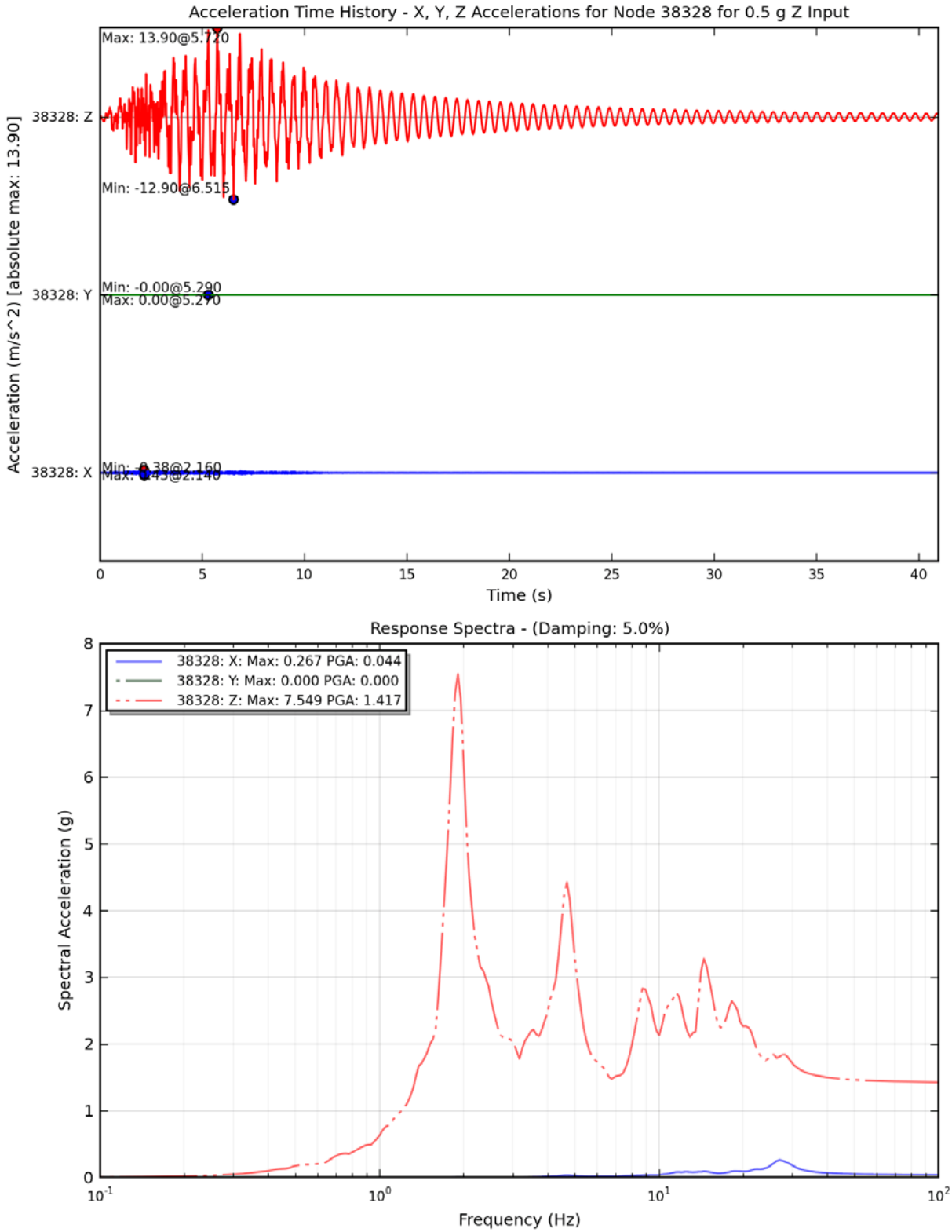

Figure 4-56 Response Acceleration Time Histories and ISRS at Node 38328 for Z Input Motion (0.5 g)

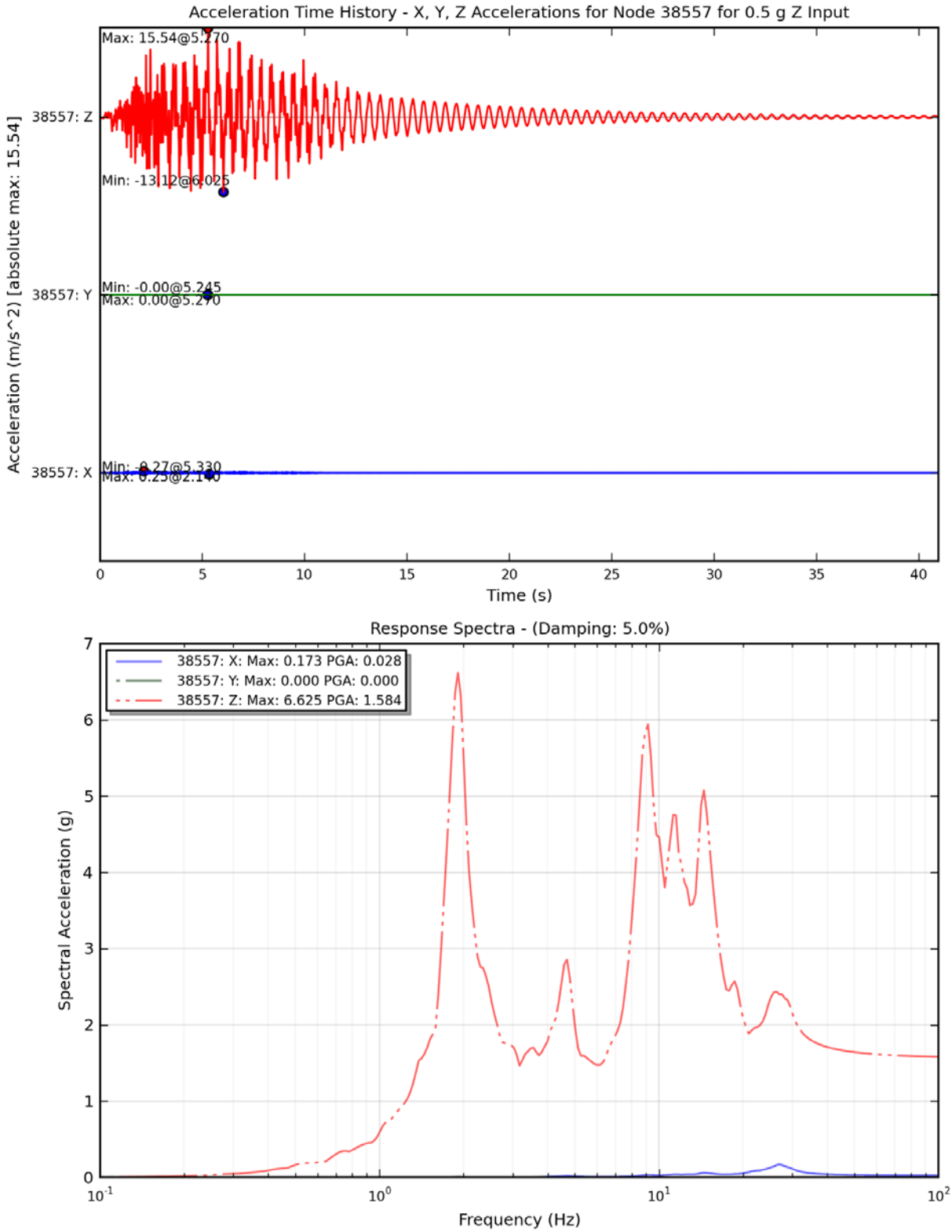

Figure 4-57 Response Acceleration Time Histories and ISRS at Node 38557 for Z Input Motion (0.5 g)

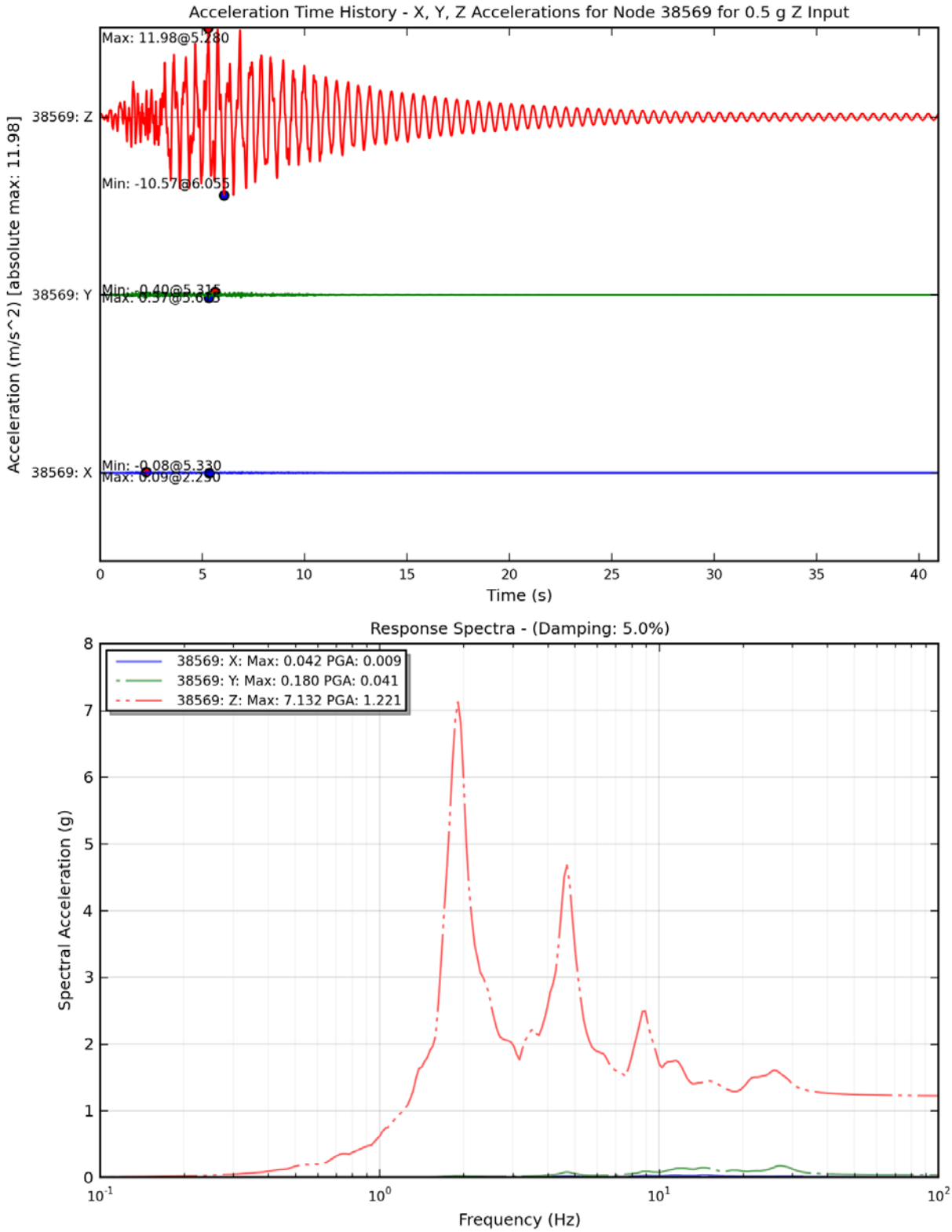

Figure 4-58 Response Acceleration Time Histories and ISRS at Node 38569 for Z Input Motion (0.5 g)

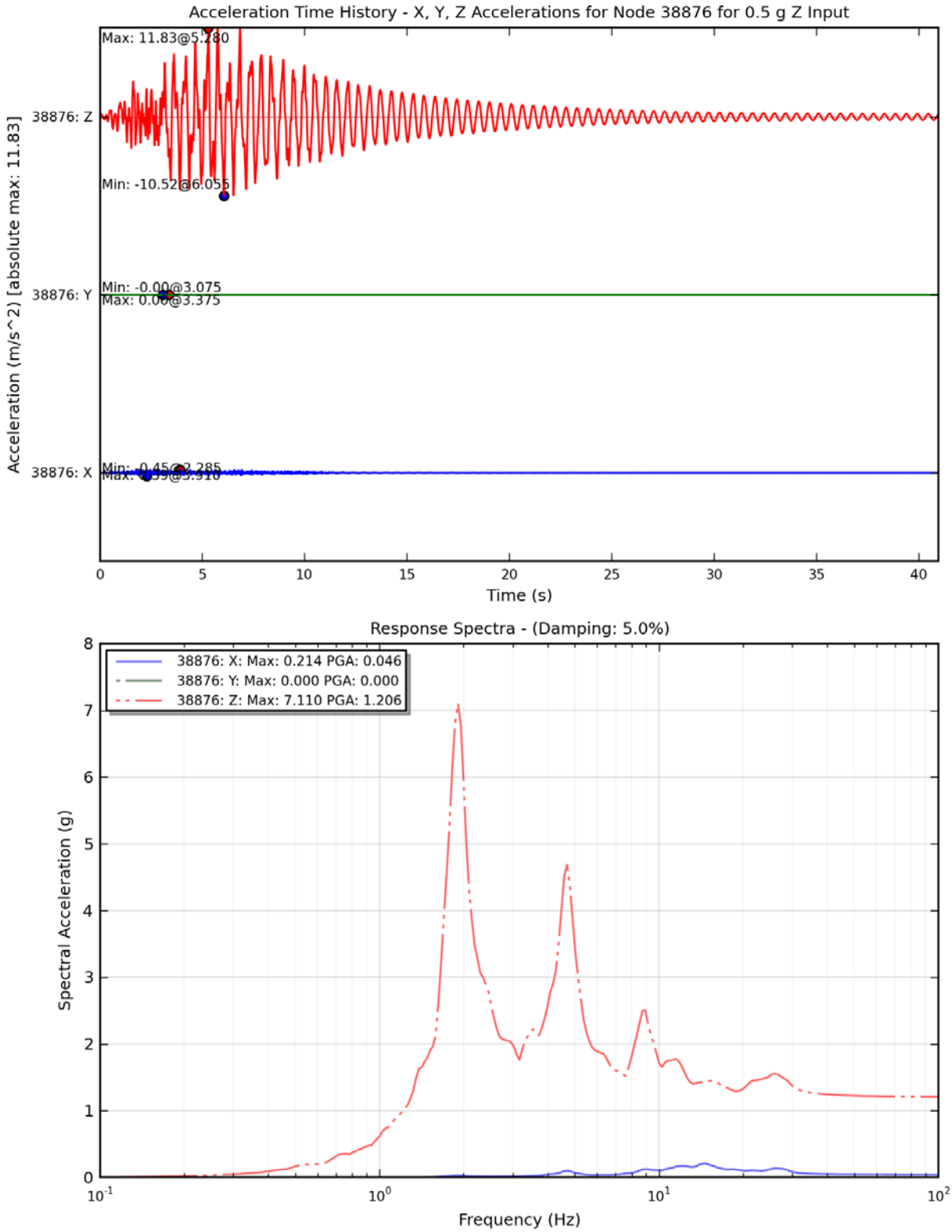

Figure 4-59 Response Acceleration Time Histories and ISRS at Node 38876 for Z Input Motion (0.5 g)

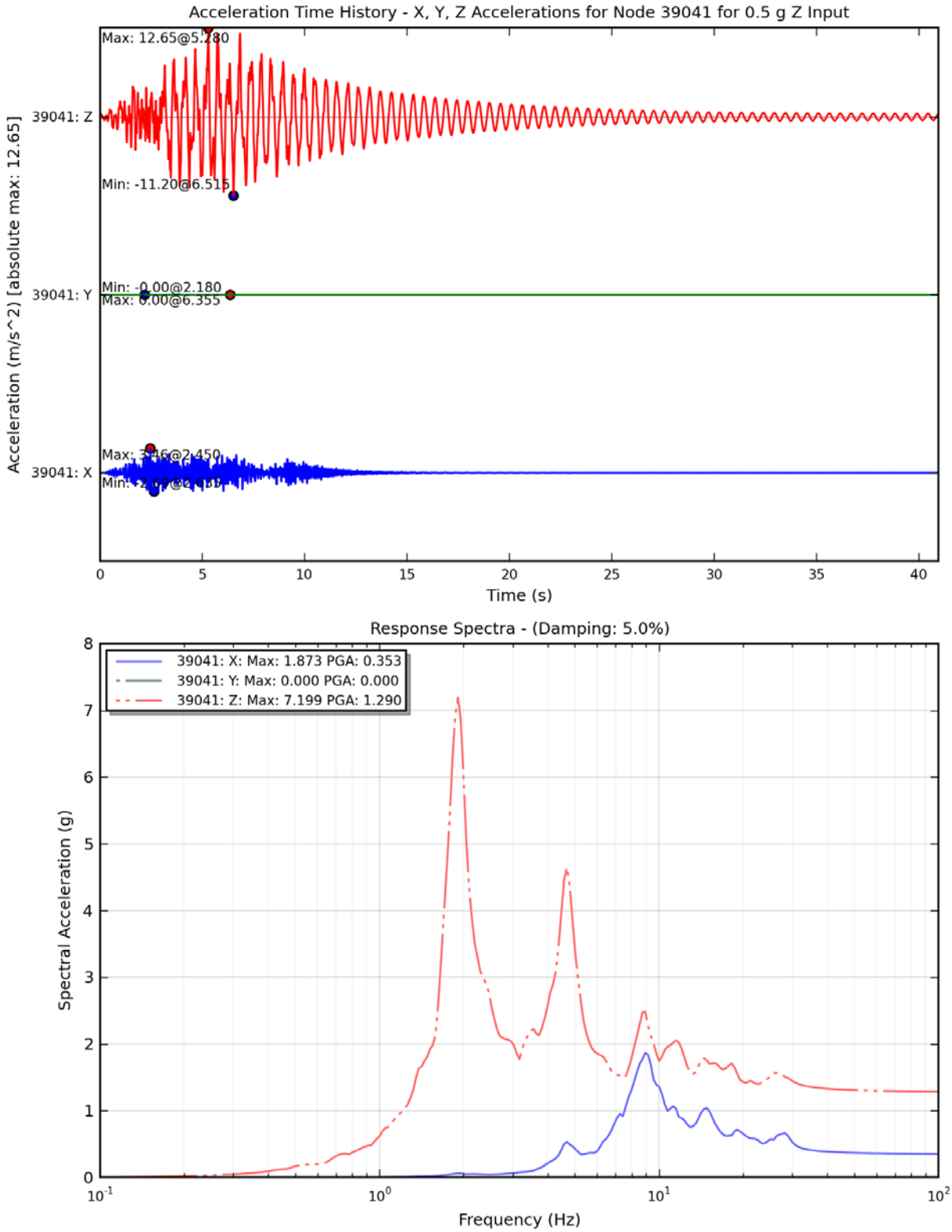

Figure 4-60 Response Acceleration Time Histories and ISRS at Node 39041 for Z Input Motion (0.5 g)

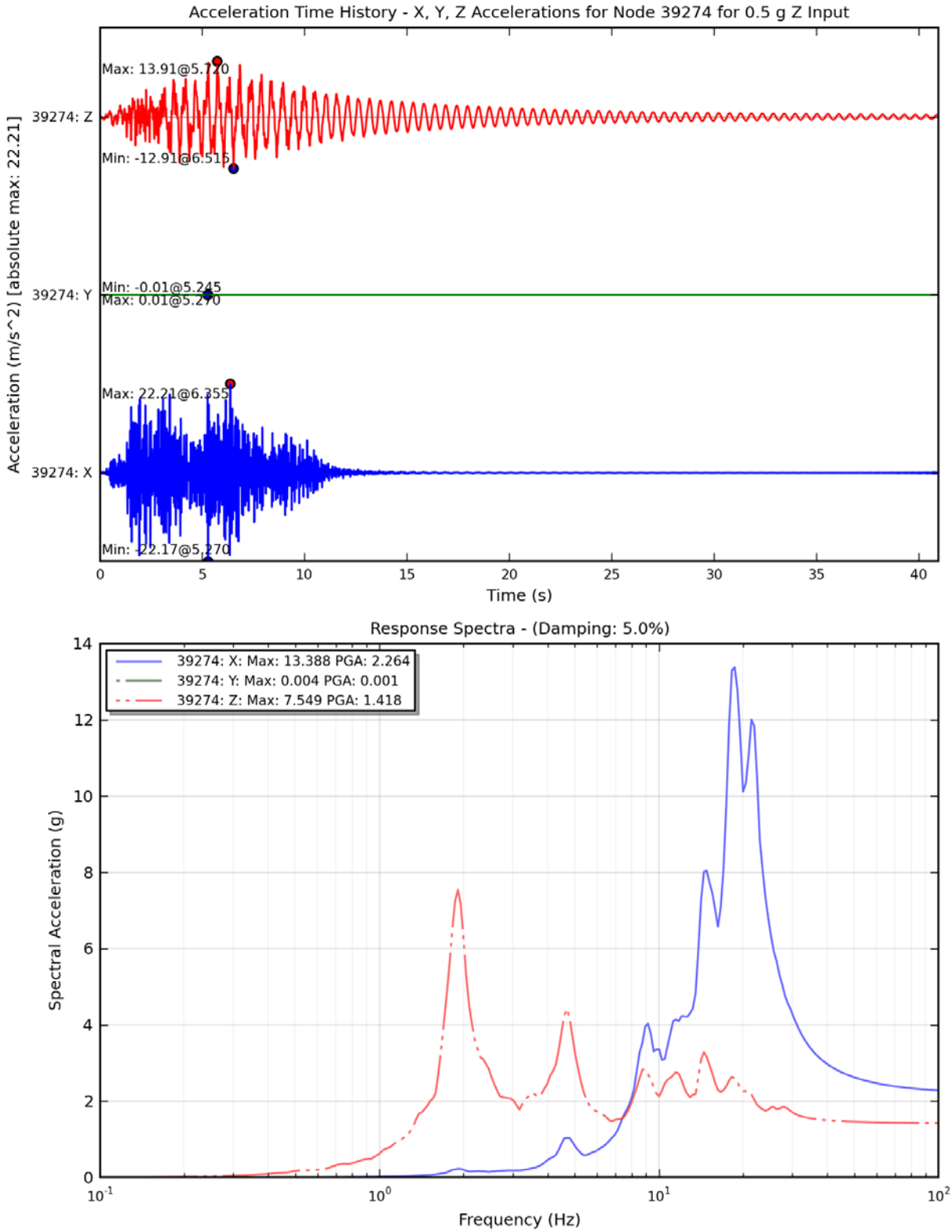

Figure 4-61 Response Acceleration Time Histories and ISRS at Node 39274 for Z Input Motion (0.5 g)

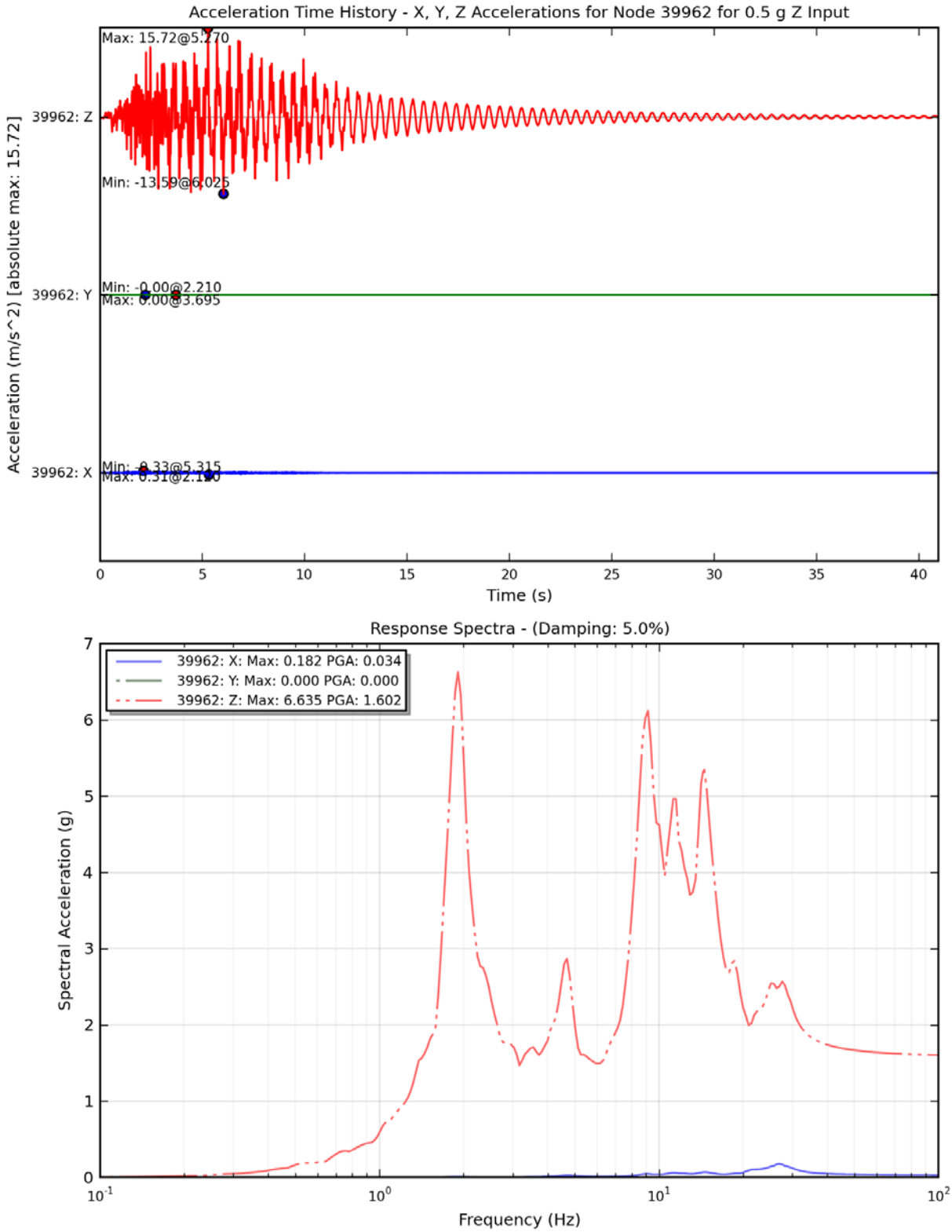

Figure 4-62 Response Acceleration Time Histories and ISRS at Node 39962 for Z Input Motion (0.5 g)

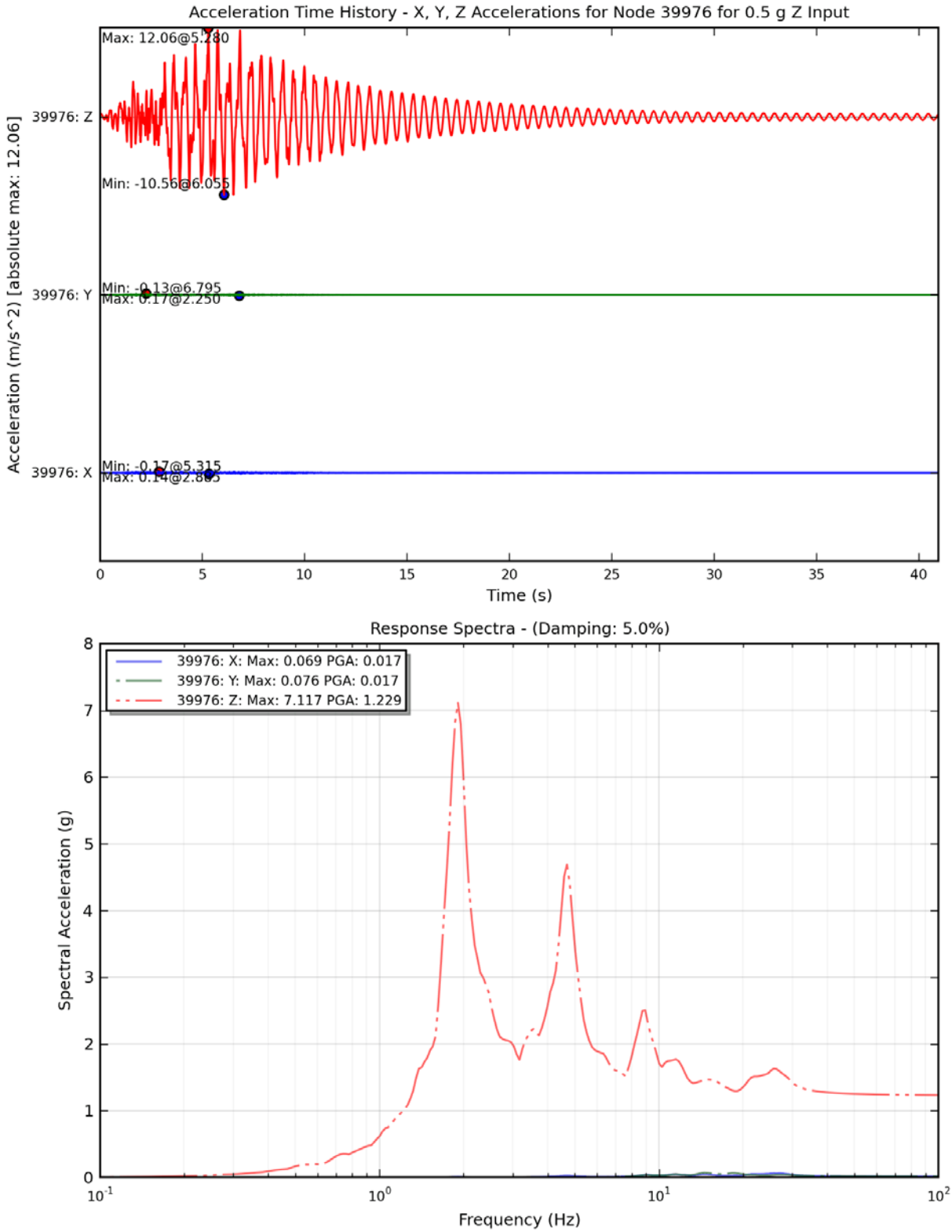

Figure 4-63 Response Acceleration Time Histories and ISRS at Node 39976 for Z Input Motion (0.5 g)

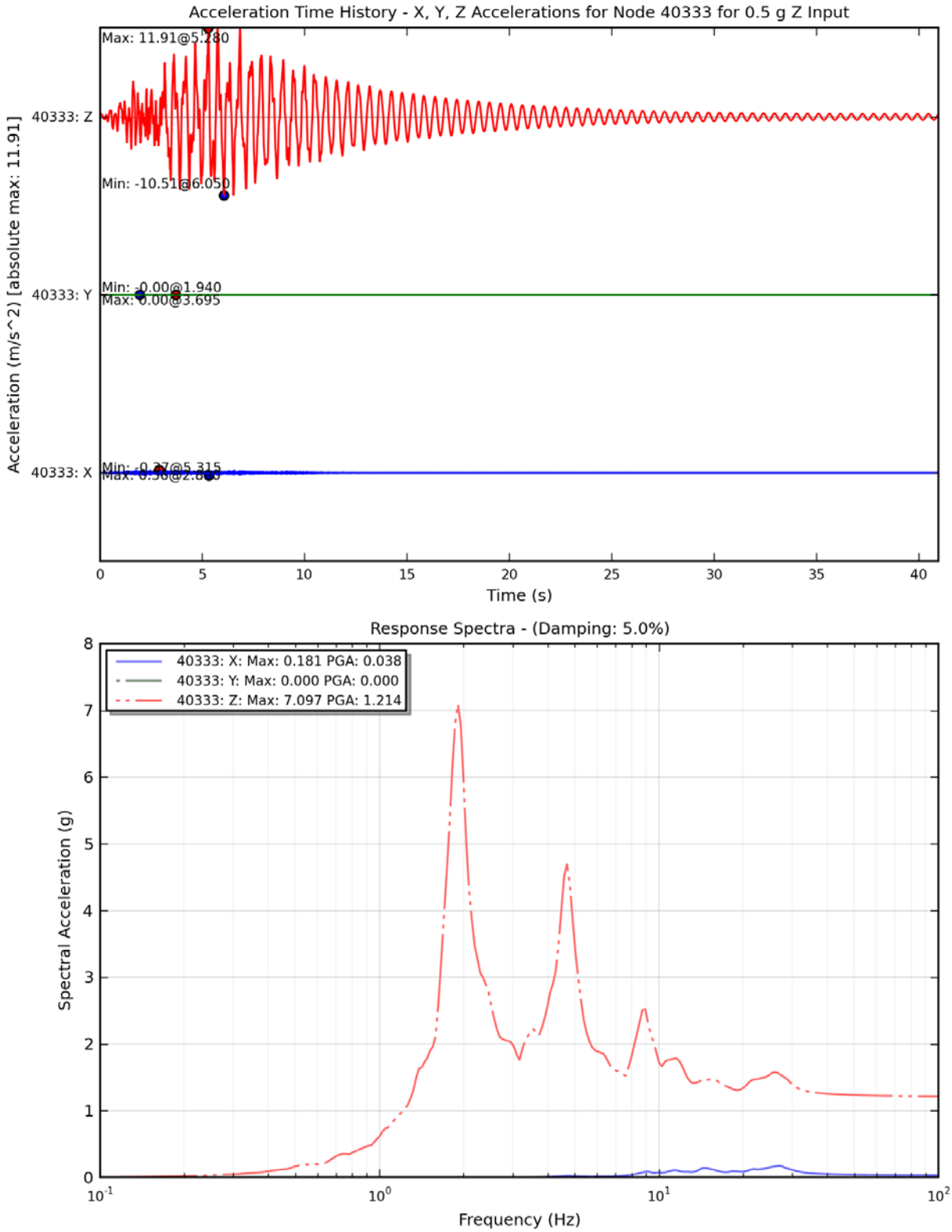

Figure 4-64 Response Acceleration Time Histories and ISRS at Node 40333 for Z Input Motion (0.5 g)

5 THE CASE OF 0.9 g

5.1 Summary of SASSI Results

This section describes the SASSI results for the case of a nominal bedrock peak acceleration of 0.9 g.

Section 5.2 includes acceleration time history and response spectral figures for the X directional input, while Section 5.3 includes figures for the Z directional input.

The acceleration time histories are output directly from the SASSI computer code. The ISRS were calculated outside of SASSI for each of these acceleration time histories, separately for the two input motions in the X and Z directions. All maximum acceleration values are rounded to the second decimal place. It should be noted that the input motion, used in both DIABLO and SASSI analyses, was not baseline-corrected, and neither were the response accelerations shown in this document. In addition, the acceleration time histories should not be integrated to obtain velocity or displacement time histories.

In summary, results are presented as follows:

Accelerations – Maximum values and time history plots
ISRS – Acceleration response spectra

The table and the footnotes were provided to BNL by LLNL in order for BNL to enter the SASSI results. All items in red denote SASSI node/element information. Where an "x" is presented in the table, the data is not available.

Table 5-1 SASSI Results for the Case of 0.9 g

Roof Slab			
Response Parameter (unit) & Location	**Response Parameter Value for**		**Remarks**
	X-Dir Input Motion	**Vertical (Z) Input Motion**	
Maximum[(1)] X, Y, Z-Directional Accelerations m/s^2) at Node xx near the center of Roof Slab	8.63 0.00 0.03	0.58 0.00 27.33	Node (EXODUS:4140, CUBIT:8789, SASSI-39962): Located (0.0,0.0,13.5)m
Maximum[(1)] X, Y, Z-Directional Displacements (m) at Node xx near the center of Roof Slab	x	x	Node (EXODUS:4140, CUBIT:8789, SASSI-39962): Located (0.0,0.0,13.5)m
Maximum[(1)] out-of-plane Bending Moment about X and Y axes (N-m/m) at Node xx near the center of the Roof Slab	x	x	Element (EXODUS:4452, CUBIT:9444, SASSI- (710, 8, 3)): Located (0.0,0.0,13.5)m
X, Y, Z-Directional Acceleration ISRSs (in 'g'unit) at Node xx near the center of Roof Slab	See figure for 39962	See figure for 39962	Node (EXODUS:4140, CUBIT:8789, SASSI-39962): Located (0.0,0.0,13.5)m
X, Y, Z-Directional Acceleration ISRSs (in 'g'unit) at Node xx and Node YY near the edges of Roof Slab	See figures for 40333 and 39976	See figures for 40333 and 39976	Node (EXODUS:3962, CUBIT:4922, SASSI-40333): Located (14.0,0.0,13.5)m Node (EXODUS:4145, CUBIT:1142, SASSI-39976): Located (0.0,14.0,13.5)m
Third Floor Slab			
Maximum[(1)] X, Y, Z-Directional Accelerations (m/s^2) at Node xx near the center of Slab	7.58 0.00 0.03	0.50 0.00 26.32	Node (EXODUS:3436, CUBIT:8193, SASSI-38557): Located (0.0, 0.0, 6.5) m
Maximum[(1)] X, Y, Z-Directional Displacements m) at Node xx near the center of Slab	x	x	Node (EXODUS:3436, CUBIT:8193, SASSI-38557): Located (0.0, 0.0, 6.5) m
Maximum[(1)] out-of-plane Bending Moment about X and Y axes N-m/m) at Node xx near the center of the Slab	x	x	Element (EXODUS:3258, CUBIT:8250, SASSI- (146, 7, 3)): Located (0.0, 0.0, 6.5) m
X, Y, Z-Directional Acceleration ISRSs (in 'g'unit) at Node xx near the center of Slab	See figure for 38557	See figure for 38557	Node (EXODUS:3436, CUBIT:8193, SASSI-38557): Located (0.0, 0.0, 6.5) m

X, Y, Z-Directional Acceleration ISRSs (in 'g'unit) at Node xx and Node YY near the edges of Slab	See figures for 38876 and 38569	See figures for 38876 and 38569	Node (EXODUS:3321, CUBIT:4747, SASSI-38876): Located (14.0,0.0,6.5)m Node (EXODU:3493, CUBIT:39, SASSI-38569): Located (0.0,14.0,6.5)m
Second Floor Slab			
Maximum[1] X, Y, Z-Directional Accelerations m/s^2) at Node xx near the center of Slab	5.35 0.00 0.74	0.41 0.00 23.55	Node (EXODUS:675, CUBIT:5718, SASSI-27948): Located (3.125, 0.0, -9.144)m
Maximum[1] X, Y, Z-Directional Displacements (m) at Node xx near the center of Slab	x	x	Node (EXODUS:675, CUBIT:5718, SASSI-27948): Located (3.125, 0.0, -9.144)m
Maximum[1] out-of-plane Bending Moment about X and Y axes (N-m/m) at Node xx near the center of the Slab	x	x	Element (EXODUS:2627, CUBIT:7619, SASSI- (65, 6, 3)): Located (3.125, 0.0, -9.144)m
X, Y, Z-Directional Acceleration ISRSs (in 'g'unit) at Node xx near the center of Slab	See figure for 27948	See figure for 27948	Node (EXODUS:675, CUBIT:5718, SASSI-27948): Located (3.125, 0.0, -9.144)m
X, Y, Z-Directional Acceleration ISRSs (in 'g'unit) at Node xx and Node YY near the edges of Slab	See figures for 28514 and 27782	See figures for 28514 and 27782	Node (EXODUS:2676, CUBIT:3872, SASSI-28514): Located (14.0,0.0,-9.144)m Node (EXODUS:2993, CUBIT:231, SASSI- 27782) Located (-0.1818,14.0,-9.144)m
First Floor Slab			
Maximum[1] X, Y, Z-Directional Accelerations m/s^2) at Node xx near the center of Slab	4.81 0.00 0.76	0.62 0.00 22.00	Node (EXODUS:435, CUBIT:5532, SASSI-14522): Located(3.125,0.0,-22.5552)m
Maximum[1] X, Y, Z-Directional Displacements (m) at Node xx near the center of Slab	x	x	Node (EXODUS:435, CUBIT:5532, SASSI-14522): Located(3.125,0.0,-22.5552)m
Maximum[1] out-of-plane Bending Moment about X and Y axes (N-m/m) at Node xx near the center of the Slab	x	x	Element (EXODUS:2224, CUBIT:7216, SASSI- (279, 5, 3)): Located(3.125,0.0,-22.5552)m

X, Y, Z-Directional Acceleration ISRSs (in 'g'unit) at Node xx near the center of Slab	See figure for 14522	See figure for 14522	Node (EXODUS:435, CUBIT:5532, SASSI-14522): Located(3.125,0.0,-22.5552)m
X, Y, Z-Directional Acceleration ISRSs (in 'g'unit) at Node xx and Node YY near the edges of Slab	See figures for 15095 and 14364	See figures for 15095 and 14364	Node (EXODUS:2055, CUBIT:4122, SASSI-15095): Located (14.00,0.0,-22.5552) Node (EXODUS:2363, CUBIT:486, SASSI- 14364): Located(-0.1818,14.0,-22.5552)
Base Mat			
Maximum[(1)] X, Y, Z-Directional Accelerations (m/s^2) at Node xx near the center of Slab	5.95 0.00 0.03	0.14 0.00 21.34	Node (EXODUS:1319, CUBIT:6413, New basemat 9828, SASSI- 1942): Located (0.0,0.0,-34.5)
Maximum[(1)] X, Y, Z-Directional Displacements (m) at Node xx near the center of Slab	x	x	Node (EXODUS:1319, CUBIT:6413, New basemat 9828, SASSI- 1942): Located (0.0,0.0,-34.5)
Maximum[(1)] out-of-plane Bending Moment about X and Y axes (N-m/m) at Node xx near the center of the Slab	x	x	Element (EXODUS:1299, CUBIT:6413, New basemat 19363 (+X+Y to node 9828), SASSI- (351, 4, 3)): Located (0.0,0.0,-34.5)
X, Y, Z-Directional Acceleration ISRSs (in 'g'unit) at Node xx near the center of Slab	See figure for 1942	See figure for 1942	Node (EXODUS:1319, CUBIT:6413, New basemat 9828, SASSI- 1942): Located (0.0,0.0,-34.5)
X, Y, Z-Directional Acceleration ISRSs (in 'g'unit) at Node xx and Node YY near the edges of Slab	See figures for 2949 And 1887	See figures for 2949 And 1887	Node (EXODUS:1384, CUBIT:4447, SASSI- 2949): Located (14,0.0,-34.5)m Node (EXODUS:1700, CUBIT:835, SASSI- 1887): Located (0.909,14.0,-34.5)m
Reactor Vessel and Supports			
Maximum[(1)] X, Y, Z-Directional Displacements (m) at Node xx near the top Cover Plate of the Reactor Vessel	x	x	Node (EXODUS:27, CUBIT:5122, SASSI-32546): Located (0.0,0.0,-4.5)m

Maximum[1] out-of-plane Bending Moments about X and Y axes (N-m/m) at Node xx near the top Cover Plate of the Reactor Vessel	x	x	Element (EXODUS:14, CUBIT:5006, SASSI- (14, 1, 3)): Located (0.0,0.0,-4.5)m
Maximum[1] out-of-plane Bending Moments about X and Y axes (N-m/m) at Node xx of the Reactor Support Ring Plate		x	Element (EXODUS:4460, CUBIT:9452, SASSI- (2, 9, 3)): Located (2.0,0.0,-20.5)m Element (EXODUS:4486. CUBIT:9478, SASSI- (28, 9, 3)): Located (0.0,2.0,-20.5)m
Reactor Building Walls			
Maximum out-of-plane bending moments about X and Y axes (N-m/m) at Elev XX (4 Nodes, one in each wall near the center)	x	x	Elevation 1 Element (EXODUS:4503, CUBIT:13), SASSI- (13, 10, 3) located: (0.0,14.0,0.0)m Element(EXODUS: 8351, CUBIT:3861), SASSI- (3861, 10, 3) Located: (14.0,0.0,0.0) Element (EXODUS:5751, CUBIT:1261) , SASSI- (1261, 10, 3) Located: (0.0, -14.0,0.0)m Element(EXODUS: 6999, CUBIT:2509) SASSI- (2509, 10, 3) Located: (-14.0, 0.0, 0.0)m Elevation 2 Element (EXODUS:7571, CUBIT:3081), SASSI- (3081, 10, 3) Located: (-14.0,0.0, -16.36541)m Element (EXODUS:6323, CUBIT:1833) SASSI- (1833, 10, 3) Located: (-0.1818, -14.00, -16.36541)m Element (EXODUS:8637, CUBIT:4147), SASSI- (4147, 10, 3)Located: (14.00, 0.0, -16.36541)m Element (EXODUS:5075, CUBIT:585) SASSI- (585, 10, 3): Located: (-0.1818, 14.00, -16.36541)m

Maximum soil pressure in X and Y direction (in psi Pa) at 4 Nodes, one in each outer wall near the center	x	x	Elevation 1 Element(EXODUS: 8351, CUBIT:3861) StructSoil: 24702, SASSI-(900, 101, 1) Located: (14.0,0.0,0.0) Element(EXODUS: 6999, CUBIT:2509) Located: (-14.0, 0.0, 0.0)m Elevation 2 Element (EXODUS:7571, CUBIT:3081) StructSoil: 22828, SASSI-(1060, 102, 1) Located: (-14.0,0.0, -16.36541)m Element (EXODUS:6323, CUBIT:1833) StructSoil: 22282, SASSI-(514, 102, 1) Located: (-0.1818, -14.00, -16.36541)m Element (EXODUS:8637, CUBIT:4147) StructSoil: 22321, SASSI-(553, 102, 1) Located: (14.00, 0.0, -16.36541)m Element (EXODUS:5075, CUBIT:585): StructSoil: 22516, SASSI-(748, 102, 1) Located: (-0.1818, 14.00, -16.36541)m

Maximum in-plane shear stress(Pa) in the reactor building X and Y-Dir outer walls at 8 Nodes, two in each outer wall (one near the center, one near the edge)			Set 1 Element (EXODUS:5544, CUBIT:1054) SASSI- (1054, 10, 3) Located: (-0.1818,14.00,-34.5) Element (EXODUS:5554, CUBIT:1064) SASSI- (1064, 10, 3) Located: (10.7272,14.00,-34.5) Set 2 Element (EXODUS:9106, CUBIT:4616) SASSI- (4616, 10, 3) Located: (14.00, 0.0, -34.5) Element (EXODUS:9116, CUBIT:4626) SASSI- (4626, 10, 3) Located: (14.00,-10.7692,-34.5) Set 3 Element (EXODUS:6791, CUBIT:2301) SASSI- (2301, 10, 3) Located: (-0.1818,-14.00,-34.5) Element (EXODUS:6781, CUNIT:2291) SASSI- (2291, 10, 3) Located: (-11.00, -14.00,-34.5) Set 4 Element (EXODUS:8039, CUBIT:3549) SASSI- (3549, 10, 3) Located: (-14.00, 0.0, -34.5)
Lumped-Mass Stick Models			

X, Y, Z-Directional Acceleration ISRSs (in 'g'unit) at the top and the bottom node of each stick	See figures for the ISRSs for these nodes.	See figures for the ISRSs for these nodes.	Node EXODUS 1893, Cubit 9396 Node EXODUS 1330, Cubit 9400 Node EXODUS 2554, Cubit 9404 Node EXODUS 2001, Cubit 9420 Node EXODUS 3163, Cubit 9428 Node EXODUS 2674, Cubit 9436 Node EXODUS 3830, Cubit 9452 Node EXODUS 3619, Cubit 9456 See the following for beam bottom and top Node CUBIT 6918, Cubit 9396 SASSI-1021, 4904 Node CUBIT 6426, 9400 SASSI- 1182, 4905 Node CUBIT 7475, 9404 SASSI-13774, 22080 Node CUBIT 6993, 9420 SASSI-13886, 18132 Node CUBIT 7980, 9428 SASSI-27184, 31566 Node CUBIT 7550, 9436 SASSI-27296, 35500 Node CUBIT 8543, 9452 SASSI-38274, 39041 Node CUBIT 8338, 9456 SASSI-38328, 39274
Maximum Accelerations (m/s^2) at the top and bottom nodes of each "stick."	5.96 24.04	16.45 18.16	CUBIT 6918, 9396 SASSI-1021, 4904
	5.96 8.05	17.01 17.05	CUBIT 6426, 9400 SASSI- 1182, 4905

	4.87 9.08	16.69 16.70 24.33 (X, 22080; This denotes that the response in X direction is larger than the response in the Z direction*)	CUBIT 7475, 9404 SASSI-13774, 22080
	4.86 4.40	19.07 19.11	CUBIT 6993, 9420 SASSI-13886, 18132
	5.37 6.81	18.38 18.39 20.66 (X, 31566; see * above)	CUBIT 7980, 9428 SASSI-27184, 31566
	5.36 11.16	19.76 19.79 20.30 (X, 35500; see * above)	CUBIT 7550, 9436 SASSI-27296, 35500
	7.56 10.92	19.52 19.56	CUBIT 8543, 9452 SASSI-38274, 39041
	7.57 8.74	23.30 23.31 34.13 (X, 39274; see * above)	CUBIT 8338, 9456 SASSI-38328, 39274

Notes:

(1) The term "Maximum" is used to mean the maximum considering the entire time period for which the time-history analysis was performed.

5.2 Acceleration Time Histories and ISRS for the X Directional Input Motion

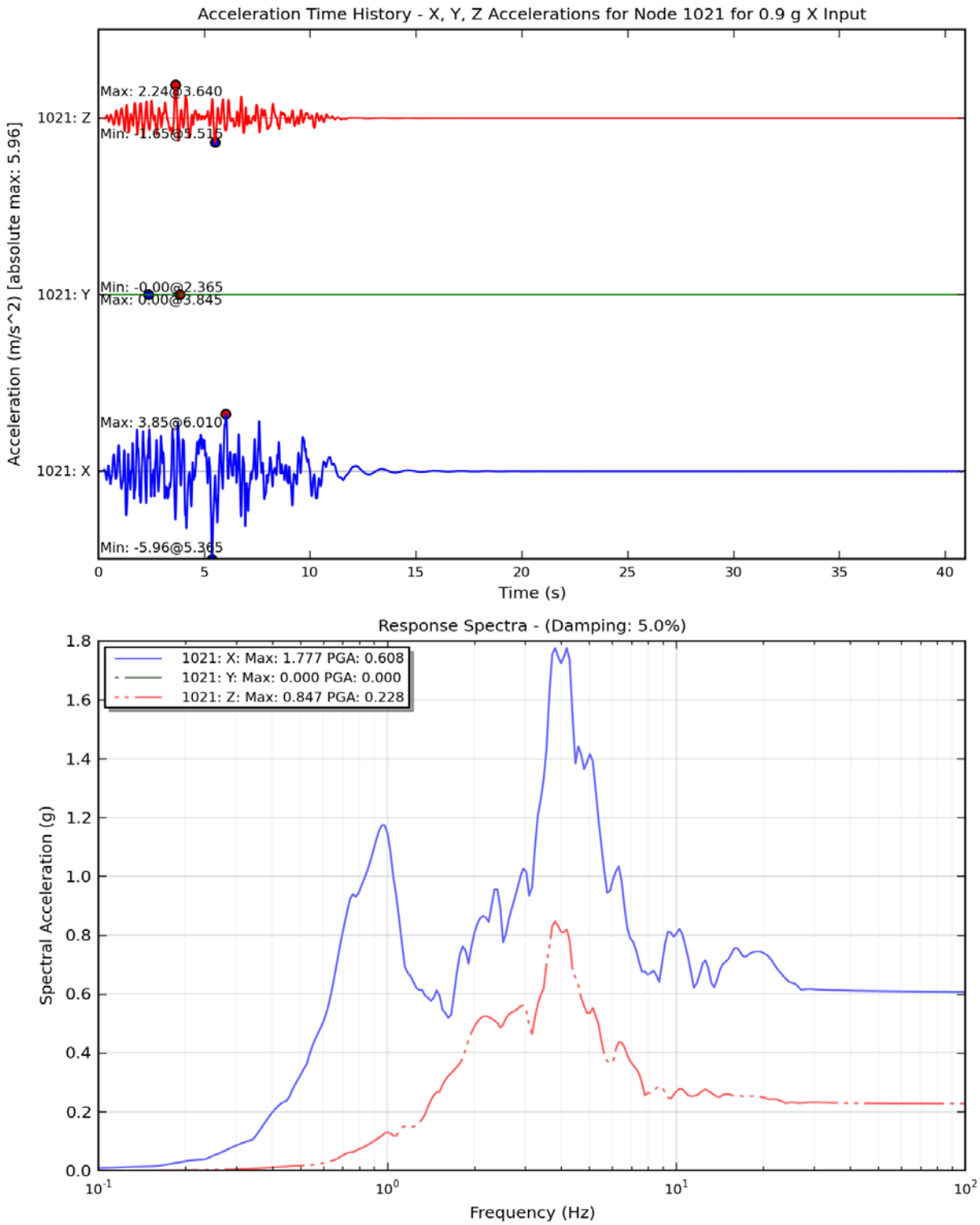

Figure 5-1 Response Acceleration Time Histories and ISRS at Node 1021 for X Input Motion (0.9 g)

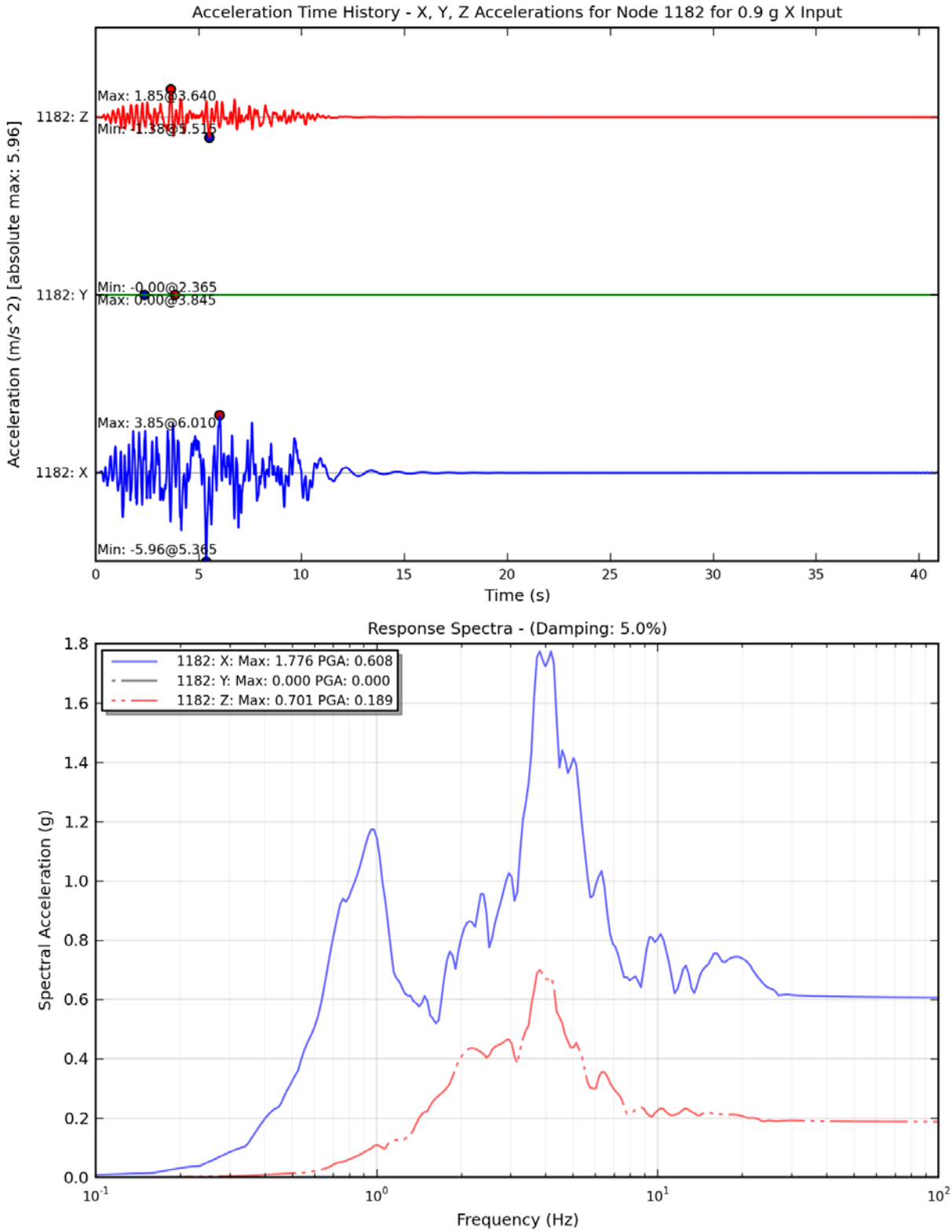

Figure 5-2 Response Acceleration Time Histories and ISRS at Node 1182 for X Input Motion (0.9 g)

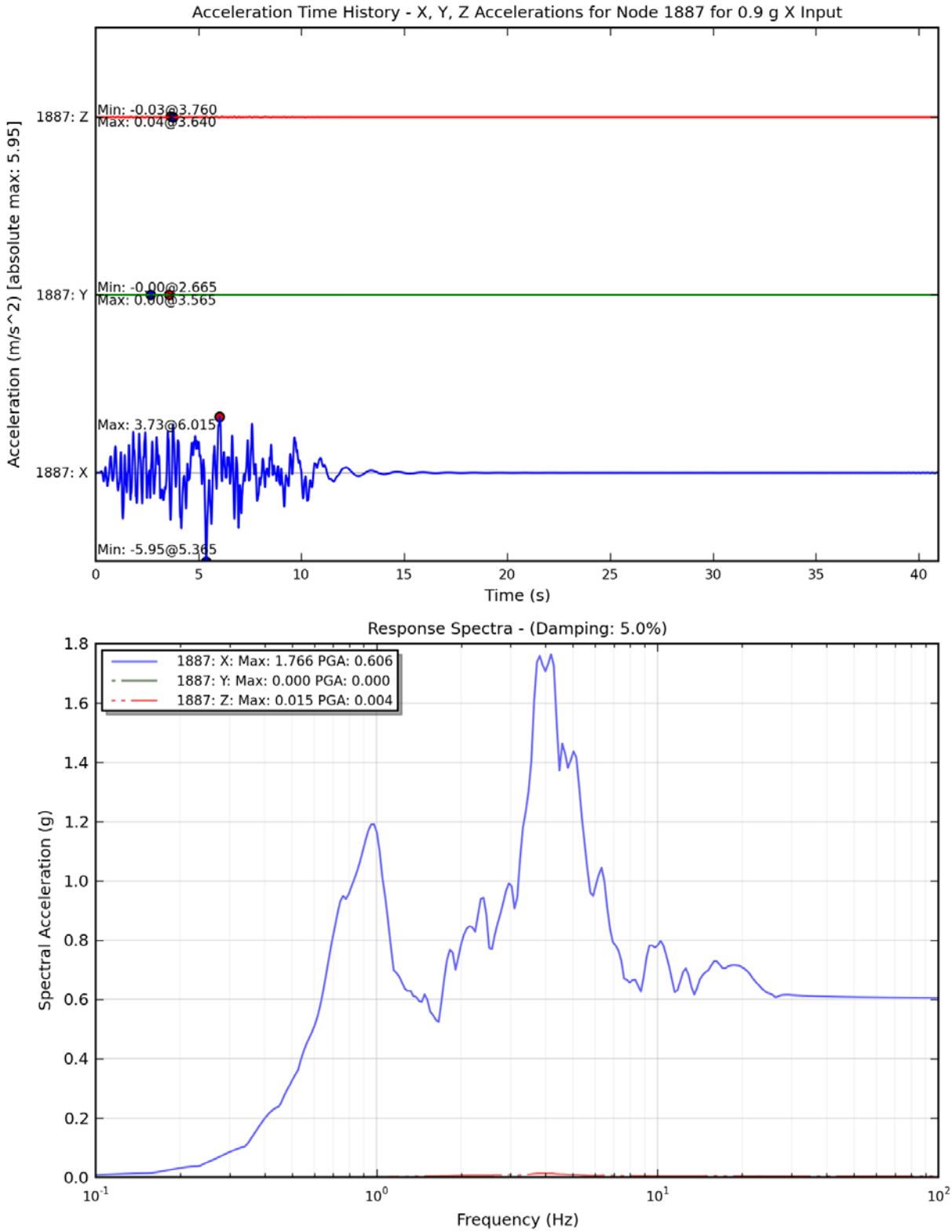

Figure 5-3 Response Acceleration Time Histories and ISRS at Node 1887 for X Input Motion (0.9 g)

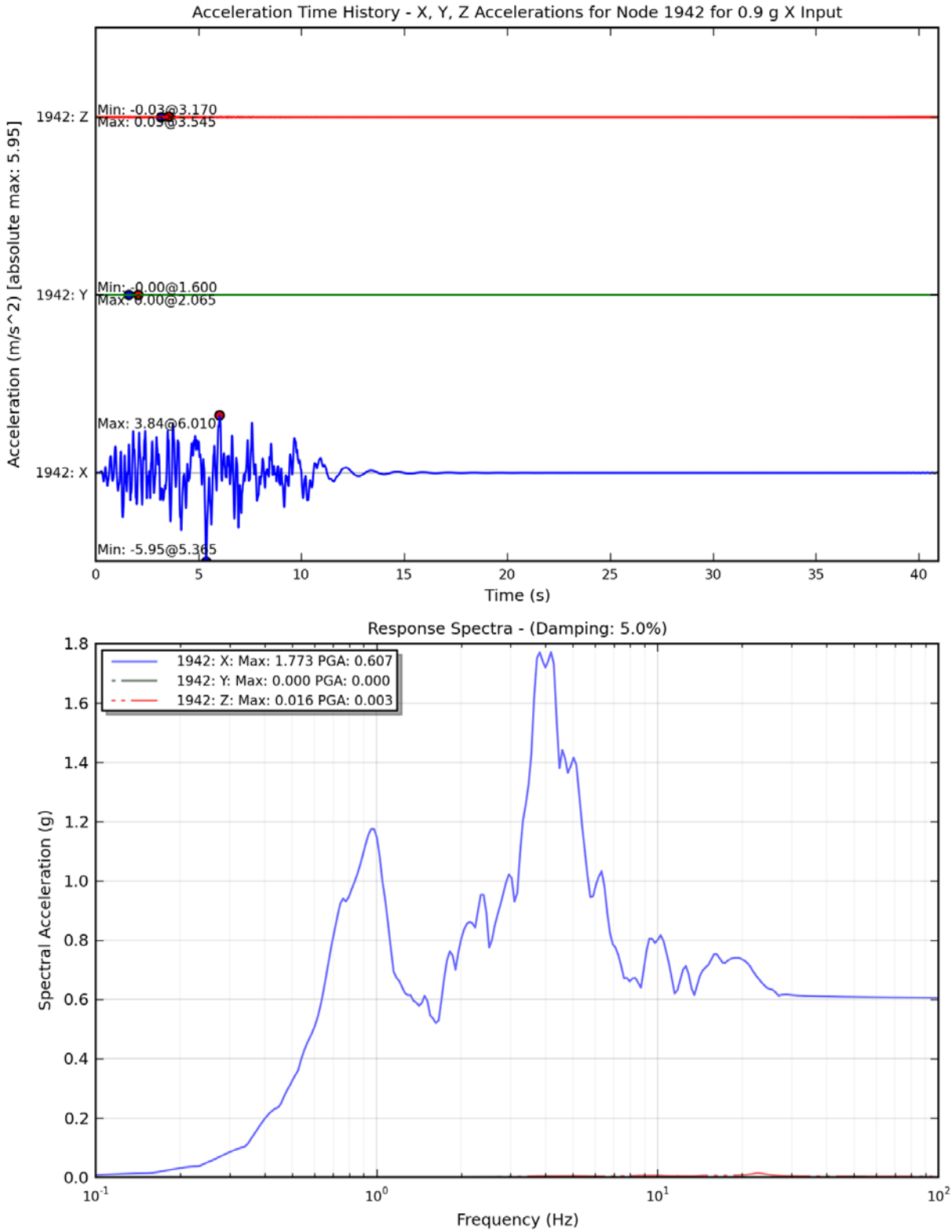

Figure 5-4 Response Acceleration Time Histories and ISRS at Node 1942 for X Input Motion (0.9 g)

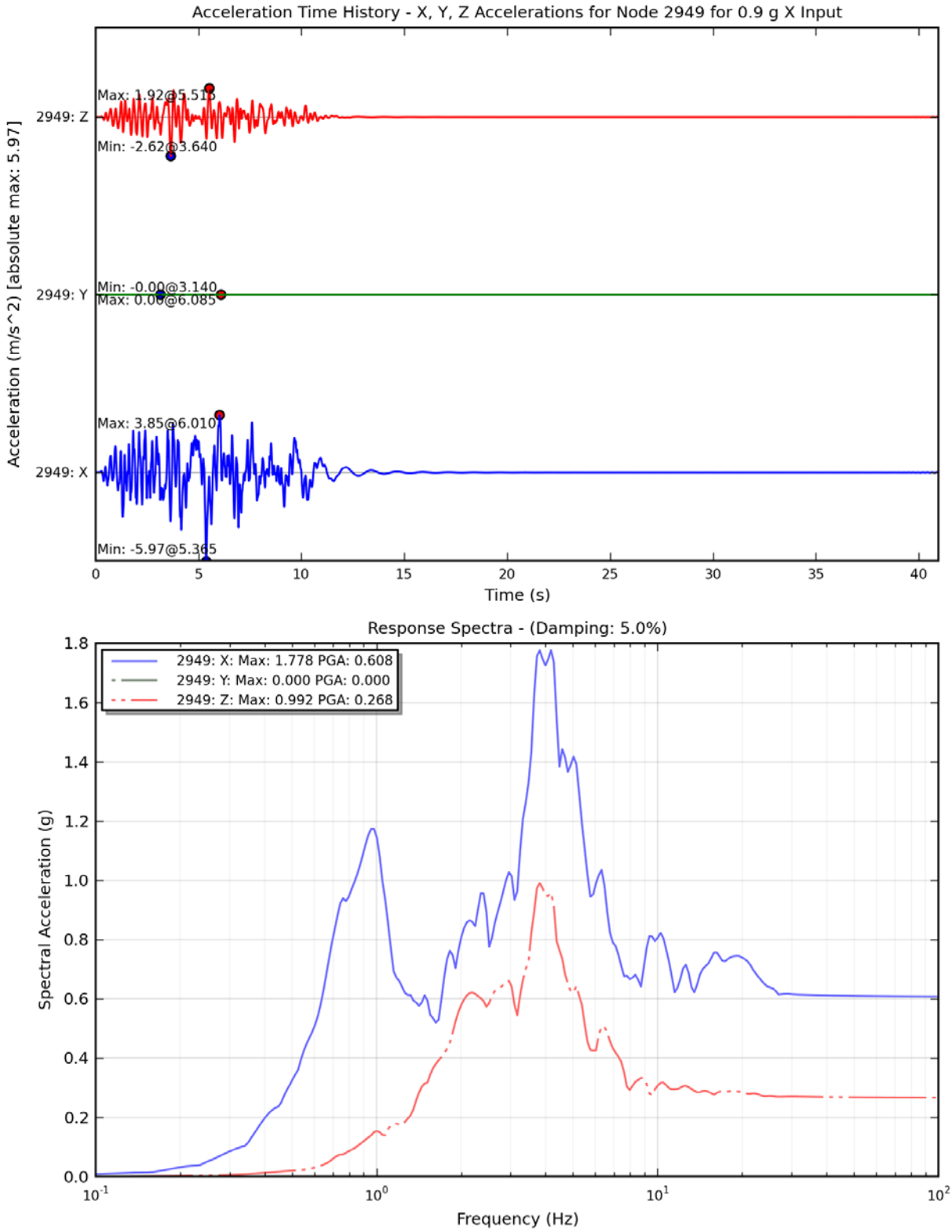

Figure 5-5 Response Acceleration Time Histories and ISRS at Node 2949 for X Input Motion (0.9 g)

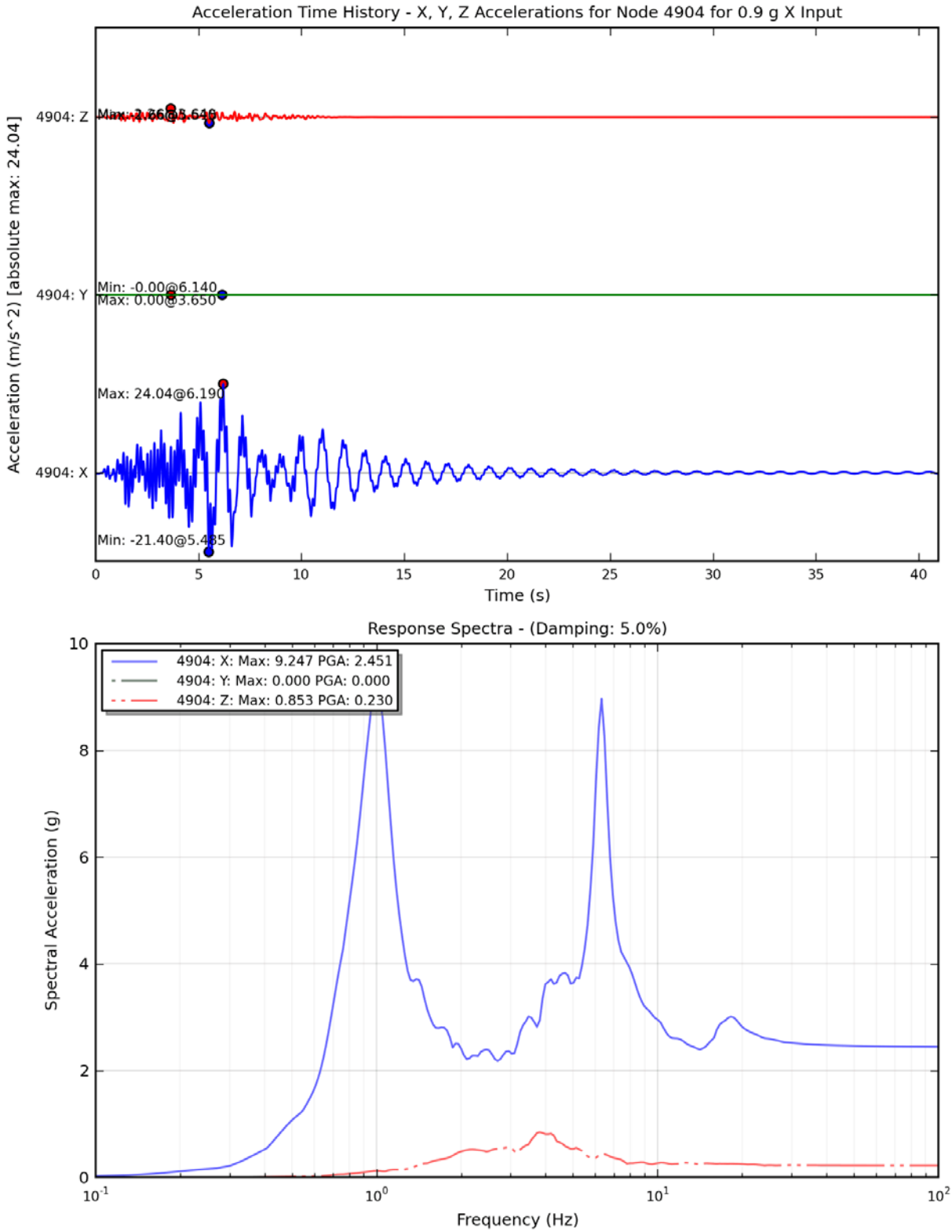

Figure 5-6 Response Acceleration Time Histories and ISRS at Node 4904 for X Input Motion (0.9 g)

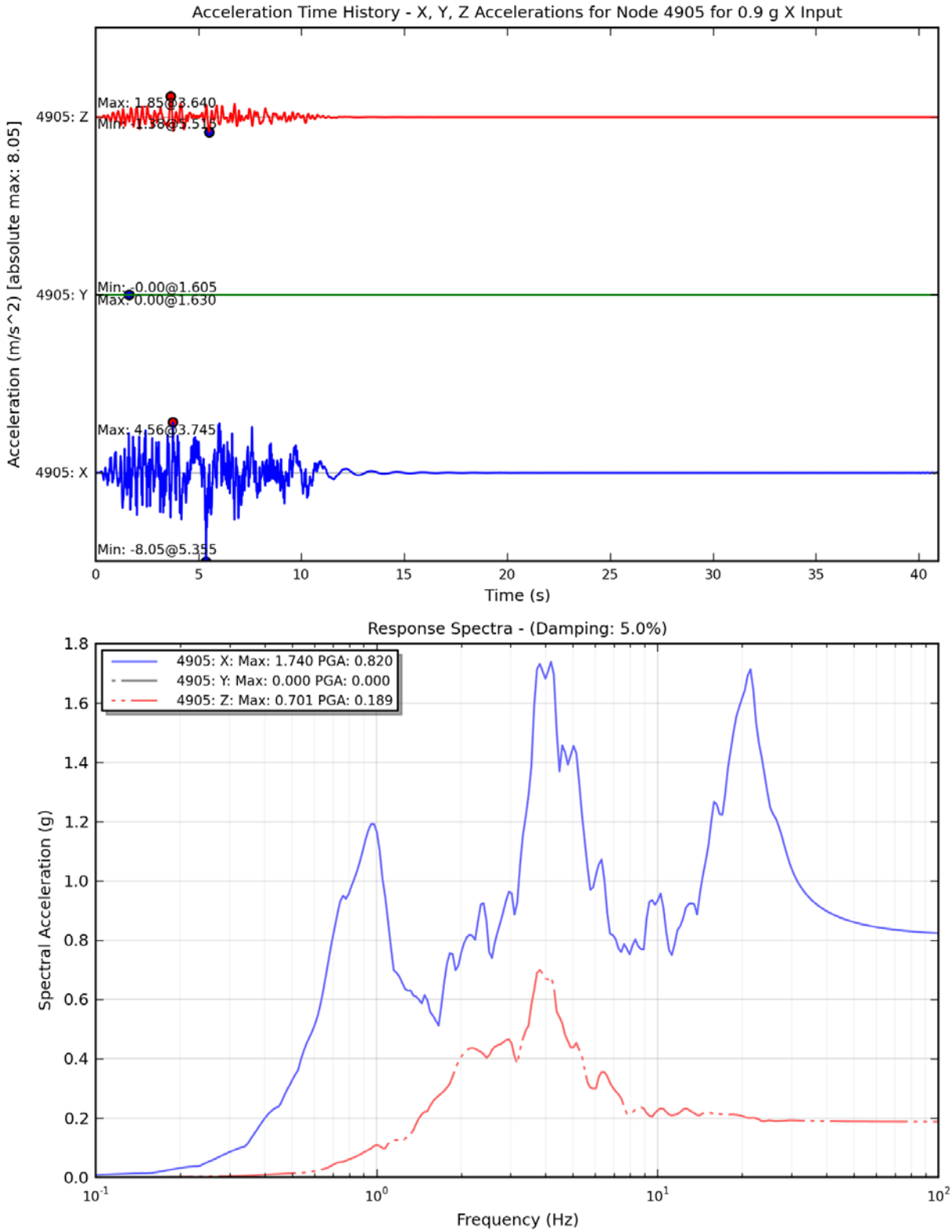

Figure 5-7 Response Acceleration Time Histories and ISRS at Node 4905 for X Input Motion (0.9 g)

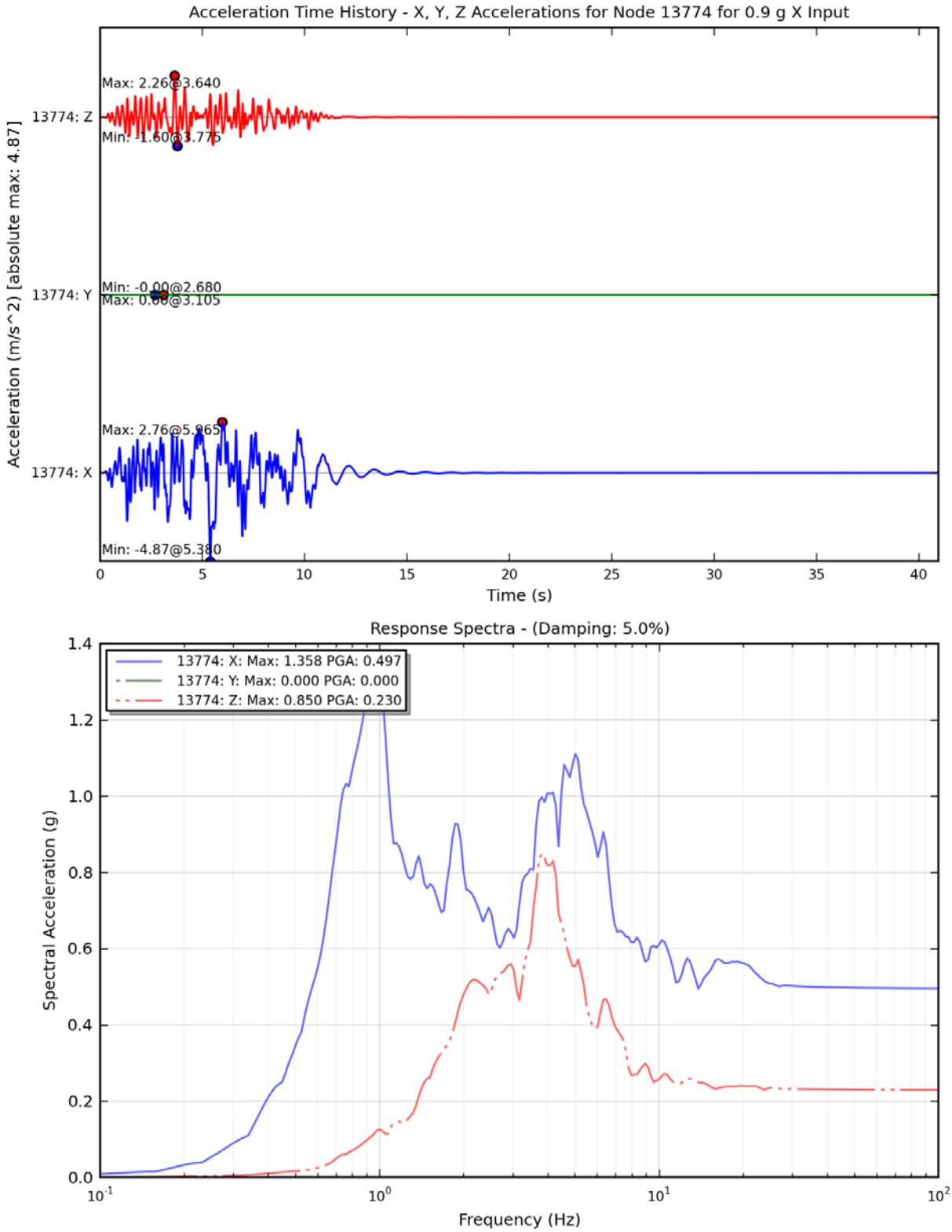

Figure 5-8 Response Acceleration Time Histories and ISRS at Node 13774 for X Input Motion (0.9 g)

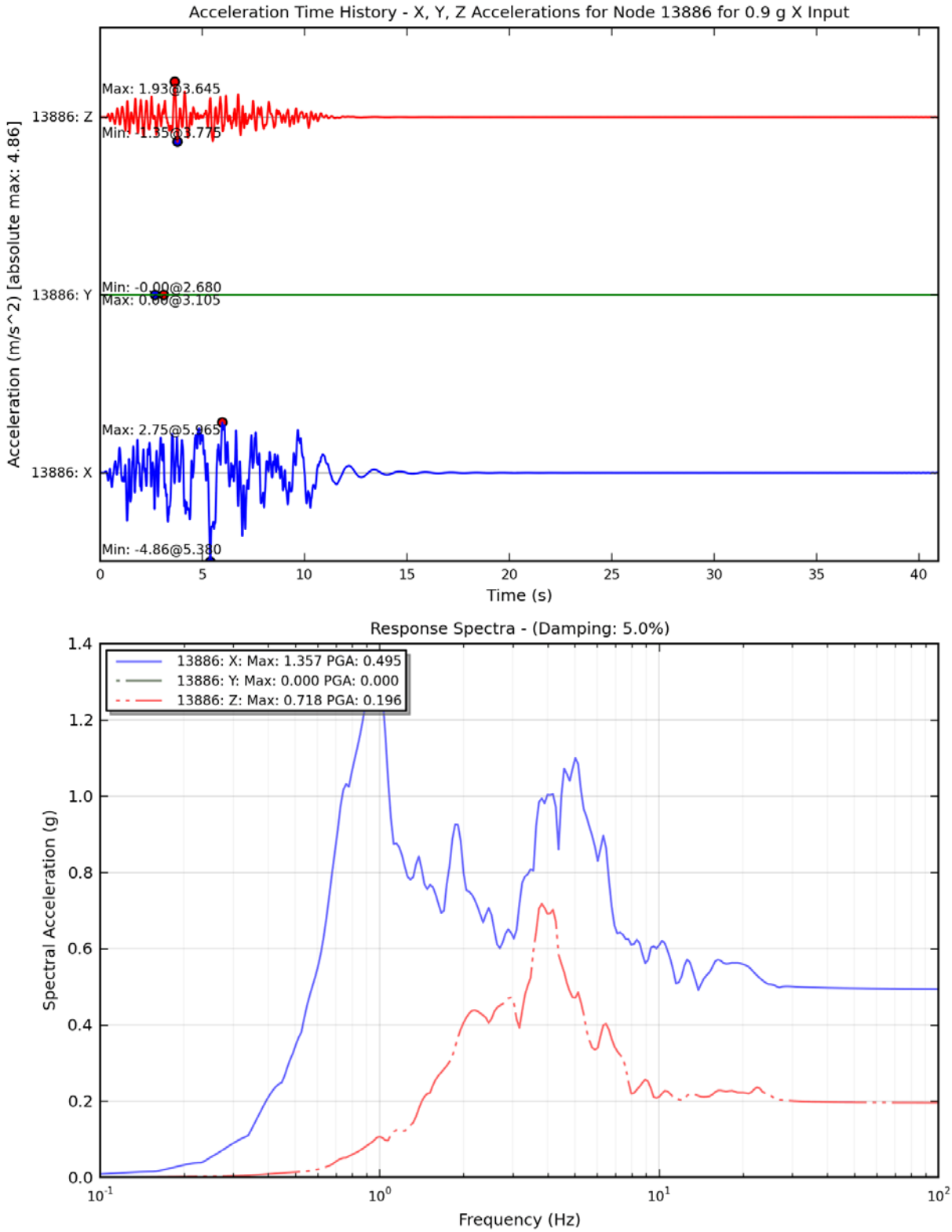

Figure 5-9 Response Acceleration Time Histories and ISRS at Node 13886 for X Input Motion (0.9 g)

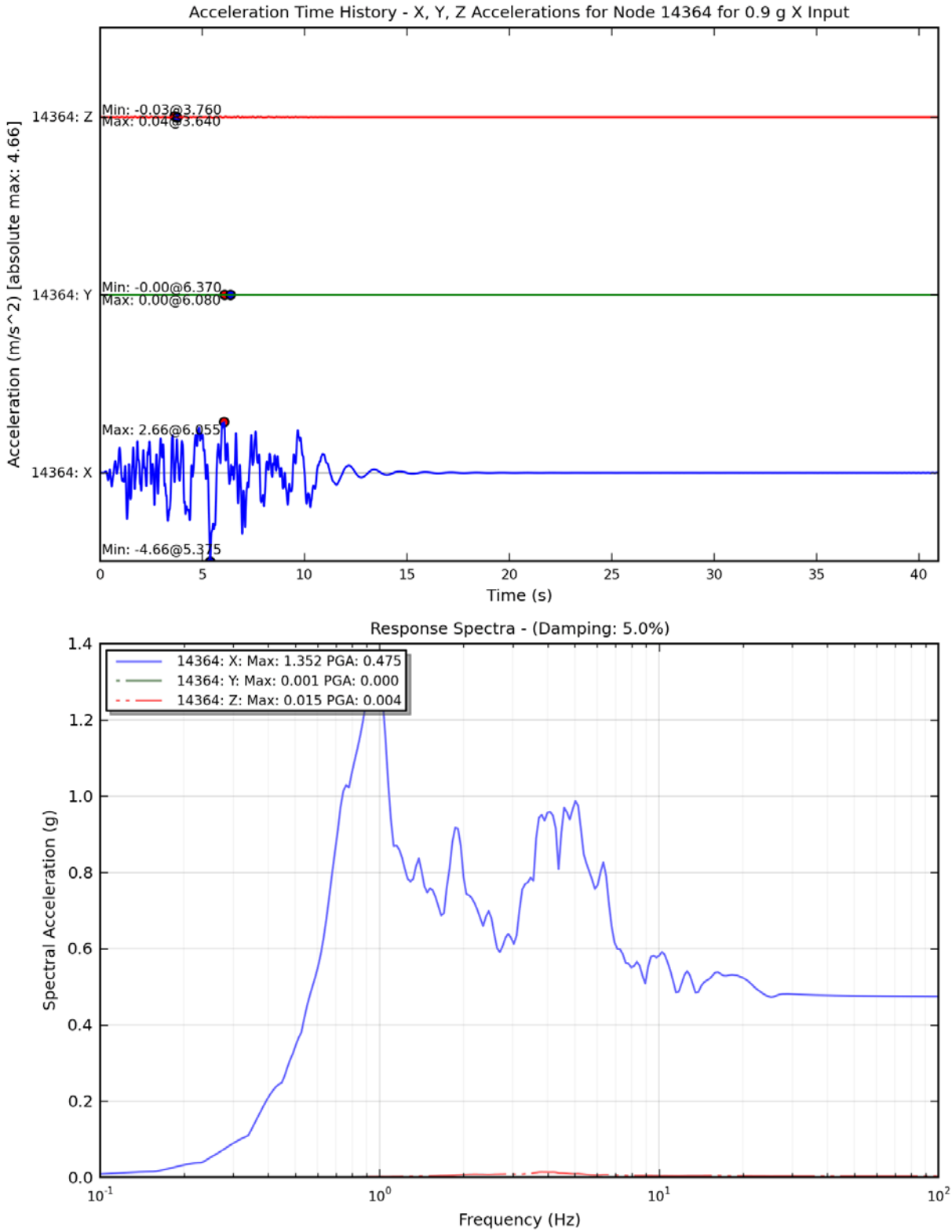

Figure 5-10 Response Acceleration Time Histories and ISRS at Node 14364 for X Input Motion (0.9 g)

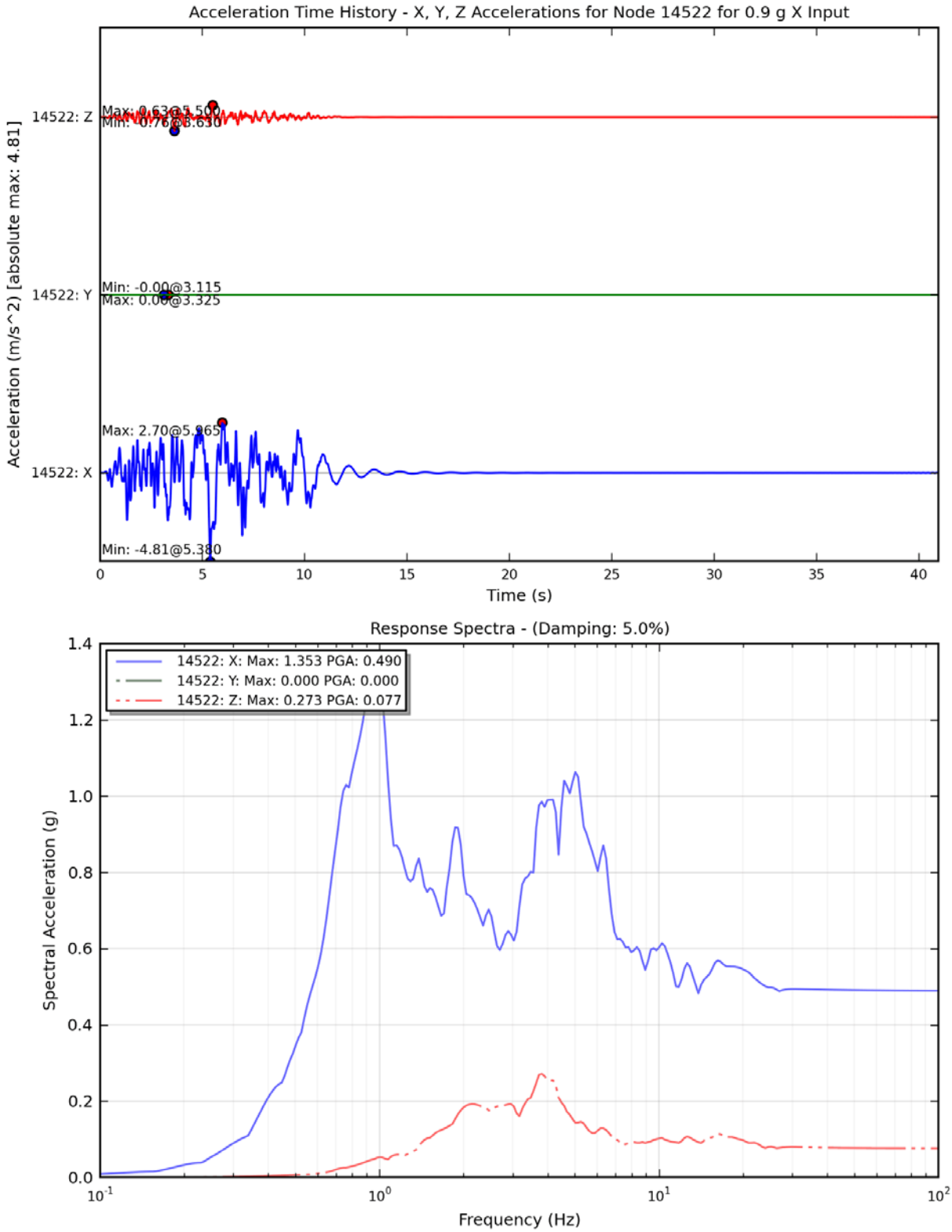

Figure 5-11 Response Acceleration Time Histories and ISRS at Node 14522 for X Input Motion (0.9 g)

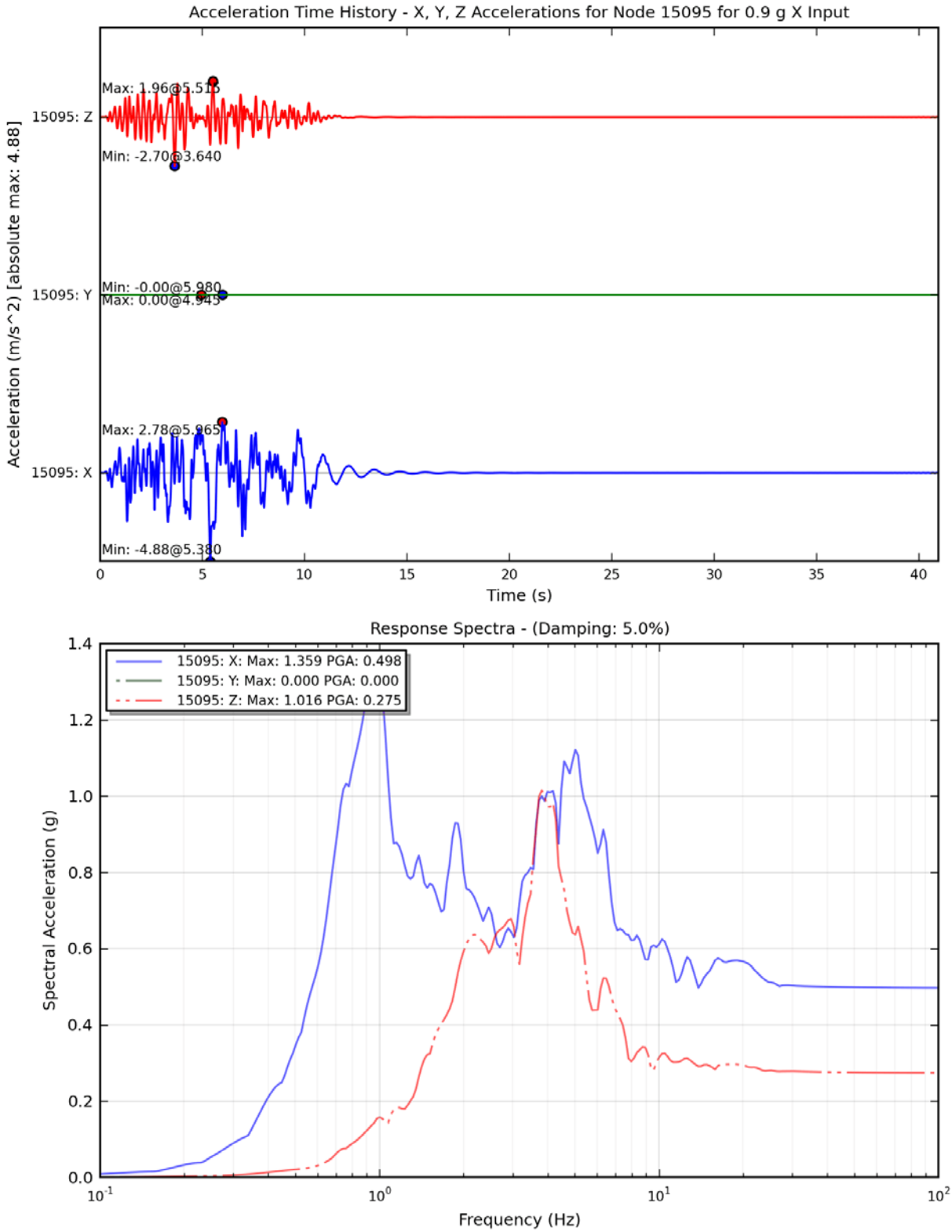

Figure 5-12 Response Acceleration Time Histories and ISRS at Node 15095 for X Input Motion (0.9 g)

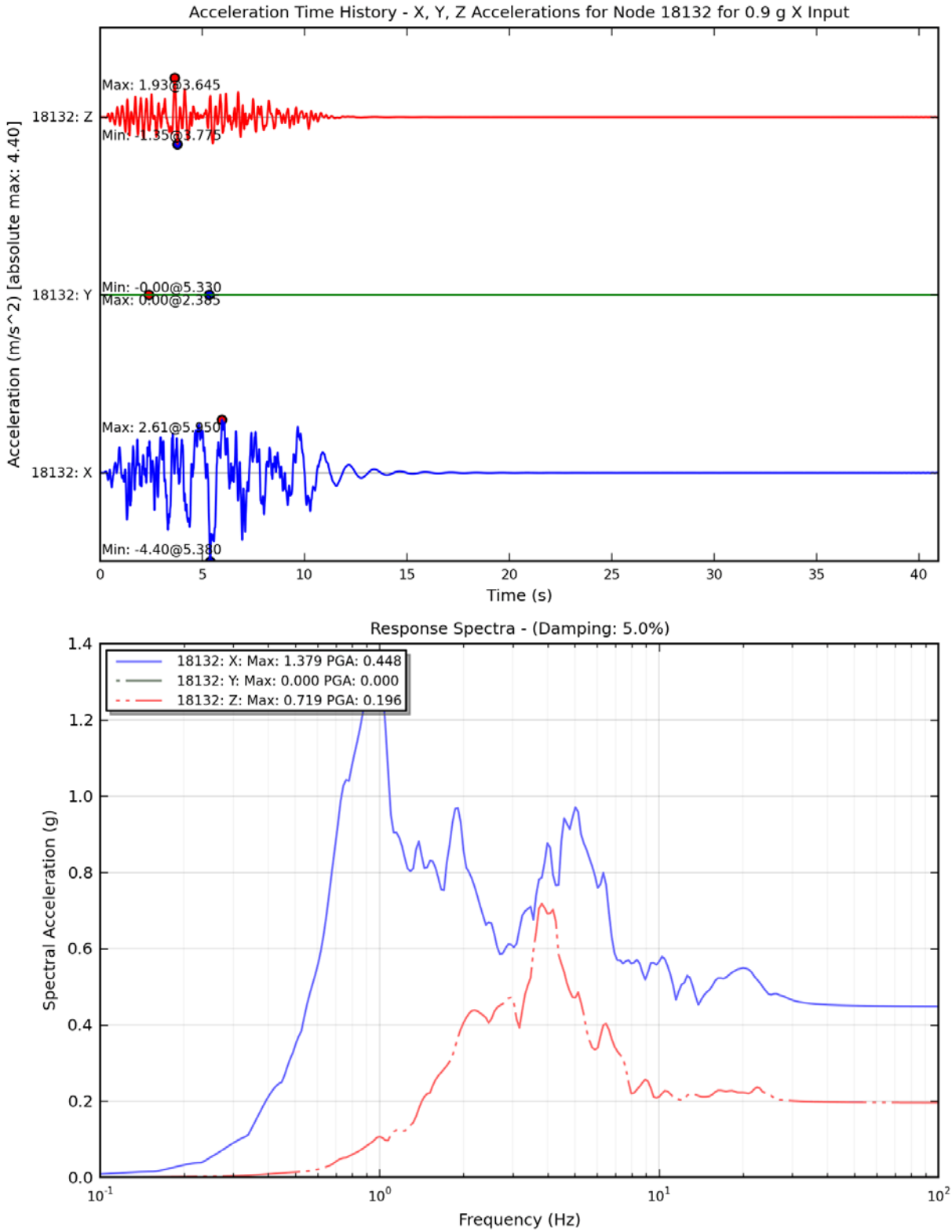

Figure 5-13 Response Acceleration Time Histories and ISRS at Node 18132 for X Input Motion (0.9 g)

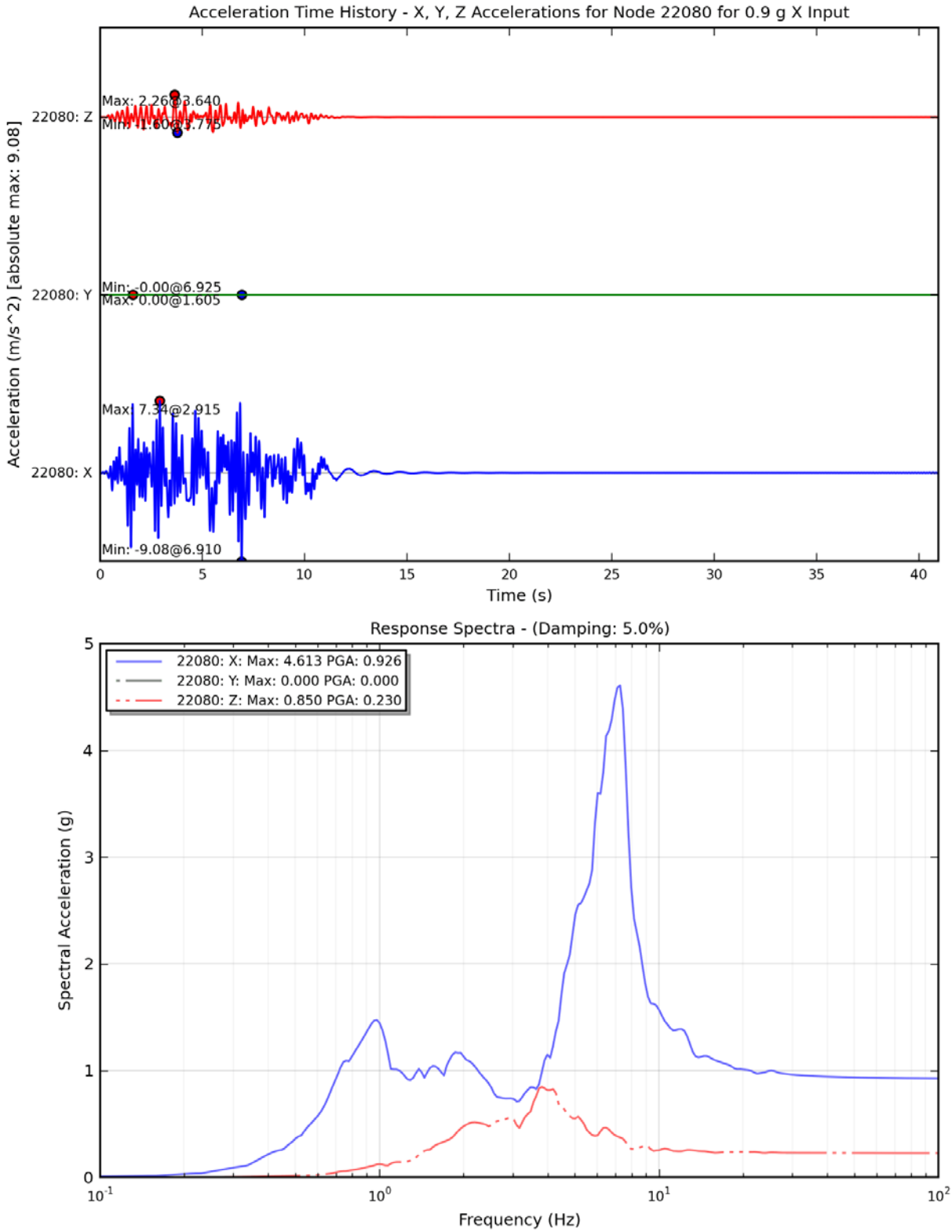

Figure 5-14 Response Acceleration Time Histories and ISRS at Node 22080 for X Input Motion (0.9 g)

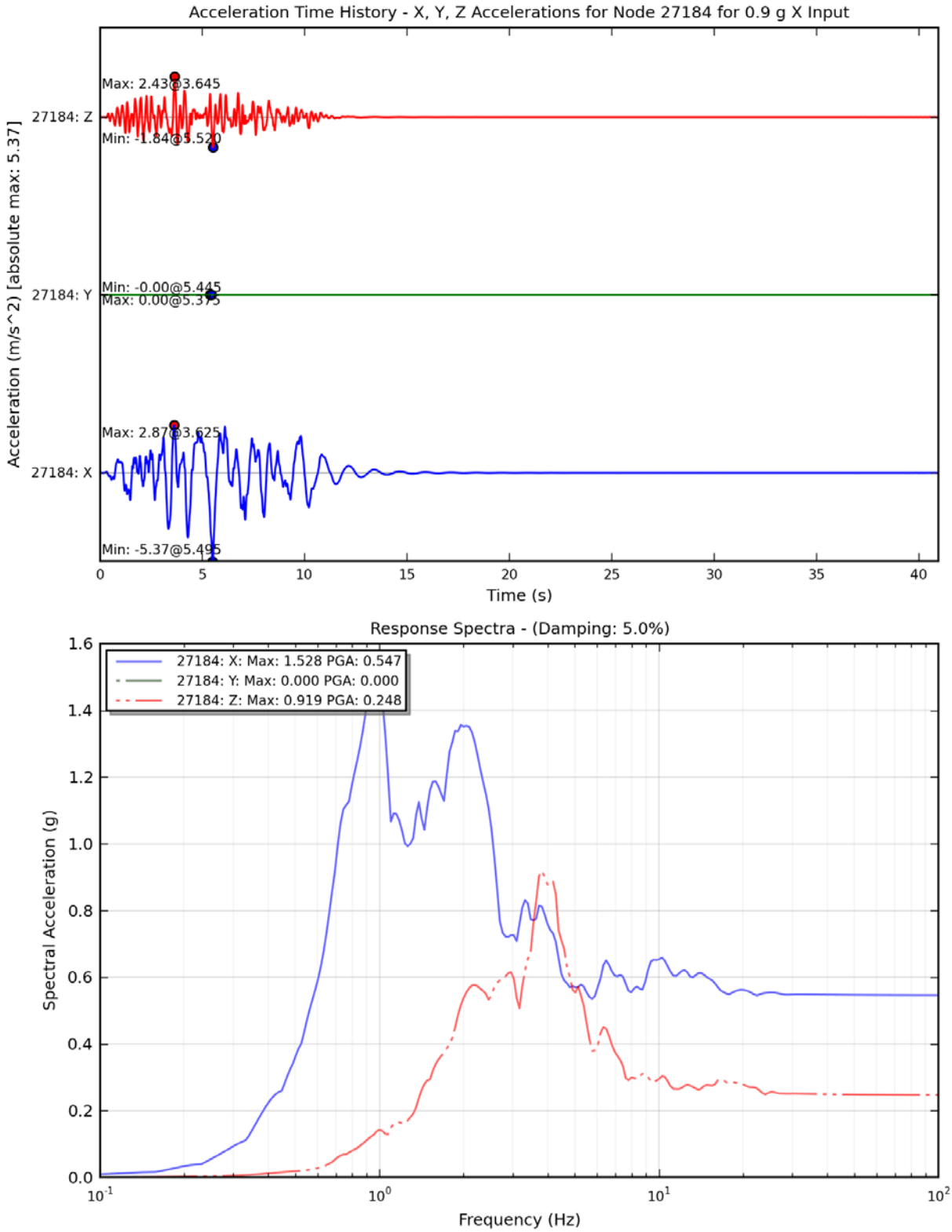

Figure 5-15 Response Acceleration Time Histories and ISRS at Node 27184 for X Input Motion (0.9 g)

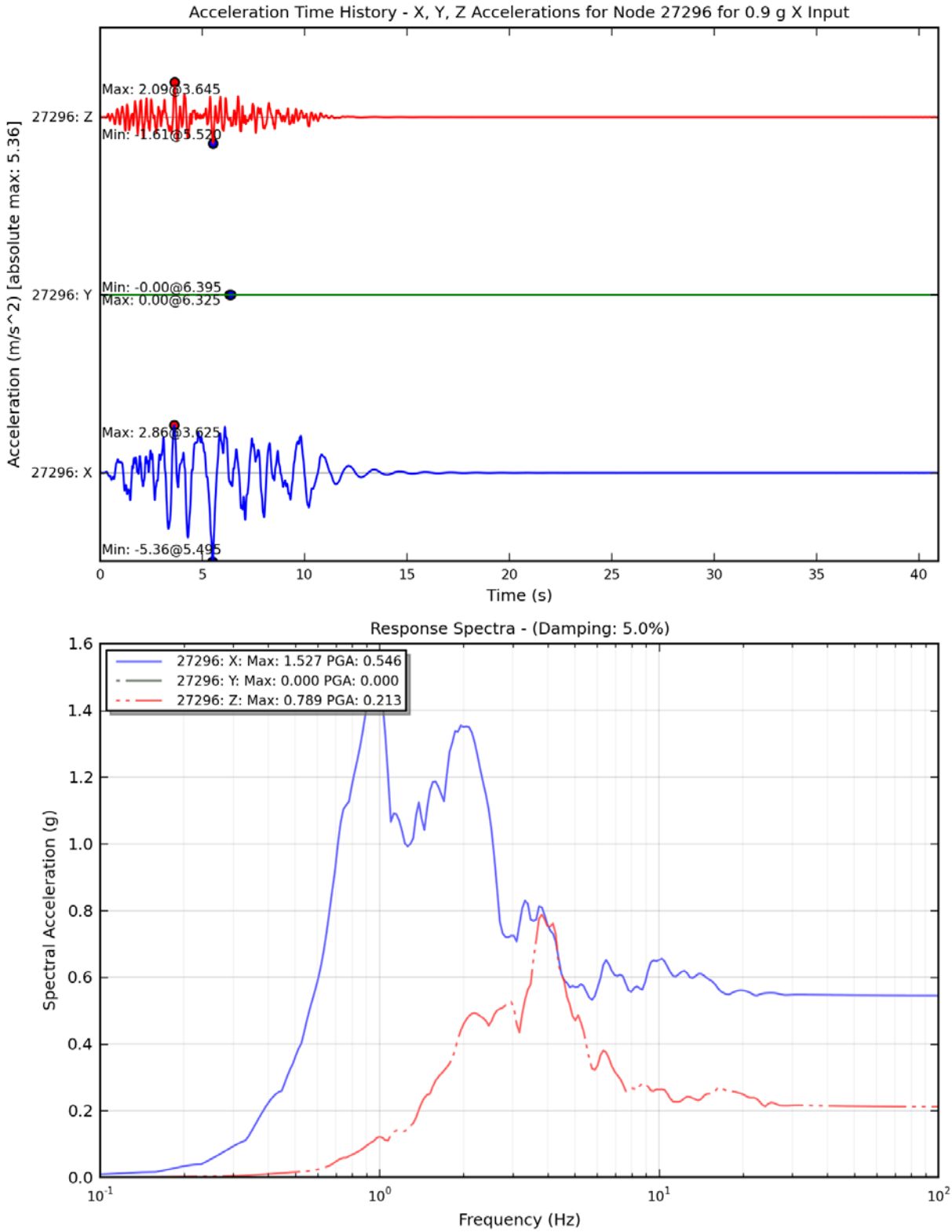

Figure 5-16 Response Acceleration Time Histories and ISRS at Node 27296 for X Input Motion (0.9 g)

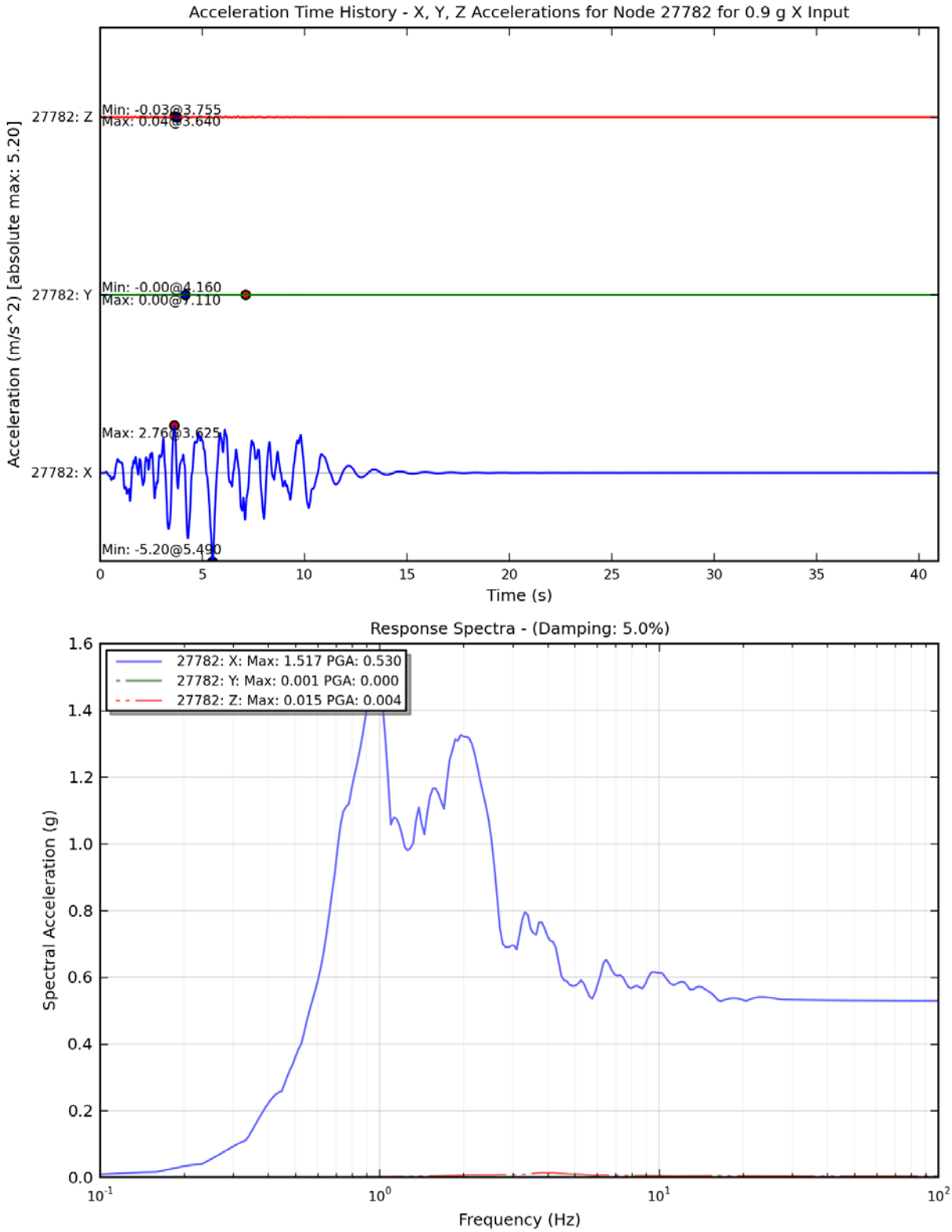

Figure 5-17 Response Acceleration Time Histories and ISRS at Node 27782 for X Input Motion (0.9 g)

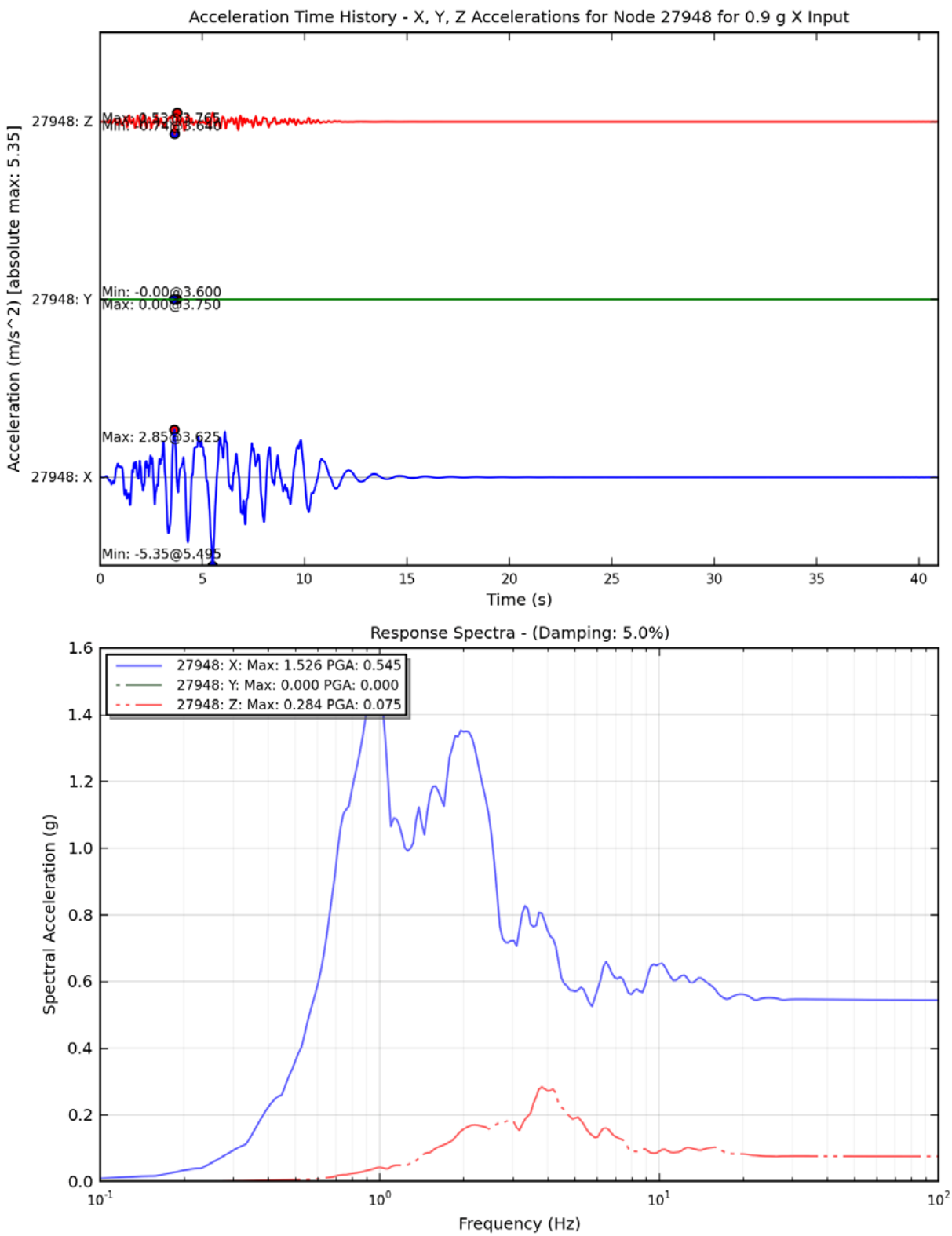

Figure 5-18 Response Acceleration Time Histories and ISRS at Node 27948 for X Input Motion (0.9 g)

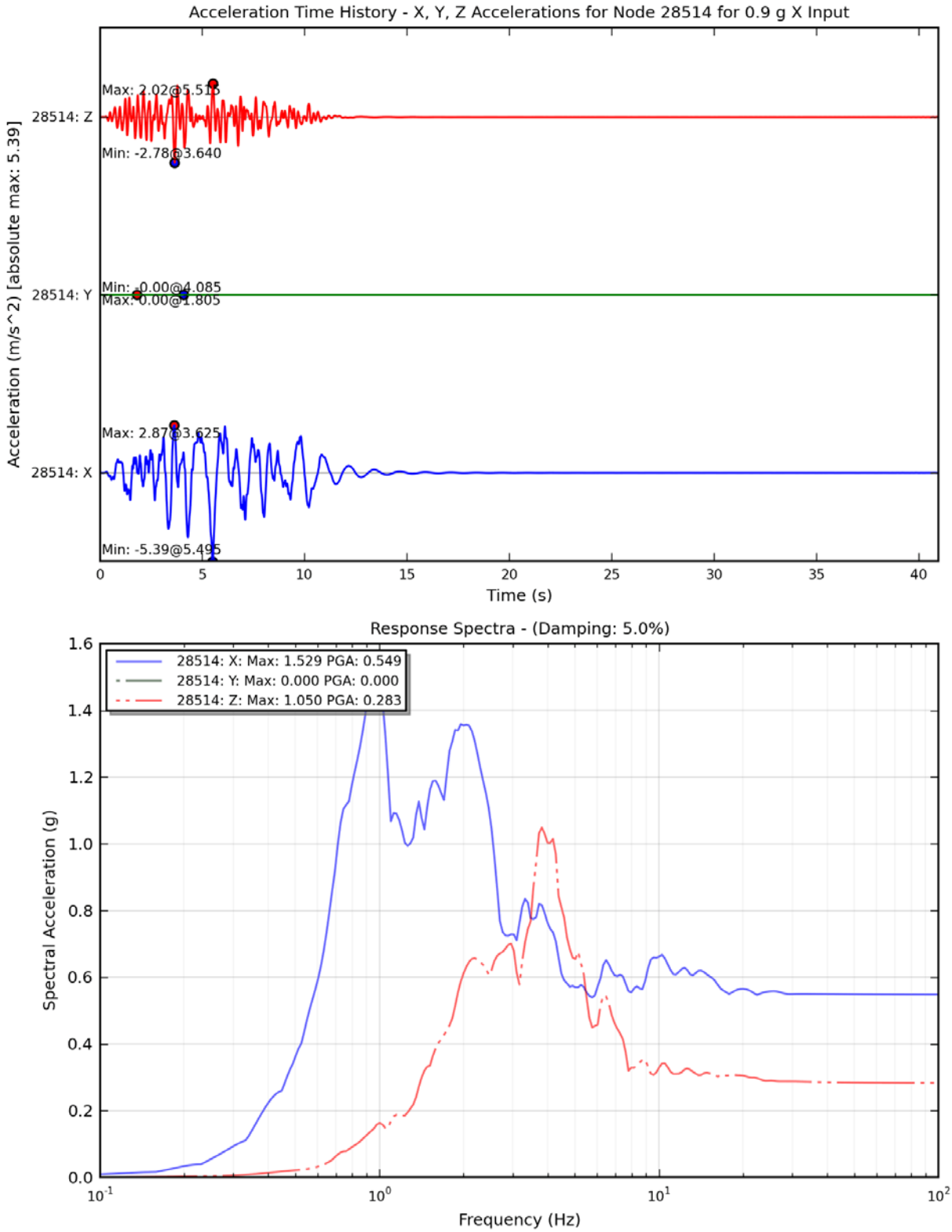

Figure 5-19 Response Acceleration Time Histories and ISRS at Node 28514 for X Input Motion (0.9 g)

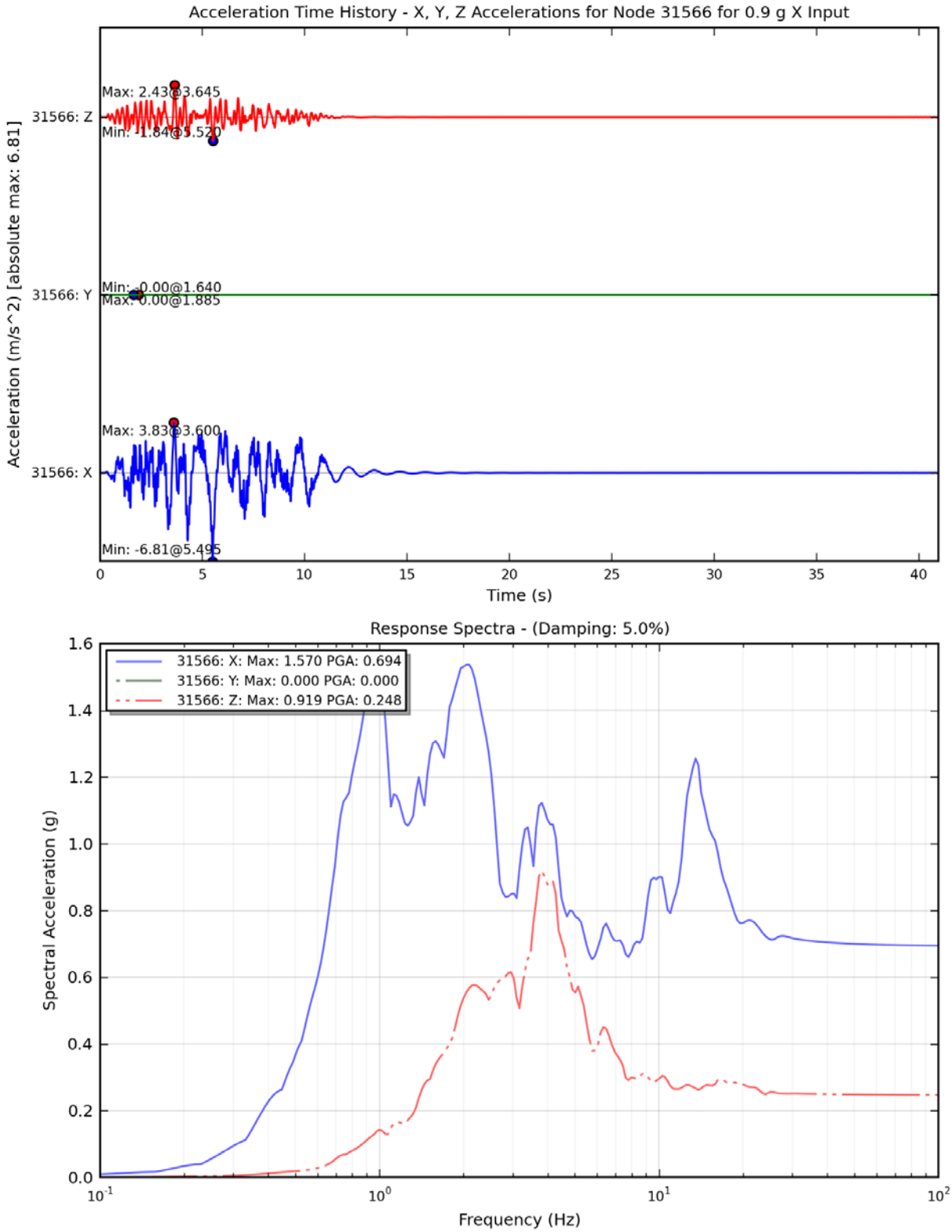

Figure 5-20 Response Acceleration Time Histories and ISRS at Node 31566 for X Input Motion (0.9 g)

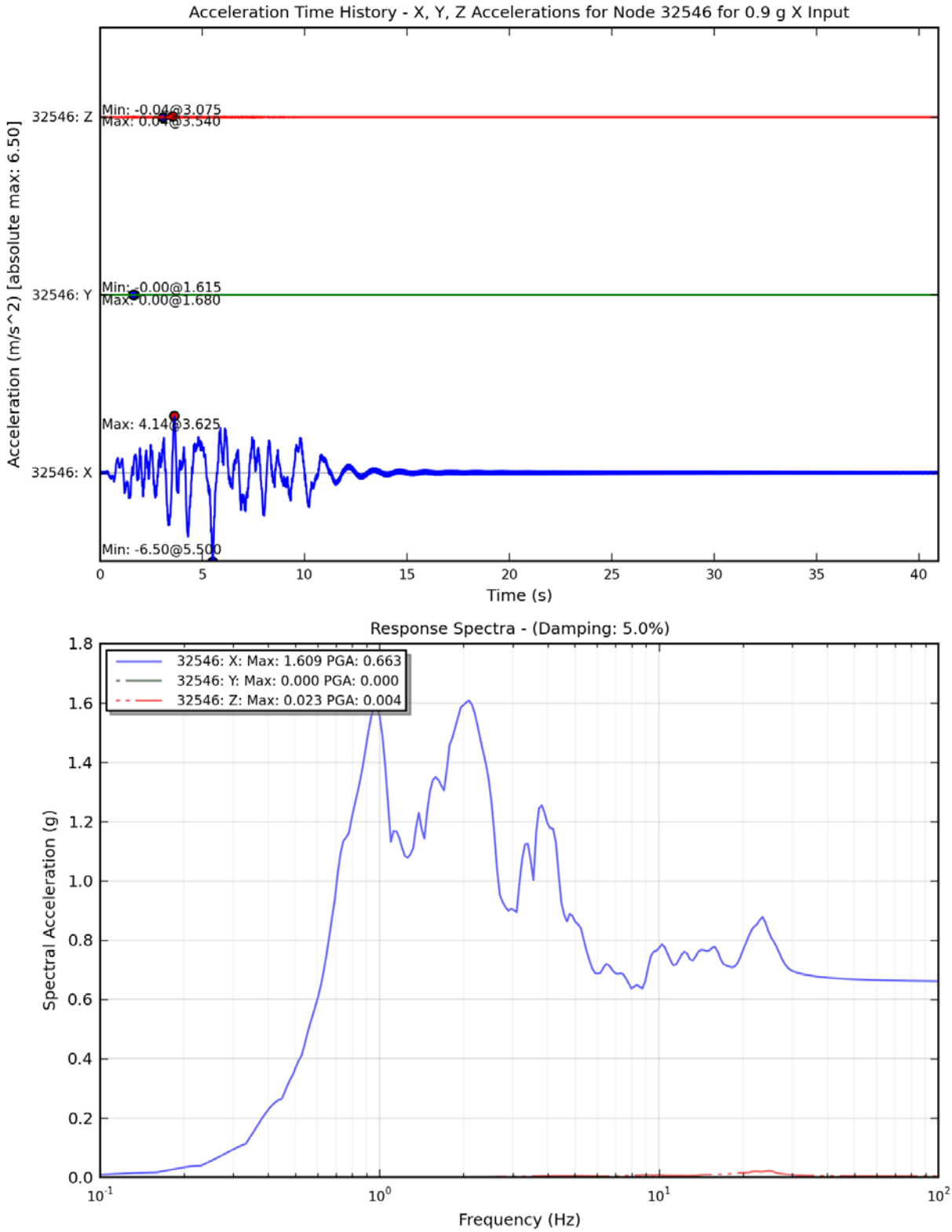

Figure 5-21 Response Acceleration Time Histories and ISRS at Node 32546 for X Input Motion (0.9 g)

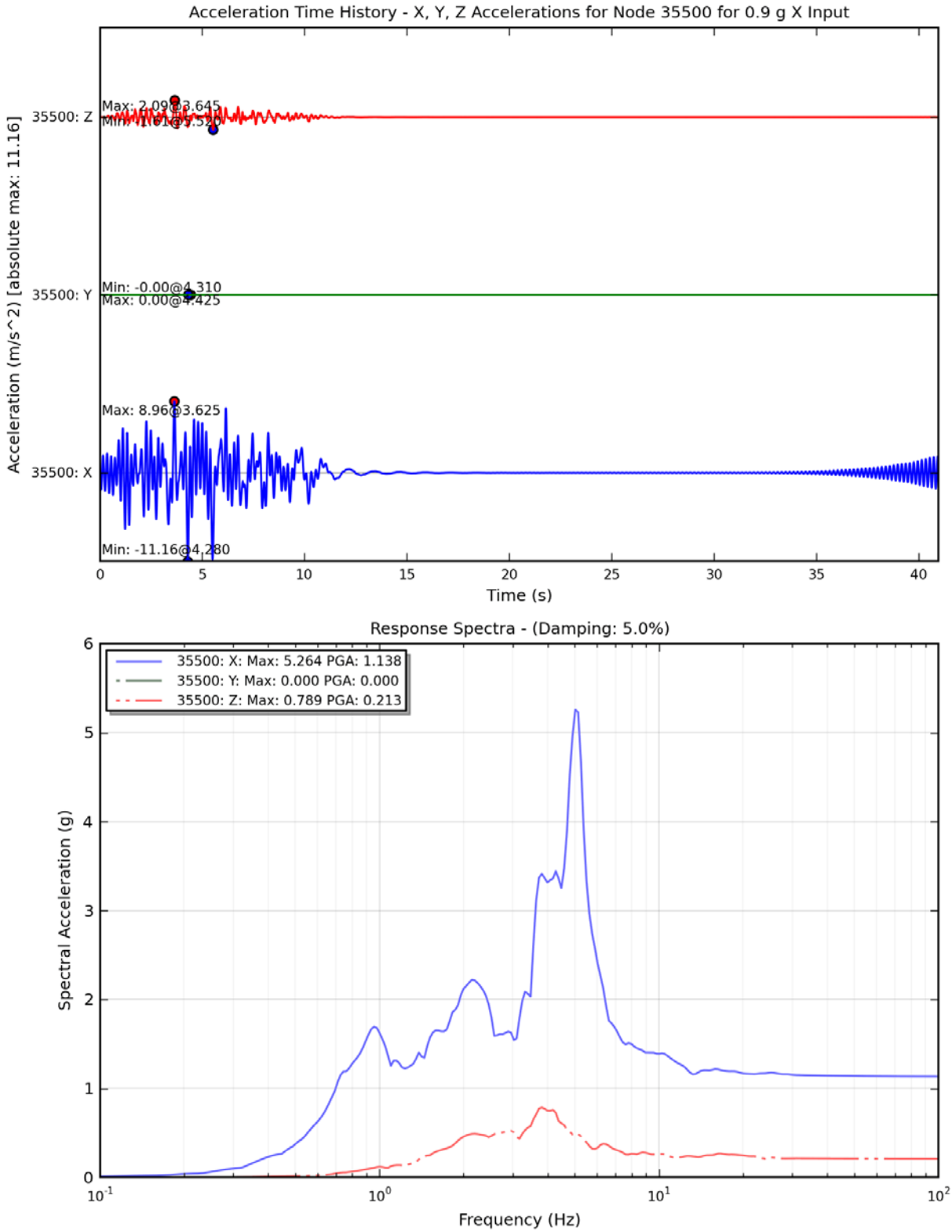

Figure 5-22 Response Acceleration Time Histories and ISRS at Node 35500 for X Input Motion (0.9 g)

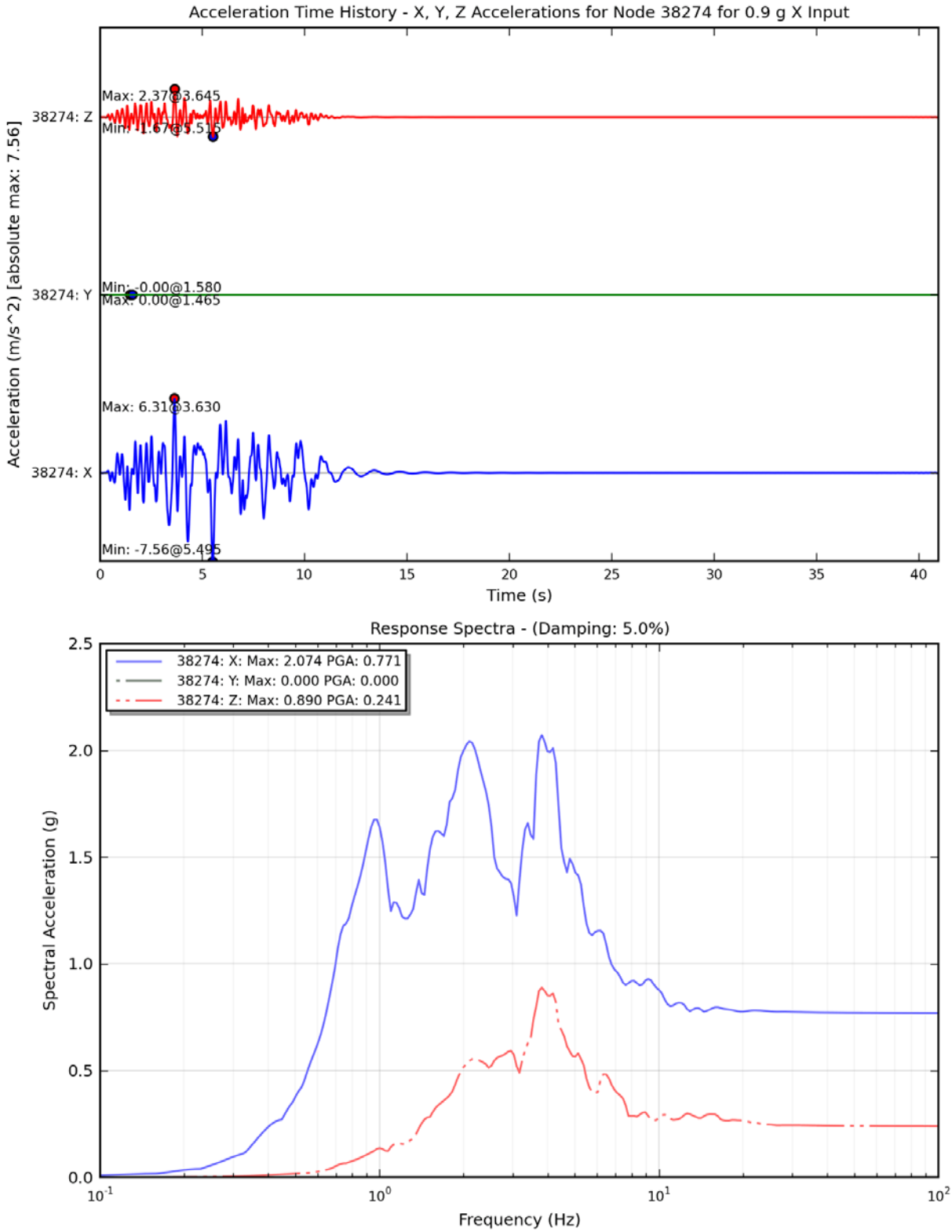

Figure 5-23 Response Acceleration Time Histories and ISRS at Node 38274 for X Input Motion (0.9 g)

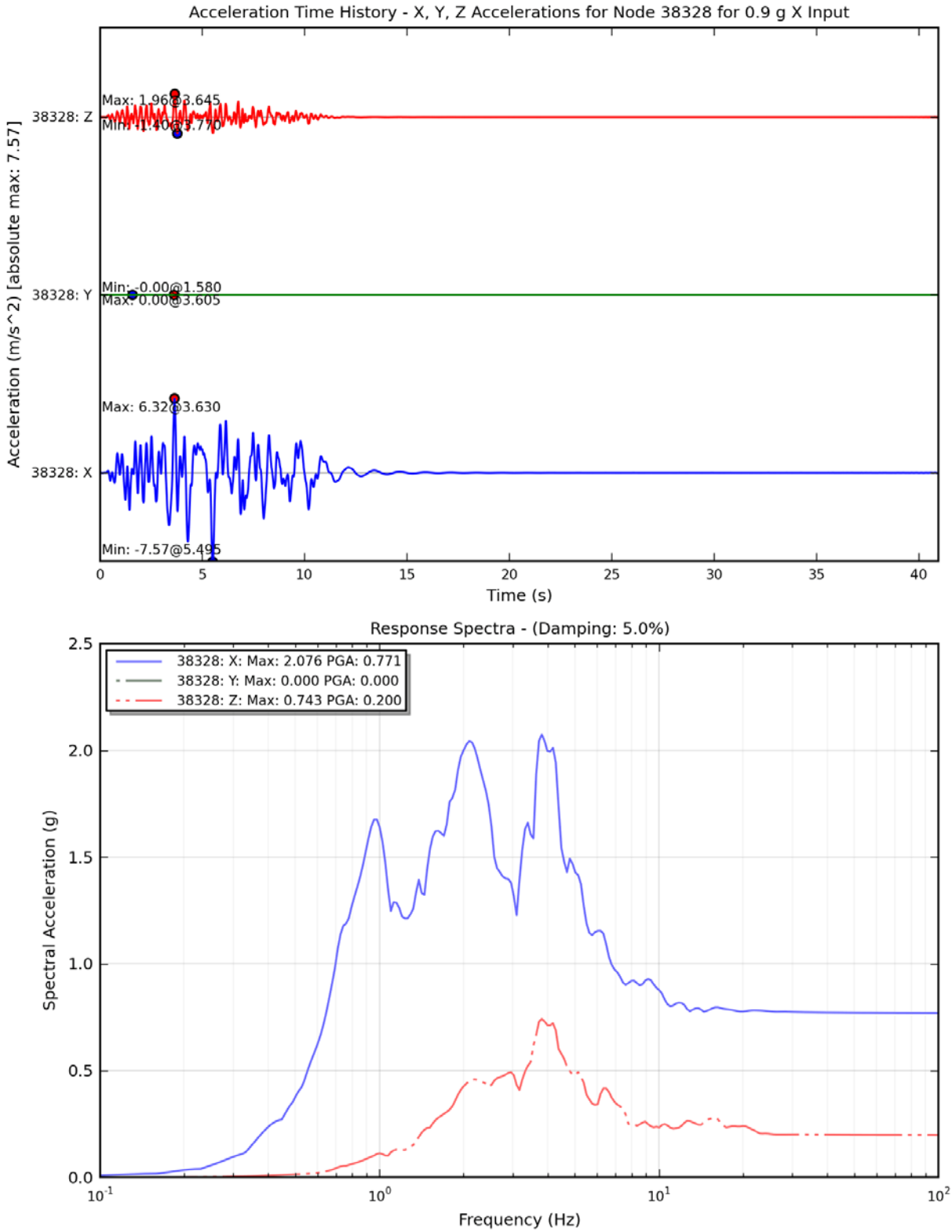

Figure 5-24 Response Acceleration Time Histories and ISRS at Node 38328 for X Input Motion (0.9 g)

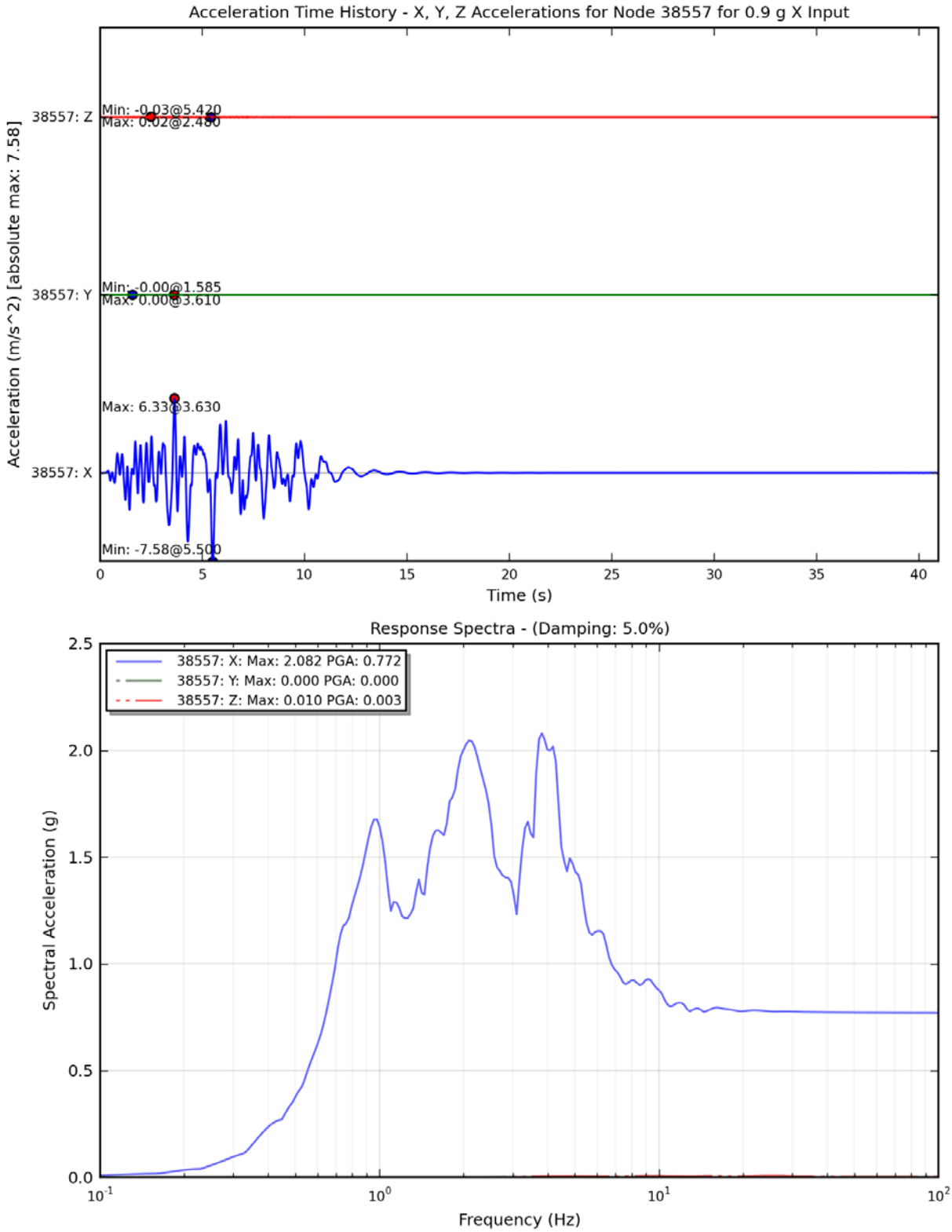

Figure 5-25 Response Acceleration Time Histories and ISRS at Node 38557 for X Input Motion (0.9 g)

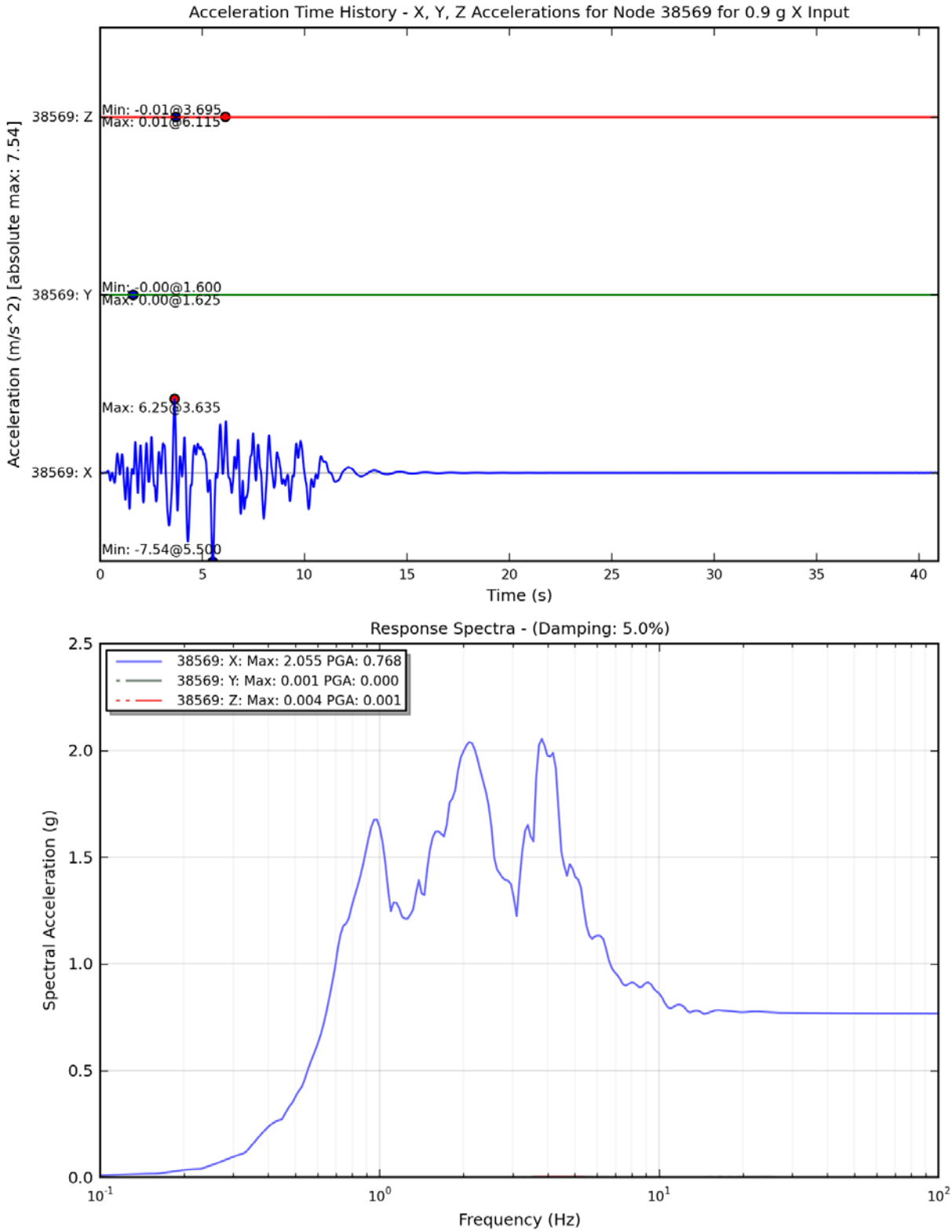

Figure 5-26 Response Acceleration Time Histories and ISRS at Node 38569 for X Input Motion (0.9 g)

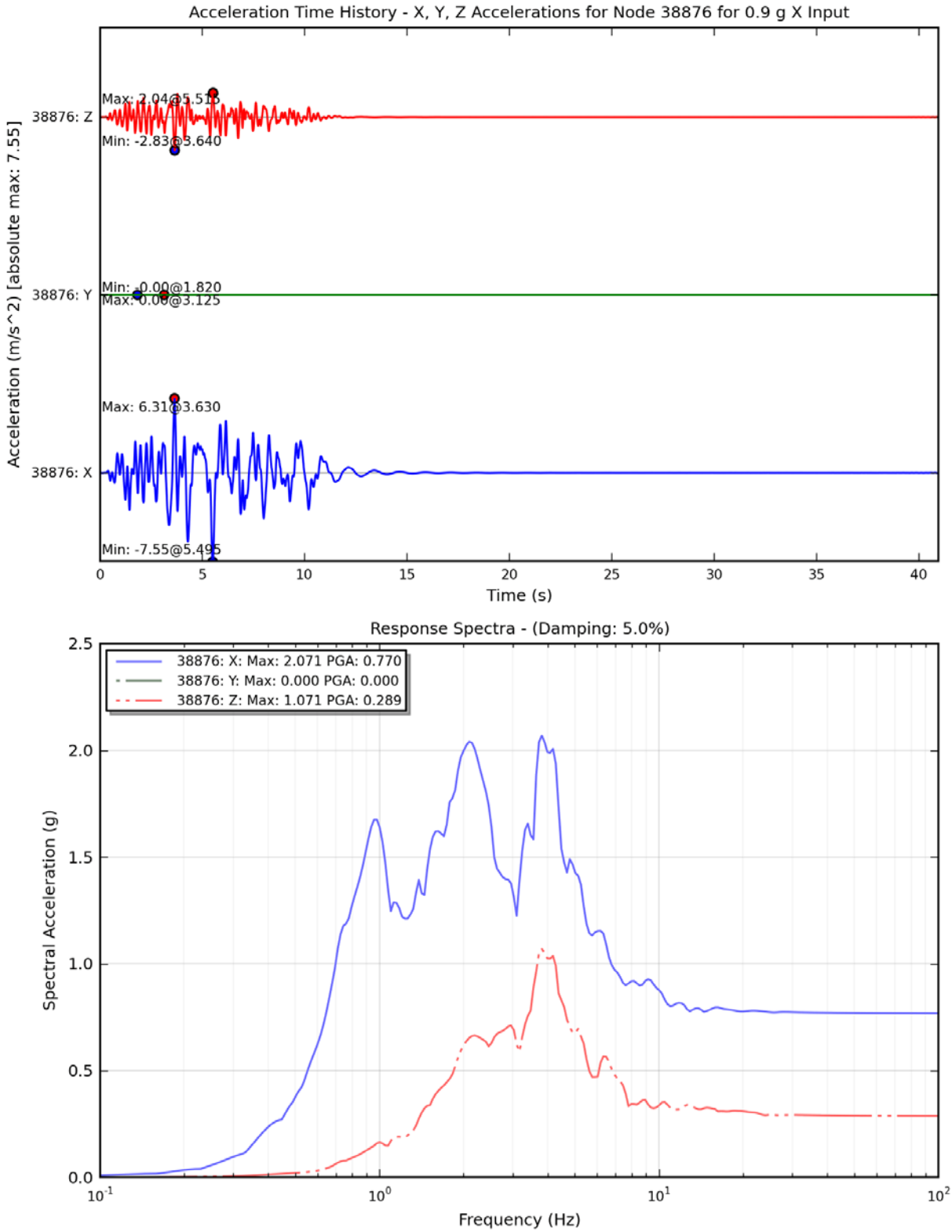

Figure 5-27 Response Acceleration Time Histories and ISRS at Node 38876 for X Input Motion (0.9 g)

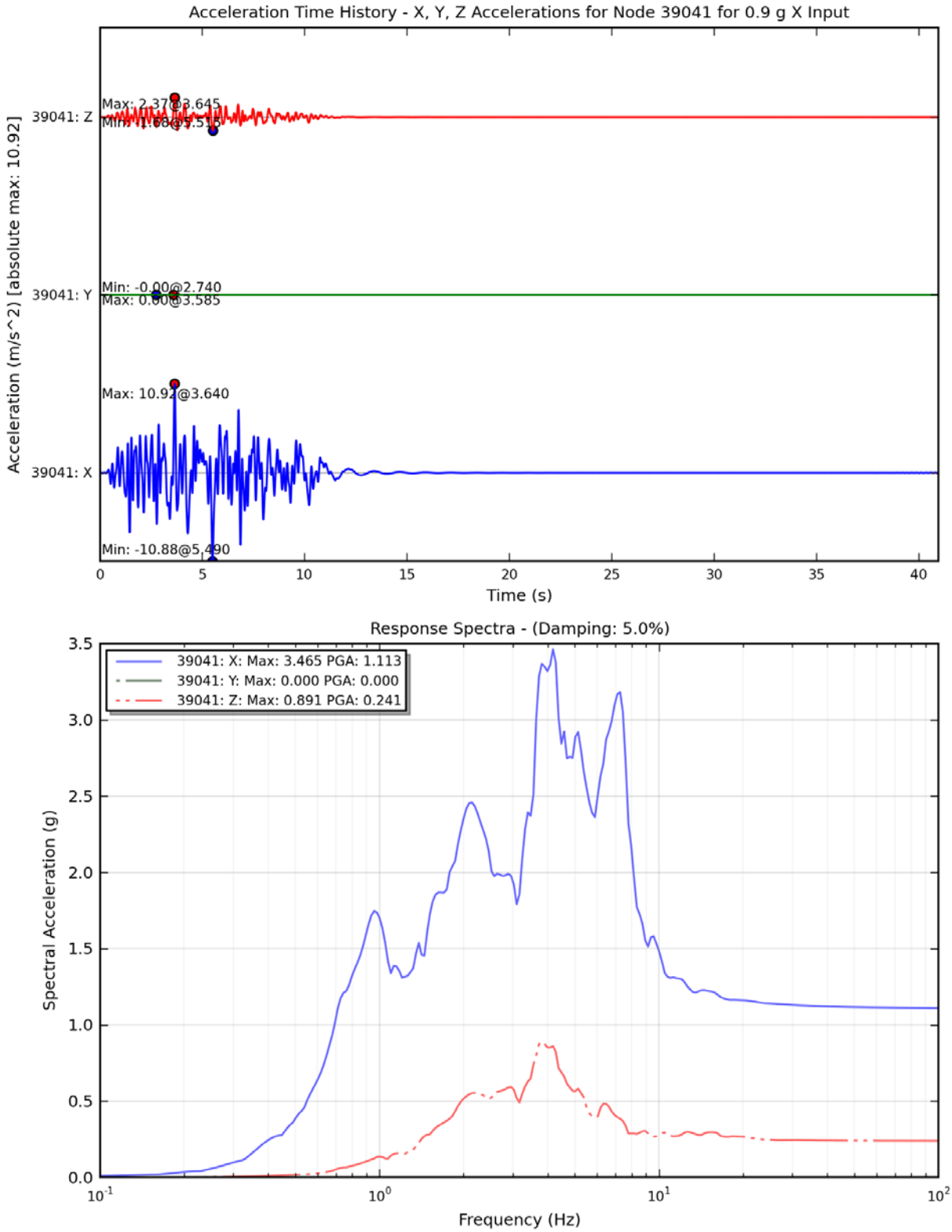

Figure 5-28 Response Acceleration Time Histories and ISRS at Node 39041 for X Input Motion (0.9 g)

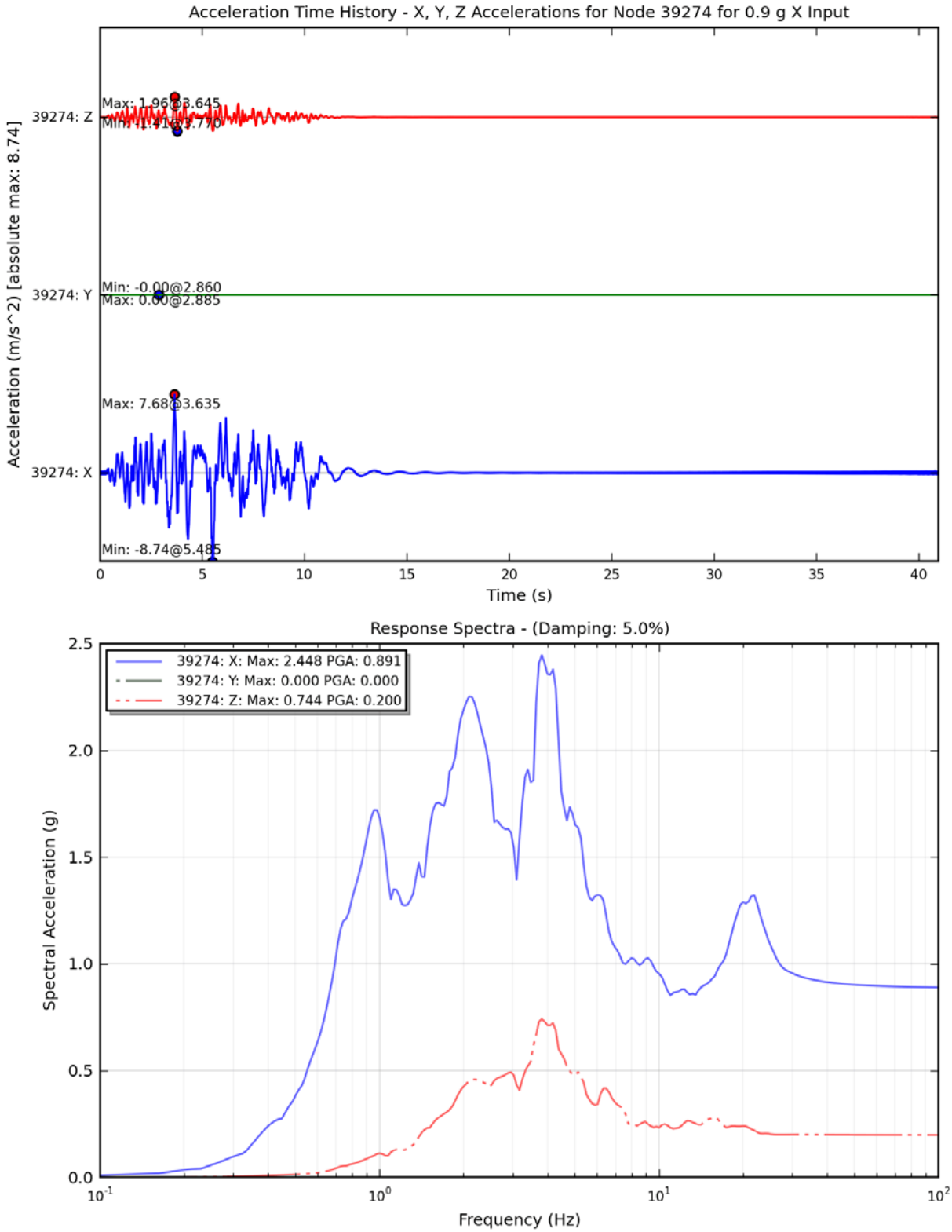

Figure 5-29 Response Acceleration Time Histories and ISRS at Node 39274 for X Input Motion (0.9 g)

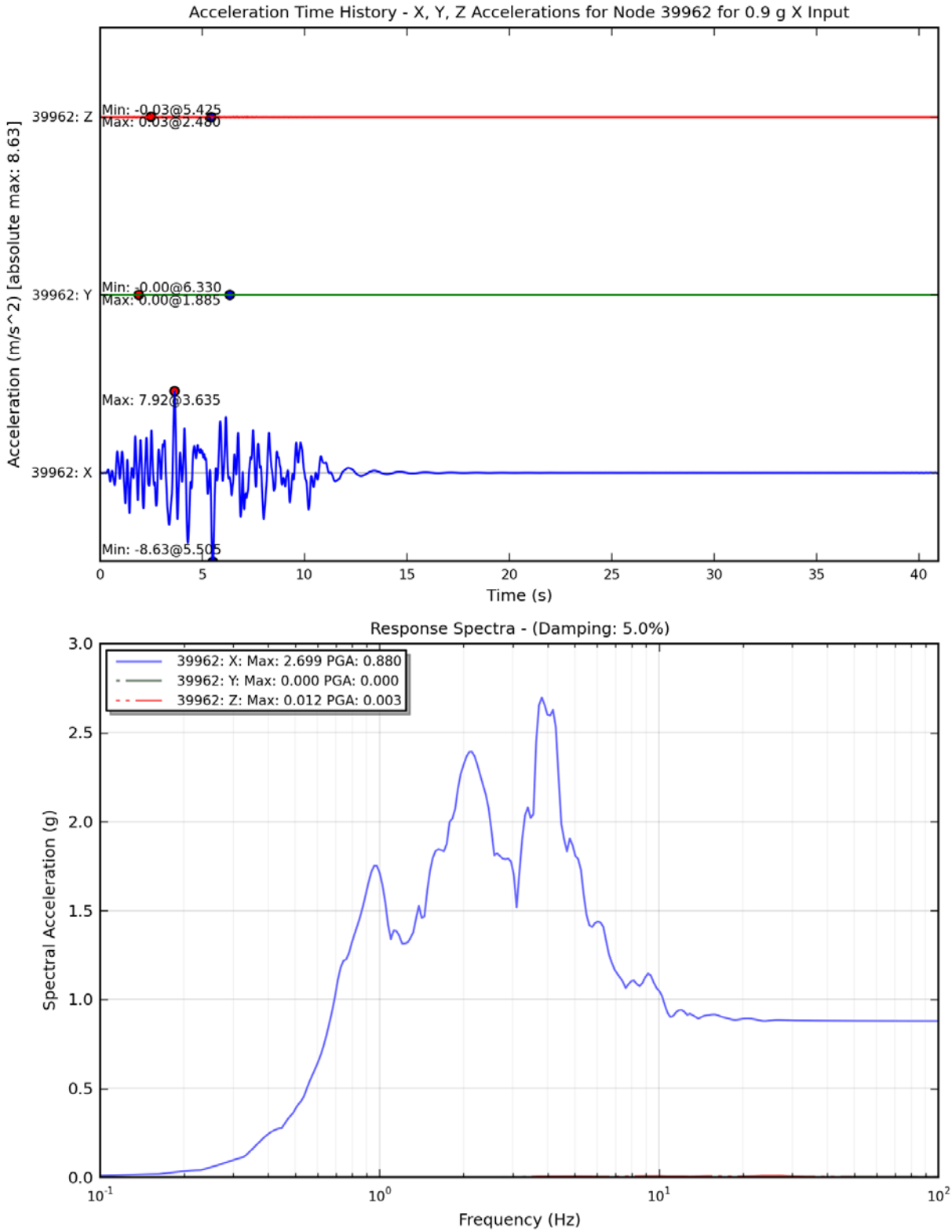

Figure 5-30 Response Acceleration Time Histories and ISRS at Node 39962 for X Input Motion (0.9 g)

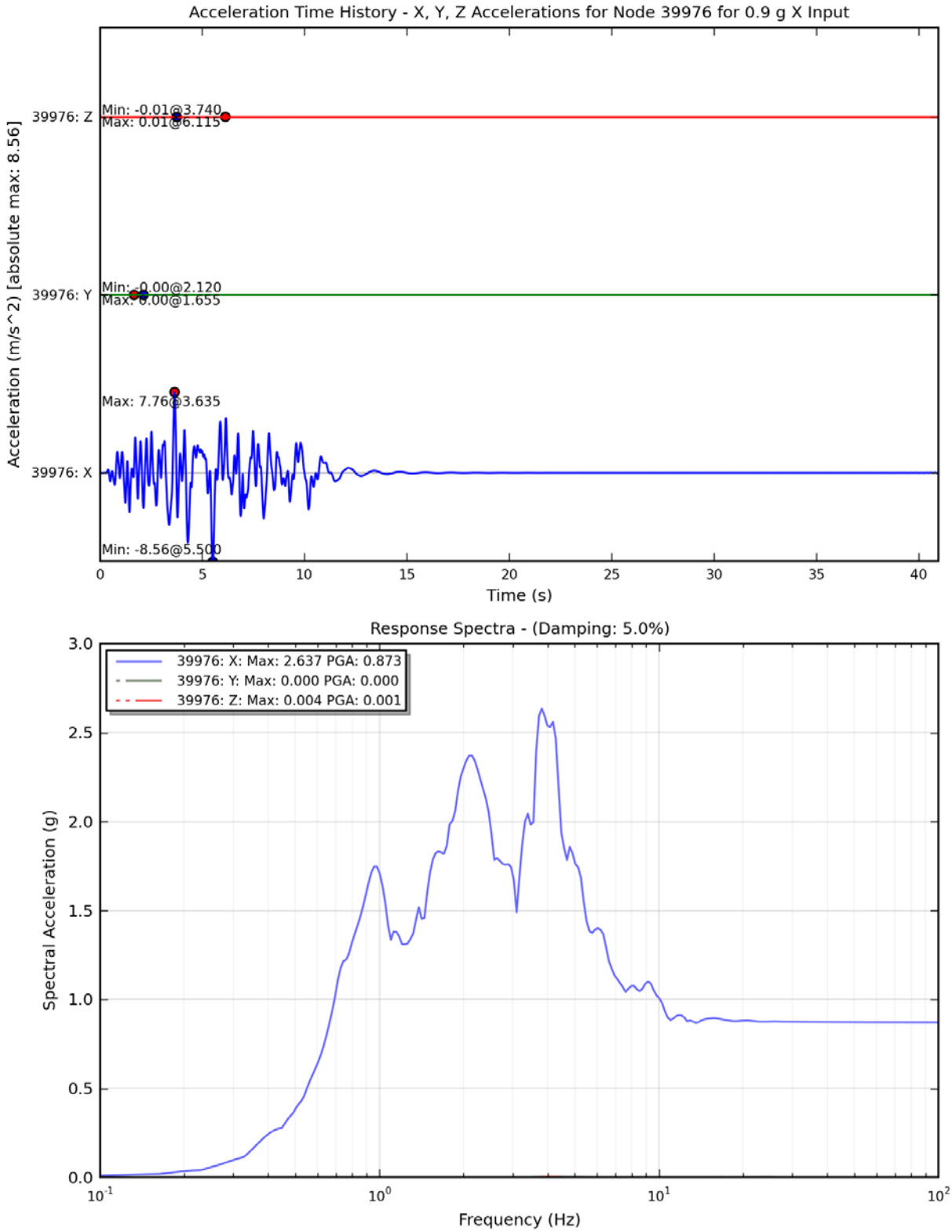

Figure 5-31 Response Acceleration Time Histories and ISRS at Node 39976 for X Input Motion (0.9 g)

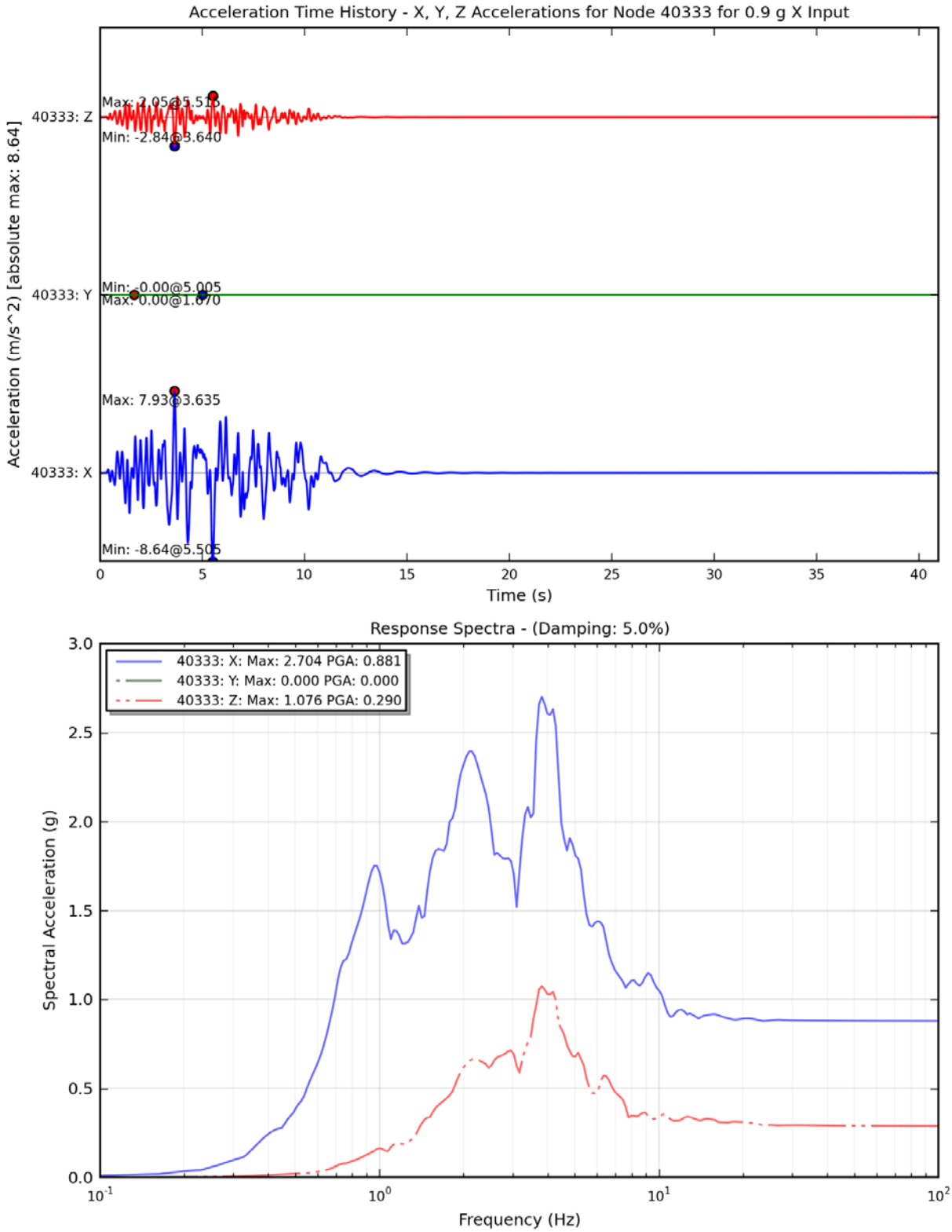

Figure 5-32 Response Acceleration Time Histories and ISRS at Node 40333 for X Input Motion (0.9 g)

5.3 Acceleration Time Histories and ISRS for the Z Directional Input Motion

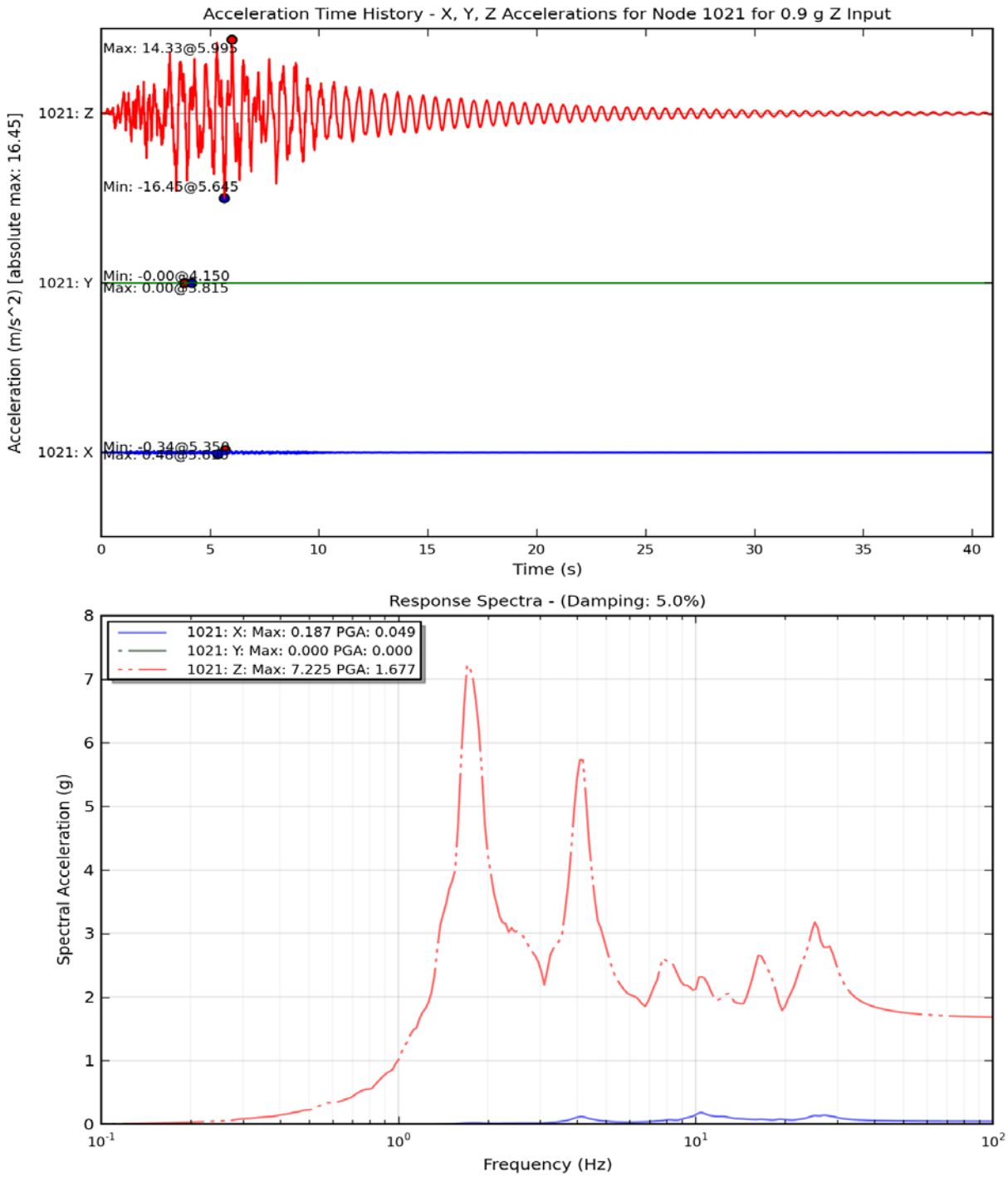

Figure 5-33 Response Acceleration Time Histories and ISRS at Node 1021 for Z Input Motion (0.9 g)

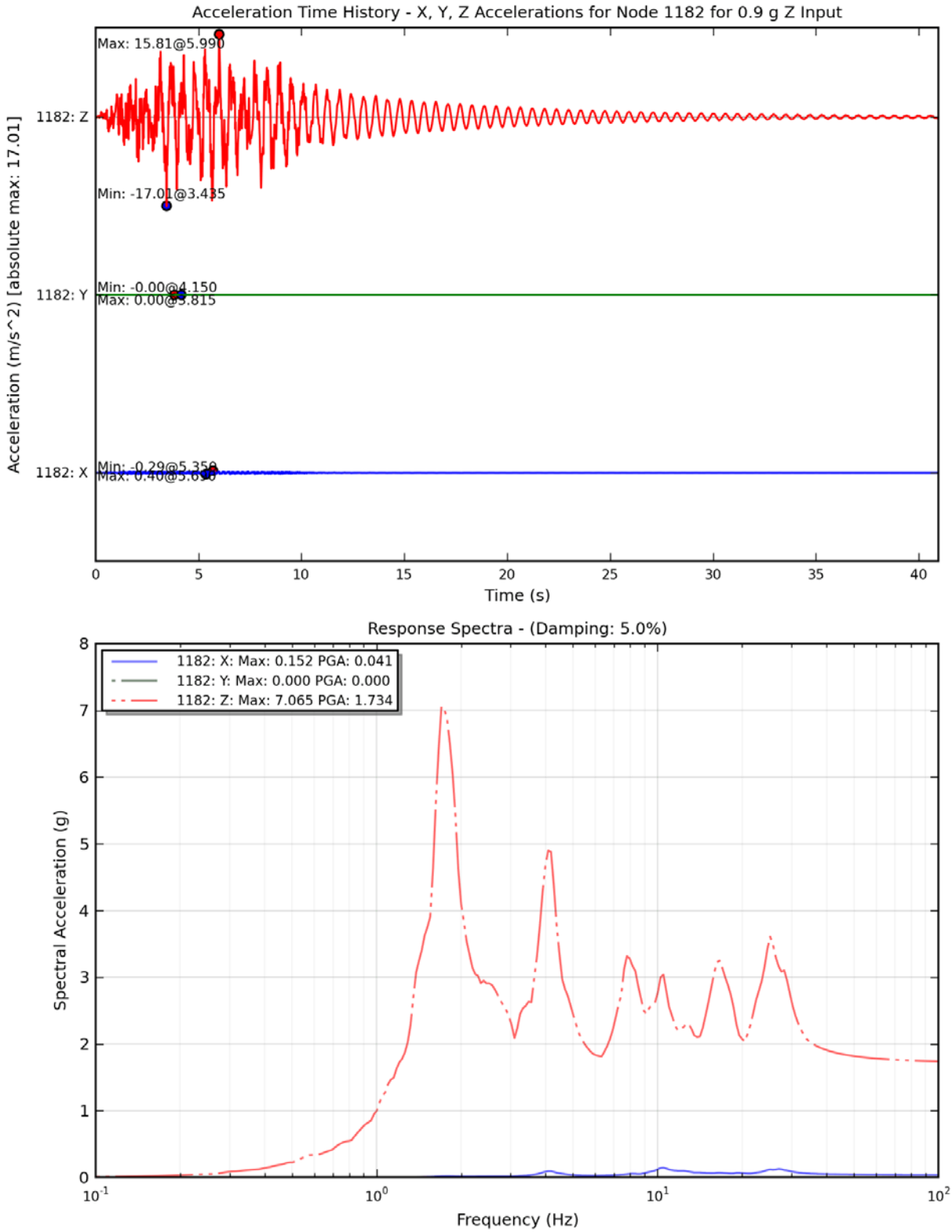

Figure 5-34 Response Acceleration Time Histories and ISRS at Node 1182 for Z Input Motion (0.9 g)

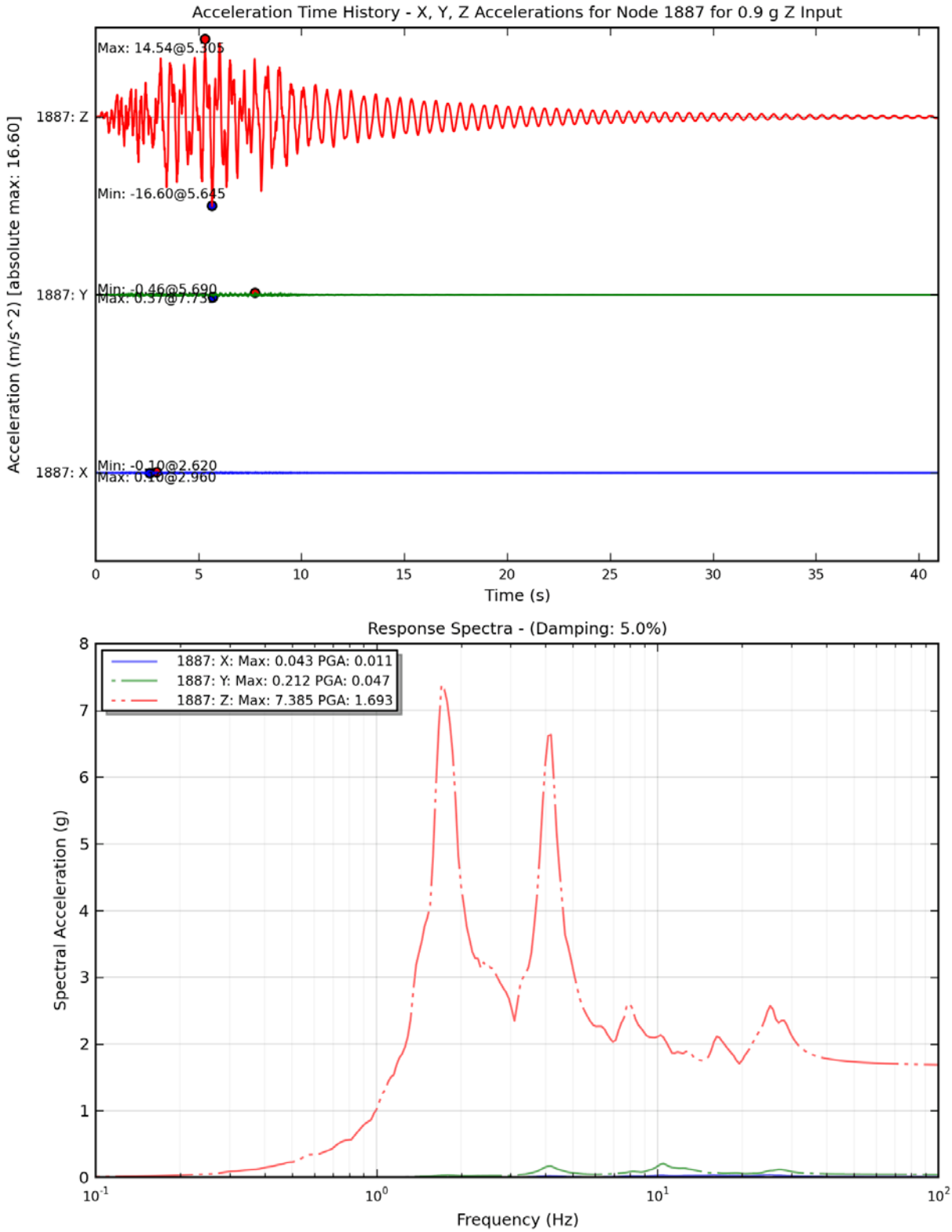

Figure 5-35 Response Acceleration Time Histories and ISRS at Node 1887 for Z Input Motion (0.9 g)

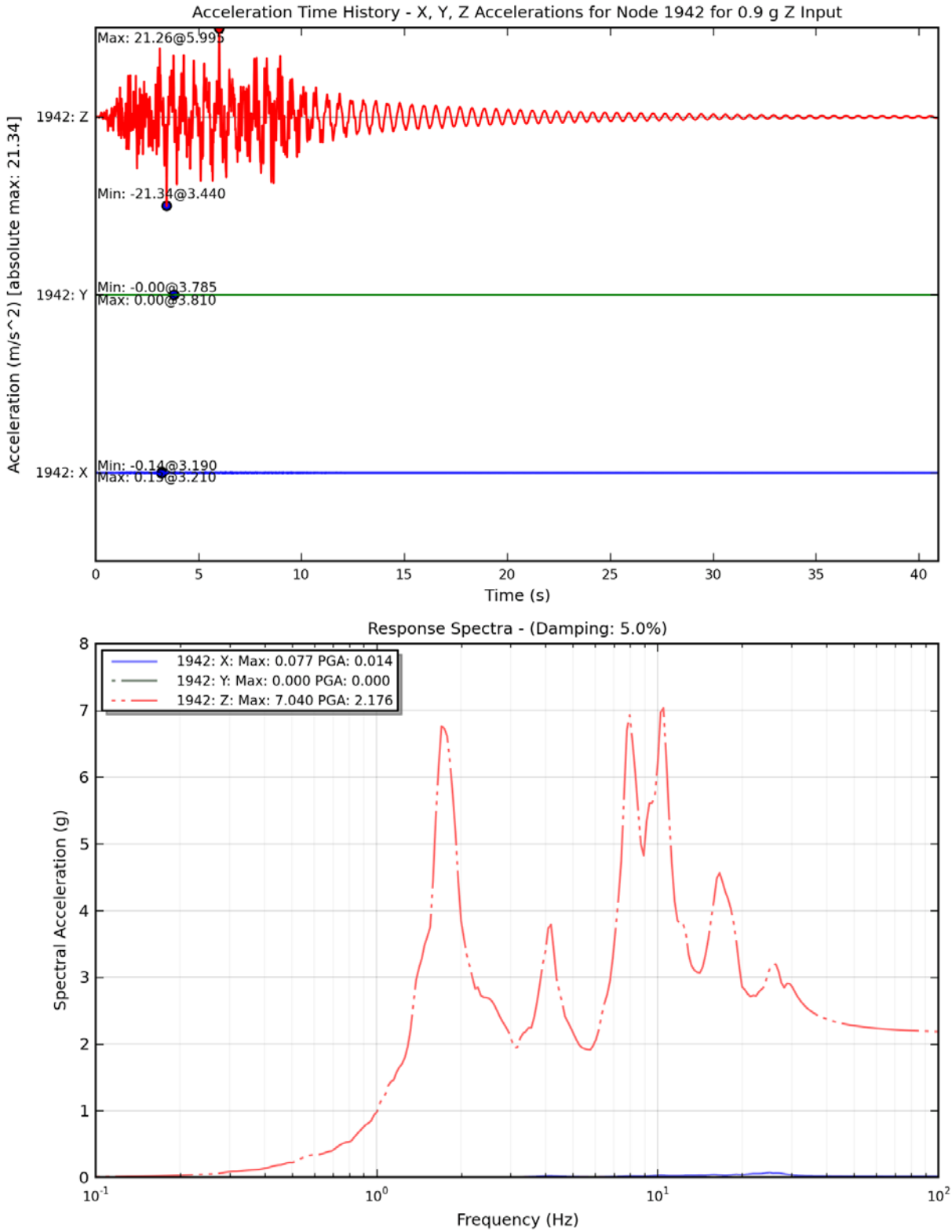

Figure 5-36 Response Acceleration Time Histories and ISRS at Node 1942 for Z Input Motion (0.9 g)

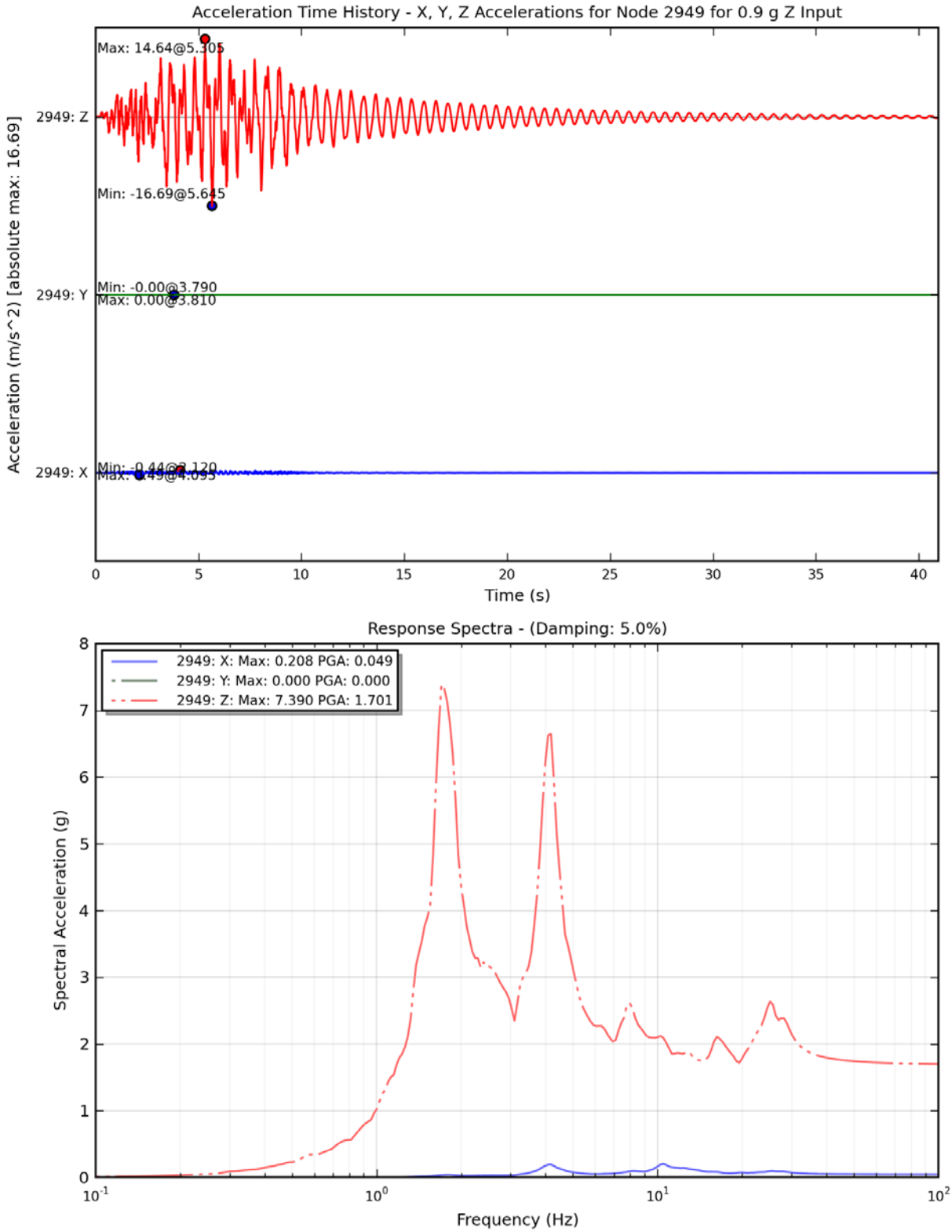

Figure 5-37 Response Acceleration Time Histories and ISRS at Node 2949 for Z Input Motion (0.9 g)

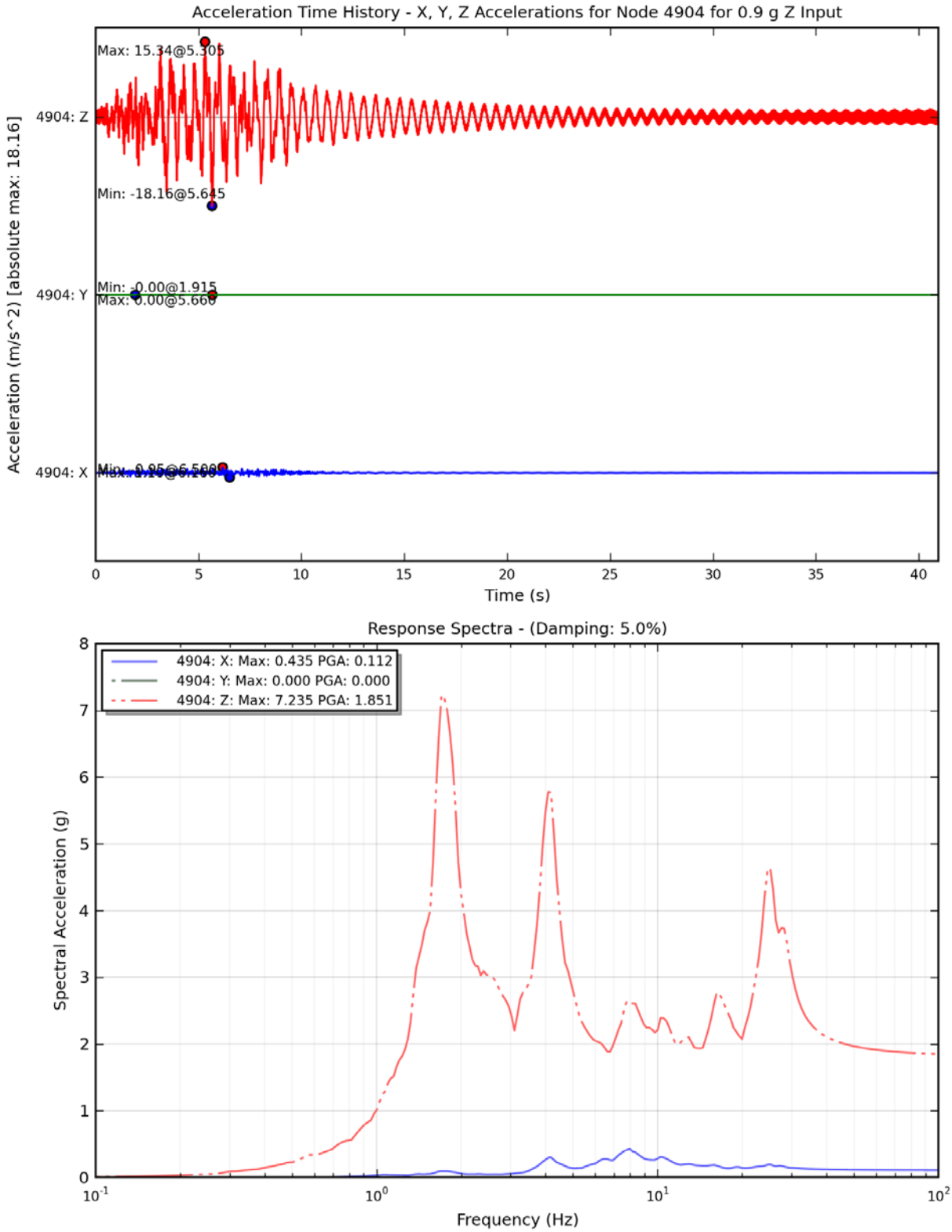

Figure 5-38 Response Acceleration Time Histories and ISRS at Node 4904 for Z Input Motion (0.9 g)

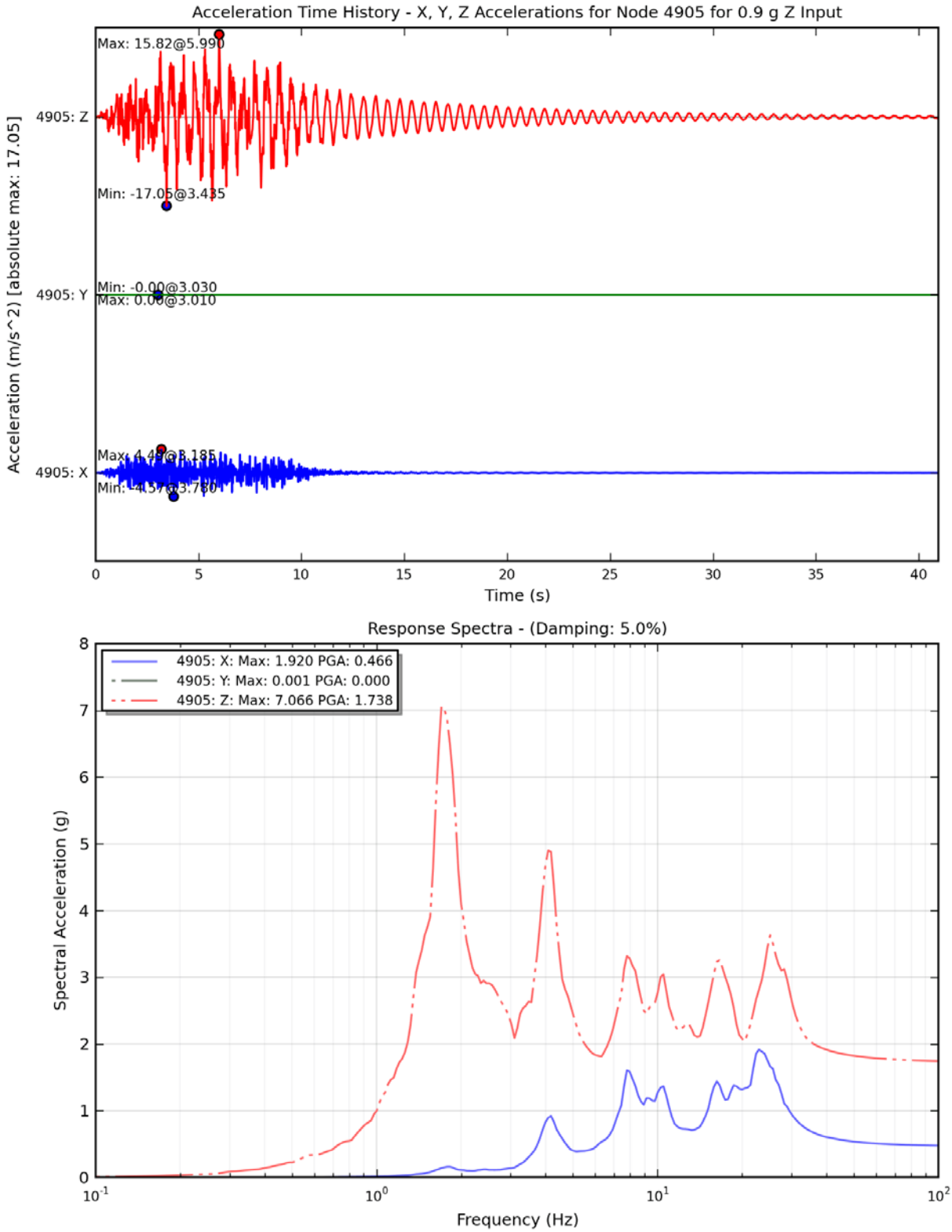

Figure 5-39 Response Acceleration Time Histories and ISRS at Node 4905 for Z Input Motion (0.9 g)

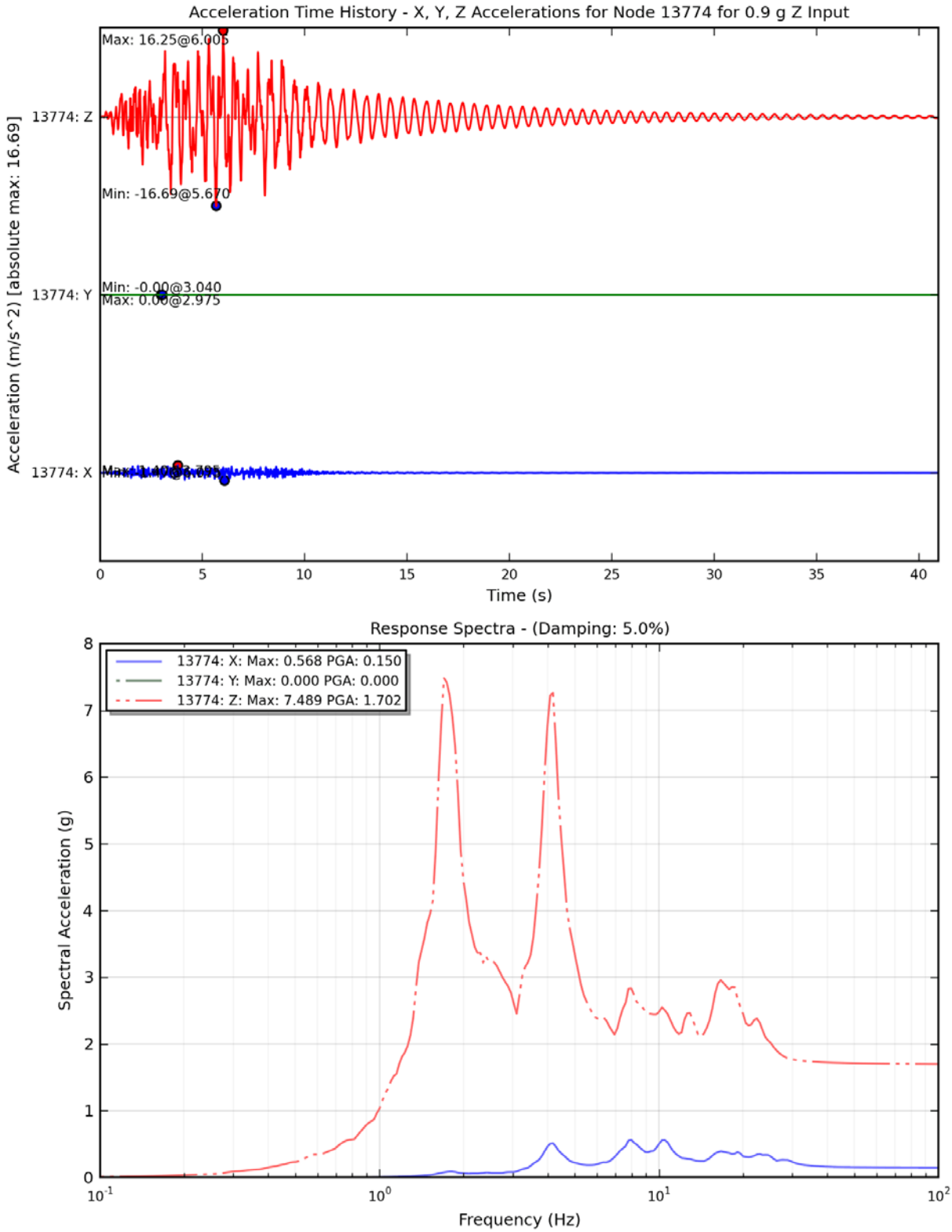

Figure 5-40 Response Acceleration Time Histories and ISRS at Node 13774 for Z Input Motion (0.9 g)

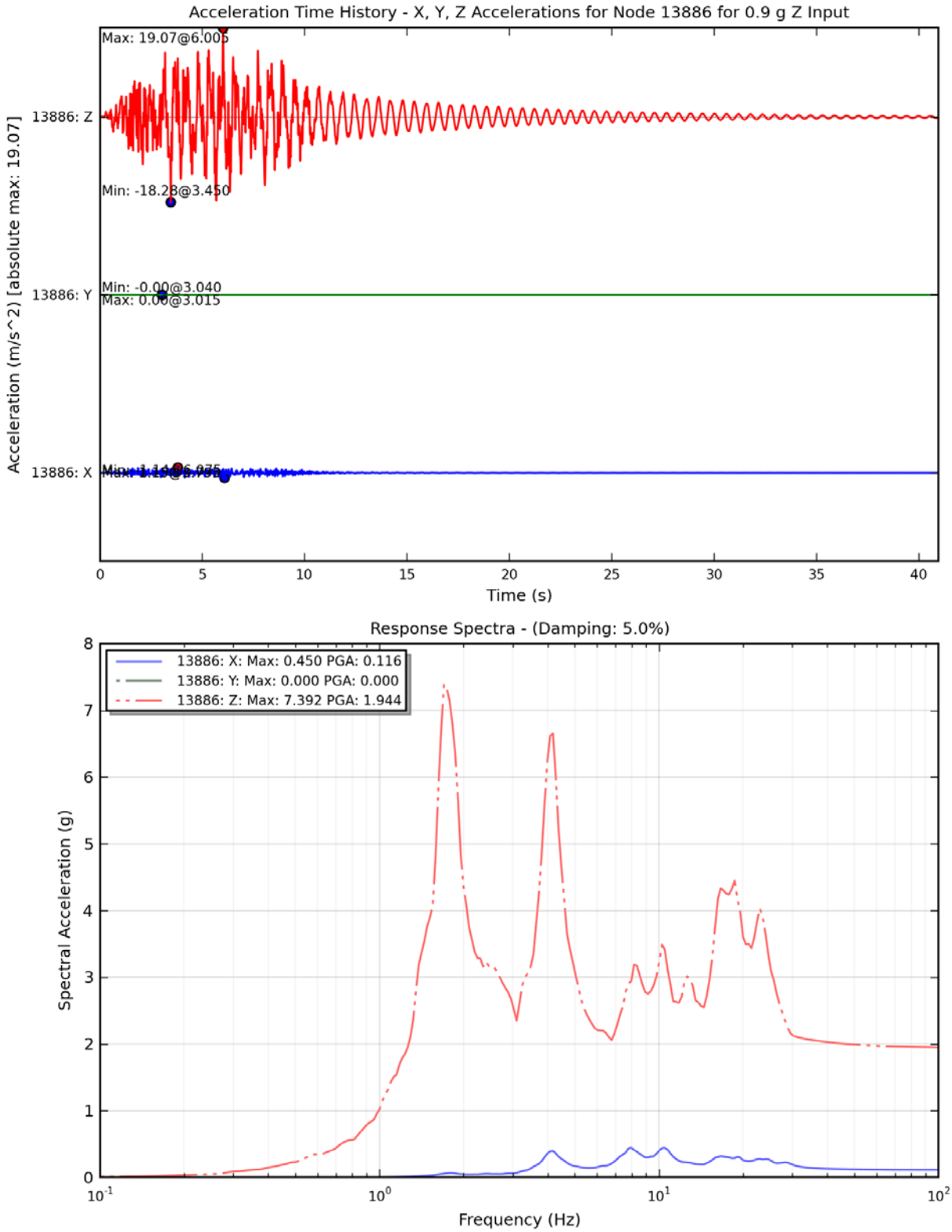

Figure 5-41 Response Acceleration Time Histories and ISRS at Node 13886 for Z Input Motion (0.9 g)

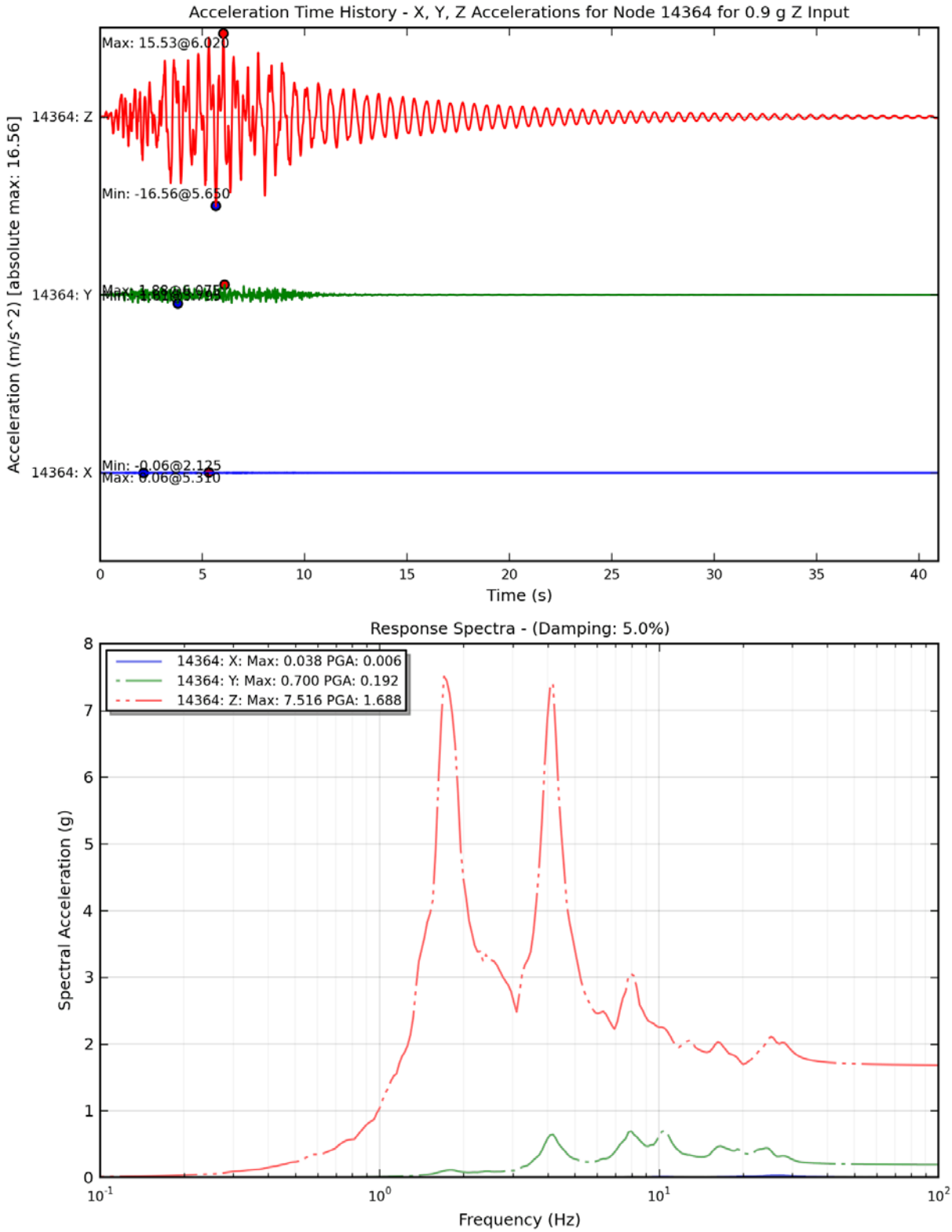

Figure 5-42 Response Acceleration Time Histories and ISRS at Node 14364 for Z Input Motion (0.9 g)

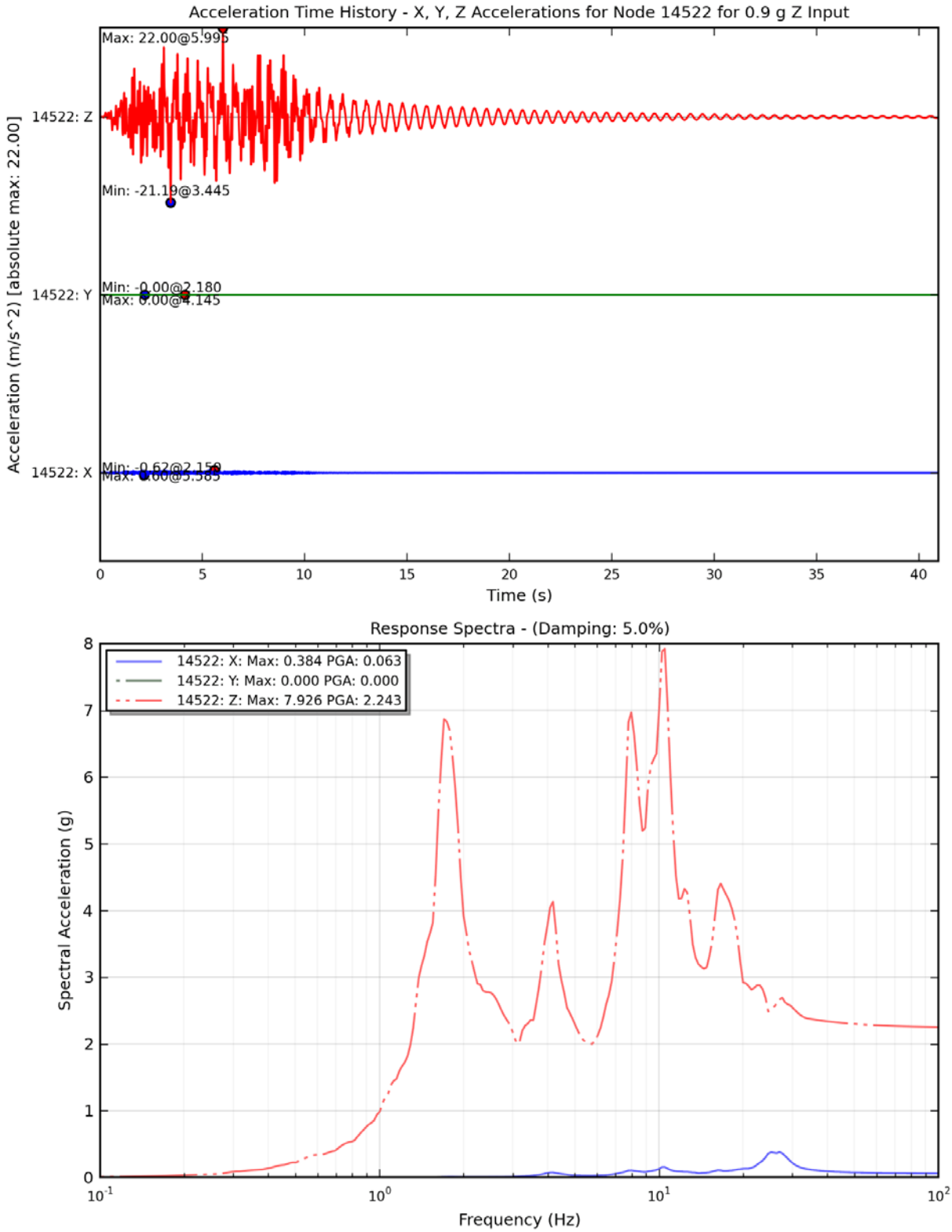

Figure 5-43 Response Acceleration Time Histories and ISRS at Node 14522 for Z Input Motion (0.9 g)

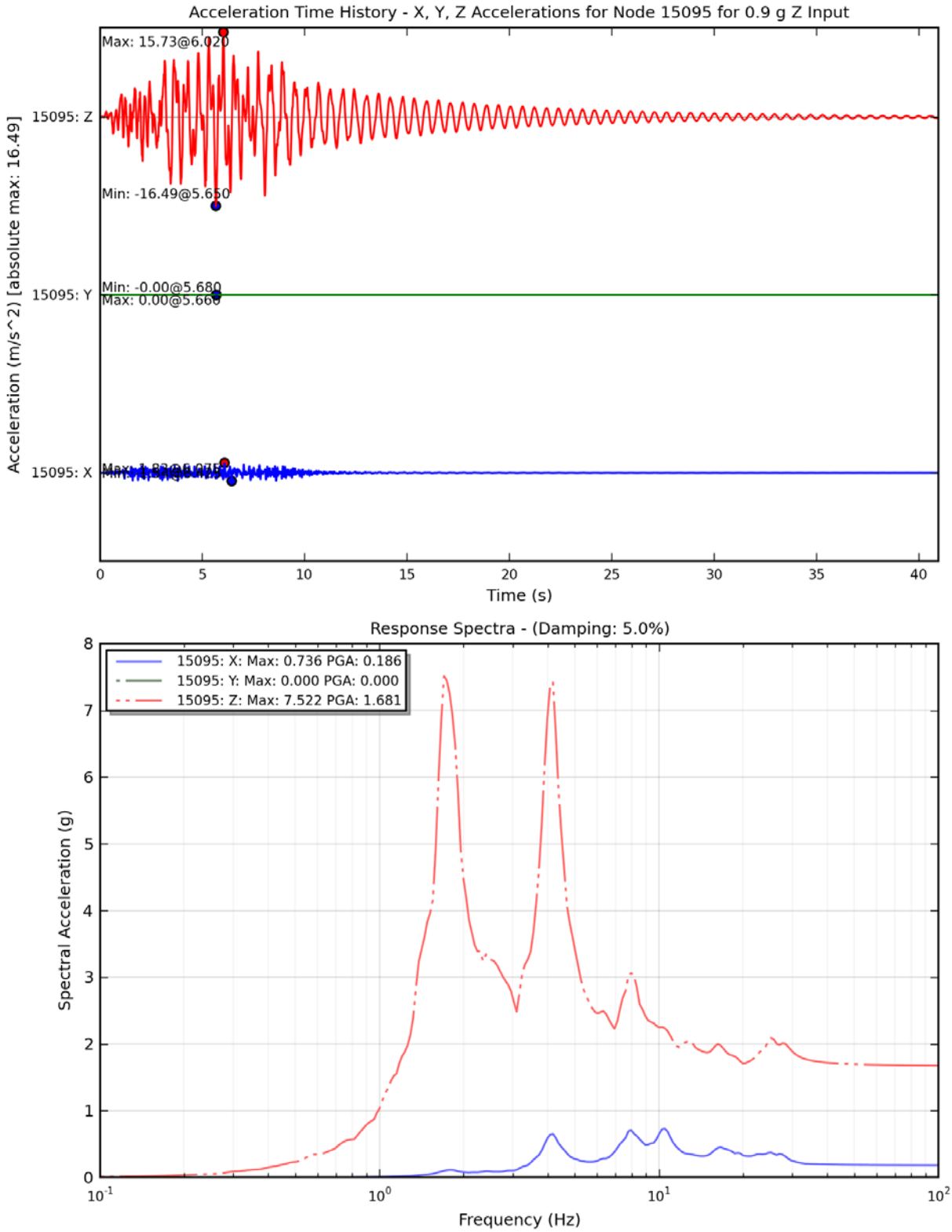

Figure 5-44 Response Acceleration Time Histories and ISRS at Node 15095 for Z Input Motion (0.9 g)

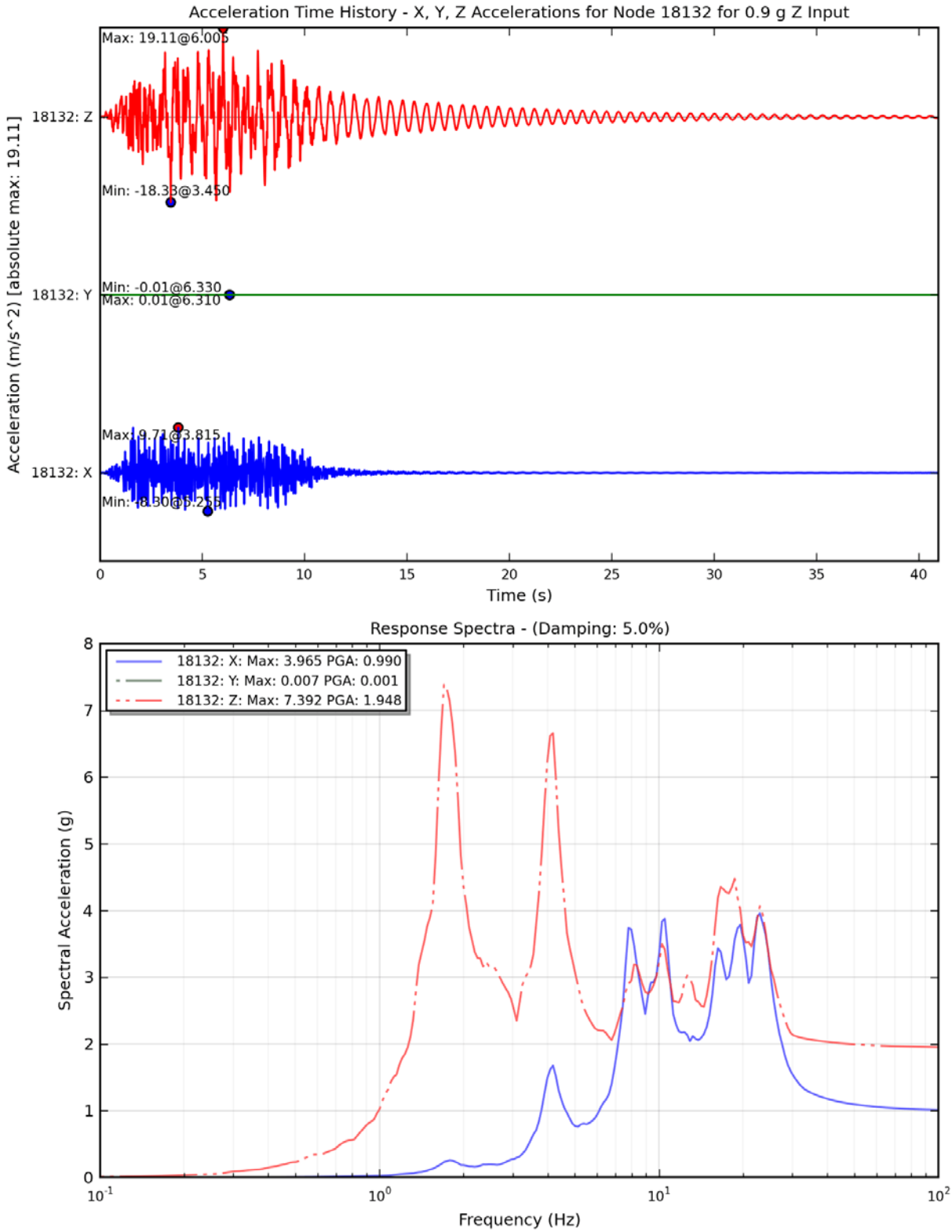

Figure 5-45 Response Acceleration Time Histories and ISRS at Node 18132 for Z Input Motion (0.9 g)

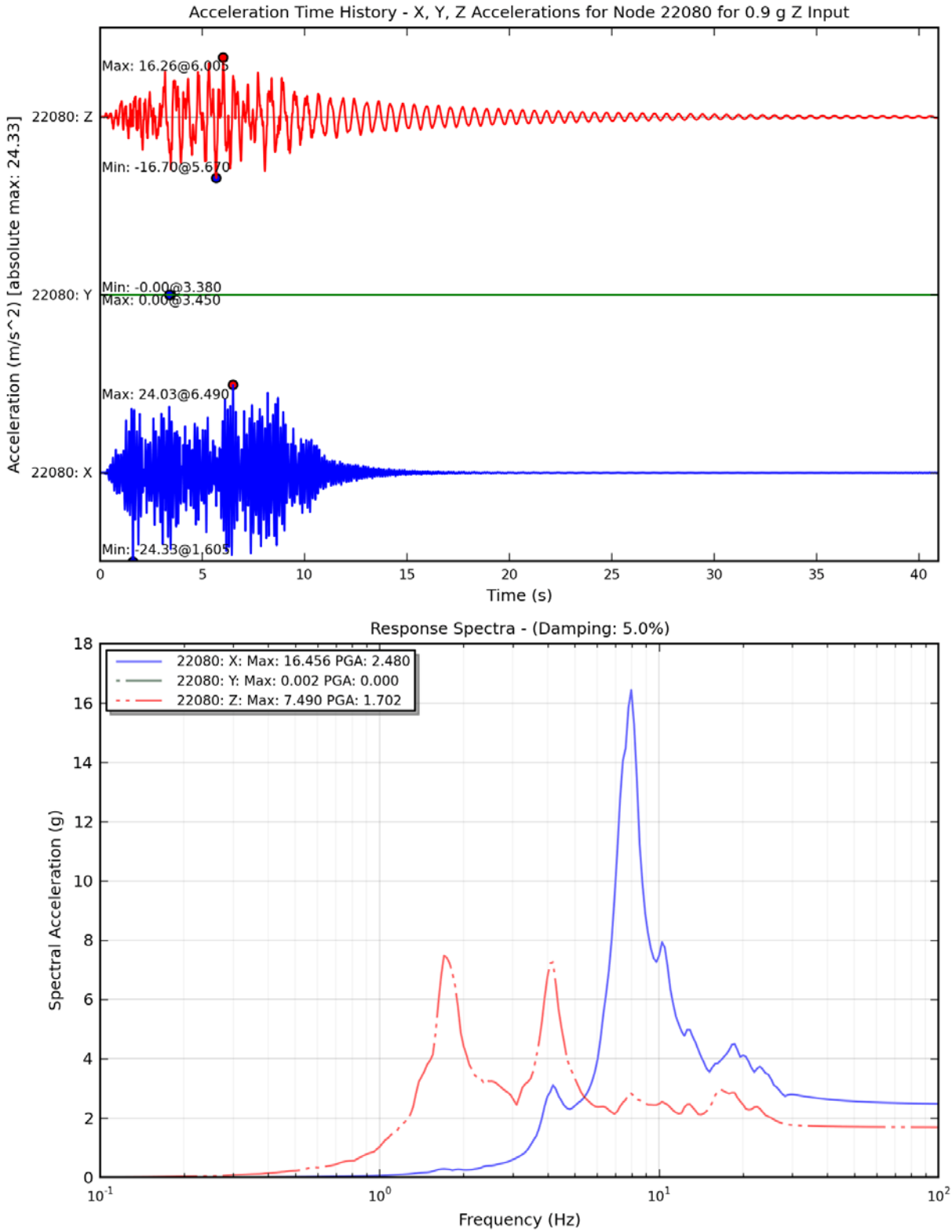

Figure 5-46 Response Acceleration Time Histories and ISRS at Node 22080 for Z Input Motion (0.9 g)

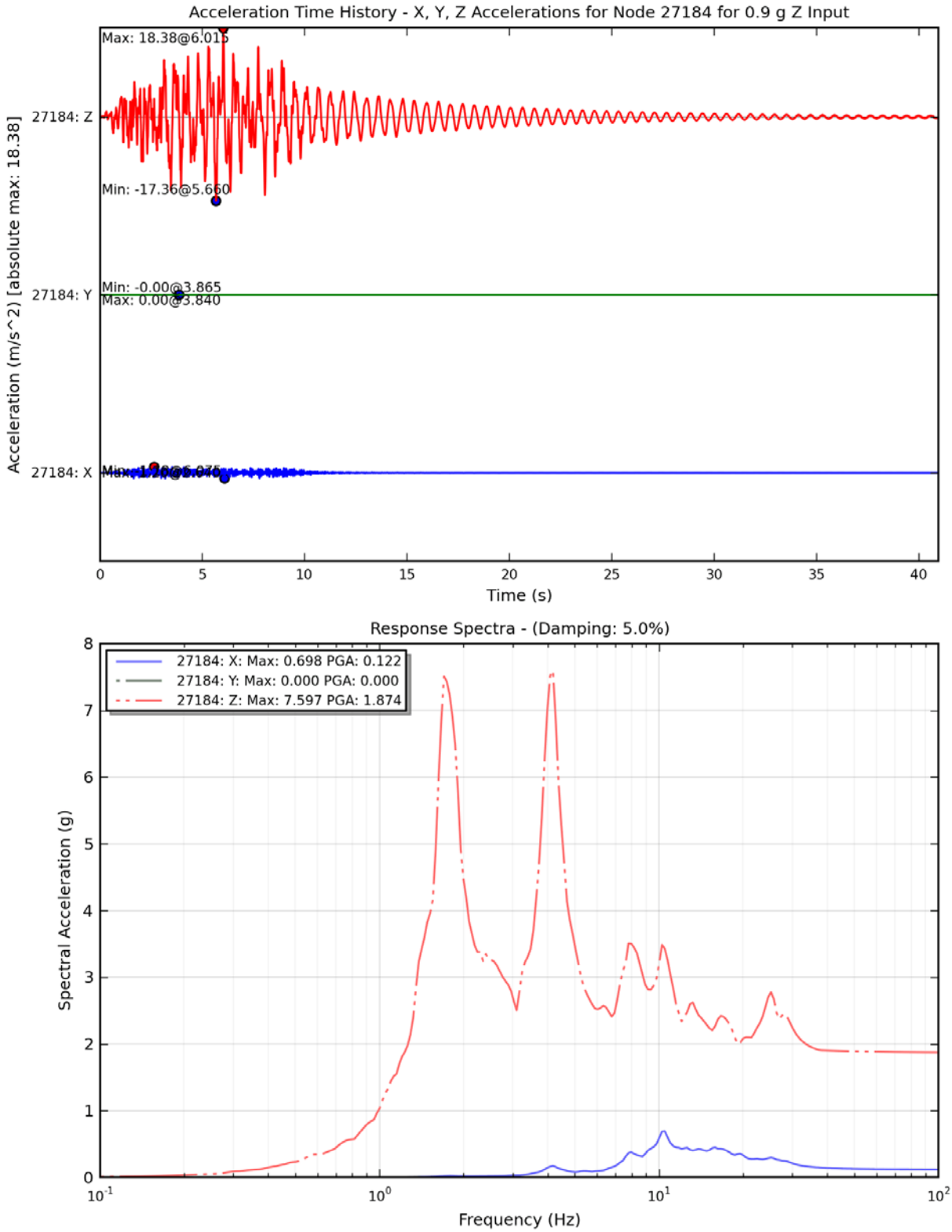

Figure 5-47 Response Acceleration Time Histories and ISRS at Node 27184 for Z Input Motion (0.9 g)

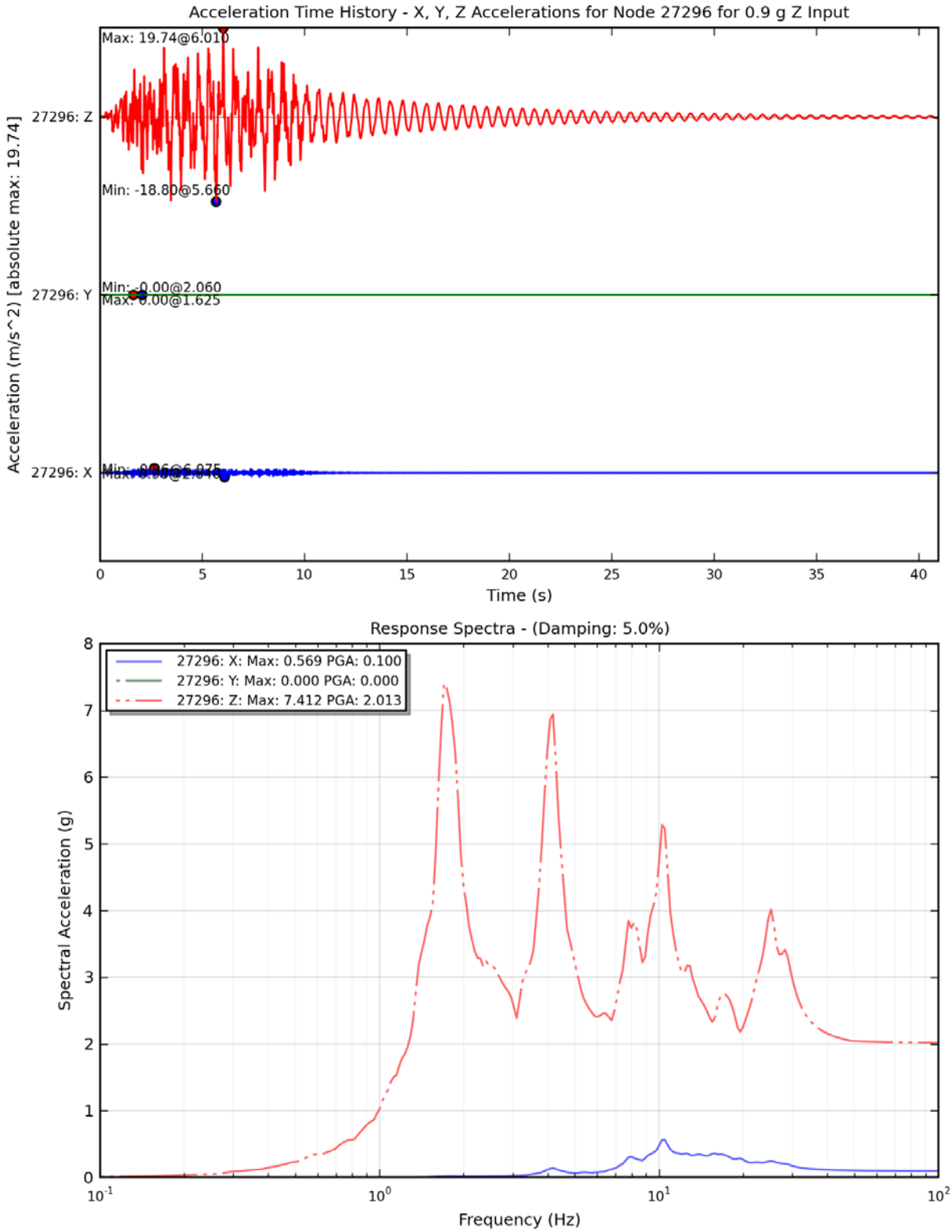

Figure 5-48 Response Acceleration Time Histories and ISRS at Node 27296 for Z Input Motion (0.9 g)

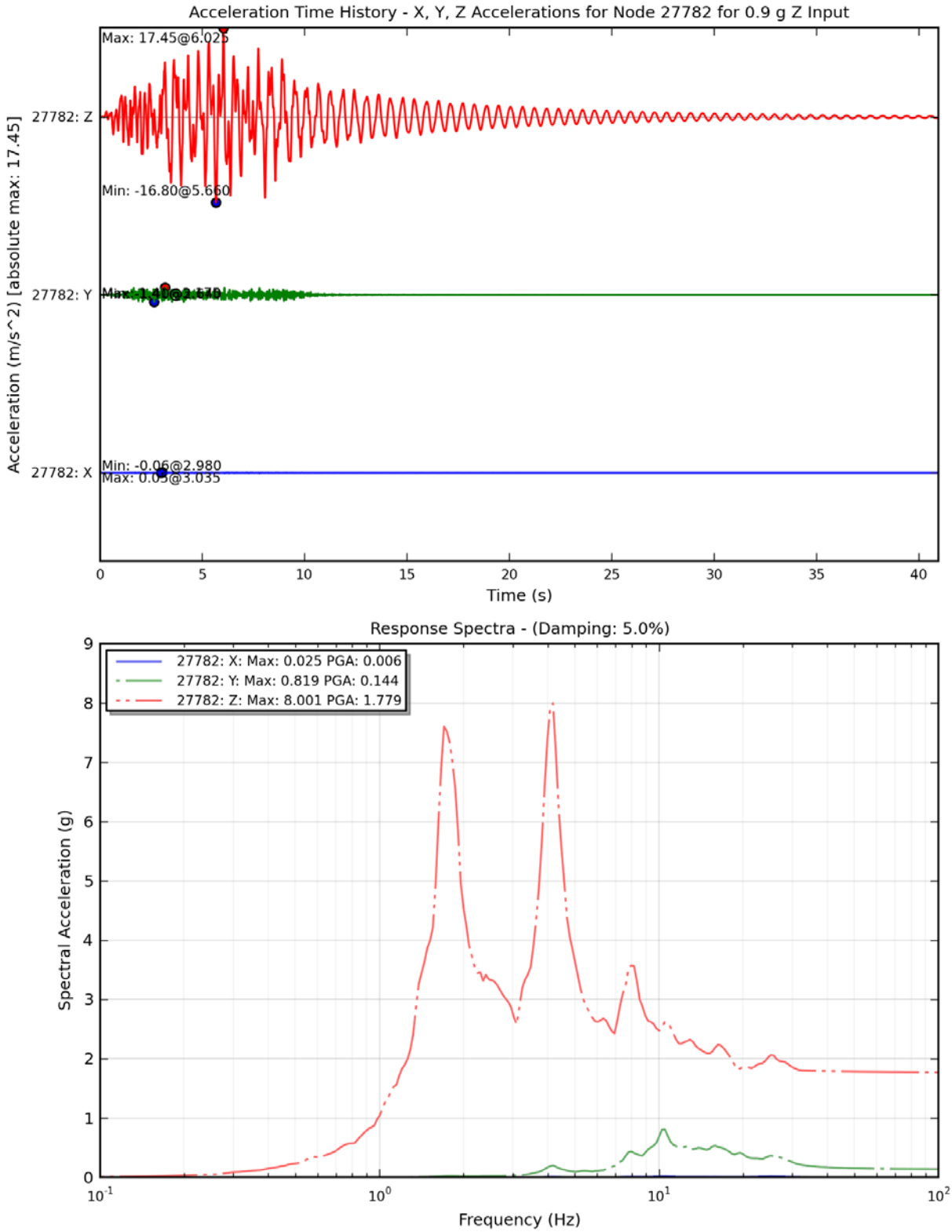

Figure 5-49 Response Acceleration Time Histories and ISRS at Node 27782 for Z Input Motion (0.9 g)

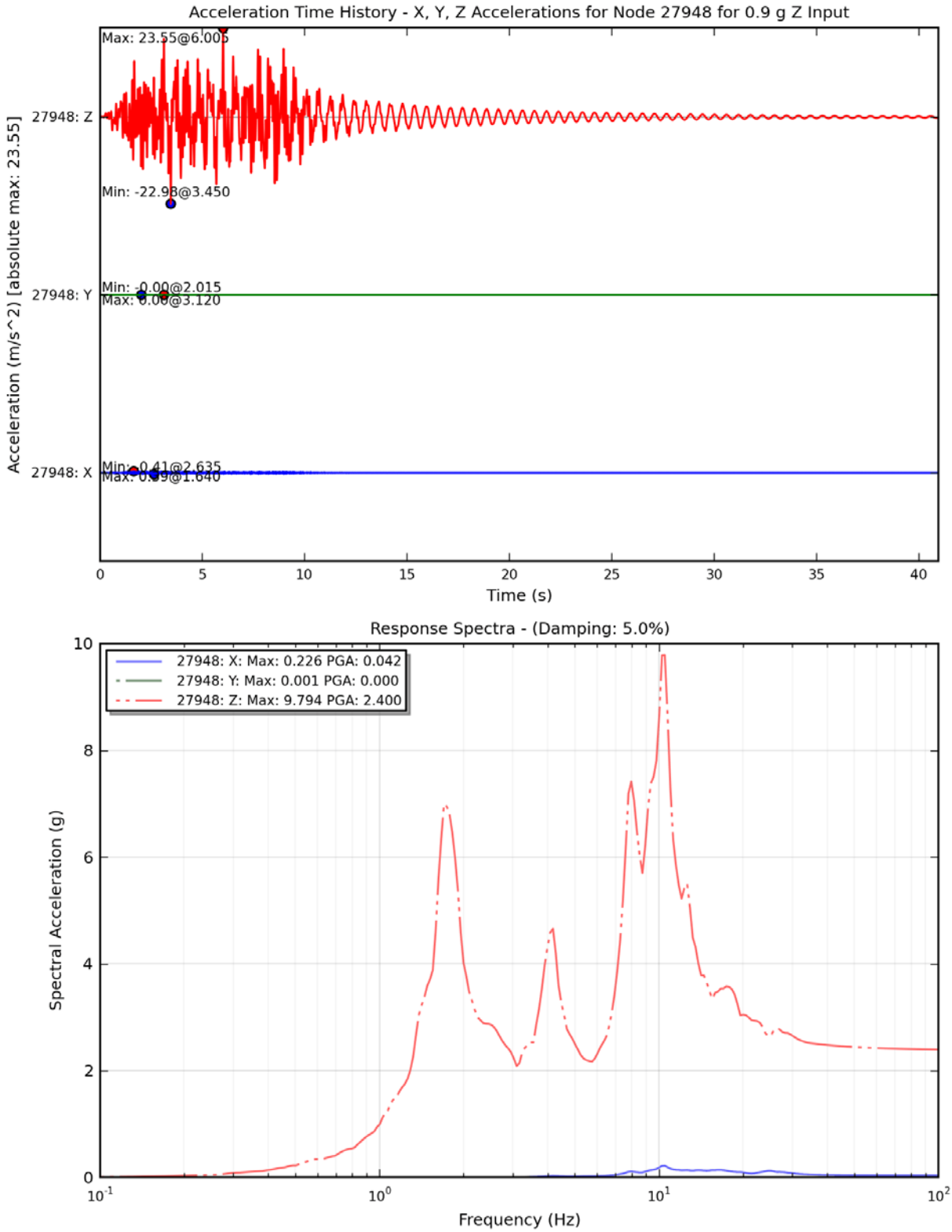

Figure 5-50 Response Acceleration Time Histories and ISRS at Node 27948 for Z Input Motion (0.9 g)

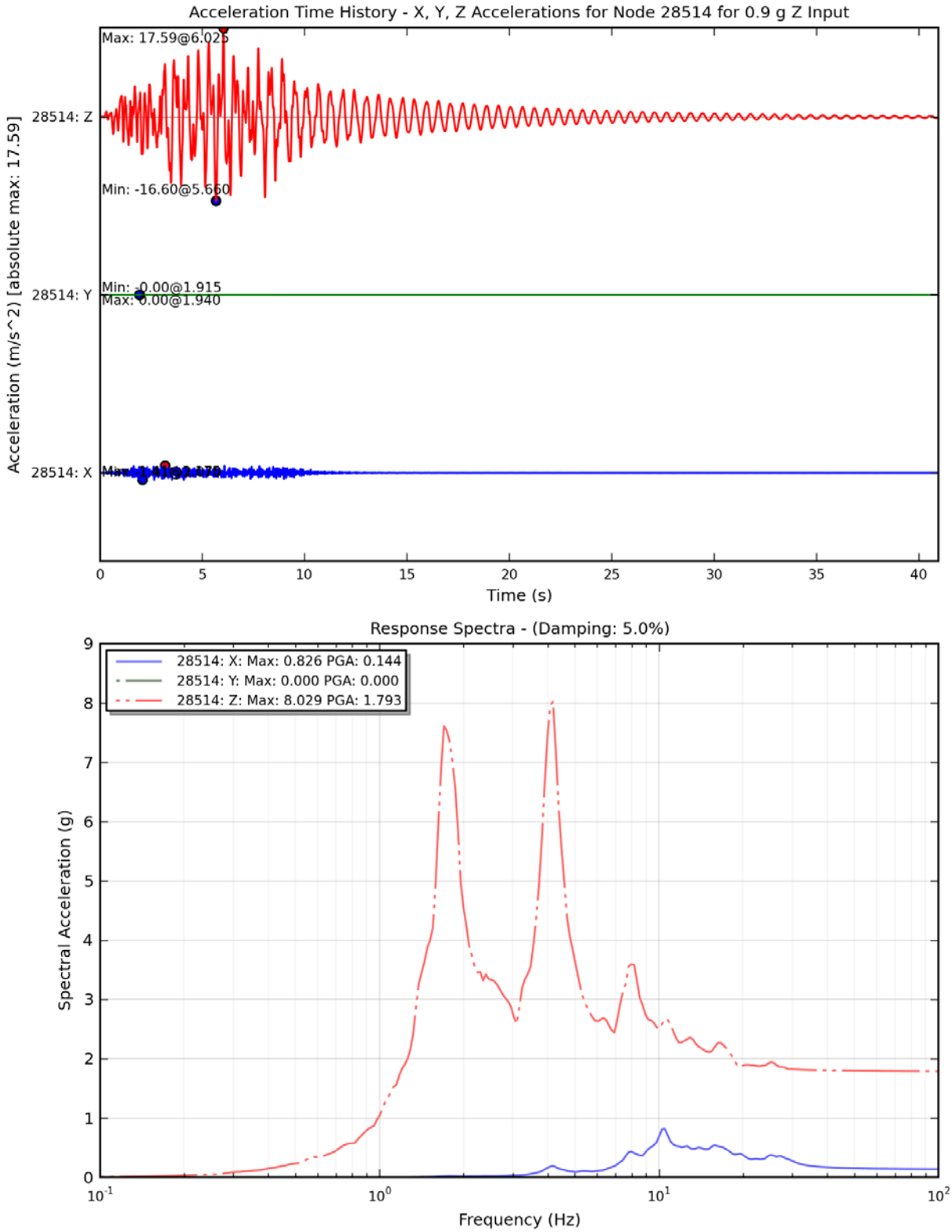

Figure 5-51 Response Acceleration Time Histories and ISRS at Node 28514 for Z Input Motion (0.9 g)

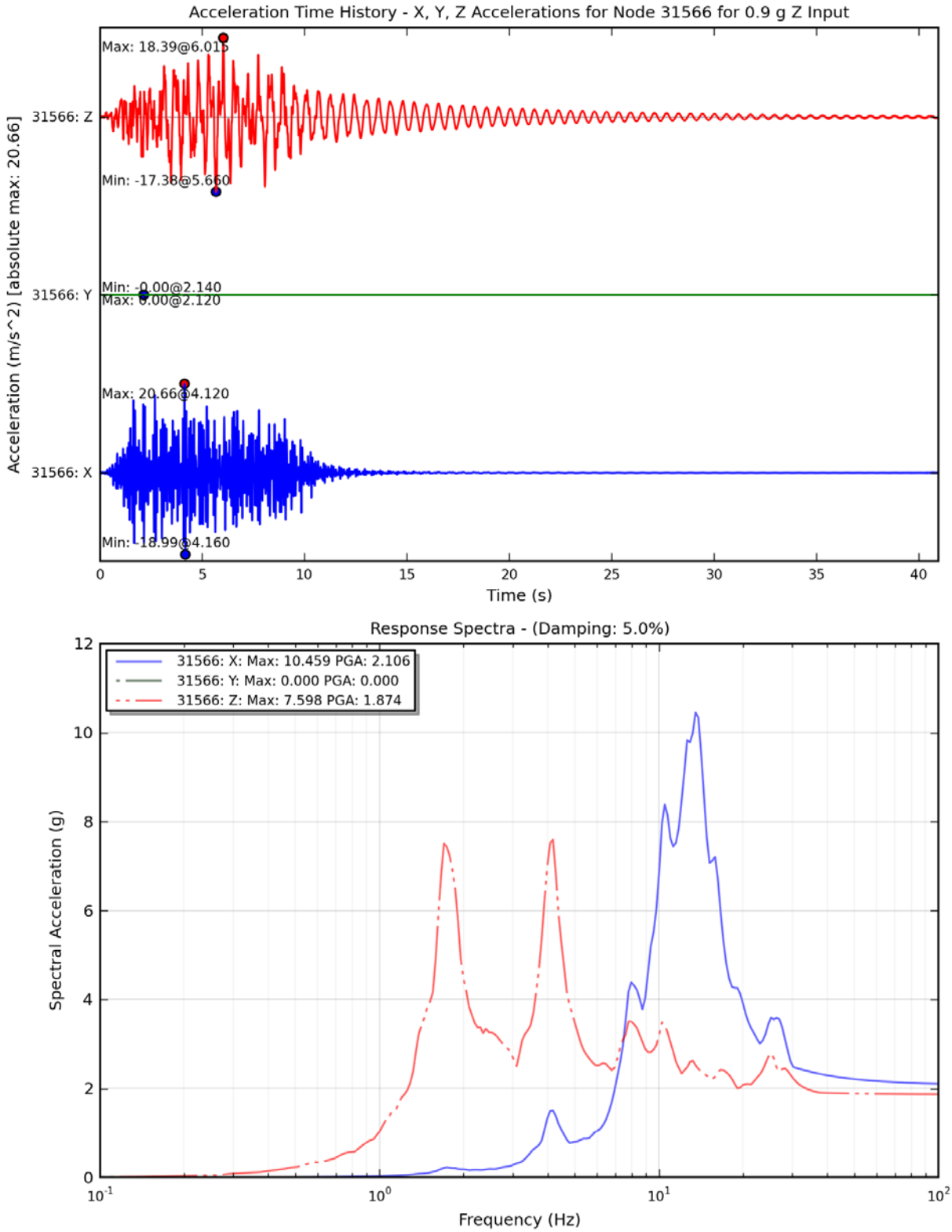

Figure 5-52 Response Acceleration Time Histories and ISRS at Node 31566 for Z Input Motion (0.9 g)

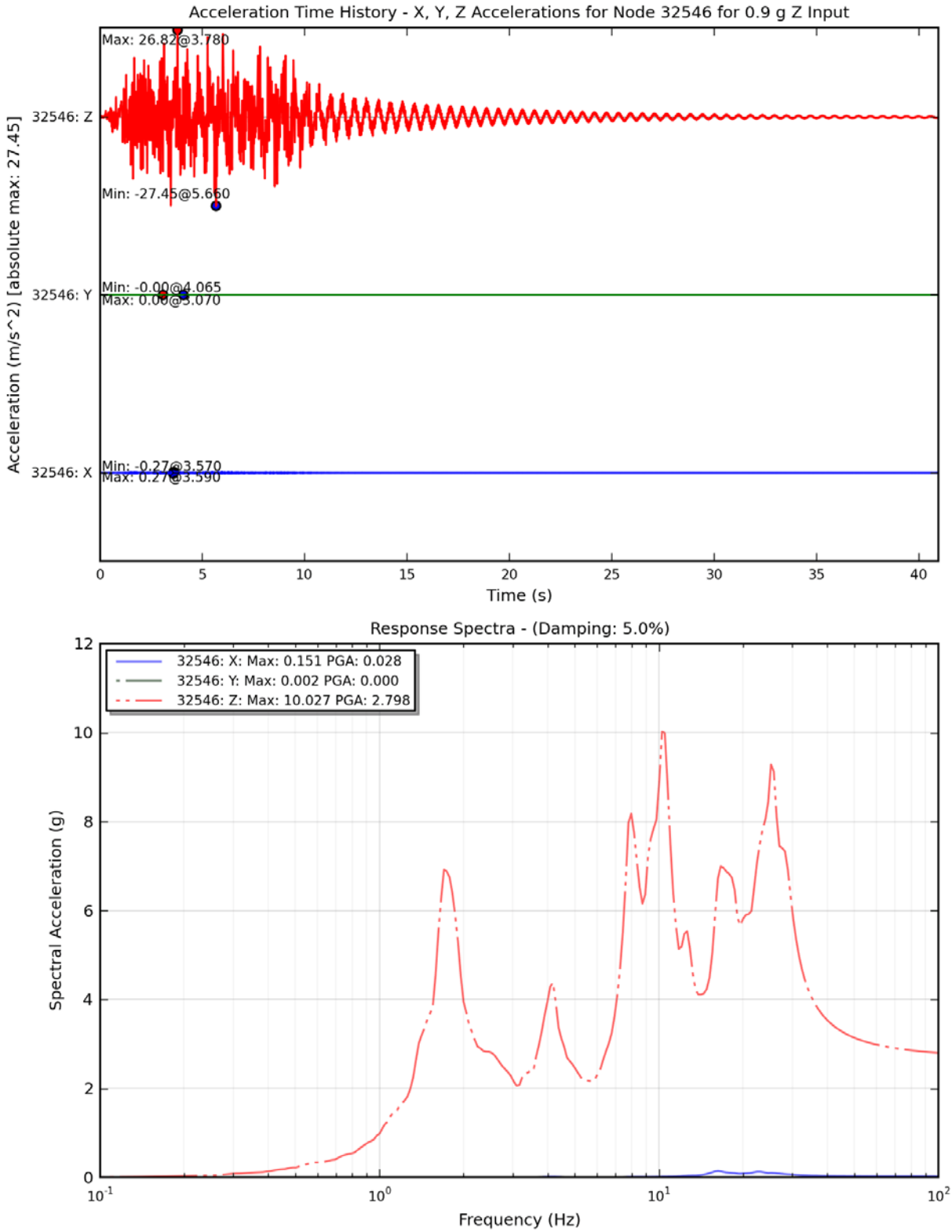

Figure 5-53 Response Acceleration Time Histories and ISRS at Node 32546 for Z Input Motion (0.9 g)

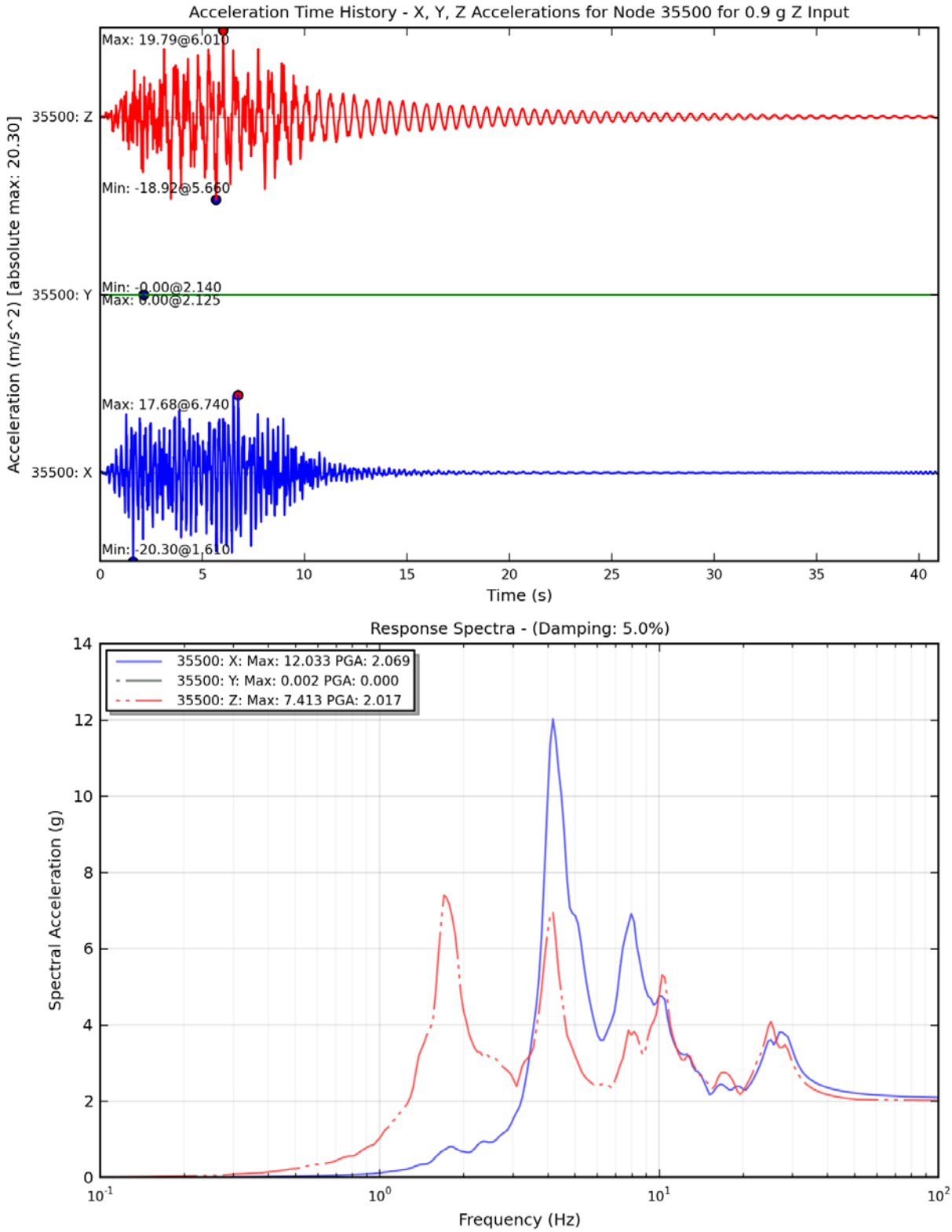

Figure 5-54 Response Acceleration Time Histories and ISRS at Node 35500 for Z Input Motion (0.9 g)

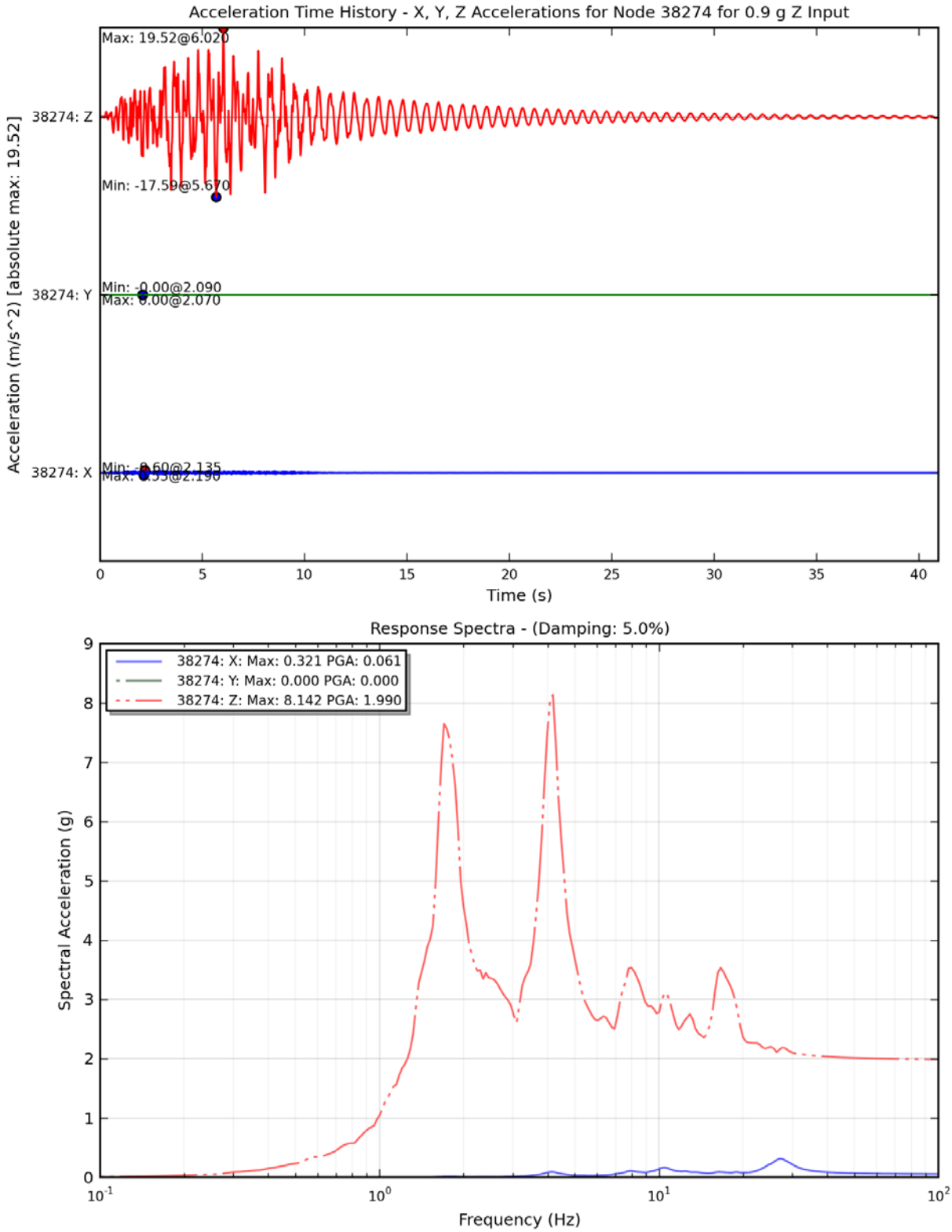

Figure 5-55 Response Acceleration Time Histories and ISRS at Node 38274 for Z Input Motion (0.9 g)

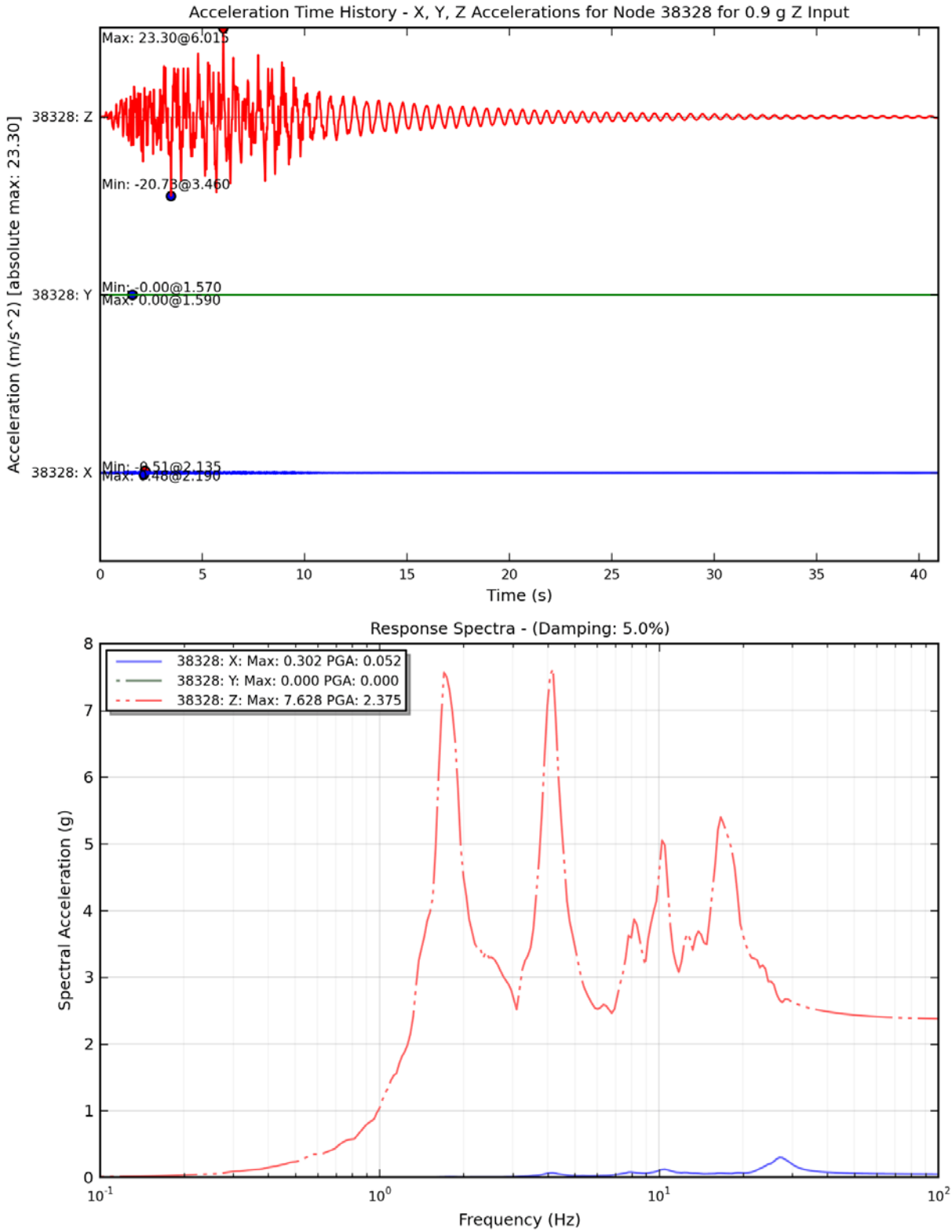

Figure 5-56 Response Acceleration Time Histories and ISRS at Node 38328 for Z Input Motion (0.9 g)

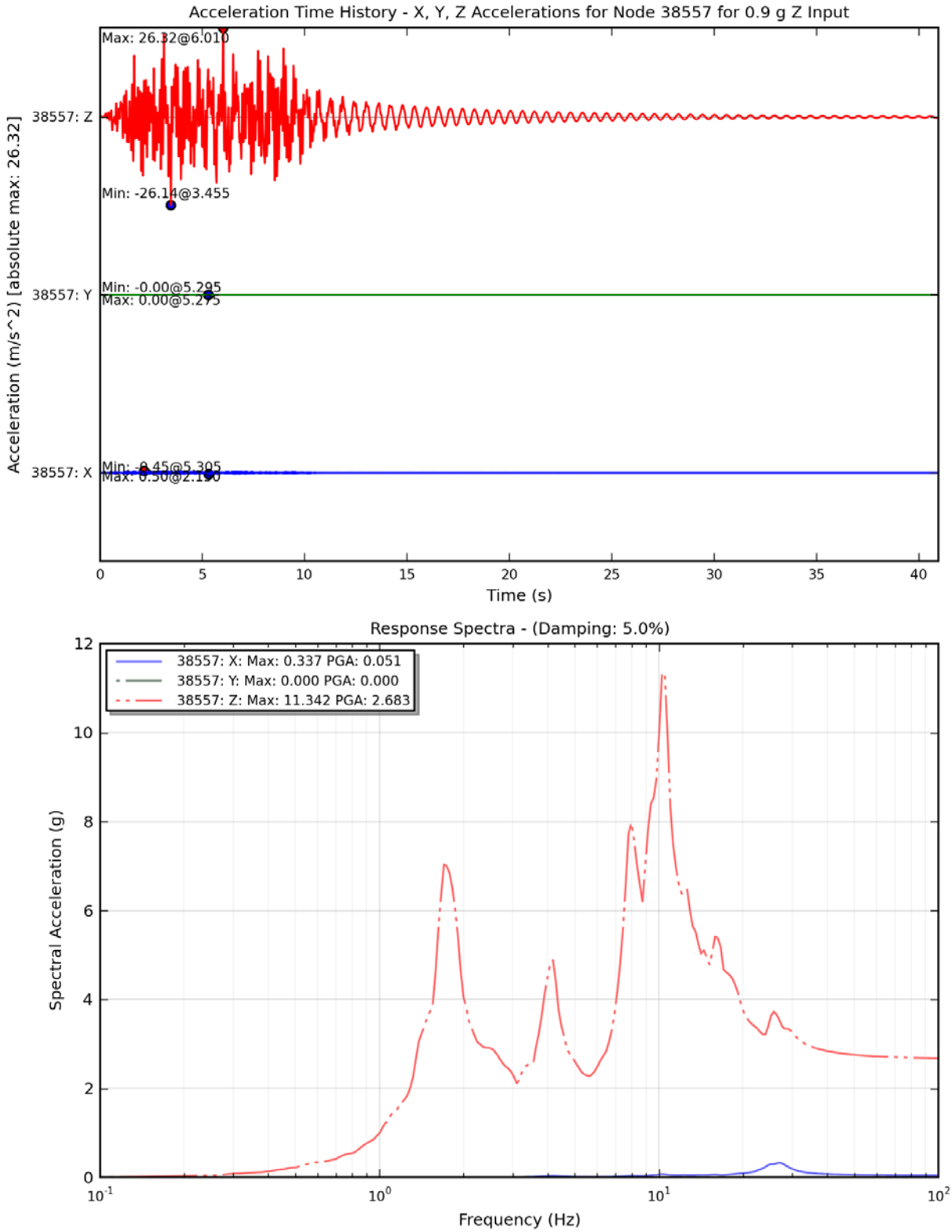

Figure 5-57 Response Acceleration Time Histories and ISRS at Node 38557 for Z Input Motion (0.9 g)

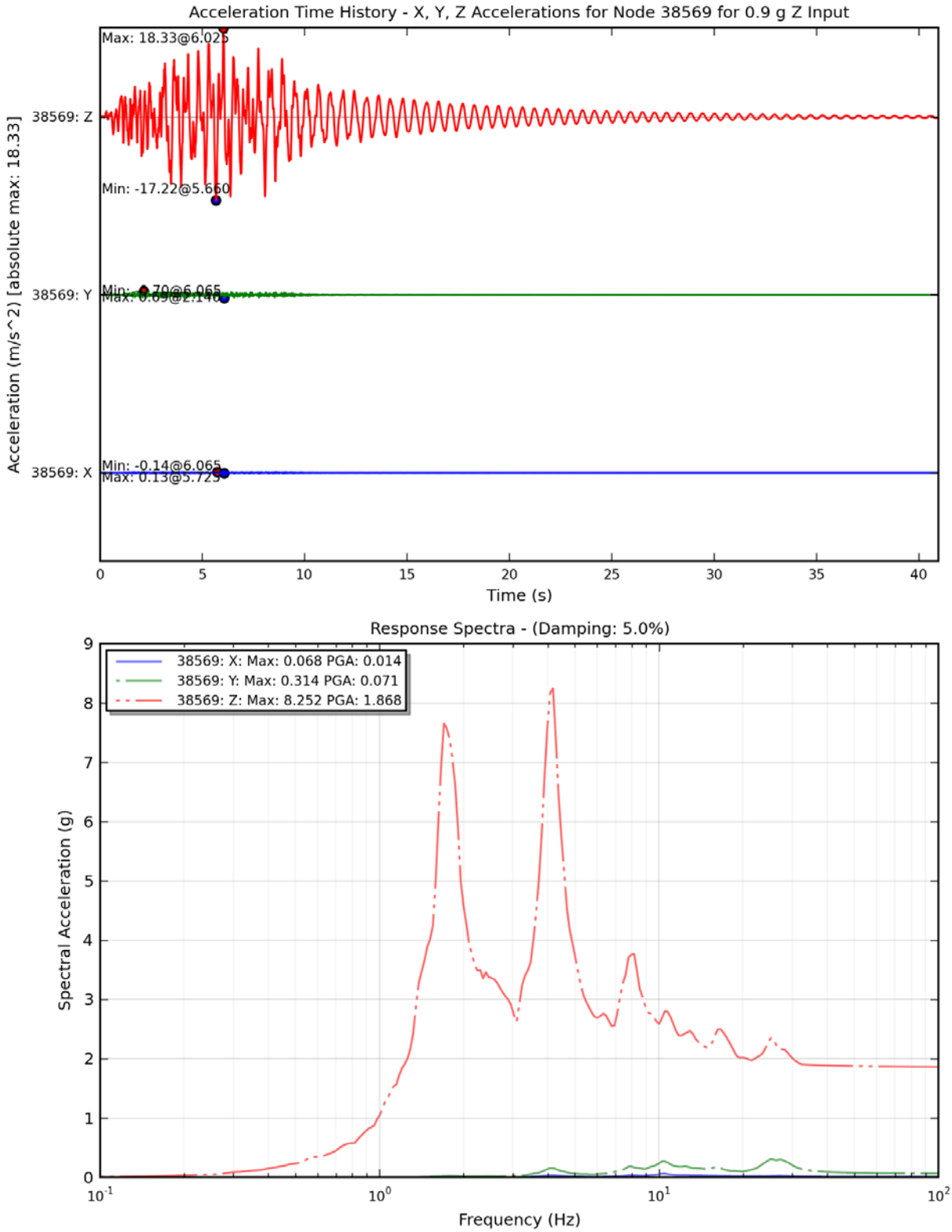

Figure 5-58 Response Acceleration Time Histories and ISRS at Node 38569 for Z Input Motion (0.9 g)

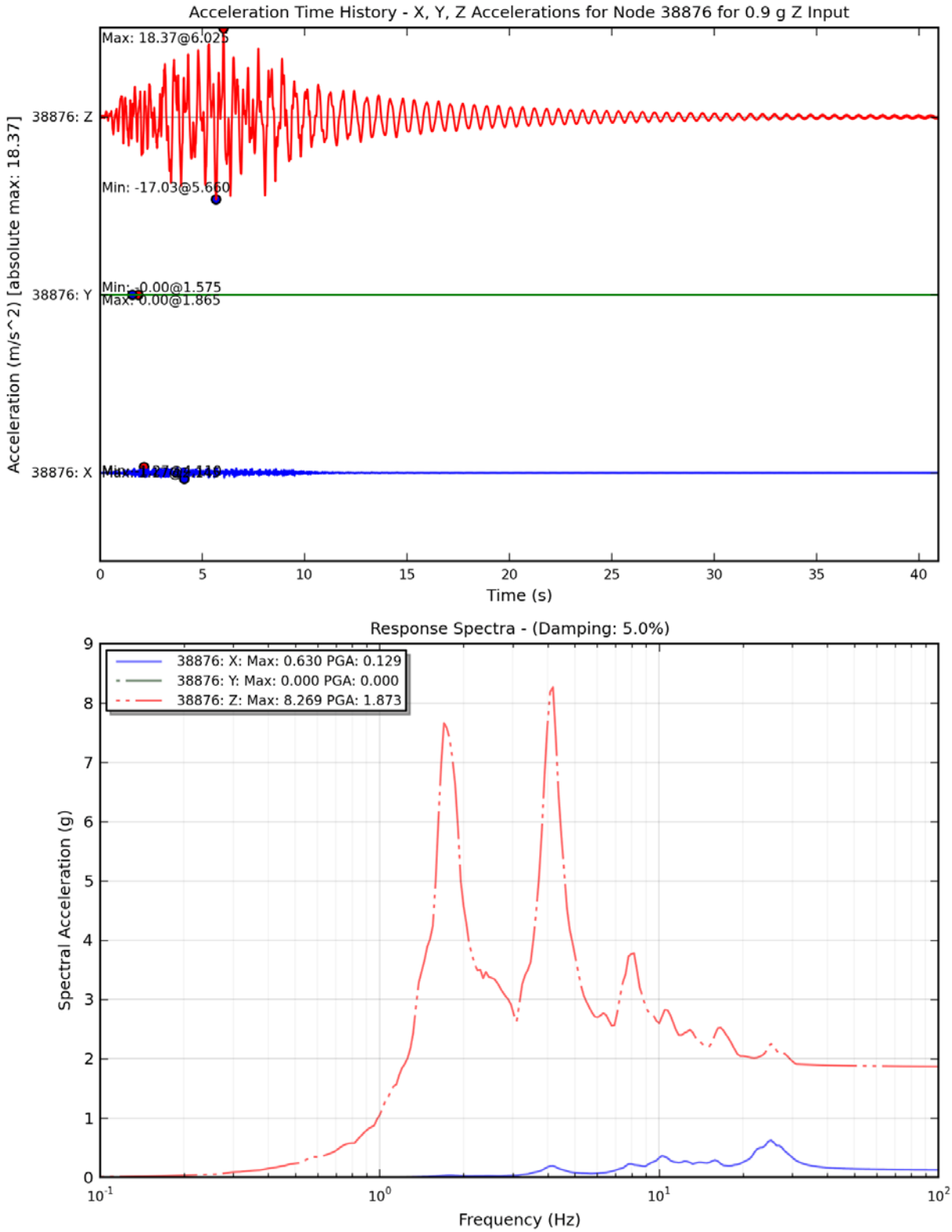

Figure 5-59 Response Acceleration Time Histories and ISRS at Node 38876 for Z Input Motion (0.9 g)

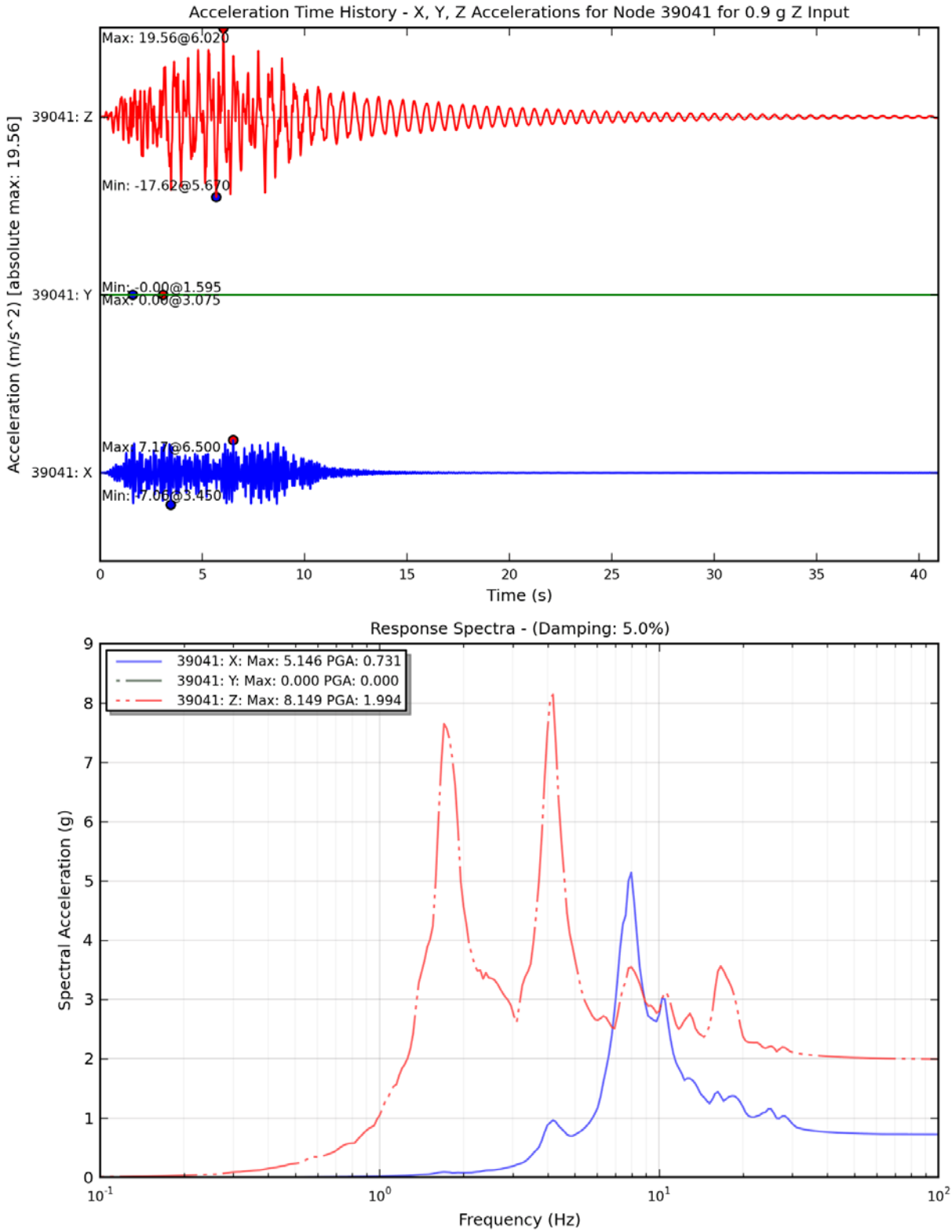

Figure 5-60 Response Acceleration Time Histories and ISRS at Node 39041 for Z Input Motion (0.9 g)

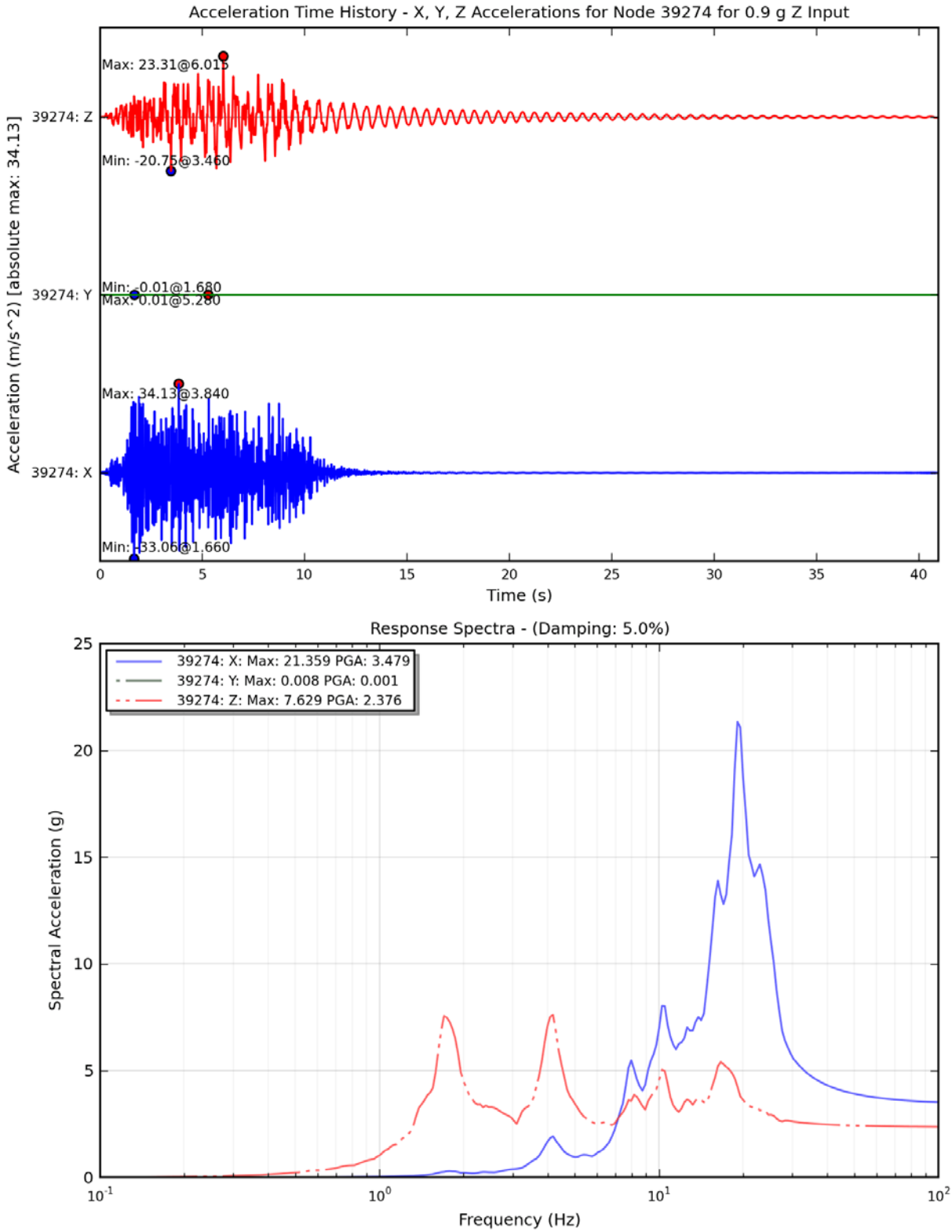

Figure 5-61 Response Acceleration Time Histories and ISRS at Node 39274 for Z Input Motion (0.9 g)

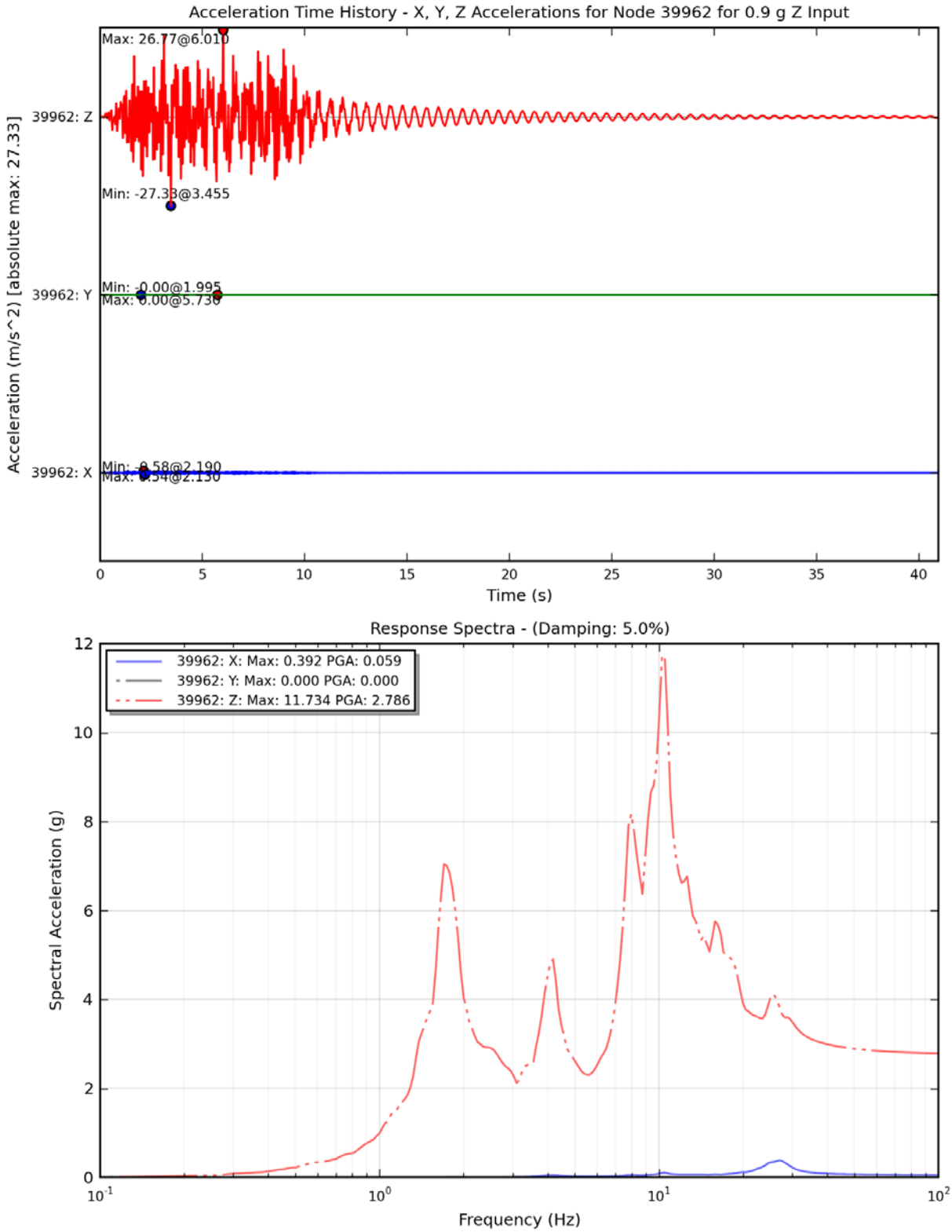

Figure 5-62 Response Acceleration Time Histories and ISRS at Node 39962 for Z Input Motion (0.9 g)

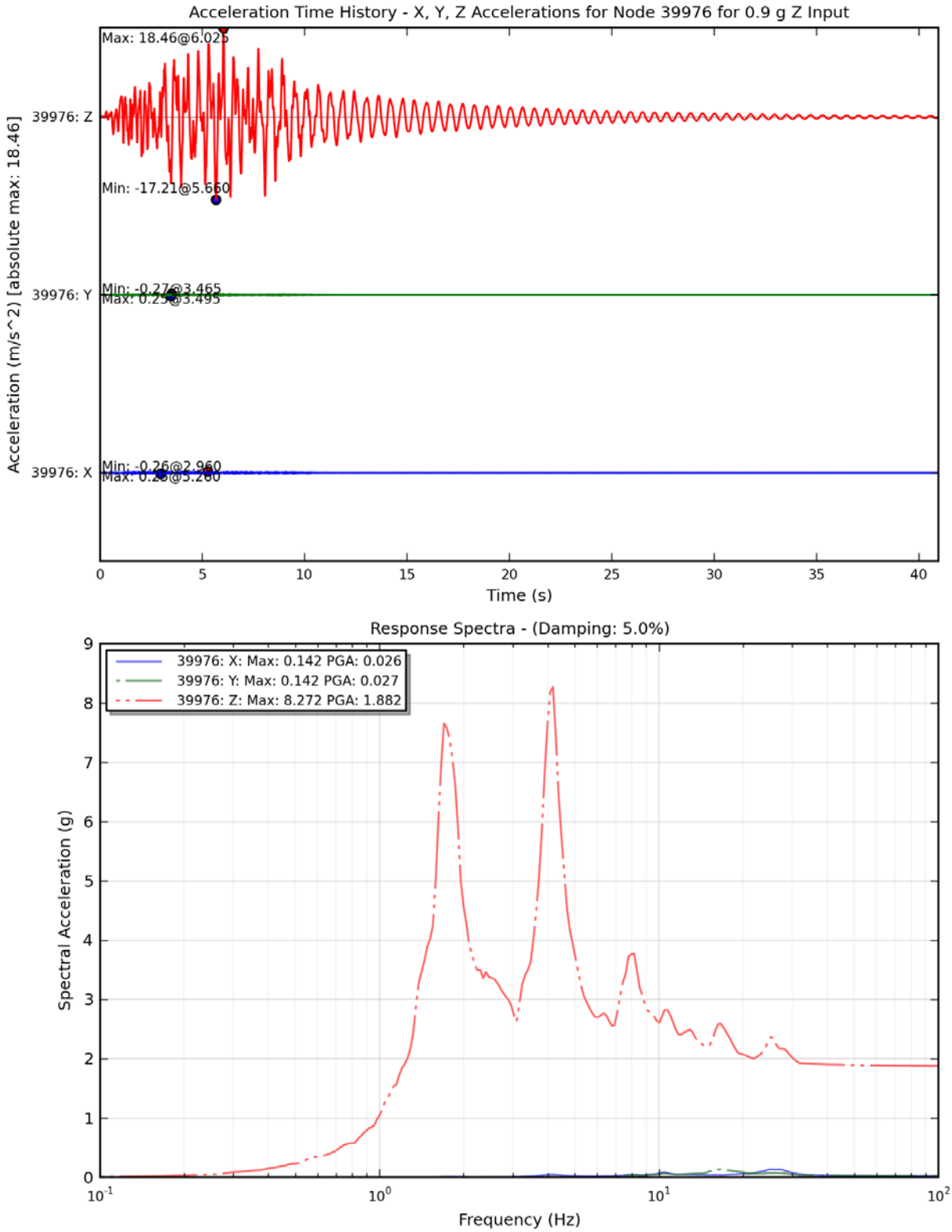

Figure 5-63 Response Acceleration Time Histories and ISRS at Node 39976 for Z Input Motion (0.9 g)

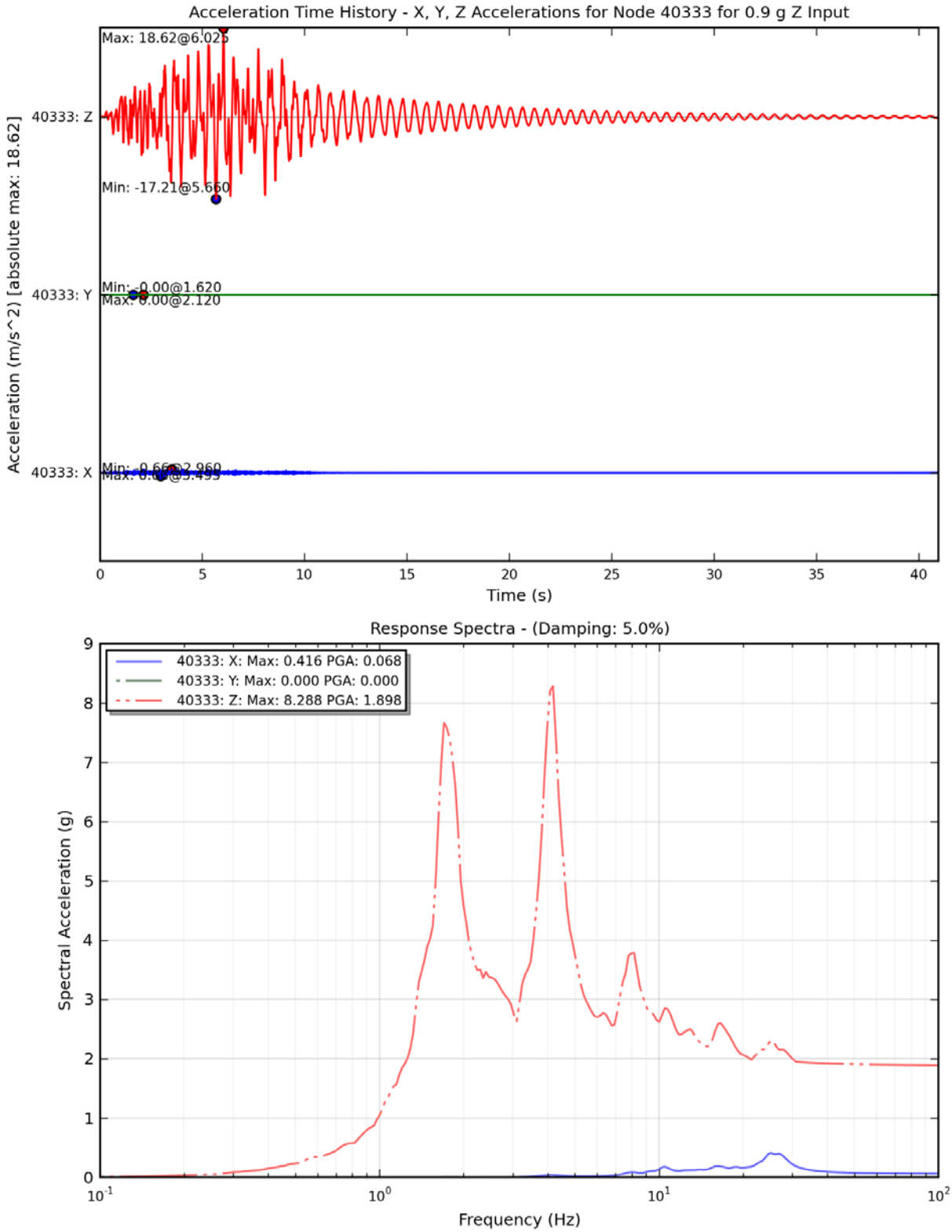

Figure 5-64 Response Acceleration Time Histories and ISRS at Node 40333 for Z Input Motion (0.9 g)

6 SUMMARY AND RECOMMENDATIONS

A.1 Summary

This report summarizes the SASSI analyses performed by BNL and CJCA, as part of the seismic soil structure interaction simulation capability project for DOE NEAMS. Another part of the project is the LLNL's DIABLO analyses of the same seismic soil-structure interaction problem. The comparison of the results from these two codes will be presented in a separate report.

The SASSI analyses included three cases: 0.2 g, 0.5 g, and 0.9g, all of which refer to nominal peak accelerations at the top of the bedrock located at a depth of 112.776 m (370 ft). The soil profiles corresponding to these input excitation levels were developed by CJCA and were used in both the SASSI analyses and the DIABLO analyses.

The MSM method was used for all SASSI analyses. This method was selected based on the transfer functions obtained from alternative methods using a quarter model.

The peak response accelerations at key locations are summarized below (m/s^2):

For the case of 0.2 g (1.96 m/s^2):

	X Input	Z Input
Center of roof (A)	2.85	6.20
Center of basemat (B)	1.85	4.36
A/B	1.54	1.42

For the case of 0.5 g (4.90 m/s^2):

	X Input	Z Input
Center of roof (A)	5.69	15.72
Center of basemat (B)	3.90	12.09
A/B	1.46	1.30

For the case of 0.9 g (8.82 m/s^2):

	X Input	Z Input
Center of roof (A)	8.63	27.33
Center of basemat (B)	5.95	21.34
A/B	1.45	1.28

As shown in the above summary, the peak response ratio (A/B) decreases somewhat as the input excitation level increases. This may indicate that as the soil column degrades due to larger excitation, soil response becomes more dominant than the structural response.

Comparing the input levels to the responses at the basemat, the soil column de-amplifies the horizontal motion while amplifies the vertical motion.

It should be noted that integration of the SASSI response acceleration time histories should not be used to obtain velocity or displacement time histories.

A.2 RECOMMENDATIONS FOR FUTURE WORK ON FREQUENCY-DOMAIN METHODS

Although the computing power nowadays makes feasible time domain solutions of large scale SSI problems, time domain codes being specifically developed for SSI problems, such as DIABLO and ESSI, are at an early stage of development and will require significantly more effort to develop and validate their capability before their practical application in design and licensing of nuclear facilities. Therefore, while efforts are being placed in the development of such time domain SSI methods, enhancements of the traditional frequency-domain methods, such as SASSI, are prudent in ensuring the continuation of the proven success of the frequency-domain methods in the nuclear industry.

It has been recognized that the currently available frequency-domain codes have some limitations regarding their capabilities and usability. Some of the limitations can be removed by adding new capabilities and others can be removed by utilizing modern computational technologies. These traditional frequency codes, especially SASSI, have undergone several revisions by different developers for enhancement. However, these efforts have been incremental and the resulting codes may be difficult to make further significant improvements. Overall, these traditional frequency-domain codes have gone through a long history of validations against theoretical solutions and field measurements (such as the large scale seismic experiment at Lotung, Taiwan) as well, and constitute a firm foundation for developing a modern frequency-domain SSI program.

Therefore, it is recommended to pursue further improvements in the frequency domain codes in parallel to the ongoing research to develop and benchmark the time domain codes. Some of the key improvements are listed below:

(1) Re-establish/develop a modern, modularized (pluggable for incorporating future capabilities), and parallel code base for SASSI;
(2) “Profile” the code (i.e., analyze the efficiency of various parts of the code) and optimize the code to expedite the execution speed;
(3) Implement/automate certain capabilities based on industry guidelines for using SASSI (e.g., addressing the need for regular excavated soil mesh for any reasonable finite element structural model, approximating local soil nonlinearity, automating the treatment of soil layering, implementing advanced data management, etc.);
(4) Investigate the number-theoretic (e.g., GLP) enhanced subtraction method (ESM, which was proposed and briefly tested in this study); and
(5) Incorporate methods to consider uncertainties in soil properties.